# THE NATURE OF HYDROTHERMAL FLUIDS ASSOCIATED WITH GRANITE-HOSTED, POLYMETALLIC MINERALISATION IN THE EASTERN LOBE OF THE BUSHVELD COMPLEX.

By

**Lauren Anne Freeman**

A thesis submitted in fulfilment of the requirements for the degree of

**PhD in Geology**

University of the Witwatersrand

1998

# ABSTRACT

Numerous small base-metal deposits occur in the acidic rocks of the Bushveld Complex, and modern exploration programs are currently re-examining this metallotect in an attempt to refine the current working hypothesis for mineralisation in these granites. The hypothesis proposed for the origin of mineralisation is multifaceted, encompassing both spatial and temporal relationships between at least three episodes of ore formation. The first episode of mineralisation (typified by the Zaaiplaats tin deposit) occurred at relatively high temperatures (>600°C to 400° C), and resulted in the formation of orthomagmatic cassiterite, scheelite and an early generation of fluorite. At lower temperatures (200°C<T<400°C), where processes were essentially fluid dominated, a mesothermal Cu-Pb-Zn-As-Ag-Au assemblage was deposited (exemplified by the Spoedwel, Boschhoek and Albert copper and silver deposits). A third episode of mineralisation resulted in the formation of an Fe-U-F assemblage and is recognised at several, but not necessarily all, of the deposits examined (for example, the Albert silver deposit). The extended nature of this three-stage paragenetic sequence is considered to reflect widespread mixing between an early fluid derived by $H_2O$-saturation of the granitic magma and an external meteoric/connate fluid, circulation of which was stimulated by the long-lived high heat-productive capacity of the Bushveld granites, as well as exhumation of the metallotect.

The early high-temperature Sn/W assemblage was precipitated while magmatic fluids dominated the system. With time, the pluton cooled and was subject to regional uplift. Fractures developed, acting as conduits for external fluids of meteoric and/or connate origin. The late magmatic fluids, enriched in incompatible metals (and volatiles), interacted with the latter fluid, resulting in the localised precipitation of a secondary, lower-temperature mineral assemblage (Cu-Pb-Zn) in the zone of fluid mixing. As the external fluid component became progressively more dominant, the paragenesis changed, forming the final Fe-U-F assemblage. The formation of these three different, temporally separate assemblages is adequately explained in terms of a fluid mixing model, wherein the concentration of metals and localisation of ore deposits are controlled by lithology and structure.

# DECLARATION

This thesis is my own unaided work, conducted under the supervision of Prof. Laurence J. Robb. It is being submitted for the degree of Ph.D. in Geology at the University of the Witwatersrand, and has not been previously submitted for any degree or examination at any other university.

Lauren Anne Freeman

# ACKNOWLEDGEMENTS

My sincere thanks to my supervisor Laurence Robb, for his guidance, support and invaluable criticisms of this manuscript.

I am grateful to the following people who played an important role in the collection of analytical data.

-Steve Kesler and Jim O'Neil at the University of Michigan, for allowing me to use their laboratory facilities, and for discussions on the information obtained concerning the gas chemistry and stable isotopic signatures of fluids in my study area.

-Wojtek Przybylowicz at NAC for running PIXE analyses and for editing the PIXE section.

-Mark Brandriss and Hank Jones at the University of Michigan for assistance with oxygen isotope analyses.

-Rudi Boer and Gillian Drennan for help with fluid inclusions during early stages of this study.

-Angie Breithaupt for teaching me how to operate the quadrupole mass spectrometer and fluid inclusion extraction line.

-Pamela Murphy for running Raman analyses

-RTZ for providing field assistance while mapping.

-Jim Reynolds for helpful discussions of fluid inclusion petrography and microthermometry

-John Clemens for discussions of hypersolvus and subsolvus granites in the field.

-Erna Hattingh at the Council for Geosciences for assistance with cathodo-luminescence and backscatter images.

- Special thanks go to my family, for their support and encouragement throughout my studies.

# TABLE OF CONTENTS

**ABSTRACTS**

Freeman, L.A. and Robb, L.J. (1995). The nature of hydrothermal fluids associated with the granite-hosted Spoedwel Copper Mine, Bushveld Complex, South Africa. Centennial Geocongress Extended Abstracts Vol. II. 719.

Freeman, L.A., Robb, L.J., Kesler, S.E. and O'Neil, J.R. (1997). Fluid mixing and the formation of polymetallic mineralisation in the Bushveld granites. International Symposium on Plumes, Plates and Mineralisation. Abstracts. 14-18 April 1997. Pretoria South Africa. 35-36.

Robb, L.J., Freeman, L.A., and Bailie, R.H. (1998). Metallogeny of the Acid Phase of the Bushveld Complex. IAVCEI Cape Town, July 1998.

**CHAPTER 4**

**CHAPTER 5**

**Figure 5.65** Schematic diagram showing the change in salinity with time, decreasing temperature and increasing external fluid component.

**CHAPTER 6**

**Figure 6.1** Model geometry for PIXE analyses of fluid inclusions, schematically indicating the proton beam, sample and detector arrangement, and the geometric parameters used to quantify PIXE microprobe spectra. The dimensions x, y and z are determined by optical microscopy; d is determined using the Cl $K_\alpha/K_\beta$ ratio and/or optical measurement (from Heinrich *et al.*, 1992).

**Figure 6.2** Screen printout showing how finder grids assist in relocation of fluid inclusions once in sample holder.

**Figure 6.3** PIXE microprobe spectrum of quartz some distance from the finder grids showing that only Si peaks are detected.

**Figure 6.4** PIXE microprobe spectrum of quartz near the finder grid, showing that excitation of the grid (in this case Cu), interferes with the spectrum for pure quartz.

**Figure. 6.5** A) Petrographic map of quartz-hosted fluid inclusions from the Grass Valley Sn deposit. The inclusions occur along the border between quartz generations 1 and 2, both of which precede cassiterite precipitation.

B) PIXE microprobe spectrum (Q = 115 nC, I = 250 pA) of inclusion C (depth 0.57μm, thickness 2.28μm, dimensions 16μm X 12μm) in sketch A), indicating the presence of Ca, Fe and Cu.

C) Enlargement of portion of B) in which S, K and Ca peaks become more obvious.

**Figure 6.6** A) Petrographic map of quartz-hosted fluid inclusions from the Grass Valley deposit. The inclusions occur in euhedral, pegmatitic quartz associated with calcite and cassiterite. The inclusion probes occurs in a secondary trail of inclusions in quartz generation 1 preceding cassiterite precipitation.

B) PIXE microprobe spectrum of fluid inclusion A in A), indicating the presence of Fe and Ni. Only Fe is derived from the inclusion, Ni peaks are caused by excitation of the Ni finder grid.

**Figure 6.7** A) Petrographic map of quartz-hosted fluid inclusions from the Spoedwel Cu deposit. These fluid inclusions are primary with respect to the second generation of quartz precipitated at the deposit, and have variable phase proportions. Inclusion A is a Type 2 inclusion consisting of liquid , vapour and a halite daughter crystal. Inclusion B contains no visible vapour phase, only liquid and 2 solids (hematite and one unidentified crystal).

B & C) PIXE microprobe spectra (Q =213 nC, I = ~500 pA) of inclusions A (depth 0.5μm, thickness 1.57μm, dimensions 14μm X 6μm) and B (depth 0.57μm, thickness 2.28μm, dimensions 16μm X 12μm), indicating the presence of Cl, K, Ca, Ti, Mn, Fe, Zn, Pb, As, Rb and Mo in the inclusions.

**Figure 6.8** A) Petrographic map of a quartz-hosted fluid inclusion assemblage that is associated with pyrite and sphalerite mineralisation in a vein from Albert silver deposit. The inclusion probed appears to be primary in origin, however, secondary trails are also present. Magnification: X400.

B) PIXE microprobe spectrum (Q =325 nC, I = ~500 pA) of inclusion A (depth 3.99μm, thickness 0.0856μm, dimensions 12μm X 10μm) in A), indicating the presence of S, K, Ca, Fe Zn and As in the inclusion. The components detected in the inclusion reflects those of the associated minerals.

C) PIXE microprobe spectrum of the same inclusion A, but where Q = 458 nC and I =~500pA. The Fe response is enhanced and Mn and Pb are detected.

**Figure 6.9** A) Petrographic map of quartz-hosted primary fluid inclusions occurring in tourmaline spheroids from Leeufontein.

B) PIXE microprobe spectrum (Q =487 nC, I =500 pA) of inclusion A (depth 0.57μm, thickness 2.28μm, dimensions 18μm X 16μm), indicating the presence of Ca, Ti, Mn, Fe, Zn, As? And Rb in the fluids.

C) PIXE microprobe spectrum (Q =283 nC, I = 500 pA) of inclusion C (depth 2.14μm, thickness 1.71μm, dimensions 20μm X 8μm), indicating the presence of Cl, K, Ti, Fe, Zn, Pb, Br and Rb in the fluids.

**Figure 6.10** A) Petrographic map of tourmaline-hosted primary fluid inclusion occurring in a tourmaline spheroid from Leeufontein. Magnification: X400.

**CHAPTER 8**

## LIST OF TABLES

# CHAPTER 1

## INTRODUCTION

The Bushveld granites have been the subject of exploration since the late 1800's, when many small scale mining operations were established. Of particular interest were the tin deposits, and mines such as Zaaiplaats, Union, Grass Valley, Stavoren and Rooiberg came into being. Mineralisation at these deposits has been extensively studied (Wagner, 1921; Strauss, 1954; Leube and Stumpfel, 1963; Solnge, 1944, Ollila, 1981, Pollard *et al.*, 1991; Mc Naughton *et al.*,1993).

However, mineralisation in the Bushveld granites is not restricted to tin alone. Numerous small base metal deposits were mined sporadically, such as those at the Albert Silver Mine (Robb *et al.* 1994), Houtenbek molybdenum deposit, Rooibokkop-Boschhoek copper deposit (Smits, 1980), Spoedwel Copper Mine (Scoggins, 1991), and Vergenoeg Fluorite Mine (Crocker, 1985). Many of these deposits have only been looked at cursorily, and an adequate understanding of the controls of mineralisation is lacking. Furthermore, certain features are common to most of these deposits, prompting the suggestion that these pockets of mineralisation are genetically related in some way.

The granites have become increasingly attractive to exploration companies recently, and establishing a framework within which to conduct prospecting has become an urgent necessity. In particular, the similarities in geological setting and paragenesis between the large scale Olympic Dam deposit in South Australia and the deposits associated with the Bushveld granites, has given added impetus to the exploration efforts. With this objective in mind, the nature of hydrothermal fluids associated with mineralisation at five known ore deposits has been examined and compared with fluids occurring in barren granites in an area east of Marble Hall. The deposits were chosen specifically to represent each of the three major ore assemblages recognised in the Bushveld granites. The deposits selected are the Grass Valley Tin Mine, the Spoedwel Copper Mine, Albert Silver Mine, the Dronkfontein copper and tin deposit, and the Houtenbek molybdenite and sphalerite deposit.

The deposits at Grass Valley , Albert, Spoedwel and Dronkfontein have several features in common; they are all fracture related, hydrothermal replacement-type deposits, showing similar parageneses but different principal ore minerals. At Houtenbek and Dronkfontein, detailed geological mapping is yet to be undertaken, but, at first sight, the mineralisation appears similar to the other deposits. At Grass Valley, tin dominates, while at Spoedwel, a copper sulphide assemblage dominates, and at Albert a hematite-fluorite-pitchblende assemblage is well developed. Paragenetic relationships show that these three assemblages represent temporally separate events, and thus, form the basis of the proposed hypothesis for mineralisation. The fluids associated with each of these assemblages have been examined, revealing an evolution in the nature of the fluids as a function of time, temperature and source.

## 1.1 THE HYPOTHESIS

The hypothesis proposed for the origin of mineralisation is multifaceted, encompassing both spatial and temporal relationships between at least three episodes of ore formation (Figure 1.1). The first episode of mineralisation (typified by the Zaaiplaats tin deposit) occurred at relatively high temperatures (>600°C to 400° C), and resulted in the formation of orthomagmatic cassiterite, scheelite, wolframite and molybdenite. At lower temperatures (200°C<T<400°C), where processes where essentially fluid dominated, a mesothermal Cu-Pb-Zn-As-Ag-Au assemblage was deposited (represented mainly at the Spoedwel, Boschhoek and Albert deposits). A third episode of mineralisation resulted in the formation of an Fe-U-F assemblage, and is recognised at several, but not necessarily all, of the deposits examined (for example, the Albert silver deposit). The extended nature of this three-stage paragenetic sequence is considered to reflect widespread mixing between an early fluid derived by $H_2O$-saturation of the granitic magma and an externally-derived fluid, circulation of which was stimulated by the long-lived high heat-productive capacity of the Bushveld granites, as well as exhumation of the metallotect. A similar hypothesis was suggested by Robb *et al.* (1994), in a study of mineralisation at the Albert Silver Mine. However, the general applicability of the model to mineralisation in the Bushveld granites was not tested, and only preliminary studies of the fluid characteristics had been conducted.

The present study aims to test and refine the model proposed by Robb *et al.* (1994), and, in light of this hypothesis, to determine the relationships between various polymetallic deposits in the eastern lobe of the Bushveld Complex.

## 1.2 METHODOLOGY

Several analytical techniques were employed in order to gain an insight into the nature of the mineralising fluids. Initially, the fluid inclusions from the Spoedwel deposit were investigated, using conventional microthermometric techniques, Raman spectrometry, and PIXE analysis. At that early stage, indications of an external meteoric and/or connate component in the fluids were recognised, prompting further investigation as to the general applicability of fluid mixing as a mechanism for the precipitation of ore minerals in the eastern lobe of the Bushveld Complex. Consequently, the above mentioned working hypothesis served as a guide in choosing analytical techniques, aimed at verifying the notion. The analytical techniques employed in this study are briefly summarised in Table 1.1, and are shown in the flow diagram (Figure 1.2) detailing methods and procedures. Detailed fluid inclusion microthermometry for all the deposits was undertaken, and stable isotopic signatures and gas chemistry of fluid inclusion contents were analysed.

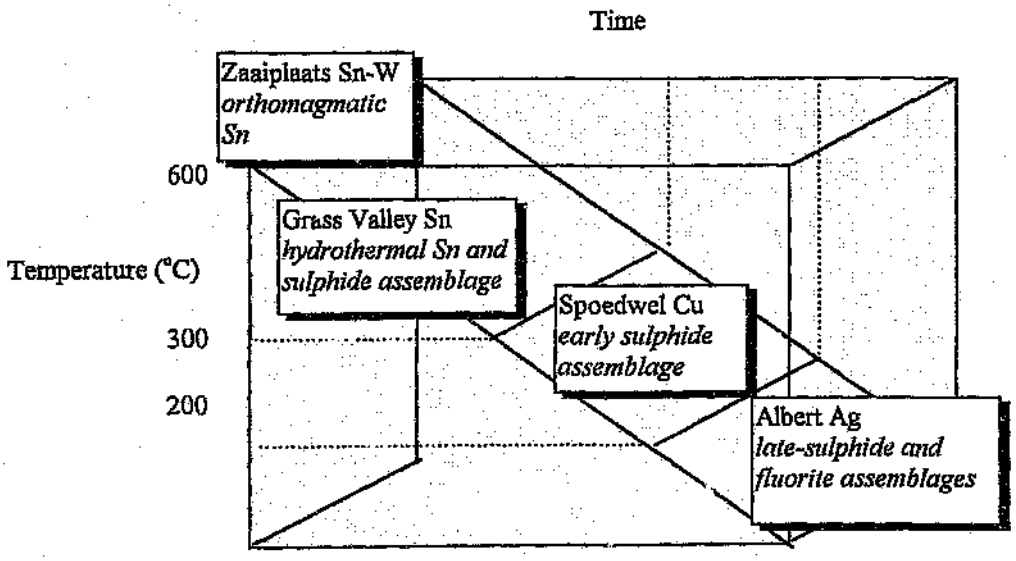


**Figure 1.1** Diagrammatic representation of the hypothesis proposed for mineralisation in the granites of the eastern lobe of the Bushveld Complex.

**Table 1.1** Analytical techniques employed to test the hypothesis.

| QUESTION | TECHNIQUE | INFORMATION OBTAINED |
|---|---|---|
| **What is the paragenetic sequence?** | Transmitted and reflected light microscopy and petrography. | The order in which ore minerals, gangue minerals, and alteration minerals were formed is determined. |
| **What is the geological setting?** | Geological mapping. Borehole core logging. Underground mapping. | The combination of these techniques provides information on the geological setting, field relations, size and geometry of the deposit, as well as the presence of any structural features (e.g. faults, folds) which may have been involved in the mineralising process. |
| **What is the temperature of ore formation?** | Fluid inclusion microthermometry. | Homogenisation temperatures indicate minimum entrapment temperatures of fluids |
| **What is the salinity of the fluids?**<br>**Which ions are in solution?** | Fluid inclusion microthermometry. | Eutectic melting temperatures ($T_e$) indicate some of the major ions in solution e.g. Ca, K, Na, and the final melting temperature provides an estimate of the salinity of the fluids. |
| | PIXE Analysis | Detects all ions in solution that are heavier than Si. |
| **Which fluids are associated with precipitation of ore suite?** | Fluid inclusion petrography and mapping. | Identify primary, secondary and pseudosecondary fluid inclusion assemblages. Trace evolution of fluids. |

**Table 1.1 (continued)** Analytical techniques employed to test the hypothesis.

| QUESTION | TECHNIQUE | INFORMATION OBTAINED |
|---|---|---|
| **Which volatiles are in solution?** | Fluid inclusion microthermometry | First melting indicates chemical system, as well as the presence of volatiles such as $CO_2$ and $N_2$. |
| | Raman Spectrometry | Detects any polyatomic solutes or solids , e.g. $CO_2$, $CH_4$, $H_2O$, $N_2$, graphite, and certain minerals. |
| | Quadrupole Mass Spectrometry | Provides quantitative data on a large number of gases present at low concentrations in fluid inclusions. |
| **What is the pressure of formation?** | Calculation and construction of isochores from fluid inclusion microthermometric data. | P-T diagrams which indicate lines of equal density, are used to infer approximate pressure conditions during the formation of the deposit. |
| | Raman Spectrometry | Methane peak position can be used to suggest pressures of entrapment. |
| **What is the origin of the fluids?** | Stable Isotopes $\delta D$ and $\delta^{18}O$ | $\delta D$ / $\delta^{18}O$ plots are used to determine whether fluids are magmatic or meteoric in origin, and whether and mixing of magmatic and meteoric water took place. |
| | $\delta^{13}C$ | Fluid $\delta^{13}C$ signatures indicate the source of the carbon. |
| | $\delta^{34}S$ | Fluid $\delta^{34}S$ signatures indicate the source of the sulphur. |

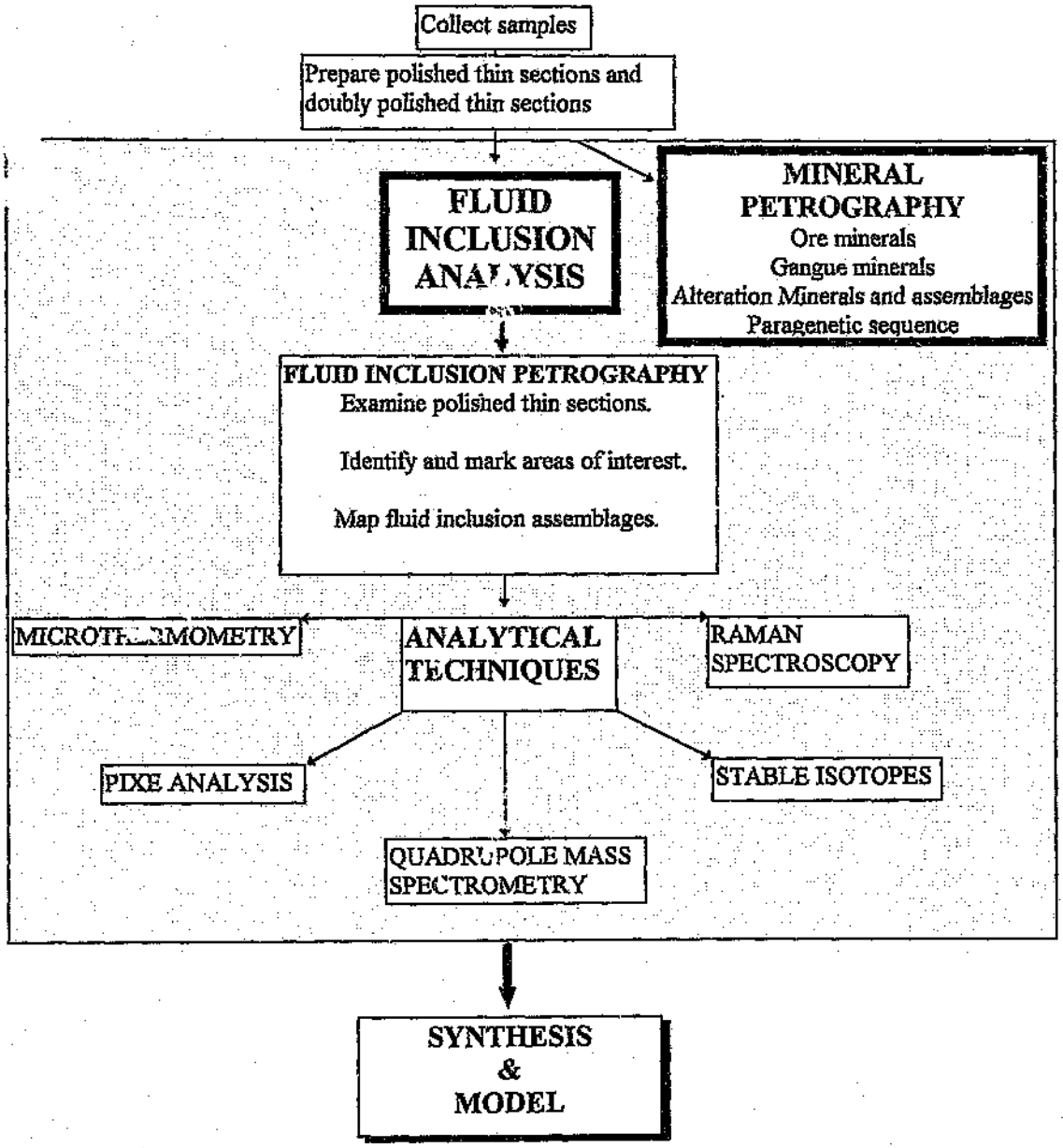


**Figure 1.2** Flow diagram showing the format of this thesis, and the analytical techniques used to test the hypothesis.

Field mapping in the area east of Marble Hall was undertaken in order to obtain sufficient knowledge of the nature of unmineralised Bushveld granites, and so be able to recognize features associated with the deposition of ore minerals. A consistent research procedure was adopted for examining the unmineralised granites, as well as the mineralised granites. Thus, comparisons between the various deposits and the unmineralised granites could be easily drawn. In each case, thorough petrographic studies of the samples were carried out, and, hence, suitable samples selected for fluid inclusion petrography and microthermometry. Once microthermometric data had been collected and fluid assemblages recognized, samples were then prepared for PIXE analysis, Raman spectroscopy, quadrupole mass spectrometry and isotopic analysis. Wherever possible, the same samples were examined using the different techniques, so that a comprehensive database, including all components of a particular fluid inclusion assemblage, could be constructed.

In the chapters that follow, the evidence gathered from each analytical technique is presented, and discussed. In the final chapter, the data are integrated and a model for the mineralisation put forward.

# CHAPTER 2

# GEOLOGICAL SETTING

## 2.1. REGIONAL GEOLOGY - the Bushveld Complex

The Bushveld Igneous Complex is early Proterozoic in age and is situated within the Kaapvaal Craton, South Africa (Figure 2.1). The mafic and ultramafic units (Rustenburg Layered Suite), the felsic rocks (Lebowa Granite Suite) and the granophyres (Rashoop Granophyre Suite), are intruded into the sedimentary rocks of the Transvaal Sequence and form the largest known A-type igneous province in the world (Kleemann and Twist, 1989). According to Hunter (1976), the intrusion covers an area of approximately 67 340km$^2$, but more recent estimates of the volume of rock preserved suggest a minimum of 300 000km$^3$ (Cawthorn and Walraven, 1997).

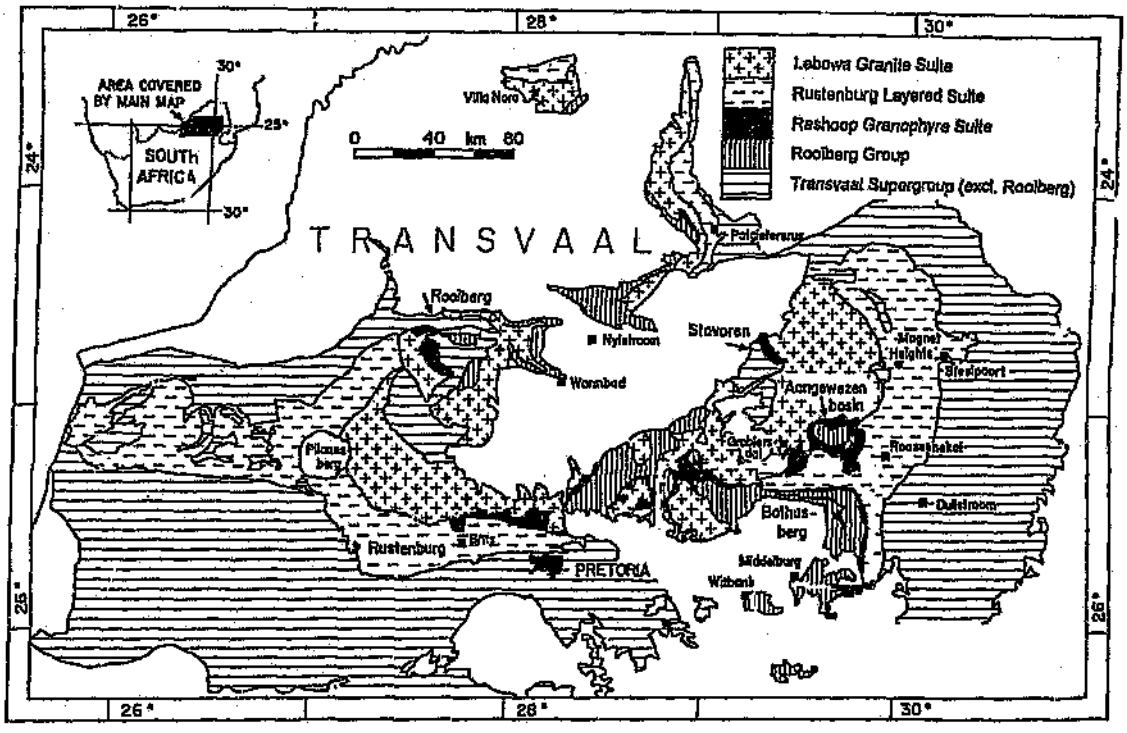


**Figure 2.1** Regional geological map of the Bushveld Complex (modified from Walraven, 1997).

*SHAPE AND STRUCTURE*

The shape of the intrusion has been described as "cruciform", consisting of four synformal lobes (Hunter, 1976) that are arranged approximately symmetrically about two perpendicular axes, aligned east north-east and north north-west (von Gruenewaldt, 1979). Two main structural trends within the Kaapvaal craton (east north-east and north north-west) were important factors controlling the configuration of the lithologies i.e. the Pongola, Dominium Reef- Witwatersrand, Ventersdorp, Transvaal and Waterberg Supergroups, preserved within the various basins on the craton (von Gruenewaldt, 1979).

A broad anticlinal warp, called the Pretoria-Zebediela anticline, stretches along the western flank of the eastern Bushveld and parallels the deep abyssal fracture (Cousins, 1959) along which the majority of layered intrusions in the Bushveld are located (von Gruenewaldt, 1979). The western flank of the eastern Bushveld was, therefore, tectonically active during emplacement of the complex (von Gruenewaldt, 1979).

LANDSAT imagery was used by Lee and Sharpe (1986) in order to assess regional structures within the Bushveld and surroundings, and it was found that there was no evidence for the concept that deep-seated crustal fractures influenced the location and form of the Bushveld Complex, as was suggested by Cousins (1959) and von Gruenewaldt (1979). Several linear structures representing joints, faults and dykes were recognised. Prominent among these lineaments is the Steelpoort Fault, trending 045° from Loskop Dam, and extends only a short distance into the Transvaal sedimentary rocks. Several 135°-trending lineaments are visible in the western sector of the complex. Faults comprising the limits of the post-Bushveld Brits graben trend 135° from Hartebeespoort Dam. The Rustenberg Fault displaces Transvaal sedimentary rocks and trends 125° through Olifantsnek Dam. In the eastern Bushveld Complex, there is a pervasive 045° to 135° pattern in the joints and dykes which are commonly occupied by dolerite dykes. The most abundant occurrence of dolerite dykes, however, is in the orientation 010° to 015°. Lee and Sharpe (1986) compiled a map of the lineaments evident on the LANDSAT image, and rated them in accordance with their prominence and orientation (Domains I to VI) (Figure 2.2).


**Figure 2.2** Lineament map showing aeromagnetic lineaments and gravity highs (< 70mgals). Prominent geological features and lineament domains are indicated (from Lee and Sharpe, 1986).

*GEOLOGY*

The geology of the Bushveld Complex has been divided into three suites of rocks (Figure 2.3), namely the Rustenberg Layered Suite, the Lebowa Granite Suite and the Rashoop Granophyre Suite (SACS, 1980). Each of these lithological units is discussed below, with the emphasis on the Lebowa Granite Suite. Furthermore, the geological relationships of the host rocks, the Transvaal Supergroup, are reviewed.

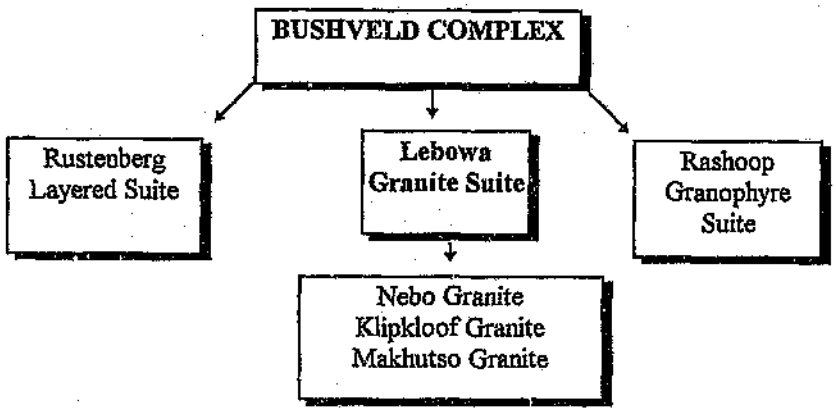


**Figure 2.3** Diagrammatic representation of the rocks of the Bushveld Complex.

**Host Rocks** - The Transvaal Supergroup

The Transvaal Supergroup is composed of the Chuniespoort, Pretoria and Rooiberg Groups which consist of chemical sedimentary rocks, clastic sedimentary rocks and volcanic rocks, respectively. The Bushveld Complex was intruded into the Transvaal Supergroup, at a palaeo-unconformity between the Rooiberg Group and the underlying Pretoria Group (Cheney and Twist, 1991). Field relationships indicate that the Rooiberg Group precedes the Bushveld Complex; however, whether the Rooiberg was part of the Transvaal Supergroup or the Bushveld Complex, was unclear for quite some time.

At one stage, the Rooiberg felsites were placed within the Bushveld Complex, as the precursor to the major magma injection (Twist, 1985). However, the consensus now is that the Rooiberg felsites represent the final stage of volcanic activity in the development of the Transvaal basin (Eriksson *et al.*, 1993; Walraven, 1997).

The Rooiberg Group is a thick succession of acid volcanic rocks which occur throughout the Transvaal sedimentary basin and forms the upper third of the Transvaal Supergroup (Eriksson *et al.*, 1993). It consists of dacite flows, rhyodacite lava, and, in places, silicic andesites. It varies from rhyodacite at the base to rhyolitic at the top (Walraven, 1997). Twist (1985) recognised three felsite magma types, which were probably generated during deep crustal anatexis, as the mafic magmas began their ascent from the mantle. Two formations are recognised in the eastern and central Transvaal basin; they are the lower, rhyodacitic Damwal Formation and the upper rhyolitic Selons River Formation. The Selons River Formation has been subdivided into the lower Doornkloof Member and the upper Klipnek Member. The Selons River Formation extends basin wide but, in the western part of the basin, in the Rooiberg area, the two members are given formation status and are called the Kwaggasnek and Schrikkloof Formations (SACS, 1980; Eriksson *et al.*, 1993).

**The Bushveld Complex**

***Rashoop Granophyre Suite***

The Rashoop Granophyre Suite is the first of the Bushveld Complex lithologies and occurs mainly as a sheet intruded into the Rooiberg Felsite Group, as well as between the Nebo and Transvaal Sequence rocks (Kleemann, 1985). The granophyres are included in the Bushveld Complex (SACS, 1980), but are generally allied more closely with the pre-Bushveld Rooiberg Group (Walraven 1987). Kleemann (1985) noticed intrusive relationships between the mafic Rustenberg Layered Suite and the Stavoren granophyres, indicating that the mafic suite post-dates the granophyre.

The granophyre is relatively homogeneous and displays a range of colours from brick-red to grey. The granophyres are composed of roughly equal proportions of quartz and feldspar which become finer-grained towards the top of the sheet (Kleemann, 1985). Kleemann (1985) maintains that the Rashoop Granophyre probably crystallised from a partial melt

extracted from the felsites on metamorphism by the Rustenberg Layered Suite. Walraven (1985, 1997) interpreted the bulk of the granophyric rocks (Stavoren Granophyre) as resulting from shallow intrusion of acid magmas immediately following, and forming a plutonic extension of, the Rooiberg Group volcanic event.

Other granophyre types are linked to the Bushveld granites and the basic layered rocks, and were formed by metamorphism of Rooiberg Group Volcanics or Pretoria Group sedimentary rocks, or by differentiation and assimilation of acid material by the basic layered rocks (Diepkloof Granophyre) (Walraven,1997). Three formal granophyre units were given by SACS (1980), namely the Stavoren Granophyre, the Rooikop Granophyre Porphyry, and the Zwartbank Pseudogranophyre. The Stavoren Granophyre includes all true granophyres, which are fairly coarse-grained and consist of intergrown quartz and K-feldspar. The Rooikop Granophyre Porphyry occurs as sill-like intrusions in the Rooiberg felsite and the Loskop Formation (Transvaal Supergroup), and consists of K-feldspar and quartz phenocrysts in a fine-grained granophyric matrix. The Zwartbank Granophyre consists of irregular quartz-feldspar intergrowths.

***Rustenberg Layered Suite***

The genesis of the Rustenberg Layered Suite has long been the subject of debate, but the general consensus is that magma mixing was involved in its evolution (von Gruenewaldt *et al.*, 1985). Cawthorn and Walraven (1997) maintained that the mafic layered rocks are the product of multiple magmatic injections, some of which are comparable to previous magmas, and others which are of a different composition.

The Rustenberg Layered Suite forms the lowermost unit of the Bushveld Complex and is subdivided into four stratigraphic units, from the base upwards, the Lower, Critical, Main and Upper Zones (von Gruenewaldt, 1973).

The Lower Zone is composed of a layered sequence of harzburgite to orthopyroxenite cyclic units (Teigler, 1990 in Kruger, 1994). The Lower Critical Zone is characterised by orthopyroxenite with lesser harzburgite and the Upper Critical Zone by orthopyroxenite, norite, and anorthosite (Teigler, 1990 in Kruger, 1994). The Critical Zone is characterised by major chromite layers. Cawthorn and Walraven (1997) have modelled the formation of

the Lower and Critical Zones in terms of six magma pulses, each one kilometre thick which underwent 20% differentiation prior to the addition of the next pulse. The calculations of Cawthorn and Walraven (1997) show that the entire Lower and Critical Zones accumulated in about 25 000 years.

The lower Main Zone consists of chromite deficient norites and in the upper part of this zone, gabbronorite becomes the dominant rock type. The Upper Main Zone is chemically differentiated and consists of homogeneous gabbronorite. The base of the Upper Zone is referred to as the 'Pyroxenite Marker', and this is followed by a highly differentiated sequence of norite, gabbronorite, ferrogabbronorite, and ferrodiorite interlayered with numerous layers of anorthosite, ferrodunite, titaniferous magnetite and apatite (Kruger, 1994).

Cawthorn and Walraven (1997) suggest that addition of 2km of magma occurred at the top of the Critical Zone, and the Lower Main Zone was calculated to have formed in a further 35 000 years. Major addition of magma then occurred at the level of the Pyroxenite Marker, and is considered to be the last injection of magma into the Complex.

***Lebowa Granite Suite***

The Lebowa Granite Suite represents the final stage in the evolution of the Bushveld Complex. In the literature it is commonly described as a "sheet-like intrusion of batholithic dimensions" (von Gruenewaldt, 1979). Strauss (1954) recognised a zonation in the 2-3km thick, gently dipping, sill-like pluton. Subsequent work has shown that the sheet has a variable thickness (~2.5-3.5km), covering an area of at least 30 000km$^2$ and dipping centripetally towards the centre of the Complex at angles less than 10°. The sheet is buckled and exposes inliers of the underlying sedimentary rocks, such as the Marble Hall Fragment (Kleemann and Twist, 1989).

The nomenclature of the Bushveld granites has evolved since the first description of the "Red Bushveld" granite (Molengraaf, 1901). Since then, it has been called the Red Granite (Merensky, 1909), the Bushveld Granite (Hall, 1906) and the Main Granite (Strauss and Truter, 1944; Strauss, 1954). The Main Granite was renamed when detailed mapping elucidated differences between the granite in the eastern and western portions of the

Bushveld Complex, and the local terms Veekraal, Sekhukhuni, Magnet Heights, Steelpoort Park and Verena granites were introduced.

The Bushveld granites were collectively referred to as the Lebowa Granite Suite by Coertze *et al.* (1978), and formed the basis of the SACS (1980) terminology for the Bushveld granites. SACS (1980) recognised seven categories of granite in the Lebowa Granite Suite, namely the Nebo Granite, the Verena Porphyritic Granite, the Klipkloof Granite, the Bobbejaankop Granite, the Lease Granite, the Balmoral Granite, and the Makhutso Granite. Other names, such as the Red Granite, Sekhukuni Granite, Steelpoort Park Granite, Magnet Heights Granite and Veekraal Granite, have been incorporated in the Nebo Granite category, since they are identical in appearance, mineralogy, chemistry and age (Walraven and Hattingh, 1993).

In addition, the Bobbejaankop and Lease Granites, which are local terms for the coarse- and fine-grained granites at the Zaaiplaats Mine, and which have been informally adopted by many geologists in other areas of the Bushveld, have been recognised as varieties of the Nebo Granite (Pollard *et al.*, 1991). Walraven and Hattingh (1993), however, consider the Bobbejaankop, and Lease, as well as a variety of other granites named in the literature (Klipkloof, Foothills and Klipvoor Granites), as differentiates from the Nebo Granite magma. The term Klipkloof Granite has been adopted for the fine-grained aplitic granite which occurs as dykes and sills within the upper portions of the Nebo Granite and in the overlying granophyric roof rocks. Thus, the terms Nebo and Klipkloof Granite have replaced the numerous synonymous terms in the literature.

The Verena Porphyritic Granite differs from the Nebo Granite in that it contains rapakivi-textured feldspar phenocrysts, and the fine-grained equivalent contains atypical trace element chemistry (Walraven and Hattingh, 1993). It is shown in subsequent chapters that the nature of this granite is completely different to the Nebo Granite and justly deserves a category of its own. The Makhutso Granite is younger than the Nebo and Klipkloof Granites and is placed in a separate category. Thus, the Lebowa Granite Suite is currently composed of the Nebo Granite, the Klipkloof Granite and the Makhutso Granite. The position of the Verena Porphyritic Granite and the Balmoral granite is yet to be determined.

*Nebo Granite*

The Nebo Granite forms the bulk of the granite of the Lebowa Granite Suite. It is a coarse-grained, hypersolvus granite which is composed mainly of quartz and perthite, and normally interstitial hydrous mafic phases (biotite). A well developed mineralogical and chemical zonation exists in the Nebo Granite; from the base to the top there is an increasing albite component of the plagioclase, increasing Al/Si ordering in alkali feldspars, increasing quartz and perthite contents, decreasing plagioclase and hornblende contents, increasing Si, K and Rb, and decreasing Fe, Ti, Ca, P, Ba, Sr, and Zr (Kleemann and Twist, 1989).

*Klipkloof Granite*

According to Kleemann and Twist (1989), the Klipkloof Granite is composed of three facies, namely, the Coarse, Fine, and Albitised Klipkloof Granites. These facies are comagmatic and have a similar mineralogy to the Nebo Granite, except that they are more evolved and commonly aplitic. The Klipkloof Granite contains a greater proportion of secondary and hydrothermal phases.

Kleemann and Twist (1989) suggest that the fine-grained Klipkloof is the result of quenching through pressure release, and concomitant volatile loss during incipient fracturing of the cooling body. It forms narrow dykes and sills intruding Nebo and other Klipkloof intrusions and corresponds to the Lease Granite. The coarse-grained Klipkloof is interpreted as forming in the transitional zone between the water saturated (above) and undersaturated (below) zones near the roof of the magma chamber. It represents the hydrothermally altered roof facies of the Nebo Granite and resembles the Bobbejaankop Granite at Zaaiplaats. The albitised Klipkloof is a typical aplite that has been subject to intense Na-silicate metasomatism (Kleemann and Twist, 1989).

The Klipkloof Granite was described by SACS (1980) as a medium- to fine-grained, porphyritic granite which forms dykes and sills in the Nebo Granite, and may also be developed between the Nebo Granite and the country rocks. The SACS (1980) description of the *Lease granite* differs slightly from that of the Klipkloof Granite, and is referred to as a fine-grained aplitic granite characterised by coarse pegmatitic patches. It is typically developed along the margin of the Nebo Granite (SACS, 1980).

The *Bobbejaankop Granite* was described as a coarse-grained, red, biotite granite which may be partially or completely altered, and which appears to be developed in the higher levels of the intrusion.

From the descriptions of the Lease and Klipkloof Granites, it is apparent that quenched marginal Nebo Granite, as well as late stage, aplitic dykes and sills, are currently classified as the same rock type. A distinction between these two modes of occurrence should be made, since detailed petrographical studies (see Chapter 4) have revealed that they are two different granite types. Furthermore, the fine-grained quenched margins of the Verena Porphyritic Granite should be distinguished from true Klipkloof aplite and quenched Nebo Granite.

*Makhutso Granite*

The Makhutso Granite represents the final phase of granitic intrusion in the Bushveld Complex, and occurs as small dykes, stocks and gently dipping sills in the Nebo Granite (SACS, 1980). The rock is white to pink and contains 10 to 15% femic minerals, the dominant mineral being biotite (altered to chlorite) (De Bruiyn, 1980). Trace element geochemistry, particularly K/Rb, Ba/Sr ratios, Ba and Zr values are lower in the Makhutso Granite than in the Nebo Granite. The outcrop is limited to the northern part of the Verena Dome (Figure 2.4). This granite has received very little attention and, hence, reference literature is lacking.

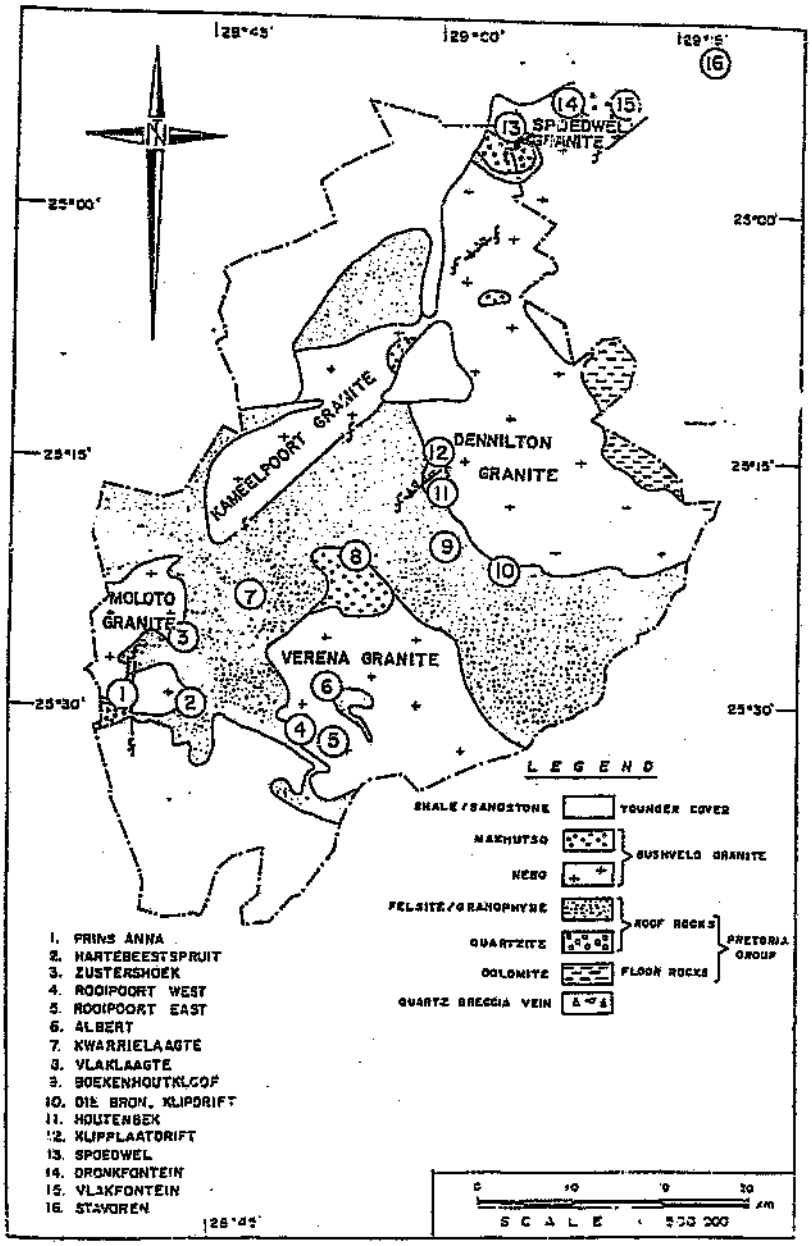


**Figure 2.4** Geological map showing granite plutons in the eastern lobe of the Bushveld Complex, and known mineral occurrences (from Scoggins, 1991).

*GEOCHRONOLOGY*

Age determinations of the various units in the Transvaal Supergroup host rocks, as well as in the Bushveld Complex, have been carried out by several authors. Chronostratigraphic data for the Transvaal Supergroup and Bushveld Complex from various sources are shown in Table 2.1 and Table 2.2, respectively.

**Table 2.1** Age determinations relevant to the Transvaal Supergroup (from Walraven, 1997). Ages in bold print are the best current age estimates according to Walraven (1997).

| Transvaal Supergroup | Age (Ma) | Method (Reference) |
|---|---|---|
| Rhyolite intercalation, Rust de Winter Formation | 2060 | U-Pb, bulk zircon, (Walraven, 1981) |
| Rooiberg Group | | |
| Rhyolite | 2030 ± 50 | Rb-Sr, whole rock (Burger and Coertze, 1973) |
| Rhyolite, Selons River Formation | **2061 ± 2** | Pb-Pb, single zircon (Walraven, 1997) |
| Rhyolite and rhyodacite | 1605 ± 28 | Rb-Sr, whole rock (Walraven, 1987) |
| Rhyolite and rhyodacite | 2003+ 289/-360 | Pb-Pb, whole rock (Walraven, unpublished data) |
| Rooiberg Group | 2018+58/-60 | Pb-Pb, whole rock (Farrow, 1988) |
| Rooikop Granite Porphyry | **2060 ± 2** | Pb-Pb, single zircon (Walraven, 1997) |
| Dullstroom Basalt Formation | 2234 ± 443 | Rb-Sr, whole rock (Walraven, 1987) |
| Dullstroom Basalt Formation | **2101 ± 28** | Various, whole rock (Schweitzer, 1986) |
| Hekpoort Andesite Formation | 2224 ± 21 | Rb-Sr, whole rock (Burger and Coertze, 1973) |
| Pretoria Group | | |
| Timeball Hill Formation | 2208 ± 63 | Rb-Sr, whole rock (Hunter and Hamilton, 1978) |
| Chuniespoort Group | | |
| Oak Tree Formation | 2550 ± 3 | Pb-Pb, Walraven and Martini (in press) |
| Wolkberg Group | | |
| Abel Erasmus Formation | 2138 +46/-47 | Pb-Pb, whole rock (Armstrong, 1987) |
| Godwan Formation | 2325 +69/-73 | Pb-Pb, whole rock (Armstrong, 1987) |

**Table 2.2** Lithostratigraphic subdivisions of the Bushveld Complex according to SACS (1980), and Walraven (1997). Ages in bold print are the best current age estimates according to Walraven (1997).

| BUSHVELD COMPLEX | Radiometric age (Ma) | Method (Reference) |
|---|---|---|
| Lebowa Granite Suite | | |
| Makhutso Granite | 1670 ± 30 | U-Pb, bulk zircon (Coertze *et al.*, 1980) |
| Nebo Granite | 1920± 40 | U-Pb, bulk zircon (Coertze *et al.*, 1980) |
| | **2054 ± 2** | Pb-Pb, single zircon (Walraven and Hattingh, 1993) |
| Rashoop Granophyre Suite | 2090 ± 40 | U-Pb, bulk zircon (Faurie, 1977) |
| Stavoren Granophyre | **2053 ± 12** | U-Pb, bulk zircon (Coertze *et al.*, 1978) |
| Rooikop Granophyre (Granite) Porphyry | 2066 ± 10 | U-Pb, bulk zircon (Faurie,1977) |
| Rooikop Granite Porphyry | 2060 ± 2 | Pb-Pb, single zircon (Walraven, 1997) |
| Rustenberg Layered Suite | 2095 ± 24 | Rb-Sr, Hamilton, 1977 |
| Lower Zone | 2049 ± 152 | Sm-Nd, (M.R. Sharpe |
| Critical Zone | 2054 ± 32 | Rb-Sr, unpublished data in |
| Main Zone | 2058 ± 155 | Sm-Nd, von Gruenewaldt *et* |
| Upper Zone | 2057 ± 24 | Rb-Sr, *al.*, 1985) |
| Upper Zone | **2061 ± 27** | Rb-Sr, single zircon (Walraven *et al.*, 1990) |

Age determinations of the Transvaal basin have shown that the formation of the basin, beginning with the deposition of sediments at 2643 ± 2 (Walraven *et al.*, in press) and ending with the volcanism which produced the Dullstroom basalts and Rooiberg felsites at 2061 ± 2 (whole rock, Walraven, 1997), occurred over a time period of 600 m.y.

Recent studies have demonstrated that the base of the Transvaal Supergroup is significantly older than was previously considered (Walraven and Martini, in press; Walraven *et al.*, in press). Walraven (1997) has produced the first precise and reliable age determinations for the upper part of the Transvaal Supergroup, showing that the Rooiberg volcanism and the emplacement of the Rustenberg Layered Suite and Lebowa Granite Suite of the Bushveld Complex, occurred in a time span of only 7 million years.

Three important points emerge from the age determinations of Walraven (1997) for the Rooiberg Group and the Rooikop Granite Porphyry, when compared with existing data for the Bushveld Complex. Firstly, the similarity of ages implies that the Rooikop Granite Porphyry was intruded almost immediately after, or even contemporaneously with, the later stages of the extrusion of the Rooiberg Group. Secondly, the best current ages for the Bushveld Complex, Rooiberg Group and related rocks are indistinguishable, and thirdly, the data show that the duration of magmatic activity of the Rooiberg Group and the Bushveld Complex did not exceed 7 million years.

**Rashoop Granophyre Suite**

Ages for the Rashoop granophyre were determined by Faurie and von Gruenewaldt (1979) as 2000 ± 30 Ma using the U-Pb isotopic system. Ages for the Stavoren granophyre of 2084 ± 62 Ma (Walraven *et al.*, 1981) have been published, but, according to Walraven (1997), the only reliable ages are from U-Pb zircon determinations which indicate an age of 2053 ± 12 (Coertze *et al.*, 1978). Whole-rock Pb-Pb isochron ages for the Rashoop granophyre in the Zaaiplaats area show a relatively restricted range from 961±129 Ma (Mc Naughton *et al.*, 1993) and represents a reset age (or final closure age).

**Rustenberg Layered Suite**

The emplacement of the Rustenberg Layered Suite took place at ca. 2050 Ma and the radiogenic isotope systems closed immediately (McNaughton *et al.*, 1993). The rocks of the Lower Zone have been dated at 2049±152 Ma (Sm/Nd), the Critical Zone at 2054±32 Ma (Rb/Sr), the Main Zone at 2058±155 Ma (Sm/Nd) and the Upper Zone at 2057±24 Ma (Rb/Sr) (M.R. Sharpe unpublished data in von Gruenewaldt *et al.*, 1985).

**Lebowa Granite Suite**

The available age determinations for the various components of the Lebowa Granite suite are shown in Table 2.3. The table includes data from the compilation by Walraven and Hattingh (1993) of geochronological data on the Nebo and related variants, as well as data from the Zaaiplaats Tin Mine (Mc Naughton *et al.*, 1993) and Albert Silver Mine (Robb *et al.*, 1994).

**Table 2.3** Compilation of existing geochronological data for the Lebowa Granite Suite.

| Rock Unit | Date (Ma) | Method and material | Reference | Comment |
|---|---|---|---|---|
| **Makhutso Granite**, eastern Bushveld Complex | 1645+64-59 | U-Pb zircon | Coertze *et al.* (1978) | Severely discordant zircons |
| **Makhutso Granite**, eastern Bushveld Complex | 2046 ± 55 | Rb-Sr whole rock | Walraven (1988) | Minimum age limit for Bushveld Complex Granites |
| **Makhutso Granite**, eastern Bushveld Complex | 2049+69-72 | Pb-Pb whole rock | Walraven (1988) | Minimum age limit for Bushveld Complex Granites |
| **Makhutso Granite**, eastern Bushveld Complex | 2045+122-133 | Pb-Pb whole rock | Walraven (1988) | Minimum age limit for Bushveld Complex Granites |
| **Klipkloof Granite**, eastern Bushveld Complex | 1531+157-142 | U-Pb zircon | Coertze *et al.* (1978) | Data are severely discordant, date is much too low |
| **Klipkloof Granite**, eastern Bushveld Complex | 2065±70 | Rb-Sr biotite | Walraven (1987a) | Uncertainty on initial ratio too large to be meaningful |
| **Klipkloof Granite**, eastern Bushveld Complex | 1788 ± 112 | Rb-Sr whole rock | Walraven (1987a) | Uncertainty on initial ratio too large to be meaningful |
| **Klipkloof Granite**, eastern Bushveld Complex | 2038+170-192 | Pb-Pb whole rock | Unpubl. Data of Walraven | |
| **Nebo Granite**, Bushveld Complex | 1904 ± 243 | Rb-Sr whole rock, feldspar, biotite | Schreiner (1958) | Within uncertainty of accepted age |
| **Nebo Granite**, Bushveld Complex | 1791 to 2055 | Rb-Sr model date on mica | Nicolaysen *et al.*(1958) | Highest date from Rustenberg Plats; lower dates from various Nebo Granite samples |
| **Nebo Granite**, central Bushveld Complex | 1982+246-81 | U-Pb monazite | Nicolaysen *et al.*(1958) | Within uncertainty of accepted age |
| **Nebo Granite**, central and eastern Bushveld Complex | 1993+90-78 | U-Pb monazite, zircon | Nicolaysen *et al.* (1958) | Within uncertainty of accepted age |

**Table 2.3 continued** Compilation of existing geochronological data for the Lebowa Granite Suite.

| Rock Unit | Date (Ma) | Method and material | Reference | Comment |
|---|---|---|---|---|
| Nebo Granite, Bushveld Complex | 1955+37-36 | U-Pb monazite, zircon | Burger *et al* (1967) | |
| Nebo Granite, Bushveld Complex | 1915 ± 18 | Pb-Pb monazite, zircon, feldspar, apatite | Burger *et al.* (1967) | |
| Nebo Granite, western Bushveld Complex | 1946 ± 45 | Rb-Sr whole rock | Davies *et al.* (1970) | |
| Granite, Bushveld Complex | 1871 ± 102 | Rb-Sr whole rock | Hunter & Hamilton (1978) | Isotopic disturbance results in low date |
| Nebo Granite, eastern Bushveld Complex | 2050+51-49 | U-Pb zircon | Faurie (1977) | |
| Nebo Granite, various parts of Bushveld Complex | 1948+42-39 | U-Pb zircon | Coertze *et al.* (1978) | Data are discordant, date is lower than accepted age |
| Nebo Granite, Bushveld Complex | 2052 ± 48 | U-Pb zircon | Walraven *et al.* (1981) | |
| Nebo Granite, eastern Bushveld Complex | 1982 ± 63 | Rb-Sr biotite | Walraven *et al.* (1985) | Within uncertainty of accepted age |
| Nebo Granite, eastern Bushveld Complex | 1779 ± 102 | Rb-Sr whole rock | Walraven *et al.* (1985) | Date too low compared to accepted age |
| Nebo Granite, Fairfield, NE of Pretoria | 1905 ±186 | Rb-Sr whole rock | Walraven (1987b) | Low but within uncertainty of accepted age |
| Nebo Granite, Fairfield, NE of Pretoria | 2037 ± 92 | Rb-Sr whole rock | Walraven (1987b) | Date obtained by regression of magnetite gabbro together with Nebo Granite |
| Nebo Granite, Fairfield, NE of Pretoria | 1842+350-397 | Pb-Pb whole rock | Walraven (1987b) | |
| Nebo Granite, Bushveld Complex, area NW of Potgietersrus | 1990 ± 9 | U-Pb zircon | Walraven *et al.* (1987b) | |
| Nebo Granite, eastern Bushveld Complex | 2082+80-85 | Pb-Pb whole rock | Unpublished data Walraven | Within uncertainty of accepted age |

**Table 2.3 continued** Compilation of existing geochronological data for the Lebowa Granite Suite.

| Rock Unit | Date (Ma) | Method and material | Reference | Comment |
|---|---|---|---|---|
| Nebo Granite, Veekraal, western Bushveld | 1857±328 | Rb-Sr whole rock | Unpublished data of Walraven | Low date but very large uncertainty; indicative of isotopic disturbance |
| Nebo Granite, Veekraal, western Bushveld | 2171+105-113 | Pb-Pb whole rock | Unpublished data of Walraven | Outside uncertainty limits of accepted age; indicative of isotopic disturbance |
| Bobbekaankop Granite from area nothwest of Potgietersrus | 2074+9.9-9.4 | U-Pb cassiterite | Gulson and Jones (1992) | Interpretation problematical |
| Nebo Granite dyke from area nordwest of Potgietersrus | 2054±1.8 | Pb-evaporation zircon | Walraven and Hattingh (1993) | Accepted age of Nebo Granite |
| Verena Porphyritic Granite, Albert Silver Mine, Bushveld Complex | 2050 | Pb-Pb whole rock | Robb *et al.* (1994) | Unaltered coarse-grained porphyritic granite |
| Verena Porphyritic Granite, Albert Silver Mine, Bushveld Complex | 500 | Pb-Pb whole rock | Robb *et al.*(1994) | Altered samples associated with mineralisation |
| Verena Porphyritic Granite, Albert Silver Mine, Bushveld Complex | 2050 | Rb-Sr whole rock | Robb *et al.* (1994) | Unaltered coarse-grained porphyritic granite |
| Verena Porphyritic Granite, Albert Silver Mine, Bushveld Complex | 1672 | Pb-Pb galena | Robb *et al.* (1994) | Galena from quartz sulphide vein in phyllic alteration zone |
| Verena Porphyritic Granite, Albert Silver Mine, Bushveld Complex | 1574 | Pb-Pb galena | Robb *et al.* (1994) | Galena from quartz sulphide vein in phyllic alteration zone |
| Verena Porphyritic Granite, Albert Silver Mine, Bushveld Complex | 400 | Pb-Pb galena | Robb *et al.* (1994) | Galena from propyllitic altered zone comprising late vuggy fluorite, galena and carbonate |

**Table 2.3 continued** Compilation of existing geochronological data for the Lebowa Granite Suite.

| Rock Unit | Date (Ma) | Method and material | Reference | Comment |
|---|---|---|---|---|
| **Lease Granite, Zaaiplaats** | 1033 ± 71 | | McNaughton *et al.* (1993) | All data |
| **Lease Granite, Zaaiplaats** | 1187 ± 51 | Pb-Pb whole rock | McNaughton *et al* (1993) | Least altered samples |
| **Lease Granite, Lenticular orebody, Zaaiplaats** | 1101 ± 51 | Pb-Pb whole rock | McNaughton *et al.* (1993) | Towards low grade orebody with altered samples omitted |
| **Lease Granite, Lenticular orebody, Zaaiplaats** | 1166 ± 52 | Pb-Pb whole rock | McNaughton *et al.* (1993) | Towards low grade orebody with altered samples included |
| **Rashoop Granophyre, Zaaiplaats** | 961 ± 129 | Pb-Pb whole rock | McNaughton *et al.* (1993) | |

The ages shown in Table 2.3 for various units of the Lebowa Granite Suite suggest that isotopic exchange was active for approximately 1000 m.y. after emplacement of the magma. Mc Naughton *et al.* (1993) found that samples from the Bobbejaankop Granite, Lease Granite and Rashoop Granophyre consistently record an event approximately 1b.y. after the emplacement of the granites, and that Pb isotope modelling indicates that each suite evolved independently between 2050 and ca. 1100 Ma.

The age of the Nebo has been narrowed down from 2050 Ma to 2054.4 ± 1.8 Ma using conventional zircon Pb-Pb dating of a Nebo dyke. Ages younger than 2054 Ma are interpreted as reflecting disturbance of the isotopic systems on which the determinations are based by post-crystallisation processes (Walraven and Hattingh, 1993). For example, the selective removal of radiogenic Sr from K-feldspar by late stage magmatic or hydrothermal fluids, affects the Rb-Sr isotopic system, and results in isochrons younger than the emplacement age being obtained (Walraven, 1990). Such disturbances in radiogenic isotope systems have been recognised at Zaaiplaats Tin and Albert Silver Mines. At Zaaiplaats, an event at approximately 1100 Ma caused closure of the U-Pb systems and is interpreted to

represent a blocking temperature age related to uplift and cooling of a long-lived hydrothermal system and precipitation of the late stage minerals (galena) at 200°C to 300°C (McNaughton *et al.*, 1993).

In a similar study at Albert Silver Mine, Robb *et al.* (1994) found that two episodes of isotopic disturbance are recorded in the Verena Porphyritic Granite hosting the deposit, in the veins associated with sulphide precipitation, and in the late stage vuggy fluorite. The late stage fluorite is considerably younger (400 Ma) than the samples containing suphides (1672 Ma and 1574 Ma), which in turn is considerably younger than the unaltered host granite (2050 Ma). Robb *et al.* (1994) suggested that the data could be interpreted to reflect the ages of two discrete mineralisation events, the older age (1600Ma to 1700Ma) corresponding to the age of late-stage processes affecting the Bushveld granites, while the younger age (400 Ma) would imply a later unrelated event.

***GENETIC MODEL FOR THE EVOLUTION OF THE BUSHVELD COMPLEX***

The relationships between the units of the Bushveld Complex and the sedimentary and volcanic components of the Transvaal Supergroup have been elucidated by the geochronological studies reviewed above, and, together, a model for the evolution of the Bushveld Complex has developed.

According to Walraven (1997), the Bushveld Complex developed as follows: The volcanic rocks of the Dullstroom Formation and the Rooiberg Group were intruded after the deposition of the Pretoria Group sediments (Transvaal Supergroup). Initially this volcanism was bimodal and areally restricted to the south-eastern Transvaal basin (the Dullstroom Formation), but soon became acid and, after extrusion of the Damwal Formation, extended across the entire Transvaal basin. The Rashoop Granophyre Suite was emplaced near the end of, or immediately after, the Rooiberg volcanism. The first of the Bushveld Complex units (Rustenberg Layered Suite) was then emplaced, followed by the Lebowa Granite Suite.

The Lebowa Granite Suite developed as a function of the crystallisation of the granitic magma. The Nebo and Klipkloof Granites are genetically related, and a model for their

origin was proposed by Kleemann (1985). The model suggests that the Nebo Granite was intruded at shallow depth, beneath an impermeable cover sequence of granophyre and Rooiberg Felsite. Towards the end of the crystallisation history of the Nebo Granite, a late-stage volatile-rich liquid separated, and formed thin sills and dykes referred to as Klipkloof Granite, which occur in the upper portion of the Nebo Granite. It was concluded that the more differentiated sills occurred at higher levels in the Nebo Granite. Late-stage liquids from both the Nebo and Klipkloof Granite intruded into higher levels to form the fine-grained Klipkloof dykes (Kleemann, 1985).

1

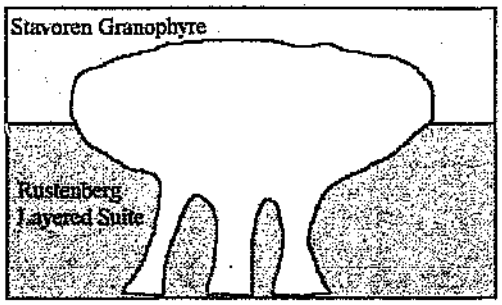


Intrusion of Nebo Granite magma and formation of intrusion breccia.

2

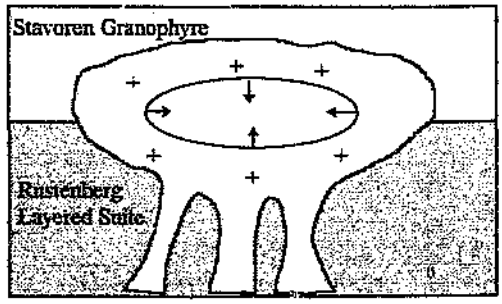


Crystallisation of Nebo Granite magma-hornblende-rich in lower portions and biotite-rich in upper portions of the sheet.

3

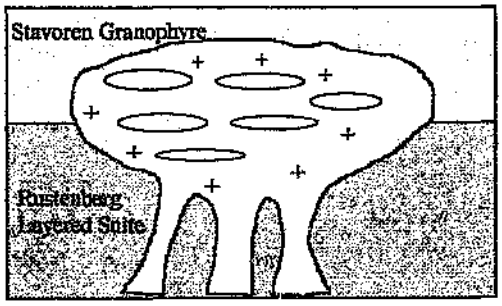


Late-stage volatile-rich rest liquids form the Klipkloof Granite sills in the upper part of the Nebo Granite.

4

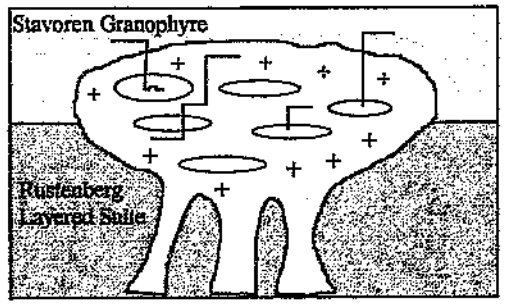


Late-stage aplite dykes are intrusive into Klipkloof Granite sills (stockwork-like) and Nebo Granite.

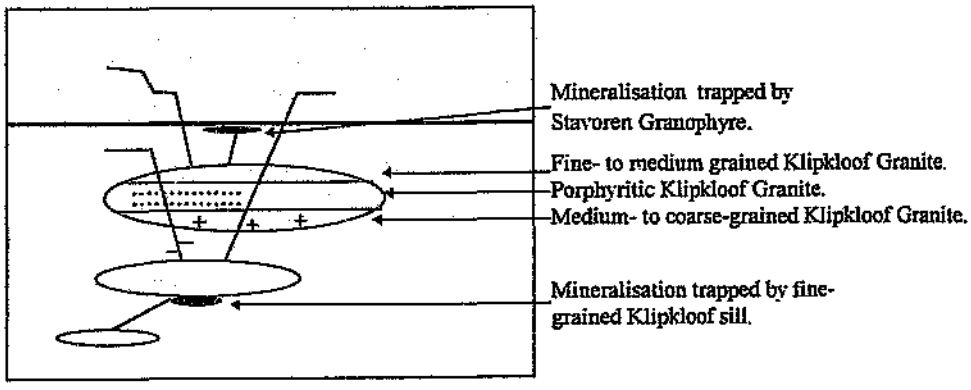


**Figure 2.5** A model for the origin of the Nebo and Klipkloof Granites (redrawn from Kleemann, 1985).

## 2.2. THE GEOLOGY OF THE AREA EAST OF MARBLE HALL - Field mapping area

Geological mapping of the area shown on Figure 2.6 was conducted in order to gain an insight into the field relationships between the Nebo and Klipkloof Granites, and to establish a framework for the barren granites, against which alteration and fluid characteristics associated with mineralisation could be compared.

The area covered by four 1:10 000 orthophoto maps spans approximately 112km$^2$ and includes land on eight farms. The area was chosen for the mapping exercise because of its ideal stratigraphic position in the Lebowa Granite Suite, being in the upper portions of the Complex, where all of the Klipkloof Granite varieties are represented as intrusions within the Nebo host rock. In addition, the area contains major WNW-ENE trending fault systems which extend right across the Bushveld Complex. Of particular importance is that the faults cutting though the mapping area may be traced westwards, and cut across the farms Spoedwel and Dronkfontein where mineralisation is known to occur. The area is approximately 5km south-east of the Boschhoek copper deposit, approximately 40km south of the Grass Valley tin deposit and approximately 50km east of the Spoedwel copper deposit. However, no mineralisation was known to occur in the area, and none was found during the mapping exercise. The area was therefore considered suitable as a standard of unmineralised Nebo and Klipkloof Granite, located sufficiently close to the mineral deposits selected, in order to make meaningful comparisons of fluid characteristics and alteration assemblages.

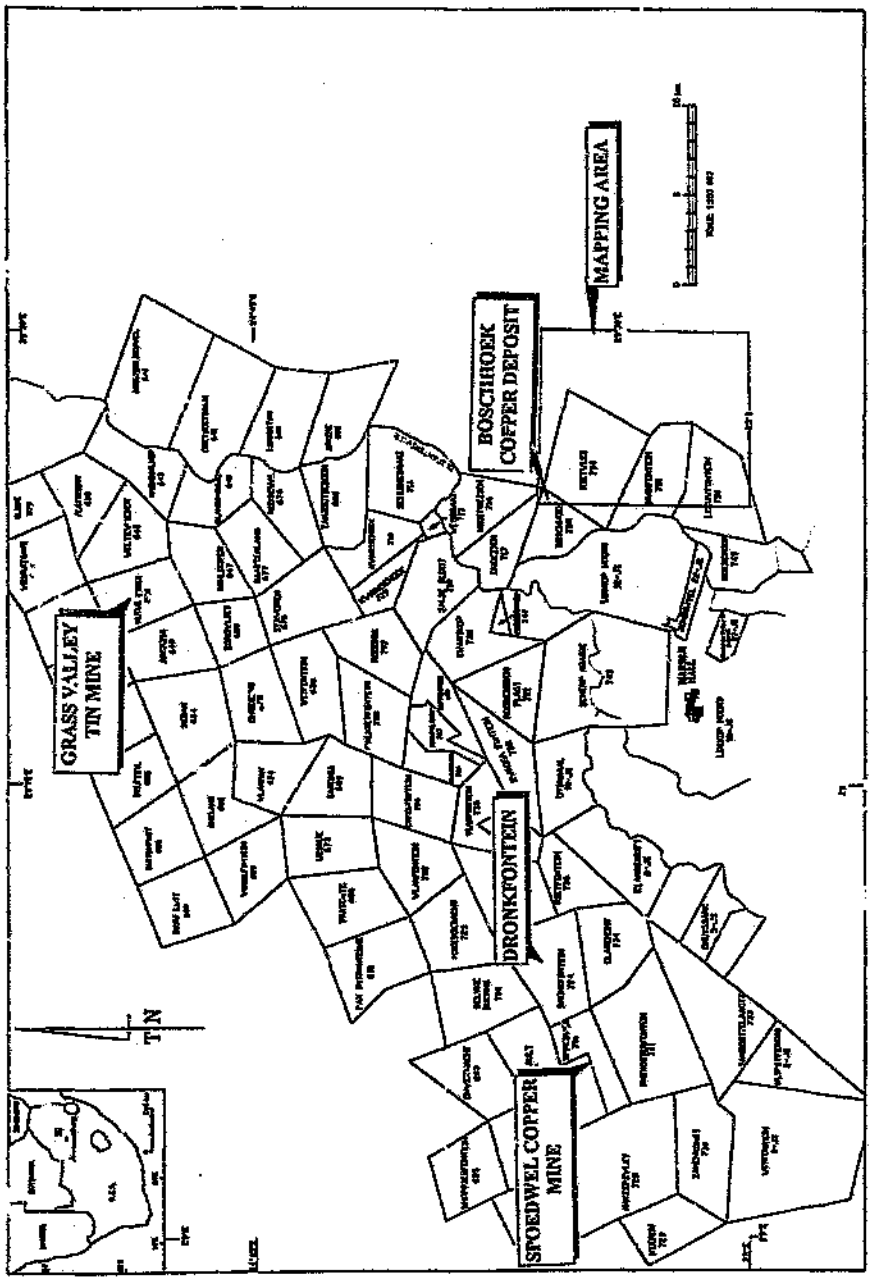


**Figure 2.6** Map indicating location of field mapping area relative to the ore deposits at Grass Valley, Spoedwel, Dronkfontein and Boschhoek.

*LOCAL GEOLOGY*

The geological map of the area marked in Figure 2.6 is shown in Figure 2.7. Each of the rock types indicated on the map are discussed below. The 4 individual 1:10 000 geological maps are to be found in the back pocket.

**The Nebo Granite**

The Nebo Granite is the most abundant rock type in the study area, forming the country rock into which the fine-grained aplitic Klipkloof material is intruded. The appearance of the Nebo Granite varies and three distinct types have been recognised.

- Medium- to coarse-grained equigranular granite, with discrete euhedral crystals of quartz and feldspar. Hornblende occurs as disseminated clusters and makes up 10-15% of the rock composition. The quartz is commonly orange-coloured and the feldspars cream-coloured. Weathered surfaces are cream to orange in colour, with angular feldspar crystals projecting from the surface.

- Coarse-grained to very coarse-grained rock in which the large euhedral to subhedral crystals of white perthite (feldspar) form the bulk of the rock mass. Minor amounts of interstitial quartz and hornblende are present. Localised haematisation of this rock near shear zones produces a deep red discoloration which closely resembles the Bobbejaankop (coarse-grained Klipkloof) Granite. On closer inspection, it is clear that the mafic content is too great for it to be classified as Klipkloof and the characteristic linked quartz chains which stand proud of weathered surfaces are absent. The feldspars of this Nebo variety are more resistant to weathering than those in the coarse-grained Klipkloof Granite.

- A contact facies has been observed where the original Nebo host has been partially invaded by fine-grained Klipkloof Granite. The majority of the rock is composed of medium- to coarse-grained quartz and feldspar crystals, but small amounts of fine-grained material occurs interstitially. This rock type occurs in shear zones and along contacts between typical fine-grained and porphyritic Klipkloof Granite and the Nebo host.

**Figure 2.7** Geological map of the field mapping area east of Marble Hall (see fold out overleaf).

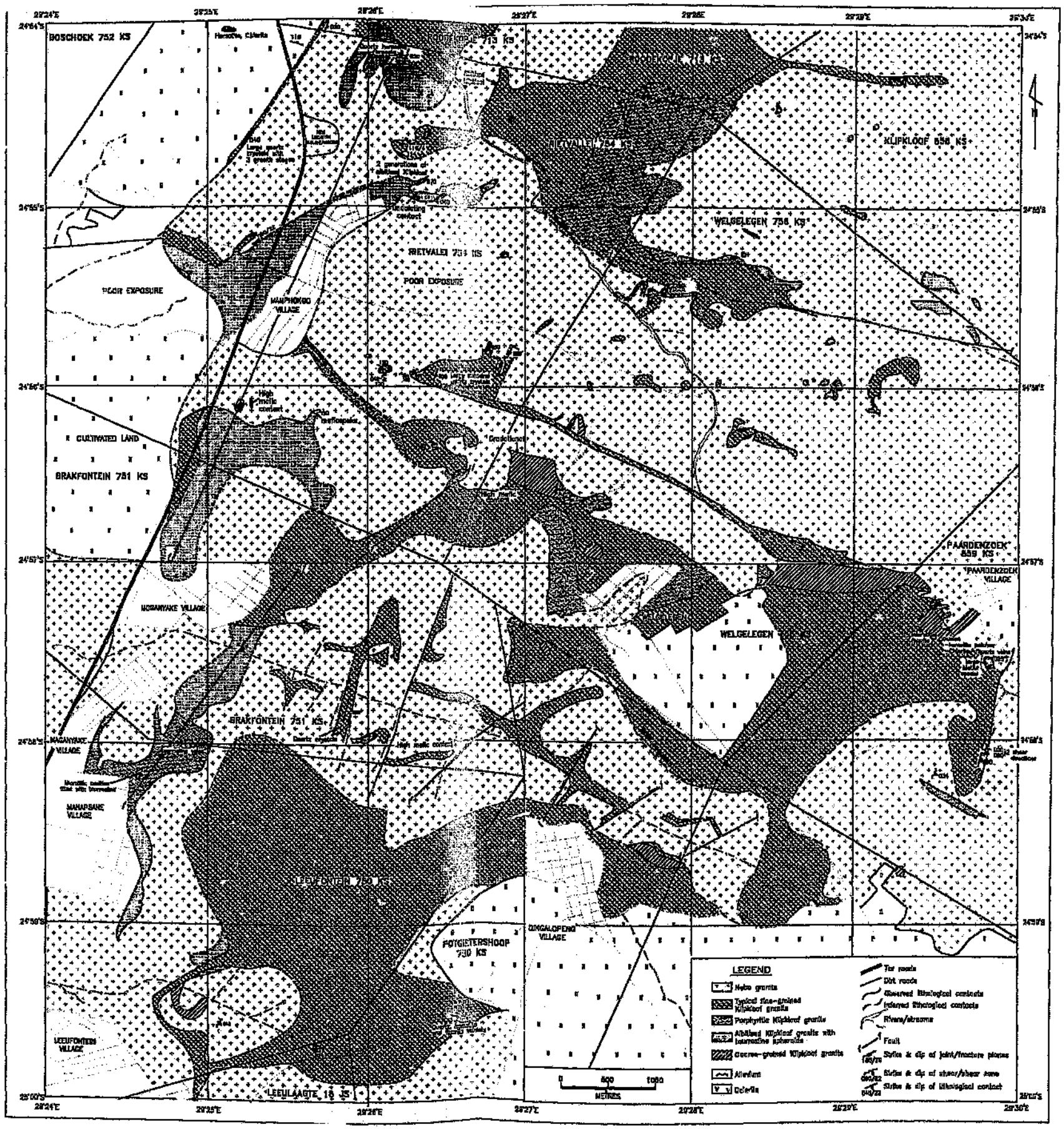
BOSCHOEK 752 KS
RIETVALEI 754 KS
KLIPKLOOF 858 KS
WELGELEGEN 756 KS
POOR EXPOSURE
MAMPHOKGO VILLAGE
CULTIVATED LAND
BRAKFONTEIN 751 KS
PAARDENZOEK 859 KS
PAARDENZOEK VILLAGE
MOSANYANE VILLAGE
WELGELEGEN
MANAPSANE VILLAGE
LEEUFONTEIN VILLAGE
POTGIETERSHOOP 730 KS
DINGALOPENG VILLAGE
LEEULAAGTE 16 JS
LEGEND
Metre
METRES

**The Klipkloof Granite**

***Typical fine-grained Klipkloof Granite***

The fine-grained Klipkloof Granite is relatively abundant in this area, occurring as dykes, sheets and plugs in the Nebo host rock. The grain size is approximately 1mm and a preliminary petrographical investigation indicates that it has subsolvus granite mineralogy i.e. plagioclase, K-feldspar and quartz, as opposed to the hypersolvus mineralogy (no primary plagioclase) of the Nebo and Bobbejaankop Granites.

Evidence for at least two generations of fine-grained Klipkloof Granite exists in the study area. Cross-cutting relationships have been observed, where the earlier dykes, sills and plugs have been intruded by a younger generation of fine-grained material. The second generation material is commonly slightly coarser-grained, and forms narrow veins and dykes composed of quartz, feldspar and, rarely, tourmaline.

***Porphyritic Klipkloof Granite***

This facies has been described as the contact facies between partially consolidated Nebo Granite and the typical fine-grained Klipkloof Granite (Kleemann and Twist, 1989). This relationship has been observed in some instances, but not all. A broad band of porphyritic granite trending roughly east-west on the farm Welgelegen 756KS is a good example, illustrating the intermediate position of the porphyritic Klipkloof Granite between the fine-grained Klipkloof and the Nebo Granite. However, several other instances where there is no porphyritic contact facies between the fine- and coarse-grained granites, have been observed.

Three types of porphyritic Klipkloof material have been observed. Types a) and b) are associated with Nebo Granite while c) is associated with Bobbejaankop Granite.

a) Large (2-4mm) disseminated, euhedral feldspar phenocrysts/xenocrysts in a fine-grained matrix. Quartz phenocrysts are minor or absent. This type of porphyritic granite is distinctive in outcrop, forming medium sized, rounded and smooth surfaced boulders that are relatively resistant to weathering. Two areas where significant amounts of this rock type are exposed are on the farms Rietvalei and Welgelegen.

b) Medium-sized (>2mm), rounded phenocrysts/xenocrysts of both feldspar and quartz occur in a fine-grained matrix that is commonly hematitised and chloritised. The outcrop is less distinctive and can easily be mistaken for typical fine-grained Klipkloof granite, since they both weather to small, angular fragments.

c) A single instance of this rock type was recognised where Bobbejaankop Granite (coarse-grained Klipkloof) was intruded by fine-grained Klipkloof granite. An intermediate rock type was produced which is deep red in colour, with red feldspars and rounded quartz blebs in a matrix of fine-grained granite. It is worth noting that the lack of mafic minerals in the Bobbejaankop Granite (coarse-grained Klipkloof) is inherited by this contact facies and no chloritisation of hornblende xenocrysts (inherited crystals) is observed.

***Albitised Klipkloof Granite***

This facies is an altered version of the typical fine-grained Klipkloof granite, and hosts tourmaline balls (Figure 2.8). The appearance of the rock varies depending on the extent of albitisation. In highly albitised zones, the rock is white in colour with a sugary texture and disseminated specks of a platey, mafic mineral, which has been identified as biotite. The size and abundance of mafic specks varies from small, barely visible particles to medium (>2mm) sized grains. Isolated occurrences of a fine-grained Klipkloof Granite with between 50-60% of disseminated tourmaline have been observed in association with tourmaline-bearing, albitised plugs of Klipkloof Granite.

A second generation of fine-grained Klipkloof aplite which contains crystalline tourmaline blebs along the central portion of the veins, cross-cuts the earlier formed fine-grained granite which bears the tourmaline spheroids. On careful inspection, it appears that the tourmaline spheroids are most abundant adjacent to the secondary aplite veins. This suggests that the tourmalinisation and albitisation of the fine-grained Klipkloof granite is a secondary overprint resulting from the action of fluids introduced with the second pulse of aplitic material. Pneumatolytic fluids containing boron (and fluorine and chlorine), percolated through the Klipkloof Granite wall rock precipitating tourmaline in miarolitic cavities, in veinlets and as spheroids of tourmaline intergrown with albite and quartz.

**Figure 2.8** Photograph of a tourmaline spheroid in albitised Klipkloof Granite at Leeufontein.

A second and more common mode of occurrence of the tourmaline balls/spheroids is within the upper 1 to 2 meters of fine-grained Klipkloof Granite, beneath the contact with the overlaying Nebo Granite. No secondary aplite dykes are in evidence and is seems possible that the pneumatolytic fluids collected beneath the consolidated Nebo Granite, inducing localised albitisation and tourmalinisation of the original fine-grained Klipkloof Granite. The mechanism which caused the formation of the tourmaline balls at this position has not yet been unravelled and further work in this field is necessary.

*Coarse-grained Klipkloof Granite*

The occurrence of this rock type is limited, and appears to form an incomplete ring observed on the farm Dikgalaopeng. Weathered exposures show the characteristic linked quartz chains that are more resistant. The mafic content is less than 5 % in areas where interstitial quartz separates the hematitised perthite crystals. In other cases, the interstitial material is fluorite, and the mafic content is even less. The grain size is fairly uniform, coarse-grained. However, a single instance where medium-grained Bobbejaankop Granite outcrops, was noted.

*STRUCTURE*

The dominant style of structural modification is faulting and associated shearing. Three categories of fault trends have emerged from the data collected. The first category comprises a set of three parallel faults trending 120°. These faults are immediately obvious on the orthophoto map, as deeply incised river valleys or gorges. The flanks of these gorges are extremely steep and show a cross-section of the geology to some depth. It is clear that the intrusive relationships are complex, and that surface mapping alone is insufficient to gain a proper understanding of the structure of the area.

Undulating sills, bifircating dykes and irregular plugs of more than one generation of fine-grained Klipkloof Granite have been intruded into the Nebo host rock. To further complicate matters, secondary faulting at oblique angles to the main fault have been observed. Two sets of parallel faults have been recognised, one set trending 030° and the other set trending 055° to 060°. The displacement along most of these faults is negligible, and where abrupt changes occur, the displacement cannot be measured since the continuing lithologies have either been removed by erosion or occur at some depth beneath the surface. Thus, it is impossible to determine the nature of the fault.

The second and third categories of fault and shear trends trend parallel to the secondary faults described in the first category. These trends reflect regional faults that are radiometrically evident. The one fault trends 040° and the other at 060°, and they are associated with a band of tourmalinised, albitised Klipkloof Granite, prompting the suggestion that the fault may have served as a fluid conduit for hydrothermal fluids.

From the geological relationships (Figure 2.9) it appears that the regional faults occur in zones occupied by fine-grained Klipkloof Granite. This material may be less competent than the Nebo Granite, and, thus, represent zones of weakness. This observation is supported by the weathering characteristics of the different lithologies. The Nebo Granite forms resistant outcrops whereas the fine-grained Klipkloof granite weathers easily, forming valleys and flat laying areas with soil and vegetation cover. An alternative possibility is that the fine-grained Klipkloof granite was preferentially emplaced into fundamental structures that were both pre- and post-Bushveld in activity.

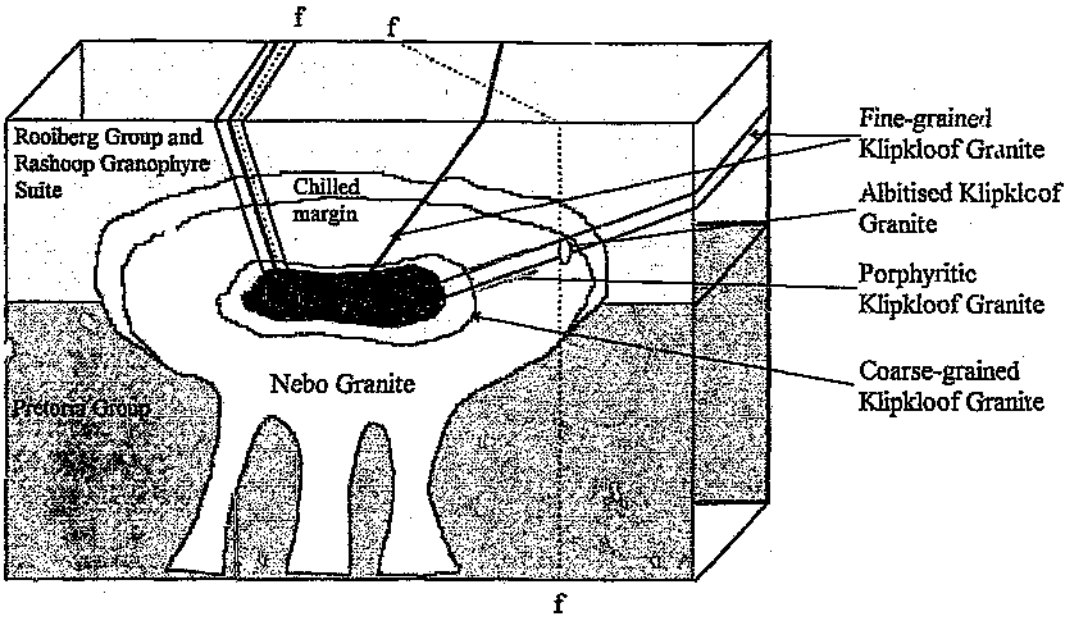


**Figure 2.9** Schematic diagram showing the intrusive relationships between the rock units in the Lebowa Granite Suite.

## 2.3 CONCLUSION

The extended nature of hydrothermal activity in the acid rocks of the Bushveld Complex has been established by numerous geochronological and radiogenic isotope studies. From the time of emplacement of the Nebo Granite magma at 2054 Ma, the radiogenic isotopic systems were exposed to disturbances caused by hydrothermal activity between 1600 Ma and 1700 Ma, as well as at 400 Ma. Ages for the closure of lead isotopic systems vary. At Zaaiplaats in the northern part of the complex, internal exchange of Pb ceased after 1100 Ma, but, at Albert Silver Mine in the south, ages of a disturbance between 400 Ma and 500 Ma were obtained. Thus, hydrothermal activity spanning approximately 1654 m.y. is recorded in the granites of the Bushveld Complex.

The relationship between the coarse-grained Nebo Granite and the various fine-grained varieties of Klipkloof Granite has been attributed to the crystallisation of the granitic magma and volatile enrichment of the residual magma. Geological mapping has revealed that two generations of fine-grained Klipkloof Granite dykes and sills have been intruded into the Nebo Granite, which are markedly different to the fine-grained chilled margins of Nebo Granite. In addition, the porphyritic Klipkloof Granite is often found to occur between the Nebo host rocks and the fine-grained Klipkloof intrusive, and is interpreted as representing portions of the magma chamber which were incompletely crystallised before the injection of the aplitic material. In cases where the porphyritic Klipkloof is absent, and sharp contacts between the Nebo and Klipkloof Granites are observed, it is suspected that the pluton was completely crystallised at the time of aplite injection. In addition, the Klipkloof Granite is often focused along large-scale fractures which extend several hundreds of metres.

# CHAPTER 3

# MINERALISATION IN THE BUSHVELD GRANITES

## 3.1 OVERVIEW

Polymetallic mineralisation in the Bushveld granites has been the subject of research and exploration for many years. However, since the discovery of the Fe oxide-rich Cu-Au±U±REE deposit at Olympic Dam (South Australia), interest in this type of mineralisation has intensified considerably. The deposit is controlled by faults or shear zones, and shows no clear association with the plutons assumed to have generated the fluids. In particular, similarities between the mineralisation at Olympic Dam, and the numerous small deposits in the Bushveld granites, have given direction to exploration efforts in the region.

The Olympic Dam deposit is hosted by the Olympic Dam Breccia Complex, which is within the Roxby Downs Granite. The granite and the breccia complex are coeval with the Gawler Range volcanics-Hiltaba Suite volcano-plutonic association, and all are products of a major middle Proterozoic thermal event on the Gawler craton, South Australia ( Haynes *et al.*, 1995). The Olympic Dam Breccia Complex comprises a large body of fractured, brecciated and hydrothermally altered Roxby Downs Granite, as well as a variety of hematite breccias, and minor tuffs and sedimentary rocks (Haynes *et al.*, 1995). The Roxby Downs Granite is an A-type granite, with high $K_2O$, REE, Zr, Y, U, Th, and F content (Johnson and McCulloch, 1995), which was produced by fractional crystallisation of a quartz-monzonite melt derived from partial melting of a deep-crustal tonalitic source (Creaser, 1989). The granite has been dated at 1588 ± 4 Ma (Creaser and Cooper, 1993).

Three mineral associations have been recognised at Olympic Dam. The early magnetite (± hematite), chlorite, sericite, siderite, and minor pyrite, chalcopyrite and uraninite (association I) is extensively overprinted by hematite, sericite, chalcocite, bornite, pitchblende, barite, fluorite, and chlorite (association II). The paragenetically latest major mineral association consists of hematite, or hematite + granular quartz ± barite (association

III). All three mineral associations display complex overlapping and indistinct boundaries. Rock relations, breccia textures, ore mineral textures, and mineral parageneses provide evidence of repetitive brecciation and mineralisation events, indicating that ore genesis was complex and multistage (Haynes *et al.*,1995).

The model (Figure 3.1) proposed for the mineralisation is one in which mixing of a hotter magmatic, or deeply circulated meteoric water, and a cooler meteoric water resulted in ore genesis. Mineral associations and their zonation, as well as fluid inclusion and isotopic data, provide evidence for the fluid mixing model, fundamental to which, is the presence of suitable fluid conduits (faults and breccias) in the host granite.

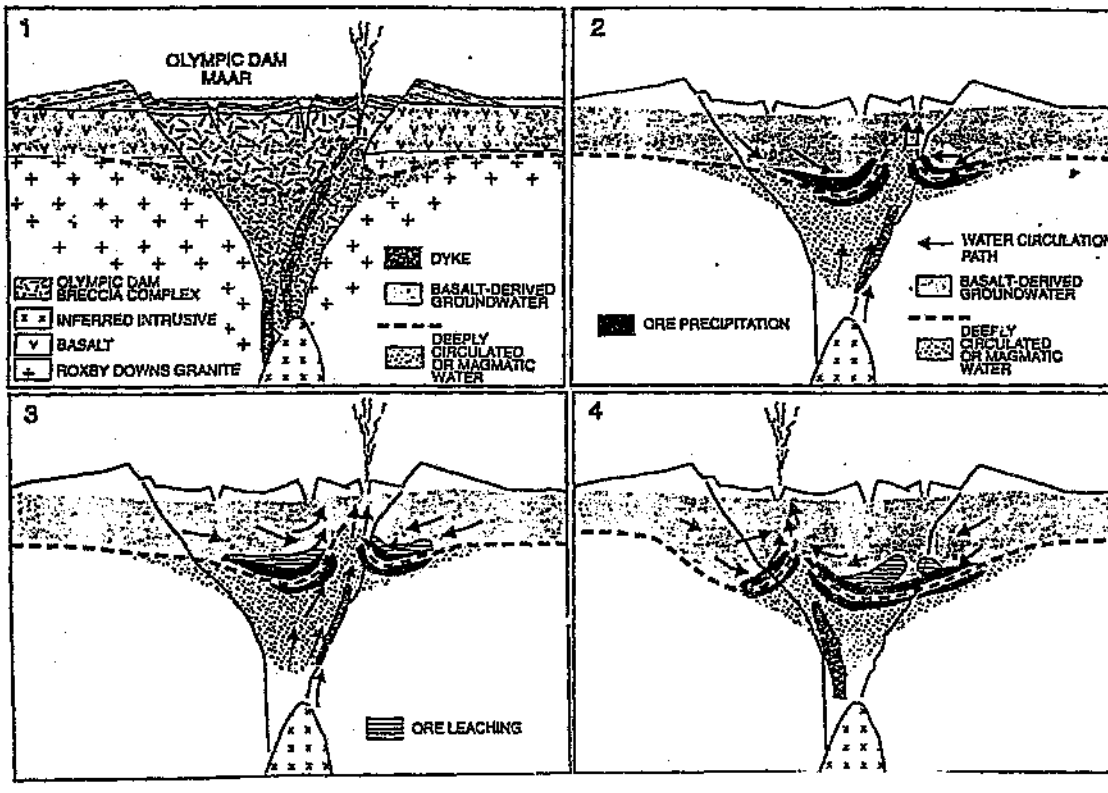


**Figure 3.1** The hypothesised water mixing, ore precipitation and ore leaching scenario in the Olympic Dam Breccia Complex and in the Olympic Dam maar volcano (from Haynes *et al.*, 1995).

In the Bushveld granites, the mineral occurrences appear to be related to the presence of large scale regional faulting, with most sizeable deposits occurring on the flanks of fault systems. A belt of mineralisation has been preserved within a graben (similar to that at Olympic Dam), which is flanked by the Wonderkop and Zebediela fault systems and trends parallel to the Steelpoort fault (see Figure 3.2). A linear fluorine anomaly has been recognised along the southern margin of the graben. The 12 deposits occurring within the graben are shown in Figure 3.3, and include the Prins Anna, Hartebeestspruit, Zustershoek, Rooipoort West, Rooipoort East, Albert, Kwarrielaagte, Vlaklaagte, Boekenhoutkloof, Klipdrift, Houtenbek, and Klipplaatdrift. The northern flank of the graben hosts the Spoedwel, Dronkfontein, Vlakfontein and Stavoren deposits. The deposits associated with the graben comprise predominantly Cu-Pb-Zn-As±Ag±Au deposits, with a later Fe-U-F assemblage becoming more pronounced in the deposits along the southern flank of the graben. Tin mineralisation occurs towards the north and north-west of the complex i.e. Zaaiplaats, Union and Rooiberg. Table 3.1 shows the variation in major ore components the Zaaiplaats and Grass Valley tin deposits, compared with deposits where the Cu-Pb-Zn-As±Ag±Au and Fe-U-F assemblages dominate. It is clear that each of the mineral assemblages are represented at the deposits, but the primary ore minerals vary in accordance with the roughly north-south Sn/ Cu-Pb-Zn-As±Ag±Au/ Fe-U-F zonation mentioned above. Thus, a regional zonation in ore minerals can be recognised in the Bushveld granites.

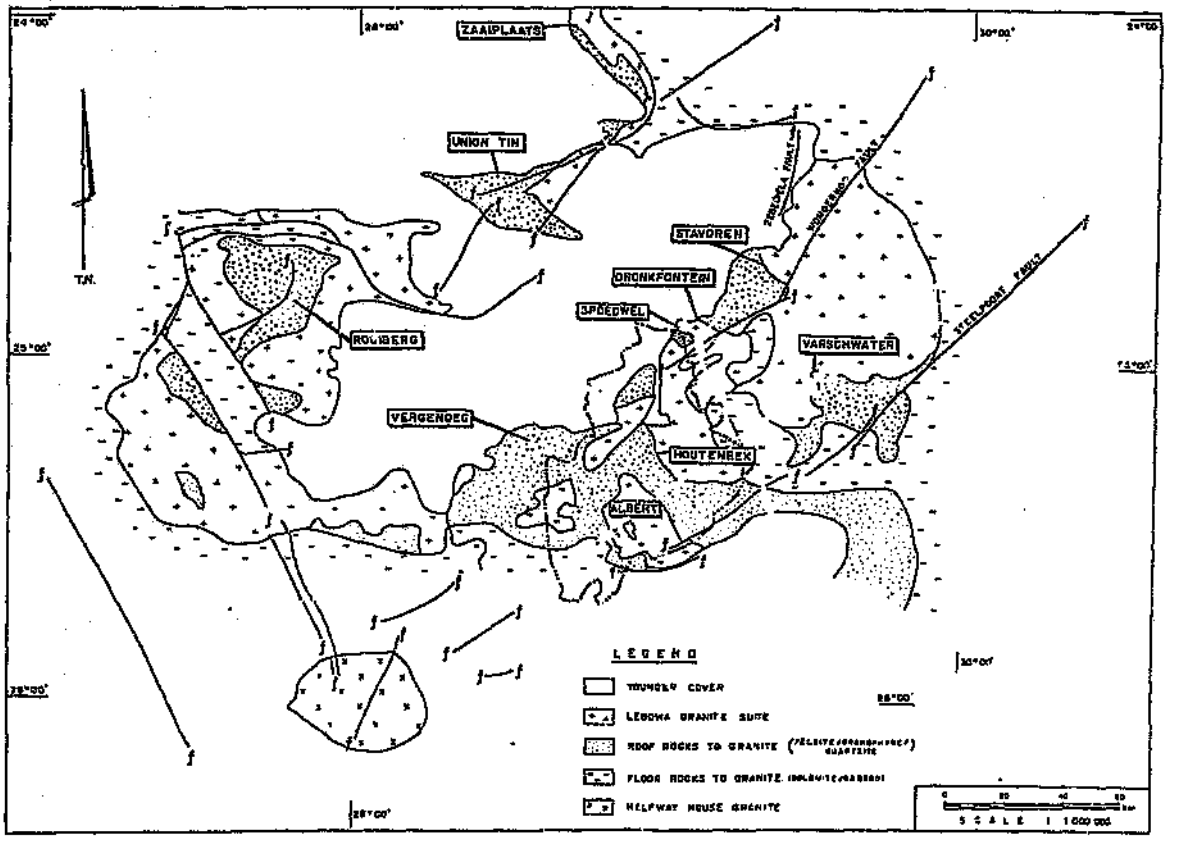


**Figure 3.2** Geological map of the Bushveld Complex showing the major fault systems and the mineral occurrences.

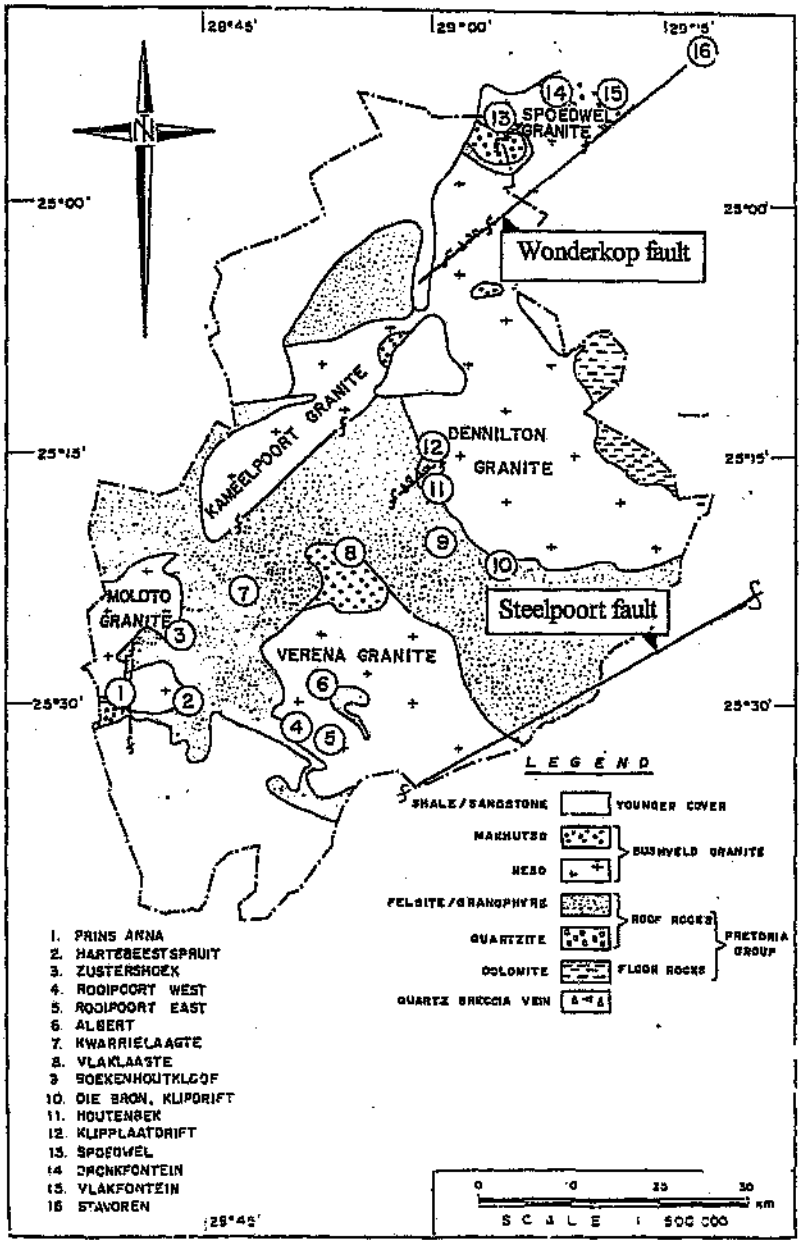


**Figure 3.3** Mineral occurrences associated with the Wonderkop and Steelpoort faults.

**Table 3.1** Mineral occurrences at deposits where tin, sulphides and/or fluorite are present (adapted from Crocker, 1979). (■ major, * common, Δ present, x accessory, • trace, not observed).

| | Zaaiplaats | Grass Valley | Albert | Houtenbek | Vergenoeg |
|---|---|---|---|---|---|
| **Quartz** | ■ | ■ | * | * | Δ |
| **Orthoclase** | ■ | ■ | | Δ | |
| **Tourmaline** | * | * | | x | |
| **Cassiterite** | * | * | | | |
| **Scheelite** | Δ | Δ | | | |
| **Bornite** | • | • | Δ | | • |
| **Chalcocite** | • | • | | | |
| **Chalcopyrite** | • | Δ | Δ | x | • |
| **Pyrite** | ■ | Δ | | x | • |
| **Pyrrhotite** | | | | | |
| **Tennantite** | • | | | | |
| **Tetrahedrite** | • | • | Δ | | |
| **Galena** | • | • | Δ | | |
| **Sphalerite** | • | • | Δ | Δ | • |
| **Arsenopyrite** | Δ | Δ | Δ | Δ | |
| **Molybdenite** | | | | * | |
| **Fluorite** | * | * | x | Δ | ■ |
| **Magnetite** | • | • | * | | ■ |
| **Hematite** | x | x | ■ | | ■ |

In addition to being generally fracture-related, mineralisation tends to be concentrated in the upper portion of the Lebowa Granite Suite (near the roof zone) and may be either endogranitic or exogranitic. Scoggins (1991) suggested that this phenomenon is related to the upward fractionation trend noted within the Lebowa Granite Suite, in which metalliferous fluids have been entrapped below an early chill phase of the granite, or released by hydraulic fracturing of the brittle roof rocks. Figure 3.4 illustrates the positions

of Spoedwel, Dronkfontein, Vlakfontein, Stavoren and Grass Valley, and the A-B section shows the stratigraphic position of the mineralisation at each deposit. The diagram shows that mineralisation is concentrated at the contact between the granite and the overlying granophyric roof rocks, or within the roof rocks themselves.

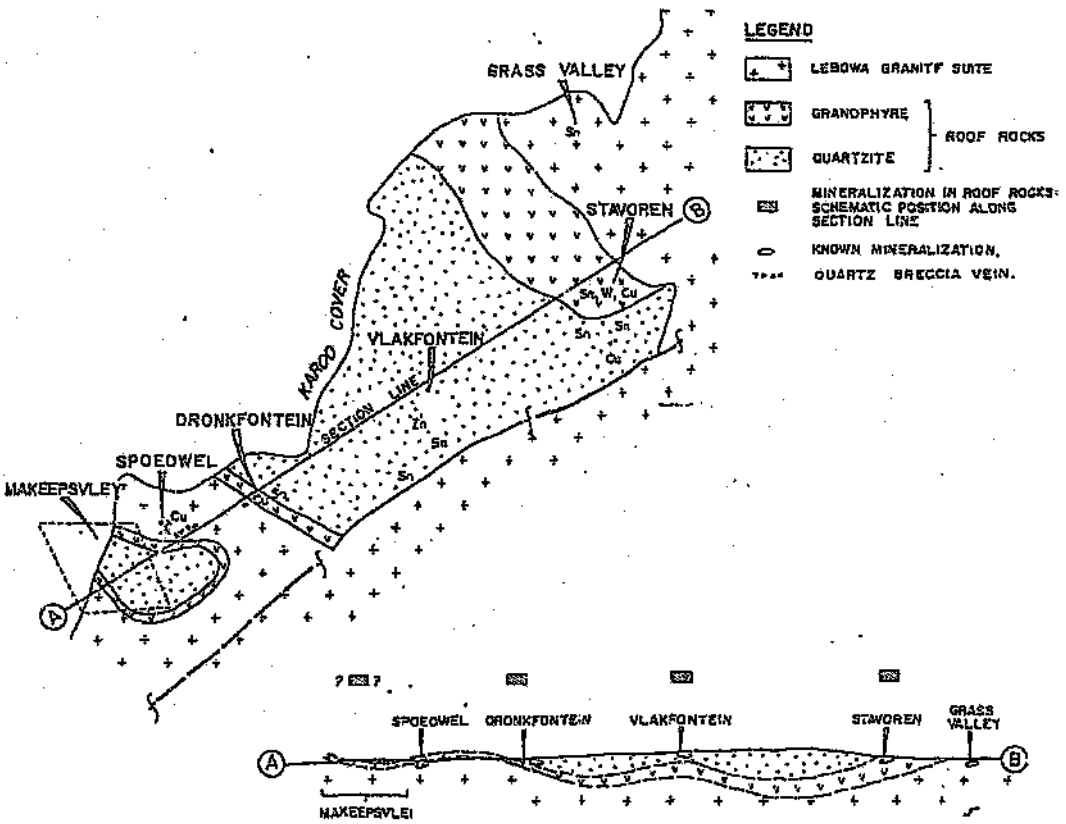


**Figure 3.4** Geological map and cross section A-B showing the stratigraphic position of the mineralisation at Spoedwel, Dronkfontein, Vlakfontein, Stavoren and Grass Valley. Modified from Coggins (1991).

Previous studies on the nature of the mineralisation at well known deposits, such as Zaaiplaats and Albert, have brought to light a number of important points related to the mineralisation in the Bushveld granites, and several attempts to model the ore genesis have been made. Crocker (1979) undertook a regional assessment of the fluorite, tin and associated rare-metal carbonate occurrences, and concluded that centripetal crystallisation of the granite pluton resulted in enrichment of the melt in non-essential residual and volatile constituents, which were released by tensional fracturing of the crystallised peripheral rind. Pneumatolytic-pegmatites developed in the fracture/joint system forming flat manto orebodies. The resulting mineral assemblages consist of either actinolite-fluorite or of magnetite-siderite-fluorite, which became altered to the common hematite-quartz-fluorite assemblage.

The results of a study by Smits (1980) on the Rooibokkop-Boschhoek copper deposit in the Marble Hall area are important, because the model proposed for the mineralisation incorporates the concepts of fluid channelling along fracture zones and subsequent mixing of magmatic and meteoric fluids. Smits (1980) found that the orebody was composed of sulphide-bearing siderite and quartz hydrothermal veins which were emplaced along an existing fracture zone in the Nebo Granite. Recurrent fracturing improved the permeability of the host rock, permitting circulation and mixing of meteoric and magmatic fluid. The veins parallel the Wonderkop Fault, as well as parallel to the mineralised fissures associated with the Stavoren and Grass Valley tin deposits. Smits (1980) recognised three major episodes of fissure formation. The first major episode produced steeply dipping crevasses with a maximum width of 7m, resulting in a composite vein system within the fracture system. The fissures were filled with large siderite crystals, enclosing sparsely disseminated pyrite and pyrrhotite. Two episodes of delayed brittle fracturing of decreasing magnitude followed the major hydrothermal event in response to the gradual release of stress. During the second episode of fracturing, fissures of less than 1m were formed and fluids channelled along the open space were silica-rich. Sulphide mineralisation and quartz veins commonly occur in the hanging wall or foot wall of the siderite veins. The third episode of fracturing occurred towards the end of the sulphide mineralisation, producing an intricate set of micro-fissures.

Smits (1980) established a paragenetic sequence of minerals in this multi-stage hydrothermal system which is related to the three fracturing events described. The paragenetic sequence is as follows:

*Early stage*: 1. Pyrite 1 - pyrrhotite - siderite 1 - quartz 1, pyrrhotite having been replaced by marcasite - pyrite 2 before the introduction of the assemblages in the 2 later stages

*Main Stage*: 2. Pyrite 3 - quartz 2
3. Sulpharsenides - quartz 3
4. Quartz 4 - bismuthinite 1 - galena 1 - sphalerite 1 - chalcopyrite -pyrite 4 - tennantite (assemblage interrupted by quartz 5)
5. bismuthinite 2 - sulphosalts - galena 2 - sphalerite 2 - quartz 6 -

*Late Stage*: 6. Sphalerite 3 - galena 3 - quartz 7
7. Siderite 2
8. Quartz 8

At the surface, the mineralisation displays a zonal distribution: a central elongated copper-rich belt is bordered on both sides by zones in which galena and sphalerite become progressively more abundant. According to Smits (1980), the introduction of meteoric water resulted in the transformation of pyrrhotite into open textured marcasite-pyrite aggregates, and the pervasive sericitisation of the host granite. At a later stage, oxygenated waters of atmospheric origin caused hematitisation of siderite, the replacement of chalcopyrite with bornite, and the chloritisation of the granite between the oxidised veins.

However, not all deposits in the Bushveld granite are fracture-related. For example, the Zaaiplaats tin deposit was formed in the absence of deeply penetrating fractures or the interaction of meteoric fluids. Pollard *et al.* (1991) have shown that primary concentration of Sn occurred by means of crystal fractionation, and that later magmatically-derived fluids further concentrated the Sn into pipe-like orebodies. Pollard *et al.* (1991) maintain that the distribution of disseminated and pipe-style mineralisation at Zaaiplaats reflects a

combination of processes including: 1) early separation of an $H_2O$-NaCl-$CO_2$ fluid enriched in boron to produce pipe-like conduits by collection and upward flow beneath crystallisation fronts, supplemented by later dissolution of granite, 2) accumulation of fluorine-rich fluids evolved at a more advanced stage of crystallisation beneath downward-advancing crystallisation fronts to produce strongly miarolitic zones of Lease Granite containing disseminated cassiterite (low grade), 3) accumulation of fluorine-rich hydrothermal fluids, possibly between upward- and downward- advancing crystallisation fronts to produce the disseminated cassiterite mineralisation zone, and 4) pervasive alteration of the granites accompanied by filling of miarolitic cavities and pipes. The crucial factor in the formation of the Zaaiplaats deposits was the lack of hydraulic or tectonic fracturing during crystallisation (Pollard *et al.*, 1991). According to Crocker (1979), this type of endogranitic deposit forms one end member of the range of mineral occurrences in the Bushveld granites, while the fault-related exogranitic Sn deposit at Rooiberg represents the other extreme.

The Rooiberg tin deposit is hosted by a sedimentary roof pendant of the upper Pretoria Group. Mineralisation occurs along bedding planes within the arkosic layers and as joint- or fracture-related lodes. However, the ore-mineral and alteration parageneses in both styles are identical. The paragenetic sequence is orthoclase-quartz followed by tourmaline-apatite-cassiterite and finally carbonate-chalcopyrite-pyrite (associated with minor galena, sphalerite bismithinite and gersdorffite) (Leube and Stumpfl, 1963). Robb *et al.* (1994) suggest that the Rooiberg mineralisation was derived from an original magmatic fluid that migrated some distance from its granitic source, and that the predominance of Sn in the paragenesis suggests that hydrothermal fluids may have interacted with a zone of primary cassiterite concentrated by progressive crystal fractionation, as at Zaaiplaats.

The concept of fluid mixing playing a role in the mineralisation process in the Bushveld granites was first put forward by Wagner (1921) in a study of mineralisation in the Mutue Fides/Stavoren tin field. Wagner (1921) recognised that the deposits were fracture-related and that the observed alteration features were produced by oxygenated surface waters.

Robb *et al.*, (1994) drafted conceptual models (Figure 3.5) of the mineralisation at Zaaiplaats and Rooiberg, and compared them to a preliminary model for mineralisation in

endogranitic, fracture-related deposits, such as Albert and Spoedwel which contain little or no Sn, and which are dominated by base and precious metals, as well as hematite-specularite, chlorite, uranium and fluorite. The Albert deposit is associated with a subparallel set of gossanous quartz-hematite veins, and consists of pyrite-chalcopyrite-sphalerite-galena-arsenopyrite-argentiferous tennantite which was followed by a chlorite-hematite-pitchblende-fluorite assemblage. The Spoedwel deposit consists chiefly of chalcopyrite and pyrite, with minor amounts of sphalerite, galena, arsenopyrite and fluorite. The mineralisation occurs at the contact between a fine-grained caprock and the underlying coarse-grained granite, and therefore is relatively stratiform. However, plunging pipe-like alteration zones do occur (Robb *et al.*, 1994). The Albert and Spoedwel deposits have been re-examined in this study and are discussed in more detail in section 3.2.

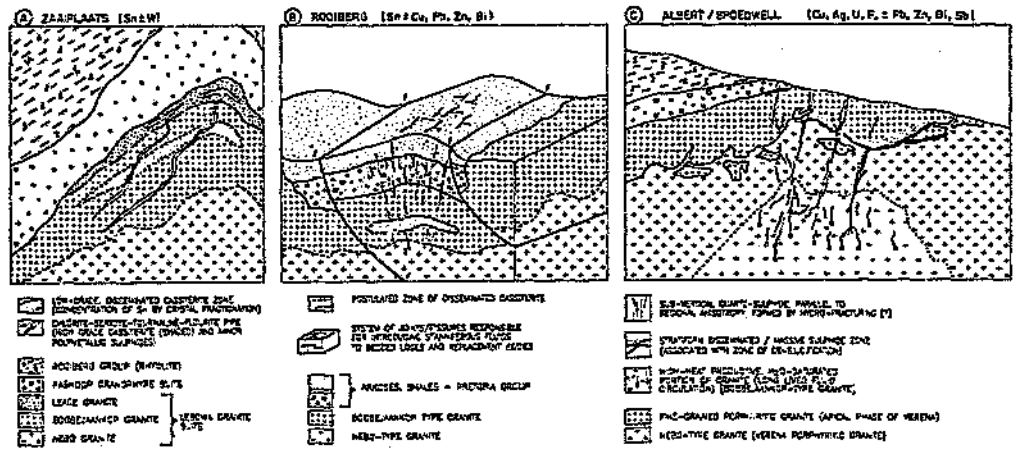


**Figure 3.5** Geological characteristics of the Zaaiplaats-, Rooiberg-, Albert- and Spoedwel- styles of mineralisation in the Bushveld Complex (from Robb *et al.*, 1994).

Hydrothermal fluids play a key role in the formation of the ore deposits in the Bushveld granites. Magmatic fluids, derived from water saturated zones within the crystallising pluton, were convectively circulated for as long as one billion years after crystallisation of the magma (Mc Naughton *et al.*, 1993), during which time, disseminated tin mineralisation, formed by crystal fractionation, was remobilised into pipe-like ore bodies (e.g. Zaaiplaats) (Pollard *et al.*, 1991), and large scale regional fractures formed, which acted as conduits

for the metal-charged magmatic hydrothermal fluids. These fractures served as conduits along which external meteoric or connate fluids were channelled into the pluton, where they interacted with the magmatic hydrothermal fluids, resulting in the deposition of ore minerals (Wagner, 1921; Smits, 1980; Robb *et al.*, 1994) and pervasive alteration of the host granites.

Previous studies on the nature of the fluids associated with granite-hosted mineralisation at Zaaiplaats have indicated a progressive evolution of the magmatic hydrothermal system from >600°C to 200°C, with cassiterite and scheelite precipitation above 400°C (McNaughton *et al.*, 1993). The fluids associated with the precipitation of the sulphide assemblage at Albert are in the range 260°C to 460°C (determined from $T_h$ measurements of fluid inclusions), while those associated with the late stage hematite-fluorite assemblage are approximately 150°C (Robb *et al.*, 1994). Applying a 1.5 kb (depth of formation at Zaaiplaats, Pollard *et al.*, 1991) pressure correction to the low temperature fluids at Albert, elevates the entrapment temperature to approximately 240°C, which compares well with chlorite geothermometry indicating equilibration temperatures of between 260°C and 290°C (Robb *et al.*, 1994). Temperatures of formation suggested by Smits (1980) for the Boschhoek copper deposit were based on features such as the predominance of fracture filling over cavity filling, the type of wall rock alteration and the structural state of pyrrhotite, and point to an upper limit for the emplacement temperature of 300°C.

The characteristics of the fluids associated with tin mineralisation at Zaaiplaats have been extensively studied by Ollila (1981) and Pollard *et al.* (1991), and are discussed in Chapter 5. However, relatively little is known about the fluids associated with the sulphide and hematite-fluorite assemblages. A preliminary study of the fluid associated with mineralisation at the Albert Silver Mine was conducted by Robb *et al.* (1994), in which two fluid populations were found, one with a final melting temperature of -20°C (equivalent to 22wt. % NaCl), and the other with a range of final melting temperatures between -5°C and 0°C ( < 8wt. % e NaCl). These populations correspond with the high and low temperature ranges measured at Albert.

Robb *et al.* (1994) proposed a general model for polymetallic mineralisation in the Bushveld Complex, integrating geochronological and structural aspects, with fluid characteristics from the Zaaiplaats and Albert deposits. This model (Figure 3.6 ) provides the framework within which the present study was conducted. The main objective of the present study was to test and refine the model, if possible, by examining the Albert and Spoedwel deposits in greater detail, and to compare the geology and fluid characteristics at these deposits with the Grass Valley, Houtenbek, and Dronkfontein deposits, as well as with fluids associated with the barren granites in the area east of Marble Hall (see mapping area described in Chapter 2). The history and geology of each of these deposits is presented in section 3.2, providing the foundation upon which the mineral petrography (Chapter 4) and fluid inclusion analysis (Chapters 5, 6 and 7) are built into a comprehensive model for mineralisation.

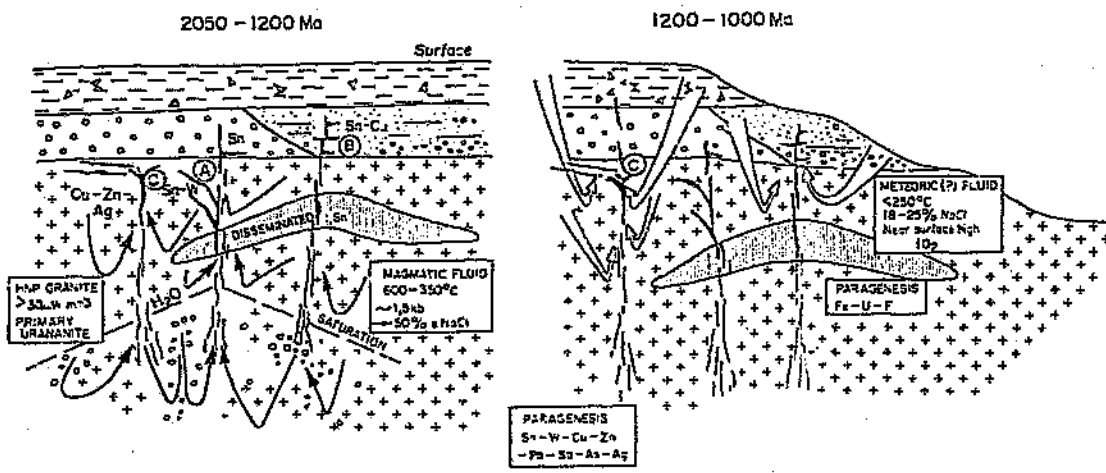


**Figure 3.6** Generalised metallogenic model for polymetallic mineralisation in granites of the Bushveld Complex (from Robb *et al.*, 1994).

## 3.2. LOCALITY DESCRIPTIONS

The five ore deposits chosen for this study, i.e. Grass Valley, Spoedwel, Dronkfontein, Albert, and Houtenbek, are located in the eastern lobe of the Bushveld Complex (Figure 3.7). Spoedwel and Dronkfontein occur on the northern flank of the Wonderkop Fault and are hosted by the Spoedwel granite pluton. Grass Valley is also associated with the Wonderkop Fault, occurring approximately 37km northeast of Spoedwel. Albert and Houtenbek are situated within the graben bound by the Wonderkop and Steelpoort Faults, and occur on the Dennilton and Verena plutons, respectively (refer to Figure 3.3 for map of plutons).

### *GRASS VALLEY*

The Grass Valley tin deposit was discovered in 1912, when prospecting in the area led to the discovery of tin on the farms Mutue Fides No.1844, Stavoren No.1871, Gaasterland No. 1972 and Roodewaal No.1948. The tin deposit on the farm Mutue Fides No. 1844 belonged to the Transvaal Consolidated Land and Exploration Company Ltd., and mining began in 1915. However, the small size and erratic nature of the orebody, the inaccessibility of the deposit, and the lack of water made mining unprofitable and it was abandoned in 1918.

#### Geology

All the deposits in the Mutue Fides/Stavoren tin field are located within a narrow zone trending in a SSE-NNW direction. The deposits are not confined to any particular horizon, and occur within the granite, granophyre and sedimentary roof rocks. The Grass Valley tin deposit is hosted by the Lebowa Granite Suite, and occurs in two modes i.e. associated with pegmatite and within fine granite. The deposits in the granite were classified into tabular replacement veins, irregular replacements or impregnations, pockets, and pipe-like orebodies (Wagner, 1921).

The granite-hosted occurrence at Grass Valley contained the greatest amount of cassiterite. Most of the ore was extracted from two large flat dipping tabular bodies, one of which outcrops at the surface, while the other was encountered at a depth of 182m. Both orebodies are replacement veins following two gently inclined fractures in the granite, the richest ore occurring at the intersection (Wagner,1921). The fractures trend parallel to the lower surfaces of pegmatite sheets (Figure 3.7a), which have trapped ore fluids and resulted in the deposition of concentrated, high-grade ore. Tin mineralisation also occurs along fractures in the granite (Figure 3.7b).

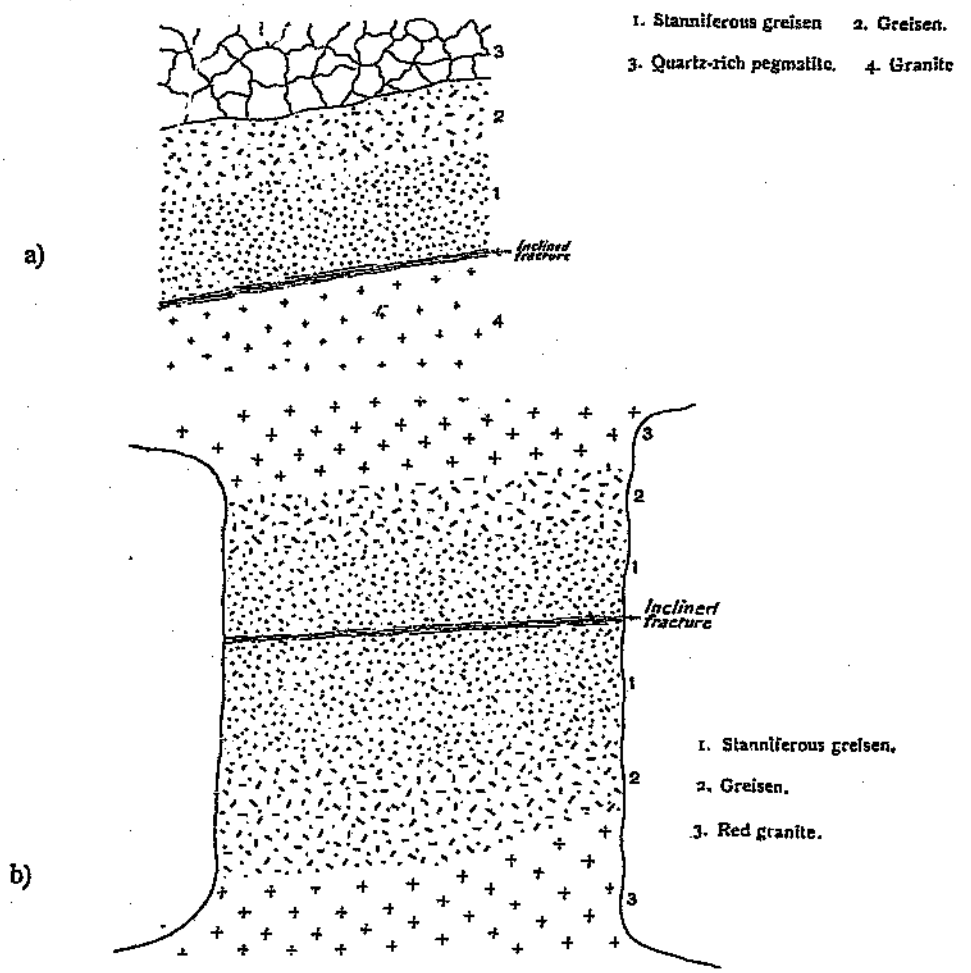


Figure 3.7 a) Fractures in granite which trend parallel to overlying pegmatite sheets. b) Cassiterite mineralisation along fractures in the granite. (From Wagner, 1921).

The relationship between the pipe-style of mineralisation and fractures is not certain. From Wagner's (1921) description, these pipes are not always associated with fractures. In Figure 3.8a, the pipe is associated with an inclined fracture, while in Figure 3.8b, no fracture was illustrated with the orebody. However, the shape of the orebody prompts the question of whether the parallel projections at the bottom of the ellipse are fault related.

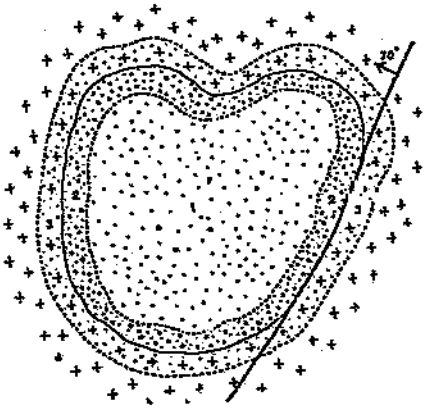

a)

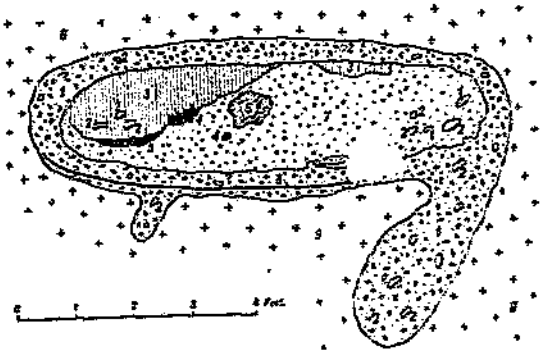

1. Red pegmatitic felspar.
2. White pegmatitic felspar.
3. Massive sulphide ore (mainly pyrite with chalcopyrite).
4. Cassiterite.
5. Arsenopyrite.
6. Fluorspar.
7. Greenish-yellow sericite-quartz rock with crystals and patches of cassiterite, arsenopyrite and fluorspar.
8. Narrow zone of soft sericitic matter.
9. Granite.

b)

Figure 3.8 a) Plan view of a small pipe at Grass Valley. b) Section of the elliptical orebody at Grass Valley, containing cassiterite and sulphide mineralisation (from Wagner, 1921).

The tin deposits in the pegmatites are irregular replacements containing the same assemblage of ore and gangue minerals as the granite-hosted deposits (Figure 3.9). Two types of pegmatite were recognised at Grass Valley, namely, intrusive and segregation pegmatites. The segregation pegmatites occur as small pockets which are zoned and grade into the surrounding granite host. These zoned pegmatites commonly contain fluorite and calcite in their central portions. Wagner (1921) suggested that these pegmatites represent localised patches of residual magma enriched in volatiles and water. The intrusive pegmatites post-date the segregation pegmatites and occur as undulating sheets with sharply defined upper and lower surfaces. Ore minerals are common in vugs within the pegmatite and are considered to have been introduced along fractures which served as favourable conduits for mineralising fluids.

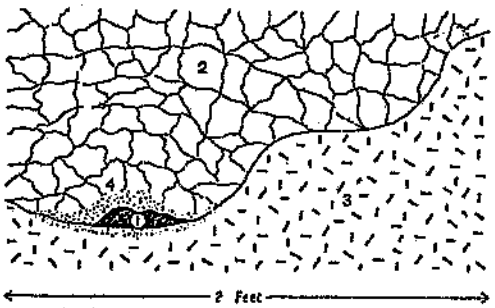

1. Massive cassiterite. 2. Pegmatitic quartz. 3. Granite. 4. Sericite.

**Figure 3.9** Replacement of pegmatitic quartz by cassiterite and sericite (from Wagner, 1921).

Wagner (1921) described the mineralogy of the Grass Valley tin deposit in detail. The paragenetic sequence was divided into three main stages (to be discussed in greater detail in Chapter 4). The principal ore mineral is cassiterite but subordinate amounts of the following minerals are present: stannite, wolframite, chalcopyrite, pyrite, arsenopyrite, molybdenite, specularite, eisenrham, zircon, titanite, magnetite, galena, sphalerite, secondary copper minerals, malachite and azurite, chalcanthite, limonite, quartz, chalcedony, feldspar, fluor-apatite, sericite, chlorite, fluorite, calcite, and ankerite. The mineralogy of this deposit has been re-examined and is presented in Chapter 4.

*SPOEDWEL AND DRONKFONTEIN*

The Spoedwel and Dronkfontein deposits are situated on adjacent farms in the Groblersdal District north-west of Marble Hall. The Spoedwel Copper Mine, located on the farm Spoedwel 701KS, and the farm adjacent to Spoedwel, Dronkfontein 724KS, both contain sulphide mineralisation in the form of veins and tabular ore bodies.

The presence of a copper ore body below the surface at Spoedwel was only detected in 1973, when a private contractor, commissioned to find and drill for ground water on the farm Spoedwel 701 KS, found chalcopyrite in the percussion chips. A period followed during which various mining companies showed passing interest in the ore body. Somerset Mining Company acquired an option to prospect in 1975. After drilling a few holes, some of which did not intersect the orebody, it was decided to first delineate the orebody by geophysical and geochemical methods.

Despite the possibility of a small high grade copper deposit, no mining companies were prepared to risk development. By 1985, Concor had acquired the option to exploit the orebody. During 1985 and 1986, a 36m vertical shaft was sunk into the orebody and a 40m development tunnel was driven across the orebody to prove the consistency of the grade (2,4% Cu). Shortly after the completion of the shaft Concor, sold all their mining interests. The company Spoedwel Copper Mine was founded by Mr. A Frick (a geologist with Concor) and a number of directors with Concor. A 100 ton/day plant was erected and production began in September 1987.

Several cores were drilled on Dronkfontein in 1989 and at least four orebodies were intersected. The northern part of Dronkfontein contains mineralisation in the overlying granophyre. The major ore components are Sn, Cu, Pb, Zn, Ag, Au and $CaF_2$ (Frick, unpubl. report, 1993). A grade of 1.5% Cu + Sn was estimated by Frick (1993) for the Dronkfontein deposit.

**Geology**

Borehole drilling and geophysical investigations at Spoedwel have shown that three tabular orebodies exist at depth (Figure 3.10) The mineralisation occurs at the contact between a medium- to coarse-grained granite and a fine-grained granite, as a tabular massive sulphide body dipping 8° to the north. The almost vertical, stockwork-like mineralisation to the south is hosted by the Nebo Granite and is interpreted as being feeder veins to the tabular body. The orebody reaches a maximum width of approximately 60m in the central portion and a thickness of up to 5m. Mineralisation and de-silicification of the host Nebo Granite occurred simultaneously, with excess silica being expelled into the immediate hanging-wall, where it manifests as crypto-crystalline quartz veins. The de-silicified Nebo is often referred to as an episyenite. The north-east-trending quartz veins outcrop at surface approximately 1 km south of the Spoedwel Mine, and are interpreted to be the result of leakage from a tabular "ponded" body trapped below the fine-grained granite/granophyre caprock (L. Robb, Pers. Comm., 1993).

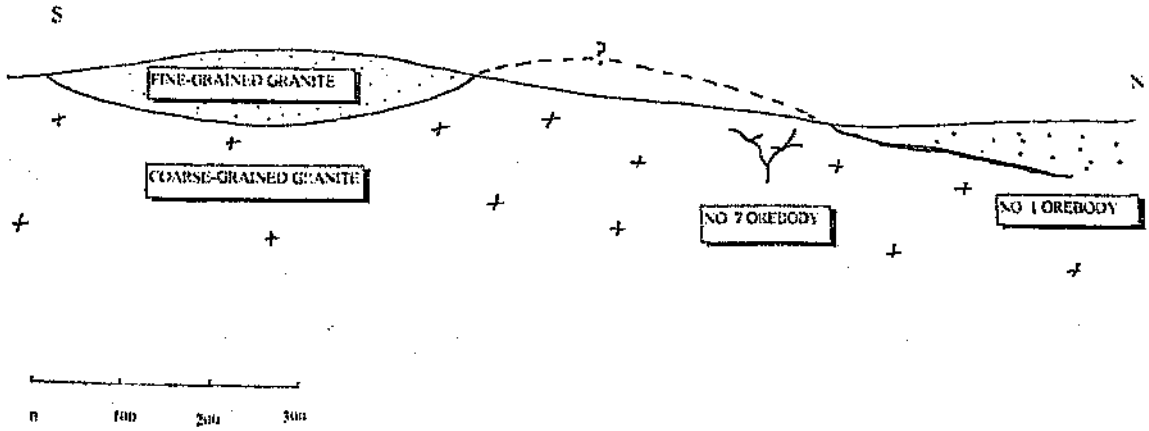


**Figure 3. 10** General section of the Spoedwel Copper deposit showing the northerly dipping No. 1 ore body and the stockwork-like No. 7 ore body (after Frick, unpubl. report, 1993).

Diamond drilled cores at Spoedwel and Dronkfontein were logged by Thomas Stone. Figure 3.11 is a composite of sketches made by Stone of the walls of the E-W tunnel at Spoedwel, and is included here as part of the previous work done on the deposit. In addition, one of the 25 borehole cores drafted by Stone is shown in Figure 3.12 indicating the Cu grades throughout the core.

In his descriptions, Stone referred to an "Upper Phase Granite", a "Lower Phase Granite" and a "Hybrid Contact Phase Granite". The Upper Phase granite (Fine-grained granite in Figure 3.11) was described as fine-grained maroon granite, in which the grain-size increases slightly with depth. It has variegated colouring and Stone called it a "mottled" granite due to the brown, bleached and orange patches which occur in places. It contains abundant interstitial hematite, a few anhedral pyrite blebs, and quartz, feldspar and amphibole phenocrysts. The feldspars show myrmekitic (granophyric?) intergrowth, and the amphibole (hornblende) is commonly altered to chlorite. Minor Fe-rich quartz veins with associated fluorite are present. Shears and fractures are occasionally coated with chlorite, hematite and limonite The Upper Phase Granite forms sharp but irregular cont. :ts with the Lower Phase Granite.

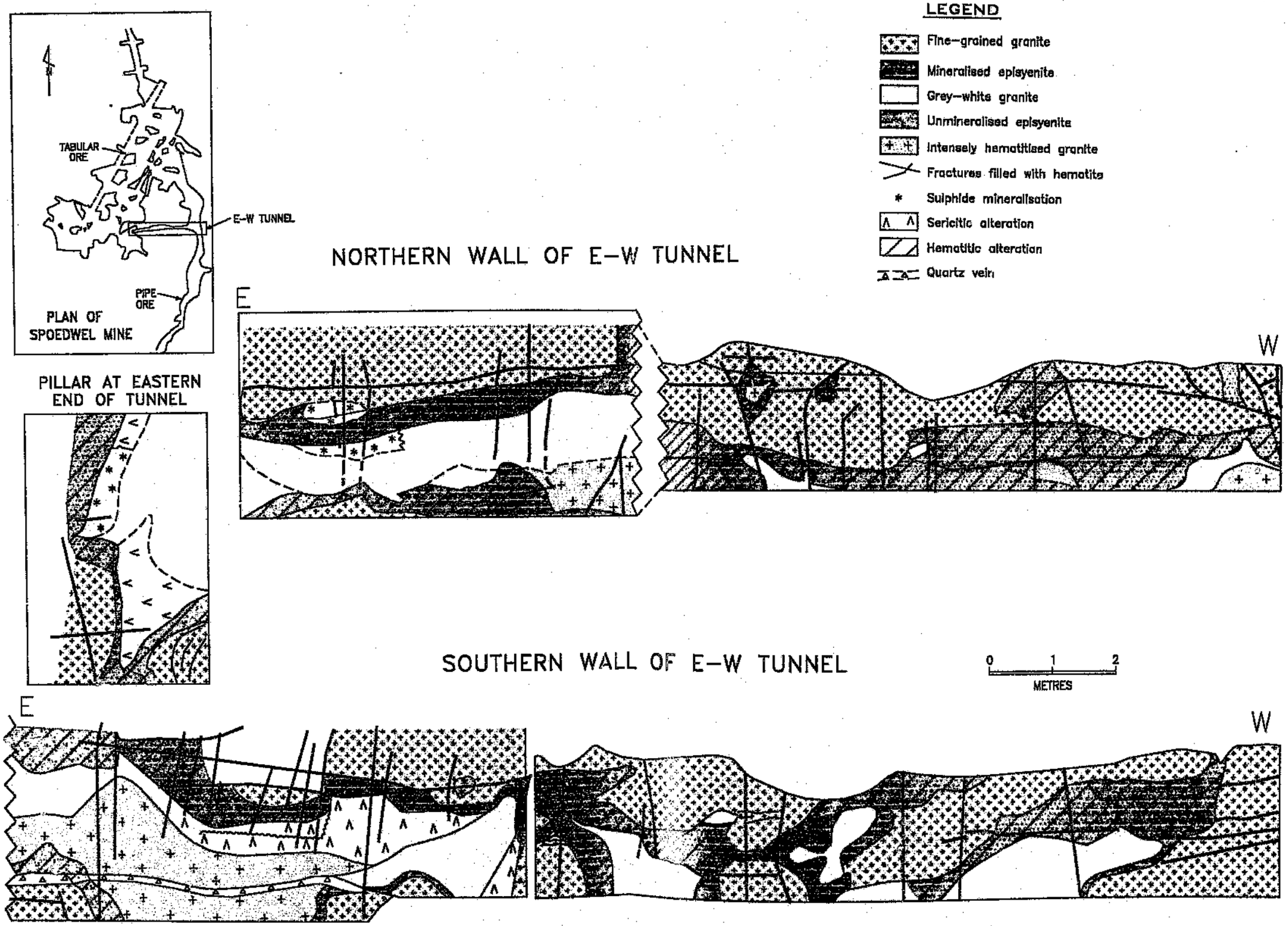


**Figure 3.11** Sketches of the walls in the E-W tunnel at the Spoedwel deposit.

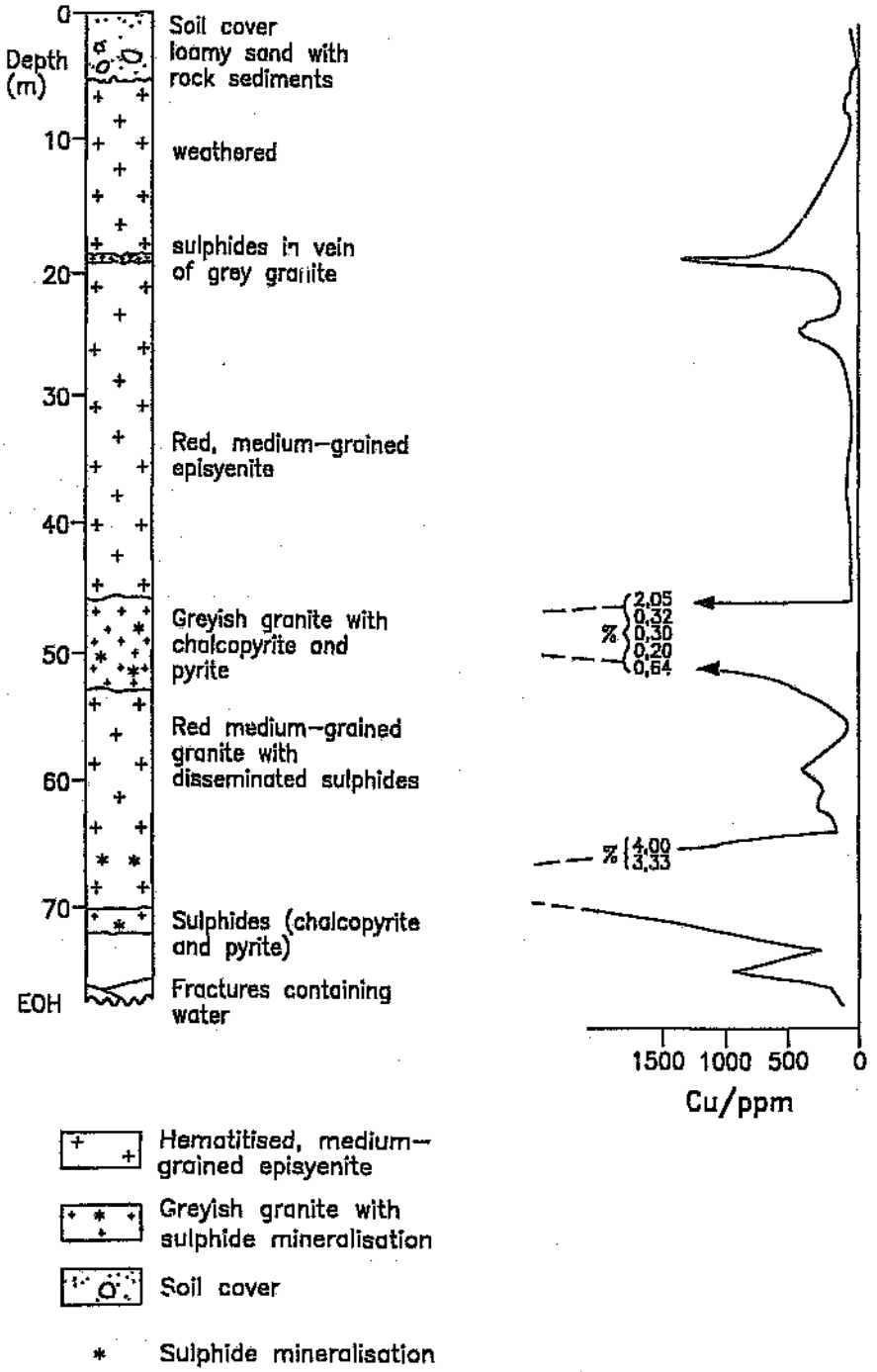


**Figure 3.12** Borehole core showing the associated Cu concentrations. Values are indicated in ppm and % in high grade samples.

The Lower Phase Granite is a pale, orange-pink, fine- to medium-grained, quartz-rich granite. The quartz and feldspar are more distinctly segregated than in the Upper Phase Granite, with discrete quartz and feldspar crystals. It contains numerous quartz, fluorite and hematite veins. Patches of chloritic alteration occur. The crystalline granite grades into vesicular, brick red, feldspathic episyenite, which contains pyrite, chalcopyrite and chalcocite (Mineralised episyenite in Figure 3.11). The highest grades of mineralisation occur in a white, bleached feldspathic granite (Grey-white granite in Figure 3.11) within the episyenite. This white granite occurs in two horizons (at around 52m depth) which are separated by the red episyenite with lower grades (Unmineralised episyenite in Figure 3.11). A third zone of highest mineralisation occurs at slightly greater depth (56m ). Several horizons of mineralisation exist.

The Hybrid contact phase consists of Fe-rich, maroon-coloured, partially assimilated Upper Phase Granite hosted by pale, orange/pink, fine-grained, chloritic Lower Phase Granite. It is porphyritic containing aggregates of quartz-amphibole and partially assimilated Lower Phase Granite blebs.

***ALBERT***

The historical aspects of the Albert Silver Mine have been researched and documented by Robb *et al.* (1994) and the reader is referred to that paper for a detailed recount. For the sake of completeness, some of the salient points are repeated below.

The Albert Silver Mine was discovered in 1885 and mined until 1910. It occurs on the farm Roodepoortjie 250JR about 80 km west-northwest of Pretoria. Four boreholes were drilled in 1952 and a further 26 in the period 1967-1969. Geophysical and geochemical surveys were carried out over the deposit by the Geological Survey of South Africa and, in 1970, an M.Sc. dissertation was submitted to the University of Natal (Champion, 1970). In 1956 scintillometer surveys showed that significant concentrations of uranium (up to 1 kg. $ton^{-1}$) are associated with the base- and precious-metal lodes. In the period 1978-1980, the property was re-examined as a potential copper-silver- uranium prospect and a further five bore-holes drilled. Present ore reserves to a depth of 150m are estimated to be 1.2 million tons at 73 g. $ton^{-1}$ Ag, 0.42% Cu, 0.27%Pb and 100 ppm $U_3O_8$; the deposit is generally

regarded as uneconomic in the present market climate. During its productive years, the mine was high graded, producing an estimated 20 000 tons of ore grading 1.14 $kg.ton^{-1}$ Ag, and 10%Cu (Voet, 1981). Recent assays of dump material report isolated samples up to 400$g.ton^{-1}$ Au and 0.48 % Sb.

Geology

The Albert Silver Mine is located within the Verena Granite pluton, and the granites in the area have been referred to locally as the Verena Porphyritic Granite. The geological relationships recognised by Robb *et al.* (1994) indicate that the fine-grained granite is the roof zone, or possibly the chilled apical phase, into which the coarser-grained granite is intruded.

The region of mineralisation is defined on surface by at least three major vein systems trending approximately east-west (Figure 3.13). On surface, the veins are distinctly gossanous and have a subvertical dip, comprising milky whit quartz, hematite and iron-hydroxide minerals (Robb *et al.*, 1994).

A preliminary investigation of these granites was carried out by Robb *et al.* (1994), in which they recognised two granite varieties; 1) Coarse-grained Porphyritic Granite (Nebo-type), and 2) Fine-grained Porphyritic Granite (Klipkloof-type). Both of these granite types are composed of plagioclase, orthoclase, quartz and biotite, with accessory phases including zircon, fluorite, apatite, bastnaesite, monazite, titanite, epidote, carbonate and magnetite-ilmenite. Alteration phenomena include chloritisation, sericitisation and argillic alteration after feldspars (Robb *et al.*, 1994). The paragenesis at Albert has been divided into two episodes of mineralisation. To begin with, a sulphide assemblage, consisting of pyrite, sphalerite, galena, arsenopyrite and argentiferous tennantite, was deposited, followed by a later assemblage of thuringitic chlorite, hematite, pitchblende and fluorite.

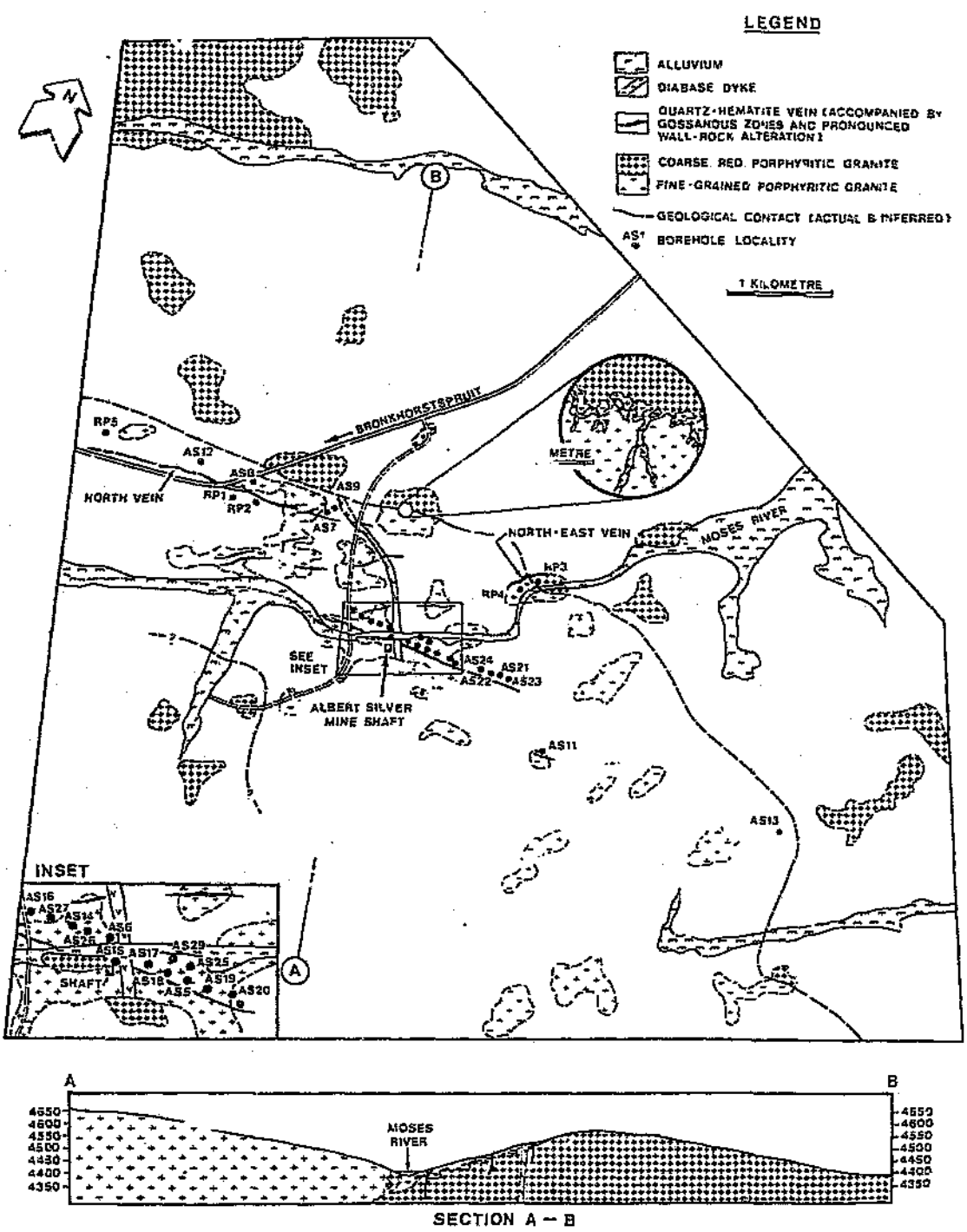


Figure 3.13 Outcrop map of the farm Roodepoortjie showing the distribution of the Albert Silver Mine veins in relation to the fine- and coarse-grained porphyritic granite host rocks. Section A-B has a 2x vertical exaggeration and shows actual elevations in feet (from Robb *et al.*, 1994).

*HOUTENBEK*

Very little is known about this deposit. It has never been studied from an academic point of view, and no literature resources exist. The deposit appears to be a pipe-style mineral occurrence, with no evidence of fractures at the surface (Figure 3.14). Highly altered sedimentary remnants are found among the rubble surrounding the pit (diameter ±15m), and contain molybdenite, sphalerite, quartz and fluorite (green and purple). The host granite is typical Nebo Granite which shows almost no hydrothermal alteration (as at Spoedwel, Albert and Grass Valley). This is a rather unusual phenomenon, and it is suggested that the pipe may represent a hydrothermal vent or breccia pipe similar to that at the Olympic Dam deposit in southern Australia. Sedimentary fragments within the pipe suggest that the vent breached the surface, or at least the Transvaal Supergroup roof rocks.

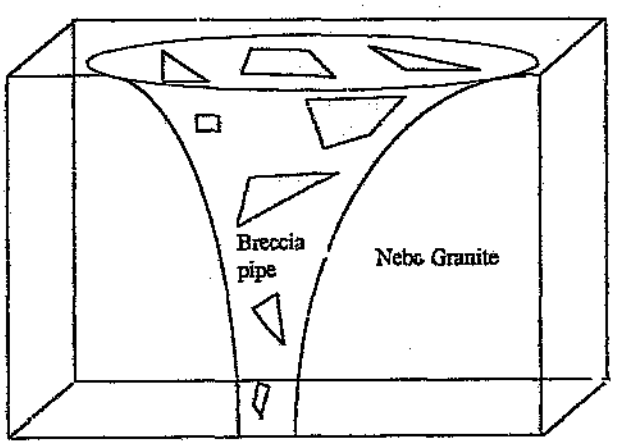


**Figure 3.14** Diagrammatic representation of the Houtenbek breccia pipe in Nebo Granite.

# CHAPTER 4

# MINERAL PETROGRAPHY

A comparative petrographic study was conducted on the rocks from the six different locations described in Chapters 2 and 3. Five of these (Grass Valley, Spoedwel, Dronkfontein, Albert and Houtenbek) are ore deposits, and the sixth (Leeufontein), a site where no ore body exists (Figures 2.6 and 3.2).

The granites in the area east of Marble Hall (which is referred to as Leeufontein) serve as the control, against which the mineralogy of the altered granites in the ore deposits are compared. The mineralogy o he different granites in the area varies, and has been described in Chapter 2. The focus of this chapter is to compare the deposits with ore mineralisation, pointing out the similarities and differences in primary assemblages, alteration and ore assemblages.

The ore and gangue minerals of all samples from each deposit examined are tabulated in the Appendix. The following sections represent a comparative discussion of the mineralogy, paragenesis and alteration assemblages at Grass Valley, Spoedwel, Dronkfontein, Albert, Houtenbek, and Leeufontein.

## 4.1. SAMPLE MATERIAL

The Spoedwel granites were mapped in 1989 by Thomas Stone, as part of an MSc project which he later abandoned. Several thin sections and polished thin sections were made at the Geological Survey of South Africa, Pretoria, and were not thoroughly examined before the project was aborted. The following mineralogical observations based on the ore and gangue mineralogy at Spoedwel are derived from a detailed examination of these 356 thin sections and polished thin sections. Additional polished thin sections were made at the University of the Witwatersrand from samples collected from the waste dumps of the non-operational mine workings. The sample material from Albert Silver mine was collected by V. Robb and L.J. Robb as part of an earlier study of the deposit. A total of 141 polished thin sections, 27 polished wedges, and 10 doubly polished thin sections were examined .

The sample material from Grass Valley and Leeufontein was collected while mapping the area for RTZ Exploration Ltd. A total of twenty seven polished thin sections, ten doubly polished thin sections and five thin sections were cut from Grass Valley. Ten polished thin sections and ten doubly polished wafers were cut from granites in the Leeufontein area.

## 4.2. SAMPLE DESCRIPTIONS

Polished thin section descriptions have been tabulated for easy reference and are shown in the Appendix. The gangue mineralogy, ore mineralogy and paragenetic sequences in each section, as well as the average grain-size and characterisation of the granite (i.e. hypersolvus, subsolvus or transsolvus) are indicated.

## 4.3 HYPERSOLVUS AND SUBSOLVUS GRANITES IN THE BUSHVELD COMPLEX

Petrographic studies of the granites hosting mineralisation at the Grass Valley, Spoedwel and Albert deposits, as well as of the barren granites in the Leeufontein area, have revealed the presence of three textural varieties in the eastern lobe of the Bushveld Complex, namely hypersolvus, subsolvus and transsolvus granites. Previous descriptions of the Bushveld granites had recognised their hypersolvus character (Kleemann, 1985; Kleemann and Twist, 1989), but the presence of subsolvus and transsolvus textures had not previously been described in the literature. Evidence for the presence of these granite types in the Bushveld is presented here for the first time.

The primary difference between hypersolvus and subsolvus granites is the presence or absence of discrete plagioclase crystals. Hypersolvus granites are characterised by the absence of a primary albitic plagioclase, except as a component of perthite. The alkali feldspars consist of coarsely perthitic microcline and are derived from relatively dry liquids in near-surface environments (Martin and Bonin, 1976). Subsolvus granites are characterised by discrete grains of K-feldspar and albite. The alkali feldspars consist of non-perthitic microcline which were derived from "wetter" liquids formed at deeper levels in the crust. The grain-size is smaller than in hypersolvus granites (Martin and Bonin, 1976). Transsolvus granites are intermediate varieties between the hypersolvus and subsolvus

extremes. They occur where crystallisation of the hypersolvus granite has been disrupted, and contain perthite in a subsolvus matrix. However, the transsolvus granites are normally not present in the study areas, and only hypersolvus and subsolvus granites occur.

In Chapter 2, the granites at Leeufontein are described, but the terms hypersolvus, subsolvus and transsolvus granite were not introduced in any detail. The Nebo Granites, which comprises the bulk of the Bushveld granites, are indeed hypersolvus granites. However, the Klipkloof Granite varieties, i.e. the fine-grained, porphyritic, and albitised Klipkloof Granites, appear to have different textures. The true fine-grained Klipkloof Granite (not the chilled Nebo Granite at the margins of the pluton), contains discrete crystals of plagioclase, the presence of which is a characteristic of subsolvus granites. In addition, the contact facies between Nebo Granite and the fine-grained Klipkloof dykes, sills and plugs, referred to as the porphyritic Klipkloof Granite, shows all the characteristics of transsolvus granites.

Thus, the characteristics of these granites correlate with those recognised by Tuttle and Bowen (1958), Martin and Bonin (1976) and Bonin (1986) in their studies of the association between hypersolvus and subsolvus granites. The hypersolvus-subsolvus granite suite of rocks is found in anorogenic areas of crustal extension and originate from mantle-derived basic liquids. Coexisting hypersolvus-subsolvus granites are commonly associated with rhyolites, granophyres, aplites, graphic granites and pegmatites within the same intrusive complex. Martin and Bonin (1976) identified and examined a number of instances where both of these genetically related granite types occur. Examples of the hypersolvus-subsolvus granite association have been recognised in the Cape Ann plutonic series, Massachusetts (Zartman and Marvin, 1971), in several plutonic complexes in Corsica (Vellutini, 1975), and in the White Mountain series in New Hampshire, North America (Karner and Bertram, 1972).

Martin and Bonin (1976) suggested a model for the evolution of these granites in which the availability of water is a critical factor in determining the nature of the granite crystallised. The model of Martin and Bonin (1976, page 228) explained the association of hypersolvus and subsolvus granites as follows: "The late influx of water, possibly of meteoric origin, "soaked" the cooling hypersolvus granite once crystallised, inducing local near complete

fusion and remobilization of the early granite. At lower temperatures the influx of water would be reflected in deuteric changes such as the alteration of mafic mineral assemblages, precipitation of late albite, replacement of pre-existing feldspars by albite and local increase in the degree of order of K-feldspar".

**Hypersolvus and subsolvus granites associated with mineralisation**

The bulk of the Lebowa Granite Suite is made up of the hypersolvus Nebo Granite, into which the aplitic, subsolvus Klipkloof Granite is intruded. The country rock hosting mineralisation and the subsolvus granites at Spoedwel, Grass Valley, Dronkfontein and Houtenbek, consists of altered, hypersolvus Nebo Granite. In contrast to the cream-coloured, barren granites in the lower portions of the pluton, the colour of the mineralised granite is brick-red, and is composed almost entirely of intensely hematitised perthite and quartz. It occurs as coarsely crystalline granite, and as a fine-grained equivalent which was rapidly chilled at the margins of the pluton.

A feature of the coarse-grained hypersolvus granite is the apparent compaction or fusion of the perthites, which may be extreme in some cases, with no interstitial spaces between grains and no euhedral crystal structure remaining (Figure 4.1). In other cases, the compaction is less pronounced, and some euhedral interlocking perthite crystals are still recognisable.

The interstitial material is predominantly secondary in origin, introduced after crystallisation or partial solidification of the perthite crystals. The material between the large perthite crystals (>2mm) is usually secondary quartz, muscovite, chlorite and fluorite in varying proportions. The degree of sulphide mineralisation is variable and has a direct influence on the gangue assemblage associated with it. In relatively unmineralised samples, minute specks of chalcopyrite (<0.01mm) occur disseminated throughout the rock. As the abundance of sulphides increases, the amount of chlorite, quartz and muscovite increases.

At Spoedwel and Grass Valley, the subsolvus granite is less abundant than the hypersolvus granite, and commonly is associated with the sulphide mineralisation (Figure 4.2). At Spoedwel, the subsolvus granite occurs as undulating dykes and sills within the Nebo Granite. In contrast, the Albert Silver deposit is situated within a large pluton of subsolvus

granite, referred to locally as the Verena Porphyritic Granite (Figure 4.3). No subsolvus granite was recognised at the Houtenbek and Dronkfontein deposits.

The occurrence of K-feldspar (microcline with no tartan twinning), primary albite and quartz intergrown with muscovite, sericite and chlorite is characteristic of the subsolvus granite (Figure 4.4). Hematitisation of the feldspars is localised near fractures; however, the fresh material is not hematitised, and the hand specimens are colourless to slightly green where chloritisation has occurred. The grain-size is typically about 1mm.

The contact between the hypersolvus Nebo Granite and the intrusive subsolvus granite is marked by a hybrid granite type, consisting of hypersolvus perthite grains in a subsolvus granite matrix (Figure 4.5). This granite type is referred to as transsolvus granite and are at Spoedwel, Grass Valley, and Albert. Portions of the hypersolvus perthite occur surrounded by albite, K-feldspar, quartz and muscovite (Figure 4.6). The amount of subsolvus granite within the hypersolvus granite varies. In some instances, the hypersolvus granite is abundant and the subsolvus granite is minor, while, in other cases, the hypersolvus remnants are minor and the matrix is composed almost entirely of subsolvus granite and sulphide minerals. The transsolvus granites are rare and limited to the marginal facies of the subsolvus granites. The geological relationships of the transsolvus granites at the ore deposits are identical to those in the barren granites at Leeufontein, where Nebo Granite is intruded by fine-grained Klipkloof dykes and sills. The porphyritic Klipkloof envelopes, which are developed along the margins of the fine-grained Klipkloof dykes and sills, are typical transsolvus granites.

The association of hypersolvus and subsolvus granites with granophyres, graphic granite, pegmatites and aplites, as documented in the Corsican and North American plutonic rocks, is recognised in the Bushveld granites. In addition to these rocks being indicative of hydrous conditions during the magmatic stage (Martin and Bonin, 1976), the abundance of muscovite associated with the subsolvus granite (Figure 4.7) and albitisation of the feldspars (Figure 4.8) further supports the hypothesis that water became available late in the magmatic stage, and persisted into the post-magmatic stage.

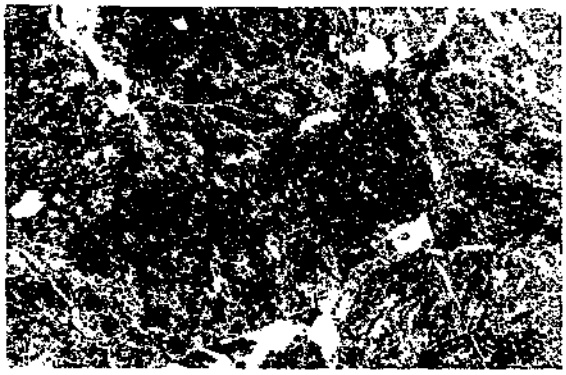

**Figure 4.1** Microphotograph of hypersolvus granite showing strongly altered and hematitised interlocking perthite crystals (PPL X40).

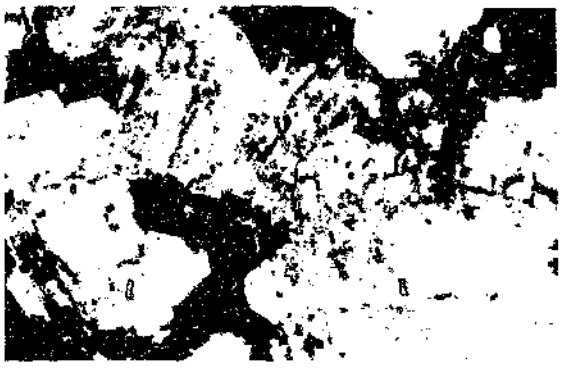

**Figure 4.2** Microphotograph of subsolvus granite associated with sulphide mineralisation at Spoedwel (PPL X100).

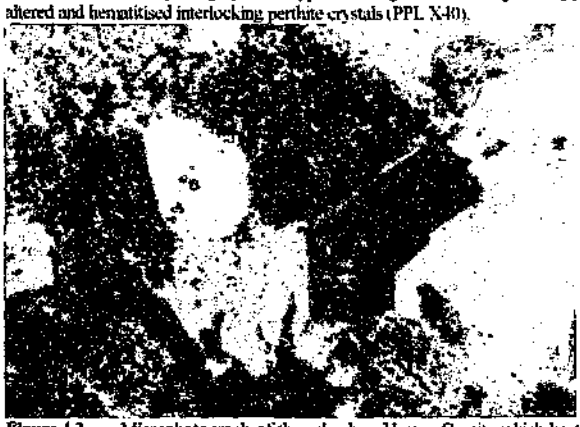

**Figure 4.3** Microphotograph of the subsolvus Verena Granite which hosts mineralisation at the Albert Silver Mine (PPL X40).

**Figure 4.4** Microphotograph of subsolvus granite containing K-feldspar, albite, quartz and muscovite. (XPL X40).

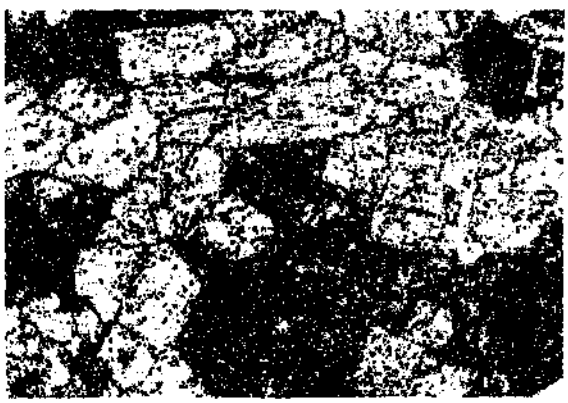

**Figure 4.5** Microphotograph of transsolvus granite composed of hypersolvus perthite in a subsolvus matrix. (PPL X40).

**Figure 4.6** Microphotograph of transsolvus granite containing perthite albite, K-feldspar, quartz and muscovite. (XPL X40).

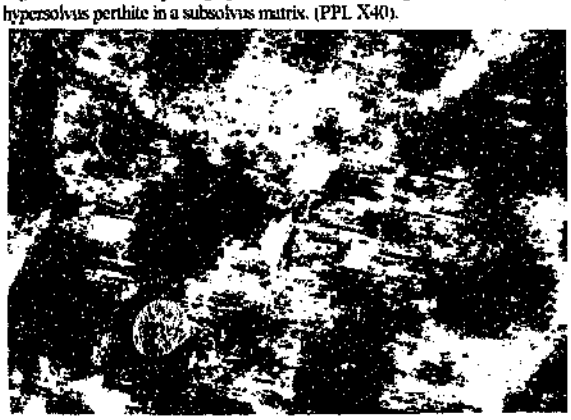

**Figure 4.7** Microphotograph showing albitisation of perthite cryst. s. (XPL X40).

**Figure 4.8** Microphotograph showing muscovitisation of subsolvus granite. (XPL X40).

## 4.4 PETROGRAPHIC OBSERVATIONS

### *GANGUE MINERALOGY*

The gangue mineralogy is directly related to the occurrence of mineralisation at each of the deposits. In areas where high-grade mineralisation is present, the primary gangue assemblage has been almost entirely obliterated, being replaced by alteration minerals such as sericite, chlorite, muscovite, and secondary albite. The ore and gangue minerals have been separated, are discussed in order of their appearance in the paragenetic sequence.

**Feldspar**

The feldspars have been discussed in some detail in the section on hypersolvus and subsolvus granites. The hypersolvus granites contain perthitised alkali feldspar and no albite. The perthites are brick-red in colour, which imparts the characteristic red colour to the rock. In contrast, the subsolvus granites contain both K-feldspar and albite. There is no perthitisation or hematitisation of the feldspars in the subsolvus granites at Grass Valley and Spoedwel. However, the host granites at Albert, which are all subsolvus in nature, exhibit varying degrees of hematitisation, particularly near the fractures and mineralisation.

Subsolvus granite samples from Spoedwel contain K-feldspar crystals, showing Carlsbad twinning, which are associated with albite, quartz and muscovite. The crystals are euhedral to subhedral and are intergrown with the quartz and muscovite. The muscovite occurs between crystals and fills cracks in the quartz. It also surrounds irregular masses of chalcopyrite. The same association occurs at Grass Valley and Albert. However, at Albert, the original albite is commonly overgrown by a second episode of albite precipitation, which has not been observed at the other deposits (Figure 4.9).

At Spoedwel, the contrast in colours between poorly mineralised, deuterically altered orange-red perthite of the hypersolvus granite, and the white unaltered feldspars of the subsolvus granite, may be observed on the scale of a single thin section. The zone containing predominantly hematitised feldspar is not well mineralised. Few small chalcopyrite grains with covellite alteration rims are disseminated among chlorite masses. Isolated grains of cassiterite occur with chalcopyrite growth on the rims. The mineralised

portion contains both hematitised perthite and unhematitised albite and K-feldspar grains, in addition to quartz and muscovite. The main ore mineral, chalcopyrite, embays feldspar grains and fills cavities formed by euhedral crystals. The perthites show chloritic alteration that was associated with crystallisation of the subsolvus granites and the sulphide mineralisation (Figure 4.10).

The host granites at Albert are all subsolvus in nature and there are no hypersolvus-subsolvus granite contacts near the zone of mineralisation. However, perthite phenocrysts in a matrix of subsolvus granite, which are typical of transsolvus granites, do occur.

**Chlorite**

Five different varieties of chlorite have been identified at Spoedwel (1-5 below). The wide variety of chlorites at Spoedwel is not present at Albert, where only the grass green chlorite occurs. The presence of chlorite at Grass Valley is not as abundant, occurring only in patches where copper mineralisation is found.

1) *Grass-green Chlorite* (Figure 4.11)

This chlorite is grass-green in colour and highly pleochroic. It occurs as fibres, flakes and rosettes, in masses filling cavities formed by the euhedral borders of feldspar and quartz crystals. It also occurs as linings of quartz veinlets cutting across feldspar crystals and pyrite grains. This chlorite is associated with chalcopyrite precipitation. Evidence for this includes co-precipitation of chlorite and chalcopyrite within pyrite grains, as chlorite rosettes within chalcopyrite, and along fracture planes within pyrite and feldspar crystals.

The chlorite invades feldspar/perthite and, in extreme cases, almost obliterates the original mineral assemblage. This chlorite is also associated with a pulse of quartz precipitation. This quartz generation post-dates the grass-green chlorite precipitation, since perfect rosettes of chlorite are found within large masses of quartz. The quartz is clearly secondary in origin, since it shows distinct triple junctions and straight crystal faces. This quartz also contains fibrous and rosette shaped muscovite crystals. The sulphide mineralisation occurs within the quartz masses and along grain boundaries. Chlorite occurs as solid inclusions within the sphalerite.

The grass-green chlorite is intergrown with muscovite and quartz. The chlorite and muscovite are intimately intergrown and assumed to have precipitated from the same fluid. Fragments of chlorite, muscovite, quartz and hematitised feldspar have been observed trapped in a vein filled with the ore minerals chalcopyrite, bornite, chalcocite and digenite.

In areas closer to the main copper mineralisation, chloritisation of the feldspars is the predominant alteration phenomenon, in contrast to the hematisation which is dominant in areas away from the orebodies.

2) A variation of this grass-green chlorite has been recognised in which the grain-size is finer and the colour tends to be tinted with brown or black flecks. The distinctive pleochroism of the normal grass-green chlorite is absent.

3) Another variation of the grass-green chlorite is extremely fine-grained, showing no fibres or rosettes, consisting of an amorphous ground mass surrounding the sulphide minerals (Figure 4.12). It is clearly distinguished from the rosette-shaped, grass-green chlorite in sections where the fine-grained material is transected by quartz veinlets lined by the rosette-shaped material. Slight colour variations between the two generations of chlorite are noticeable.

4) *Brown Chlorite*

This type of chlorite is scarce and is easily distinguished from the green chlorite by its colour, lack of well developed rosettes and its extremely fine grain size. It is light brown to olive green in colour and shows weak pleochroism (Figure 4.13).

It occurs as veinlets transecting feldspar crystals and forming a network surrounding the chalcopyrite masses. This chlorite seems to be associated with the alteration of cassiterite and titanite, forming borders around them or filling cavities into which they project.

5) *Olive-green Chlorite*

This type of chlorite looks similar to the grass-green chlorite, except that the colour tends more towards the colour of the brown chlorite discussed above. It occurs as well developed

rosettes comparable in size to those of the grass-green chlorite, filling vugs and fractures within the regions where the perthite has been hematitised.

The green and brown generations never occur together. The green species tend to be more common in quartz-rich sections associated with the ore mineralisation. In contrast, the brown and olive-green varieties are more common in the regions where haematisation of the feldspars is the dominant form of alteration and where the ore minerals, chiefly chalcopyrite, occur as disseminated flecks.

It is apparent from the mineral relationships that both generations of chlorite, the green and the brown varieties, are associated with the introduction of the copper-bearing ore suite. The green chlorite is more abundant than the brown chlorite.

**Quartz**

Quartz precipitation occurred in several episodes during the crystallisation history of the Bushveld granites. Evidence for this is obvious to the naked eye in some instances, where multiple growth episodes of quartz line fractures in the granite. In other cases, the distinction between different episodes is more subtle. However, evidence indicating a sequence of quartz precipitation in interstitial material has been identified.

Euhedral crystal faces of quartz deposited early in the sequence are commonly outlined by fluid inclusions trapped on the surface and radiating into the newly precipitated quartz in subsequent growth stages (Figure 4.14). In addition, large masses of quartz crystals terminating in triple junctions (Figure 4.15), intergrown with albite and K-feldspar, muscovite and chlorite are present. Under crossed polars, this quartz shows no undulous extinction, as opposed to the quartz grains that have been partially sericitised.

Apart from the quartz filling the interstitial spaces in the host rock, small scale (less than 1cm in diameter) and large scale (10cm to >1m)) quartz veins and stockworks form a major component of the rock. In the veins at Spoedwel, two generations of quartz have been recognised. The veins are lined by euhedral crystals projecting into the open fracture (Figure 4.16). The faces of these crystals are lined by fluid inclusions trapped by the massive quartz precipitated into the remaining space.

The vein-fill at Albert and Grass Valley is much more complex, with at least eight episodes of precipitation being recognised at each deposit (Figures 17 and 18). In addition, evidence from Grass Valley indicates that at least two episodes of quartz precipitation occurred before cassiterite was deposited, making a total of ten increments of quartz growth.

**Chalcedony**

Veins and stringers of cryptocrystalline silica have been observed at Grass Valley. They intersect the ore body and some of the veins have been re-utilised by later generations of transparent quartz and late-stage hematite.

**Muscovite and sericite**

The occurrence of muscovite is alluded to in previous sections in association with other minerals and is present at all three deposits. It occurs as relatively large fibres (~10mm) to smaller sized rosettes (~0,25mm). It is highly pleochroic, and, upon rotation of the stage, shows alternating shades of green, blue and pink. The muscovite is associated with the subsolvus granite and is intimately intergrown with albite, K-feldspar, grass-green chlorite and quartz. It occurs intersitially with quartz in spaces between perthite crystals. It also is associated with quartz filling interstices in the hypersolvus granite and subsolvus granite (Figure 4.7).

Fine-grained muscovite (sericite) is the most common alteration mineral at the Albert and Grass Valley deposits, and is formed by hydrothermal alteration of feldspars in the host granites. At Albert, sericitisation of plagioclase is extreme in some areas, obliterating the original minerals. The precipitation of secondary albite at Albert occurred after sericitisation of the core albite crystals. Perthite is not commonly highly sericitised.

**Fluorite**

Fluorite is abundant in the hypersolvus granite, where it fills vugs and open fractures. It is distinguished from quartz by its higher relief, purple coloration, and isotropism. It contains no mineral inclusions, such as chlorite, muscovite or quartz (Figure 4.19). Central portions of some vugs contain zoned crystals of $CaF_2$ which are surrounded by clear masses of fluorite commonly showing fractures along the cleavage planes.

Fluorite also occurs in vein form, intergrown with the ore minerals galena, sphalerite, tennantite and chalcopyrite. Paragenetic relationships do not suggest that fluorite precipitation occurred at any particular point in the sequence of mineralisation, but rather that precipitation continued throughout the sequence.

In addition to its association with the above mentioned ore minerals, fluorite is also associated with quartz and muscovite in the same veins. Quartz and fluorite occur in roughly equal proportions in ore veins, the quartz preceding the fluorite precipitation. Furthermore, the relationship of muscovite with the quartz and fluorite and with the other ore minerals is not easily unravelled. The quartz and muscovite were precipitated throughout the paragenetic sequence, beginning during the precipitation of pyrite.

Cathodo-luminescence imagery has shown that two main episodes of fluorite occurred at Spoedwel. An early massive in-fill of interstitial spaces is overgrown by a second generation which shows progressive growth increments. At Albert, the second generation fluorite is abundant and is associated with massive hematite and pitchblende, and post-dates the sulphide assemblage.

**Tourmaline**

Tourmaline is not present at any of the ore deposits examined, although it is found in the area east of Marble Hall (Leeufontein). Veins and spheroids of tourmaline are confined to areas where faulting is evident, and are hosted by albitised fine-grained Klipkloof Granite.

The tourmaline spheroids (Figure 4.20) consist of plagioclase, quartz and K-feldspar. The plagioclase and tourmaline are clearly secondary, being superimposed on the original granite host. Granophyric intergrowths of quartz and tourmaline are observed, suggesting

that tourmaline and quartz were precipitated together. Furthermore, colour zonation within the tourmaline is observed, implying that precipitation occurred as more than one event. Small specks of chalcopyrite and sphalerite have been noted in some tourmaline spheroids.

**Titanite**

Crystals of titanite are relatively common and are disseminated throughout the granite. They are subhedral to euhedral in shape, varying in length from small (>0,5mm) to relatively large (1,0mm). Relief in these grains is high, as in cassiterite and zircon, but the birefringence is slightly lower than that in cassiterite.

The titanite crystals are more abundant than the cassiterite crystals, showing distinctive symplectic inter-growth. Alteration of the original titanite crystals is observed at different stages in the progression towards leucoxene (a general term referring to the alteration product of Ti-bearing minerals). In specimens where the alteration is far advanced, there is almost inevitably chalcopyrite and/or fine-grained brown pleochroic chlorite surrounding the grains. Titanite/leucoxene is a similar shade of grey to altered cassiterite in reflected light, but shows the symplectic texture described above. However, this texture is not characteristic; some unaltered crystals appear homogeneous and the internal reflections resemble those of sphalerite.

**Zircon**

Zircon crystals are small in diametre (2 - 5mm) and colourless to pale brown in colour. They occur as subhedral to euhedral prisms with high relief, commonly bearing minute chalcopyrite and covellite grains along the borders (Figure 4.21). Several grains contain specks of chalcopyrite inside the grains. Zircon has a lower bireflectance / birefringence than either titanite or cassiterite, and is relatively scarce in comparison.

Evidence for at least two generations of zircon was observed at Spoedwel by petrographic means. The first generation of zircon crystals are altered and are surrounded by alteration halos caused by radiogenic decay (Figure 4.22). The second generation of zircons are unaltered, and are associated with the sulphide mineralisation (Figure 4.23). Supporting evidence for the presence of multiple episodes of zircon precipitation has been obtained by cathodo-luminescence imagery.

Figure 4. 24 is a cathodo-luminescence image which shows a euhedral zircon crystal with multiple growth stages. The zircon occurs within a fracture in early generation quartz, that has been filled by two later quartz generations.

**Monazite**

Monazite crystals are abundant in the samples associated with mineralisation at Spoedwel and Dronkfontein. The high relief crystals are euhedral and are highly birefringent. Sulphide specks are often found within the crystal, indicating that the precipitation of monazite coincided with sulphide precipitation.

**Calcite and ankerite**

Calcite and ankerite were observed only at Grass Valley and occur late in the paragenetic sequence, filling open cavities and fractures .

**Figure 4.9** Microphotograph of subsolvus granite at Albert showing secondary albite growth on sericitised primary albite. (XPL X[illegible]).

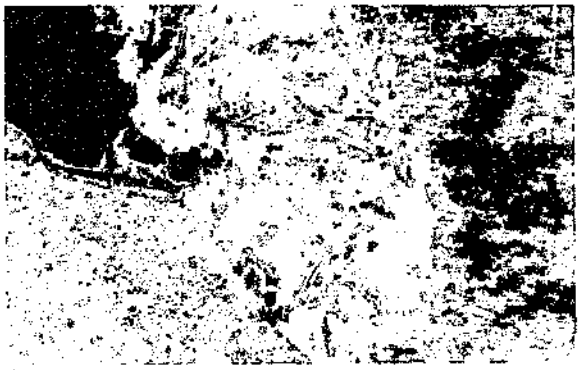

**Figure 4.10** Microphotograph showing chloritic alteration of perthite. (PPL X 40).

**Figure 4.11** Microphotograph of grass-green chlorite. (PPL X 100).

**Figure 4.12** Microphotograph of a fine-grained variety of grass green chlorite which often surrounds disseminated sulphide minerals. (PPL X100).

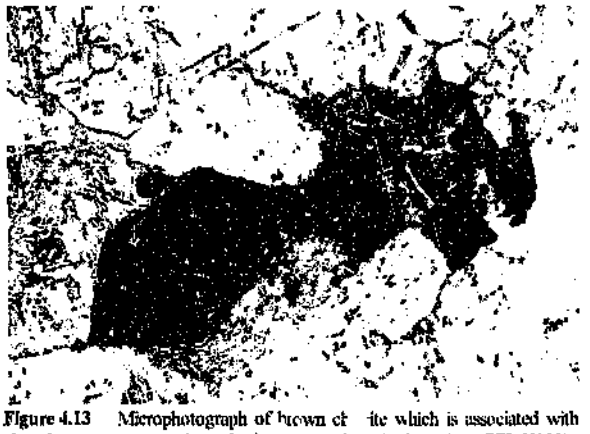

**Figure 4.13** Microphotograph of brown ch[illegible]ite which is associated with altered accessory cassiterite and sphene in unmineraised granites. (PPL X100).

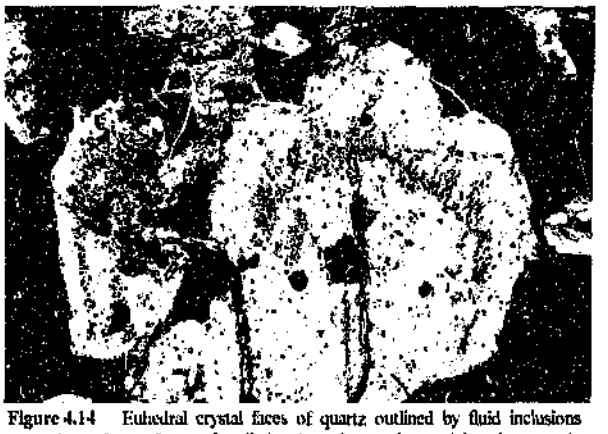

**Figure 4.14** Euhedral crystal faces of quartz outlined by fluid inclusions trapped on the surface and radiating into the newly precipitated quartz in subsequent growth stages. (PPL X40).

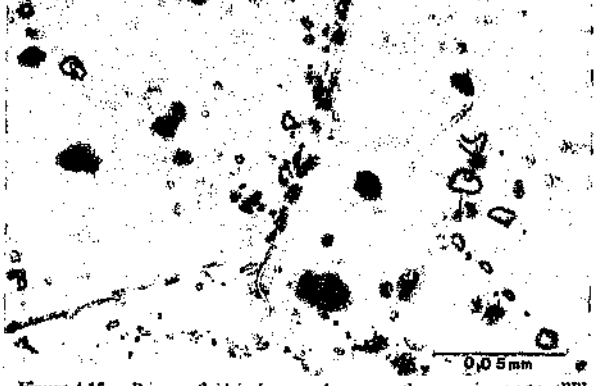


**Figure 4.15** Primary fluid inclusions along growth zones in quartz. (PPL X400).

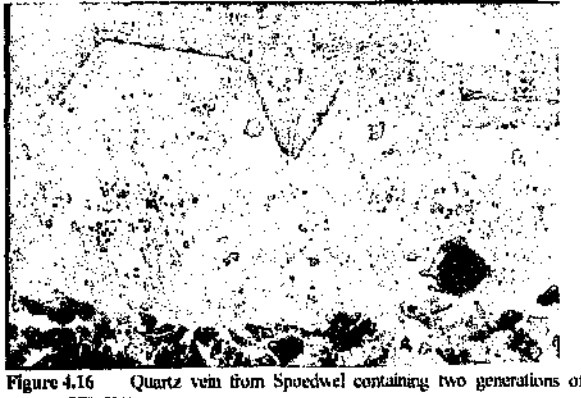

**Figure 4.16** Quartz vein from Spoedwel containing two generations of quartz. (PPL X40).

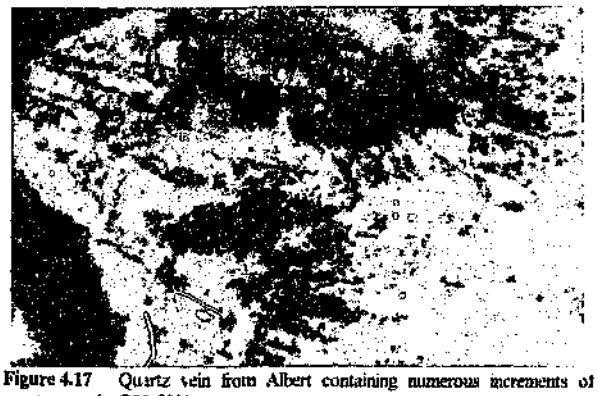

**Figure 4.17** Quartz vein from Albert containing numerous increments of quartz growth. (PPL X40).

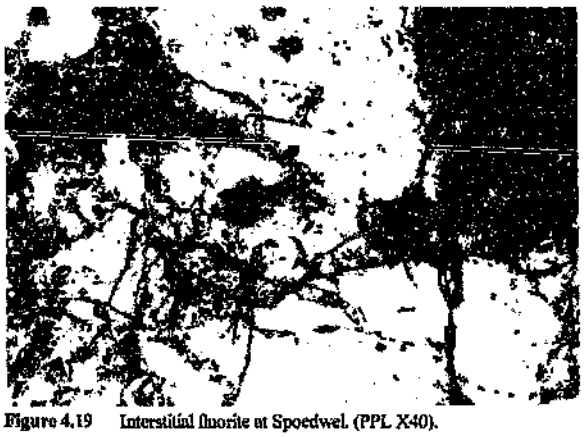

**Figure 4.19** Interstitial fluorite at Spoedwel. (PPL X40).

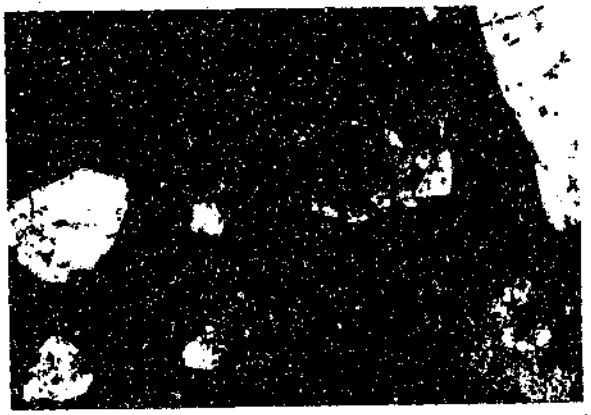

**Figure 4.21** Zircon crystal surrounded by sulphides. Note the internal growth zonation within the zircon crystal. (RL X40).

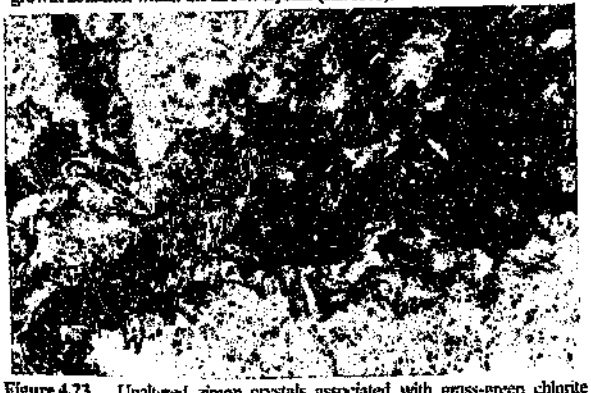

**Figure 4.23** Unaltered zircon crystals associated with grass-green chlorite and sulphide mineralisation. (PPL X100).

**Figure 4.18** Scanned image of vein quartz from Grass Valley containing numerous increments of quartz growth.

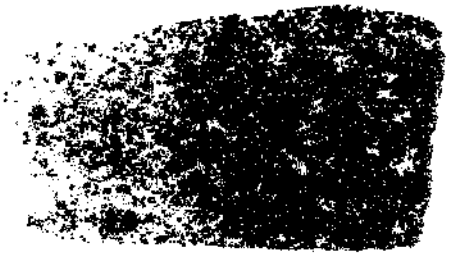

**Figure 4.20** Scanned image of a polished thin section cut through a tourmaline spheroid.

**Figure 4.22** Altered zircon crystals with radiogenic alteration halos in a chlorite matrix. (PPL X40).

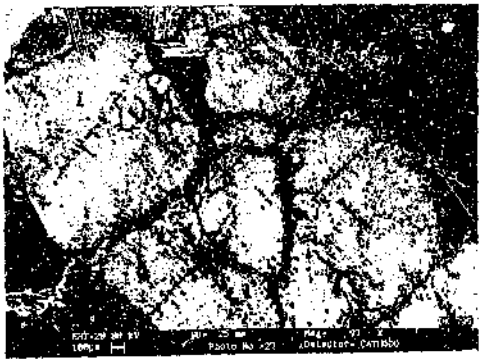

**Figure 4.24** Cathodo-luminescence image of a zoned zircon associated with the third quartz generation at Spoedwel.

The ore minerals are discussed in order of their appearance in the overall paragenetic sequence recognised in the ore deposits. The paragenetic sequence is described in greater detail in section 4.4.

**Cassiterite**

Cassiterite was the first ore mineral to be precipitated from magmatic hydrothermal fluids in the Bushveld Complex. It occurs as an accessory phase disseminated throughout barren granites. However, in certain areas, it has been concentrated into economically viable ore deposits. Cassiterite is the primary ore mineral at Grass Valley, and occurs as well formed crystals of variable dimensions. In the pegmatite, the crystals measure several centimetres in diameter whereas in the granite, they are a few millimetres in diameter. The abundance of cassiterite diminishes at Spoedwel and Dronkfontein, and is quite scarce at Albert.

Small irregular grains and larger euhedral crystals of cassiterite are present in the Spoedwel sections, measuring from 2mm to 10mm in length (Figure 4.25). The cassiterite is commonly observed as small isolated euhedral grains associated with plagioclase and alkali feldspar, either as embayments or interstitial material between crystal boundaries.

As a consequence of alteration, cassiterite, zircon and titanite are distinguished from one another with some difficulty. Under reflected light, cassiterite appears pleochroic light to dark grey, while transmitted light reveals an irregular distribution of dark red, brown and green colours. However, the reflectance of cassiterite (R=11-12%) is greater than that of either zircon or titanite, and cassiterite shows a greater tendency towards being euhedral and zoned.

The association between cassiterite and a fine-grained pleochroic brown generation of chlorite at Spoedwel is shown in Figure 4.13. The chlorite is found along the borders, and filling fractures within the cassiterite crystals. However, no evidence of resorption or embayment of the cassiterite is evident.

**Specularite**

Specularite is fairly abundant in some of the workings at Grass Valley and at Albert. However, at Grass Valley it is an early formed mineral associated with cassiterite (Wagner (1921), while at Albert it occurs as a late-stage mineral associated with the introduction of fluorite and pitchblende (see hematite).

**Molybdenite**

Molybdenite is abundant at Houtenbek, where it occurs in association with early fluorite, sphalerite and late fluorite. It was recognised in one of the workings at Grass Valley, and as small disseminated flakes in one thin section at Spoedwel.

**Arsenopyrite**

Variable amounts of arsenopyrite have been observed in thin section from most of the deposits. Minor amounts of arsenopyrite were recognised at Spoedwel, compared with the relatively large amount at Albert Silver Mine. Thin sections from Grass Valley unfortunately contained no arsenopyrite, but according to Wagner (1921), it is very abundant in the lower portions of the lower levels at Grass Valley. Some discrepancy in the paragenetic position of arsenopyrite at the various deposits seems to exist. According to Wagner (1921), arsenopyrite formed before pyrite at Grass Valley. The same relationship was observed at Spoedwel (Figure 4.26). However, at Albert, Robb *et al.* (1994) reported that arsenopyrite was deposited late in the sulphide paragenetic sequence, occurring after the formation of pyrite, galena and chalcopyrite. On re-examining the paragenesis at Albert, no evidence of this relationship was found, and it appeared that arsenopyrite was deposited before the formation of pyrite, and most certainly before chalcopyrite (Figure 4.27), since the latter two minerals surround euhedral arsenopyrite crystals.

The distinction between arsenopyrite and pyrite is made with some difficulty in most instances where they are not juxtaposed. The arsenopyrite is anisotropic, tends to be whiter in colour and is less scratched by polishing. It occurs as well formed crystals containing no inclusions of other minerals such as galena, sphalerite and chlorite.

**Pyrite**

Pyrite is abundant at all of the deposits. Pyrite is the second most abundant ore mineral visible in polished section at Spoedwel. It occurs in two forms: 1) as idiomorphic, euhedral crystals varying from 5mm to 10mm in diameter. These crystals appear hexagonal in cross-section, although smaller triangular, rectangular and trapezoid crystals are not uncommon, 2) as small rounded grains (usually not greater than 0,5mm in diametre). These small grains have irregular, wavy edges that are embayed by other sulphide and gangue minerals. An intermediate class of pyrite grains has been recognised, where in a single grain, some perfectly euhedral crystal faces have been preserved while others have been resorbed and embayed.

The pyrite crystals and rounded grains are commonly fractured, and replaced or filled by gangue and ore minerals (Figure 4.28). These planes of weakness are exploited by in-filling minerals such as chalcopyrite, chlorite, galena and bornite. The chalcopyrite filling the hairline cracks within the pyrite may be altered to bornite, chalcocite and/or covellite. Growth zoning in the euhedral crystals has been observed where muscovite precipitation has commenced between the two pyrite growth stages (Figure 4.29).

Pyrite is rarely observed as isolated crystals not associated with chalcopyrite. Rather, the pyrite and chalcopyrite are found juxtaposed, with euhedral pyrite crystals surrounded by anhedral masses of chalcopyrite. The accessory minerals cassiterite, titanite and zircon rarely occur adjacent to pyrite crystals. In the sections examined, a single instance was found where pyrite and titanite/leucoxene occur with their straight euhedral crystal faces in contact. Furthermore, cassiterite and pyrite were never found in contact.

**Galena**

At Spoedwel and Albert, galena was precipitated before chalcopyrite. However, at Grass Valley, in some instances it appears earlier than chalcopyrite, and in others later. Galena is readily identified by the characteristic triangular cleavage pits and off-white colour. It is commonly found in association with sphalerite and tetrahedrite/tennantite. At Spoedwel, Albert and Grass Valley, galena occurs as an interstitial phase to other sulphides, notably

pyrite, chalcopyrite and sphalerite. Anhedral galena and recrystallised euhedral to subhedral quartz is found surrounded by chlorite. Galena fills cavities partly resorbing crystal faces of quartz and feldspar. It forms the outermost ore mineral in cavities, lining the cavity walls. Occasionally galena occurs as large masses, almost completely filling cavities or filling veins transecting other sulphide minerals.

Galena, tetrahedrite/tennantite and chalcopyrite also occur in vein form, cutting across dark orange hematised feldspar grains at Spoedwel. At Spoedwel, zones where galena is more abundant, have been observed. These tend to be some distance away from the core of the high grade copper mineralisation, occurring toward the fringes of the deposit.

**Tetrahedrite -Tennantite**

The occurrence of tetrahedrite/tennantite is limited and generally is found only where substantial quantities of galena are present. Galena and tetrahedrite form symplectic intergrowths, and often contain inclusions of chalcopyrite. Tetrahedrite/tennantite is distinguished from galena by its lack of cleavage pits and light-greyish-brown colour, in contrast to the almost white colour of the latter. Tetrahedrite exhibits extensive chemical substitution, often containing Ag, Hg and As. The arsenic end-member is referred to as tennantite $Cu_{10}(Zn, Fe)_2As_4S_{13}$, and is common in porphyry copper mineralisation (Gribble and Hall, 1992). At Spoedwel, the As-rich member, tennantite is present, while at Albert, substitution of Ag has occurred and is referred to as argentiferous tetrahedrite. Tetrahedrite was not recognised at Grass Valley.

**Sphalerite**

Sphalerite was recognised at Albert, Spoedwel, and Grass Valley, occurring immediately before chalcopyrite in the paragenetic sequence. At Grass Valley, Wagner (1921) also recognised instances where sphalerite (together with galena) post-dated chalcopyrite. Large sphalerite crystals are present at Houtenbek, and commonly occur in veins cutting across intensely altered sedimentary rock (leptite) within the deposit. Molybdenite and two fluorite generations also occur within the metamorphosed sedimentary rock. Molybdenite appears to have been deposited before the sphalerite.

Two distinct types of sphalerite have been recognised at Spoedwel. Both have the same appearance under reflected light, showing a dark grey anhedral mass spotted by chalcopyrite blebs. In apparently uniform masses under reflected light, the same uniformity is not observed under transmitted light. Some portions within the sphalerite allow light to pass through the grain while other portions, usually surrounding the anisotropic portions, absorb all the light, resulting in total opacity of the grain.

This phenomenon is a result of the presence of Fe in the crystal lattice. Pure ZnS is transparent and colourless, but when Fe-rich, it appears opaque. Sphalerite has very high relief and is usually yellow to brownish, with dark brown bands due to iron zonation. Oxidation of iron-bearing varieties leads to brown staining, especially in fractures. It is darker than most ore minerals but brighter than gangue minerals. Pure ZnS has abundant internal reflections but, with increasing Fe content, opacity increases and internal reflections become fewer, and brownish or reddish.

The translucent sphalerite occurs as subhedral grains with partially resorbed borders and fractures (Figure 4.30). It contains no galena inclusions. However, cracks within this material are often filled with opaque sphalerite, galena, chalcopyrite and covellite. The isotropic, massive, interstitial, irregular sphalerite with chalcopyrite disease contains inclusions of muscovite and chlorite. It is intimately associated with galena and tetrahedrite.

**Chalcopyrite**

Chalcopyrite is the last of the primary sulphide minerals to be deposited, and is often altered to bornite, chalcocite, and covellite. Chalcopyrite is the most abundant ore mineral in the Spoedwel deposit, filling interstitial spaces between euhedral quartz grains, and filling cracks in gangue minerals and earlier formed ore minerals. It is also the major disseminated ore mineral at Bronkfontein. Chalcopyrite is present at Grass Valley and Albert, but is not the primary ore mineral of these deposits. It was precipitated after the sulphide paragenesis arsenopyrite-pyrite-galena-tetrahedrite/tennantite-sphalerite, and is associated with chlorite and sericite.

Chalcopyrite is intergrown with sphalerite, galena and tetrahedrite/tennantite, filling vugs and cracks, as well as in tiny blebs scattered throughout sphalerite grains. Where chalcopyrite is adjacent to gangue minerals, their borders tend to be resorbed and embayed (Figure 4.31). It is often found together with galena as infiltrations in pyrite (Figure 4.28).

In vugs lined by euhedral feldspar crystals, green chlorite lines the walls and fills most of the cavity while chalcopyrite is found in the central portions forming irregular resorbed or embayed grain contacts, transecting rosettes of green chlorite.

The chalcopyrite at Spoedwel and Albert is altered to bornite, chalcocite, and covellite. Covellite over-printing is pronounced in the high grade ores, particularly at Spoedwel. In contrast, the alteration of chalcopyrite is not well developed at Grass Valley.

**Bornite**

The presence of bornite is minor and has been recognised at Spoedwel, and Albert, but not at Grass Valley. Where present, it is limited to the areas where chalcopyrite is present (Figure 4.32). Digenite and chalcocite form rims on the outer borders of grains containing bornite and chalcopyrite.

**Chalcocite, digenite and covellite**

These three minerals occur together in veinlets traversing chalcopyrite masses. The veinlets appear dark blue owing to the blue colour of all three minerals (Figure 4.33). Covellite overprinting of chalcopyrite is referred to in the section on chalcopyrite.

The covellite exists as little plates or needles in a groundmass of chalcocite or digenite. The covellite flakes, however, are darker than the surrounding material, and shows distinct pleochroism and anisotropism. In some instances, the veinlets are completely composed of covellite. Minor amounts of an isotropic, pale blue mineral accompany the covellite in some veinlets. Although these characteristics match those of chalcocite, it cannot be ruled out that these portions merely represent basal sections of covellite, hence remaining blue and showing no anisotropism.

Both chalcocite and digenite occur in some samples (Figure 4.34). A solid solution exists between chalcocite and digenite and the two are told apart with some difficulty. Digenite is isotropic and has a grey to blueish-grey colour. Covellite, on the other hand is weakly anisotropic and has a lighter blueish grey colour. Furthermore, the reflectance of chalcocite R=33% is greater than digenite R=21%.

**Magnetite**

Magnetite occurs as a primary accessory phase in unaltered granite. The appearance of secondary magnetite is erratic, and appears locally, associated with the final stages of the paragenetic sequence where hematite, quartz and fluorite are abundant. The magnetite may occur as euhedral crystals in a quartz (Figure 4.35) or fluorite matrix (Figure 4.36) or as tongues in the coarse-grained transsolvus granites near the Klipkloof-Nebo Granite contact. The magnetite is partially oxidised to hematite. The name martite is applied where magnetite has been pseudomorphed by an intergrowth of hematite. Magnetite pseudomorphs after chlorite and muscovite have been observed locally in hypersolvus granites (Figure 4.37).

**Hematite**

Hematite schillers in the perthite crystals lend a brick-red or orange colour to the feldspars in the granite. Hematitisation of the feldspars is complete in some grains and patchy in others. Partial albitisation of perthite grains is responsible for the incomplete hematisation shown by some grains (Figure 4.38). The hematite plates follow the trend of the exsolution lamellae in the perthite, and hence producing a straight fabric to the individual grains. In some hematitised feldspar, the twin lamellae (Carlsbad twins) have been obliterated and replaced by a granular texture that goes into extinction with rotation of the stage. Other crystals still show twinning behaviour; the hematite schillers and the respective twin lamellae go into extinction simultaneously.

In sections where albitisation of the perthites is extensive, the hematite liberated from the perthite lattice occurs as rims around the individual grains and along fractures within the grains (Figure 4.39). Hematite also appears as veinlets or stringers cutting across the hematitised perthite crystals.

At Grass Valley and at Albert, large scale hematite (specularite) veins cut across the ore body, while at Spoedwel smaller scale hematite veins are present. Hematite fills the central portions of late stage quartz veins and is associated with a generation of fluid inclusions consisting almost entirely of carbon dioxide.

**Limonite**

Limonite consists of goethite and lepidocrocite with absorbed water. Goethite is associated with late stage brecciation of the host rock and occurs in the quartz filling fractures and the adjacent perthite crystals. It has a very dark red to blackish-brown colour and is present as stingers and alteration halos around iron-bearing sulphide minerals such as pyrite and chalcopyrite. The colour of the limonite is variable; in some instances it appears yellow with tinges of brown (Figure 4.40) while in others it is bright orange with red flecks.

**Other minerals**

In addition to the major minerals described above, several subsidiary minerals observed by Wagner (1921), Champion (1970) and Robb *et al.* (1994) are named below for the sake of completeness. Those present at Grass Valley are scheelite, wolframite, Eiserham, bismuthinite, galeno-bismuthinite, tungstite, cuprotungstite, scorodite, malachite, azurite, and chalcanthite. Those present at Albert are argentite and a Pb-Bi-sulphosalt.

**Figure 4.25** Disseminated cassiterite from Spoedwel associated with later stage sulphide specks (PPL X100).

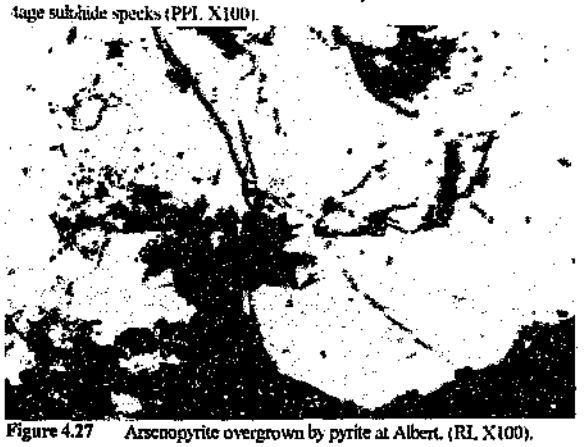

**Figure 4.27** Arsenopyrite overgrown by pyrite at Albert. (RL X100).

**Figure 4.29** Microphotograph of pyrite (opaque) showing two growth stages separated by muscovite and albite precipitation (PPL X200).

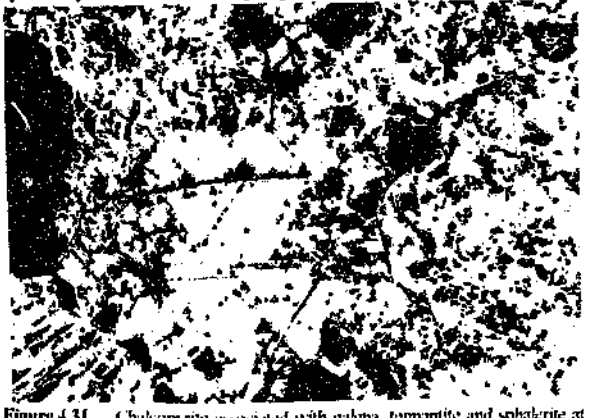

**Figure 4.31** Chalcopyrite associated with galena, tennantite and sphalerite at Spoedwel (RL X100).

**Figure 4.26** Arsenopyrite overgrown by pyrite from Spoedwel. (RL X100).

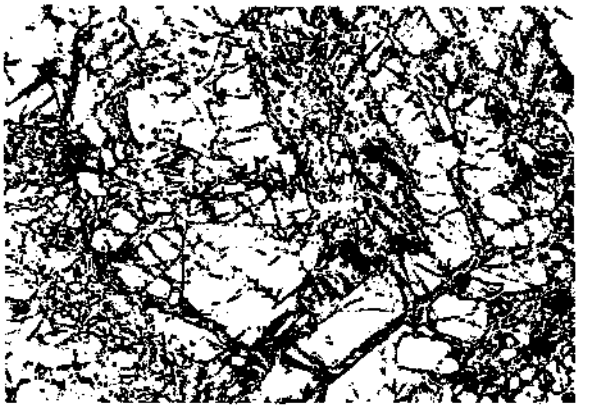

**Figure 4.28** Euhedral pyrite crystal fractured and ...ed by galena and chalcopyrite. (RL X100).

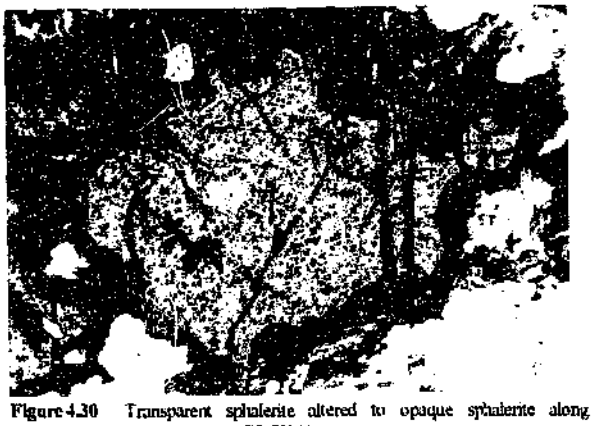

**Figure 4.30** Transparent sphalerite altered to opaque sphalerite along fractures and grain boundaries. (RL X100).

**Figure 4.32** Chalcopyrite from Spoedwel altered to bornite and chalcocite (RL X100).

**Figure 4.33** Chalcopyrite from Spoedwel altered to covellite along fractures and grain boundaries. (RL X100).

**Figure 4.34** Chalcocite, digenite and covellite completely replace chalcopyrite (RL X100).

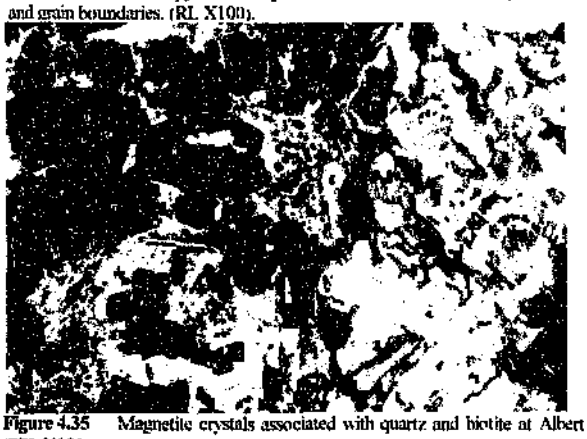

**Figure 4.35** Magnetite crystals associated with quartz and biotite at Albert (PPL X100).

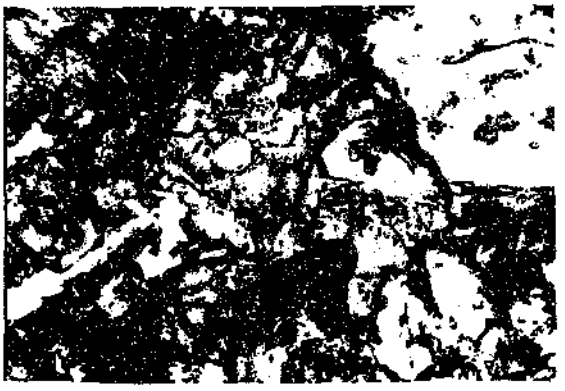

**Figure 4.36** Magnetite crystals associated with fluorite at Albert (PPL X100).

**Figure 4.37** Magnetite pseudomorphs after muscovite in Nebo granite at Spoedwel (Backscatter image).

**Figure 4.38** Hematitised perthite crystals showing partial albitisation (XPL X200).

**Figure 4.39** Hematite liberated from the perthite lattice occurs as rims around the individual grains and along fractures within the grains (PPL X100).

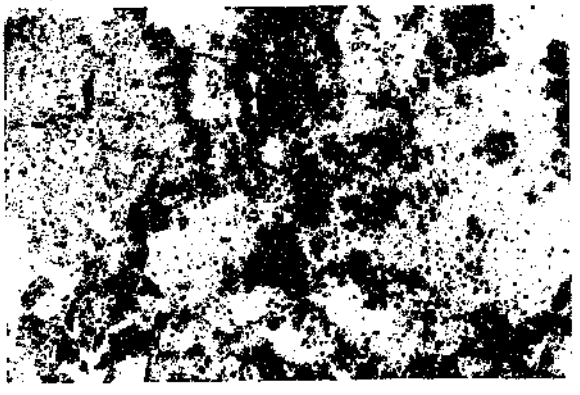

**Figure 4.40** Limonite staining associated with oxidation and hydration of Fe-bearing minerals.

## 4.5 PARAGENETIC SEQUENCE

The paragenetic sequence of ore minerals has been presented in the preceding section describing the occurrence of the different minerals. It appears that the overall paragenetic sequence at each of the deposits is similar, with some minor variations. The paragenetic sequence as described by Wagner (1921) for the Mutue Fides-Stavoren Tin Field, in which the Grass Valley deposit is situated, is shown in Table 4.1. The paragenetic sequence has been divided into three major phases with subdivisions, namely the Pneumatolytic phase, the Hydrothermal Phase, and the Phase of Alteration. This paragenetic sequence broadly compares with the sequences recorded at the Spoedwel and Albert deposits in this study. At Albert and Spoedwel, the minerals associated with the first phase of mineralisation are not well represented, but the assemblages of the Hydrothermal and Alteration Phases are abundant. Variations in the paragenetic position of certain minerals at Albert were recognised by Robb *et al.* (1994). In particular, arsenopyrite was placed after chalcopyrite in the paragenetic sequence and no early generation was observed. This was not the case at Spoedwel, where the position of arsenopyrite is the same as at Grass Valley. It is possible that a second generation of arsenopyrite was recognised by Robb *et al.* (1994). Furthermore, although minor amounts of galena and sphalerite precede chalcopyrite at Grass Valley, the paragenetic position of the bulk of the galena and sphalerite was recorded by Wagner (1921) as occurring after chalcopyrite, in contrast with Spoedwel and Albert, where galena and sphalerite were deposited before chalcopyrite.

In Chapter 3, it was mentioned that similarities between the Bushveld Complex and the Olympic Dam deposit in South Australia were responsible for stimulating the exploration efforts in the Bushveld granites, and it is worth comparing the parageneses of this deposit with that determined for mineralisation in the Bushveld.

Three mineral association have been recognised at Olympic Dam. The early magnetite (± hematite), chlorite, sericite, siderite, and minor pyrite, chalcopyrite and uraninite (association I) is extensively overprinted by hematite, sericite, chalcocite, bornite, pitchblende, barite, fluorite, and chlorite (association II). The paragenetically latest major mineral association consists of hematite, or hematite + granular quartz ± barite (association III). All three mineral associations display complex overlapping and indistinct boundaries.

Rock relations, breccia textures, ore mineral textures, and mineral parageneses provide evidence of repetitive brecciation and mineralisation events, indicating that ore genesis was complex and multistage (Haynes *et al.*,1995).

**Table 4.1** Summary of the paragenetic sequence at Grass Valley (after Wagner, 1921).

| Phase | Assemblage | Prevailing temperature, T |
|---|---|---|
| **Pegmatitic or Primary Pneumatolytic Phase** | Deposition of pegmatitic feldspar and quartz, or pegmatitic feldspar alone. | About 575 °C |
| **Secondary Pneumatolytic Phase** | *Stage 1* - Deposition of raven-mica (biotite), quartz and probably tourmaline.<br>*Stage 2* - Deposition of specularite, cassiterite, wolframite, scheelite, arsenopyrite and fluor-apatite. | 358 °C <T<575 °C |
| **Early hydrothermal Phase** | Deposition of chlorite, sericite, quartz, pyrite, chalcopyrite, some fluorite, and probably bismuthinite. | |
| **Late hydrothermal Phase** | Deposition of galena, sphalerite, fluorite, ankerite, calcite, quartz, chlorite and probably secondary scheelite. | About 150 °C |
| **Phase of Alteration by cold descending Meteoric Waters** | Formation of chalcocite, covellite, copper oxides, bismutite, tungstite, cerussite, martite, limonite, kaolin and secondary chlorite. | Ordinary atmospheric temperature |

The paragenetic sequence at Olympic Dam shows several similarities with polymetallic mineralisation in the Bushveld granites. Firstly, the three-fold subdivision at Olympic Dam (Associations I, II and III) is also present in the Bushveld. The earliest subdivision was put forward by Wagner (1921) where Pneumatolytic, Hydrothermal and Alteration phases

were recognised in the Mutue Fides-Stavoren tin fields. Smits (1980) recognised a similar three stage division in the paragenesis at the Boschhoek copper deposit, and referred to them as the Early, Main and Late Stages of mineralisation (see Chapter 3).

As discussed above, the classification of Wagner (1921) for mineralisation at Grass Valley, compares favourably with the scheme proposed in this study for Grass Valley, Spoedwel and Albert (Figures 4.41, 4.42 and 4.43). Some of the discrepancies in paragenetic sequences between these deposits may be explained by considering the paragenetic sequence proposed by Smits (1980) at Boschhoek. Smits (1980) recognised multiple generations of pyrite, bismuthinite, galena, sphalerite, quartz and siderite This may explain the varying positions of galena and sphalerite in the paragenetic sequence at Grass Valley, Albert and Spoedwel, since no distinction was made between different generations of these minerals.

Comparing the mineral assemblages of the different stages of mineralisation at Olympic Dam with that at Boschhoek, Grass Valley, Albert and Spoedwel, some striking similarities are obvious. Association I at Olympic Dam correlates with the Early Stage at Boschhoek, where the presence of siderite, hematite/magnetite/marcasite and pyrite seem to be characteristic. The Main and Late Stages at Boschhoek differ from Associations II and II at Olympic Dam. They also differ from the three subdivisions created in this study for mineralisation at Grass Valley, Spoedwel and Albert. Association I is not present at Grass Valley, Spoedwel and Albert. Stage 1 at these deposits is represented by the specularite-cassiterite-wolframite-molybdenite-scheelite-arsenopyrite-fluorapatite assemblage, which is not represented at Olympic Dam. The main episode of sulphide mineralisation in the Bushveld occurred in Stage 2. Alteration of this assemblage is associated with the introduction of the hematite-fluorite-pitchblende assemblage, and correlates with Association II at Olympic Dam.

Thus, it can be concluded that, although of smaller scale, mineralisation in the Bushveld granites is somewhat similar to that at Olympic Dam, not only in terms of the geological setting, but also in terms of the observed paragenetic sequence.

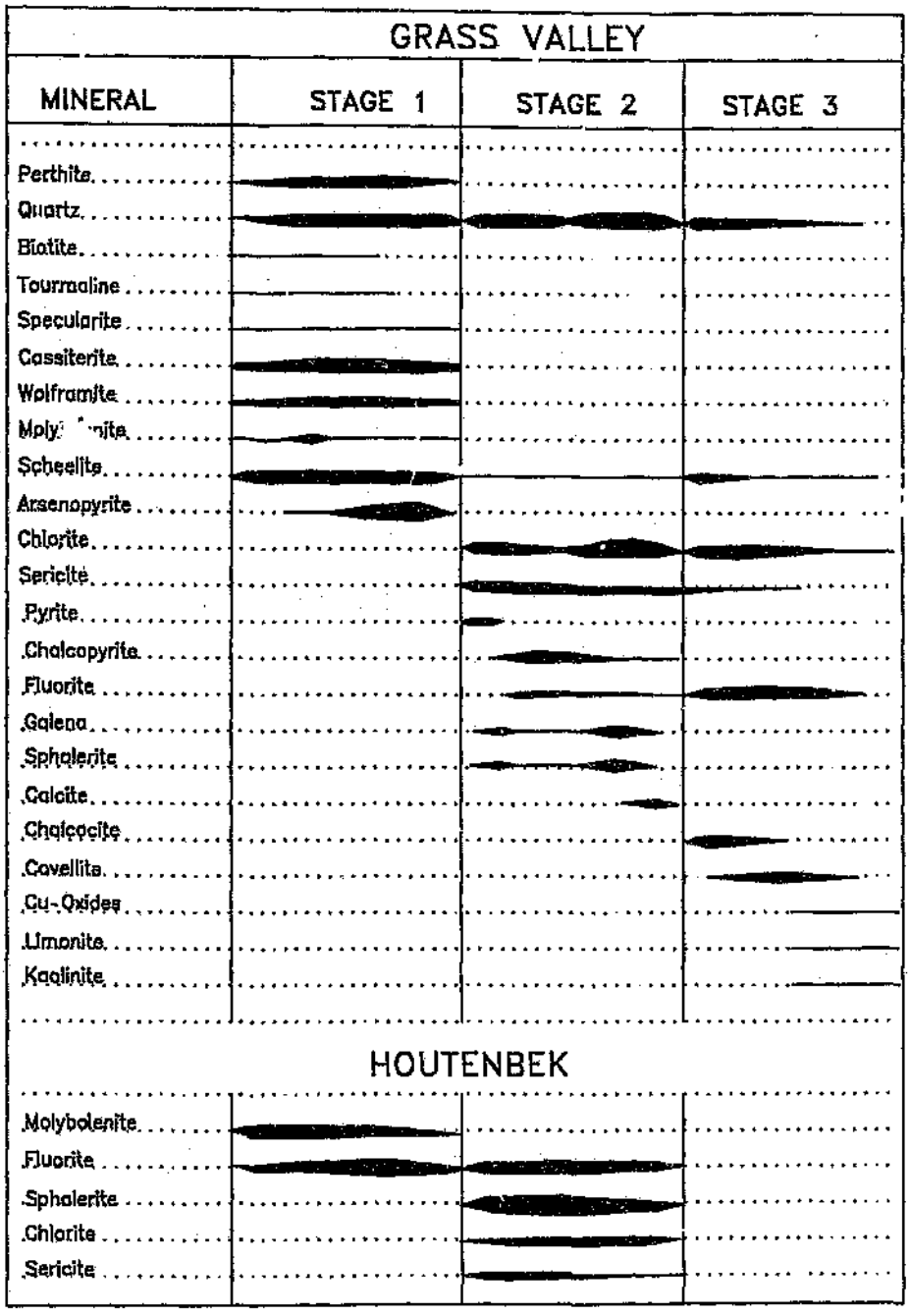


**Figure 4.41.** Paragenetic sequences at Grass Valley and Houtenbek.

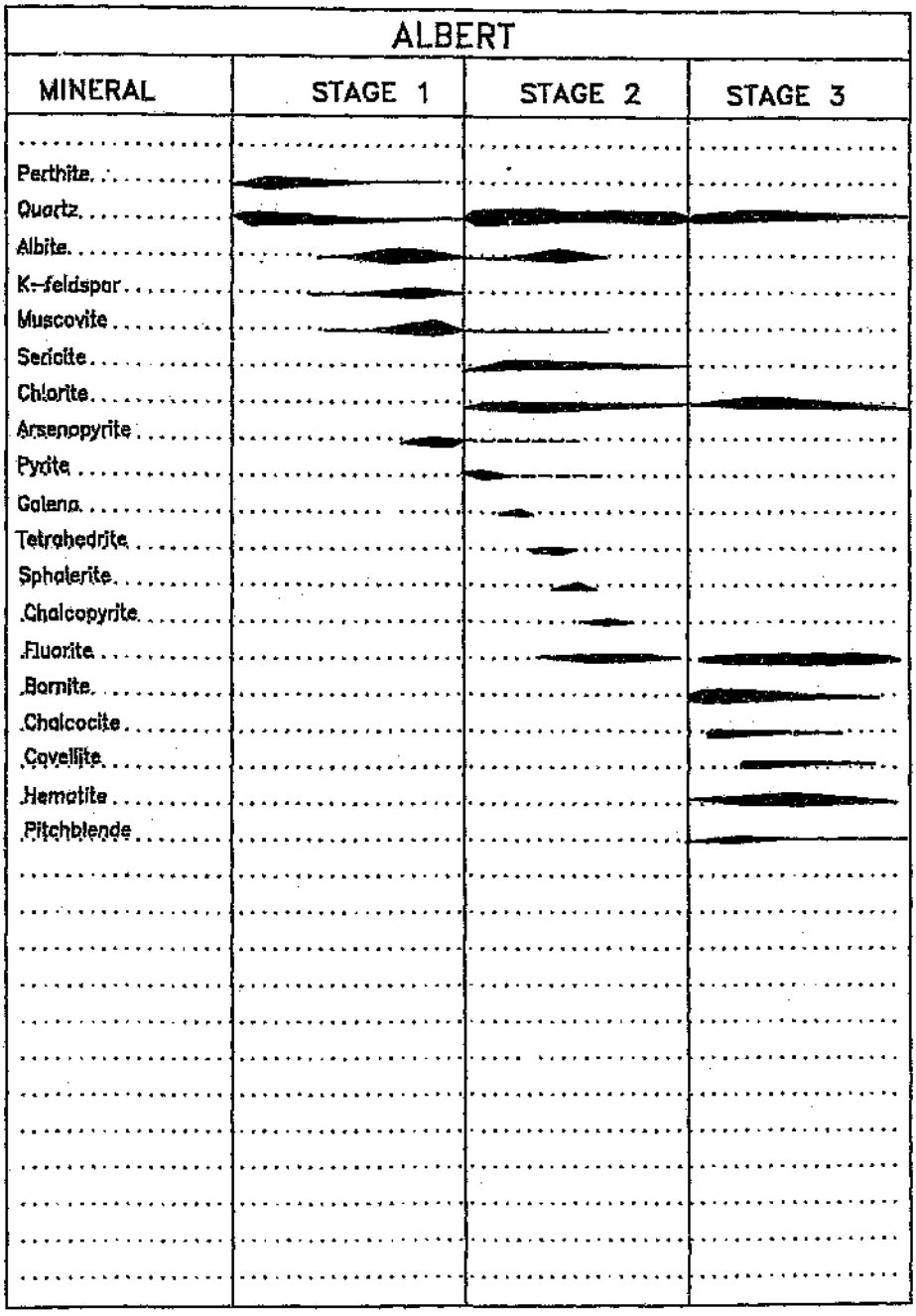


**Figure 4.42** Paragenetic sequence at Albert.

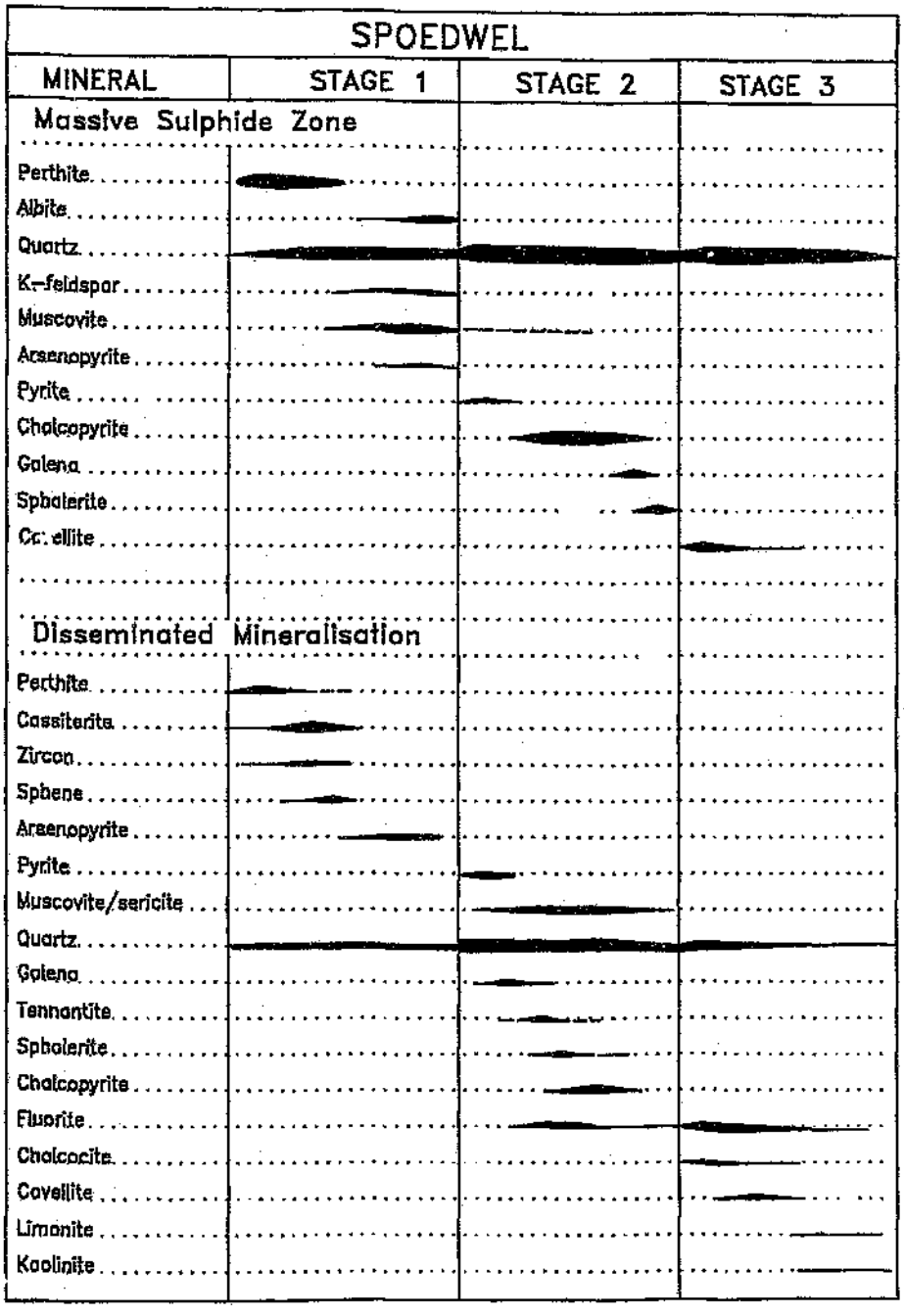


**Figure 4.43** Paragenetic sequence in the zones of massive sulphide and disseminated mineralisation at Spoedwel

## 4.6 ALTERATION

Alteration is an integral part of each of the deposits studied. The minerals and assemblages provide useful insights into the processes of mineralisation and the consequent overprinting of alteration minerals on existing ore and gangue minerals. This section deals with the types of alteration, alteration assemblages and their significance.

### *ALTERATION ASSEMBLAGES*

An alteration assemblage refers to a set of minerals that grew in equilibrium with one another during the hydrothermal process. At the Spoedwel, Grass Valley and Albert deposits, several such assemblages have been recognised, each defining a characteristic alteration assemblage, as proposed by Meyer and Hemley (1967) and discussed in detail in Barnes (1967) and Guilbert and Park (1986).

#### Advanced Argillic Alteration

According to Meyer and Hemley (1967), this type of alteration represents extreme hydrolytic base-leaching from all aluminous phases. Guilbert and Park (1986) report that it represents low $K^+/H^+$ and $Na^+/H^+$ by low activities of the alkalis and strongly acidic, high $H^+$ fluids. The resultant assemblages are characterised by dickite, kaolinite, pyrophyllite, sericite, quartz, alunite, pyrite, tourmaline, topaz, zuynite, and amorphous clays (Meyer and Hemley, 1967). This type of alteration is evident at Spoedwel and Albert, where alteration of chalcopyrite to covellite and digenite is pronounced, and where alteration of the feldspars has produced gangue minerals such as kaolinite, sericite, quartz, alunite, and tourmaline. At Leeufontein, the presence of tourmaline veins and spheroids, which are developed along fracture zones, is indicative of this type of alteration.

#### Phyllic or Sericitic Alteration

The assemblage, sericite-quartz-pyrite is the most abundant of all the alteration types. At Albert and Spoedwel, sericitic alteration is the predominant type associated with mineralisation, while, at Grass Valley, although it is pronounced, it is somewhat less abundant. Normal accessories include chlorite, rutile/leucoxene, and titanite.

**Propyllitic Alteration**

Propyllitic assemblages are characterised by epidote and chlorite, and include albite, septechlorite, and carbonate, commonly with sericite, pyrite, or Fe-oxides

**Chloritisation**

The alteration of feldspars, notably K-feldspar perthite to chlorite, is common in the granites hosting mineralisation. Chlorite is also present as masses of well-formed rosettes, associated with the sulphide mineralisation at both Albert and Spoedwel. The extent of chloritisation of the host granite is variable; in extreme cases, the original minerals are obliterated. Compositional variations have also been noted. Fe-rich grass green varieties tend to be associated with the sulphide assemblage, whereas Fe-deficient brown chlorites are associated with orthomagmatic tin deposition.

Since there is a marked absence of hornblende and biotite at Spoedwel and copious amounts of a variety of chlorites, it is probable that the original hornblende and /or biotite grains have been altered to chlorite. The subsolvus granites in particular have localised zones of extreme chloritisation of the plagioclase crystals. This type of alteration is not observed in the hypersolvus granites well removed from the sulphide mineralisation.

**Albitisation**

Albitisation occurs in patches within the fine-grained Klipkloof Granites in the area east of Marble Hall, as well as associated with the mineralisation at Albert, Spoedwel and Grass Valley. It is manifested in several forms, viz. as partial replacements in perthite, as secondary overgrowth on albite crystals of the subsolvus Verena Granite, and as complete replacement pockets in fine-grained Klipkloof Granite, where it is referred to as Albitised Klipkloof Granite. Albitisation is not associated with the introduction of sulphides, but is commonly accompanied by Fe-oxides. This relationship is evident at Albert where vast amounts of secondary albite and hematite has been precipitated.

**Potassic Alteration**

Potassic alteration involves the presence of introduced or recrystallised K-feldspar in a rock with or without biotite and sericite, commonly with traces of anhydrite, apatite, thorite, calcite, scheelite, chalcopyrite, molybdenite, pyrite, magnetite, or hematite.

This assemblage is present at all the ore deposits studied, and is associated with the subsolvus granites. At Spoedwel, the hypersolvus granites were composed primarily of K-feldspar, which subsequently became hydrothermally altered by the fluids associated with the subsolvus granite. The introduction of secondary K-feldspar is associated with the crystallisation of the subsolvus granite. The secondary K-feldspar is in equilibrium with muscovite (sericite). Biotite is limited to the highly differentiated pegmatitic and aplitic portions of the intrusion. In contrast, the subsolvus Verena Granites which host mineralisation at Albert contain significant amounts of biotite disseminated thought the rock. Biotite is scarce in the Grass Valley deposit and occurs associated with hematite as specks and patches in Albitised Klipkloof Granite.

Potassic alteration played a major role in the mineralising process, particularly during the introduction of the sulphide paragenesis, and suggests high $K^+/H^+$ conditions at the time.

*ALTERATION REACTIONS*

The chemical processes identified as being responsible for the observed alteration are the following:

1) hydrolysis
2) hydration-dehydration
3) alkali or alkali-earth metasomatism
4) silicification
5) oxidation-reduction
6) sulphidation

**Hydrolysis ($H^+$ metasomatism)**

Examination of the alteration minerals suggests that hydrolysis was a major contributor to the evolution of the wall rock and fluid composition. Hydrolysis reactions involve $H^+$, and hence have a large influence on the pH of the fluids. Buffering of pH by the conversion of anhydrous silicates like feldspars to hydrolysed silicates like mica and clay minerals has a pronounced effect on the solubility and association-dissociation relationships (Guilbert and Park, 1986).

The consumption of $H^+$ to alter the feldspar to muscovite affects the pH of the fluid and the degree of dissociation of the hydrogen containing complexes, such as HCl. As a consequence the degree of associatic ~f NaCl and KCl and metal chloride complexes and the solubility of metals in solution is affected.

Apart from consuming $H^+$ in reactions like

$3KAlSi_3O_8 + 2H^+_{(aq)} \leftrightarrow KAl_3Si_3O_{10}(OH)_2 + 6SiO_2 + 2K^+(aq)$

K-feldspar Muscovite

(Sericite)

$H^+$ ions may be liberated by reactions between metals and $(HS)^-$ to produce sulphides. Thus, hydrolysis controls the stability of the feldspars, micas and clays, as well as the transfer of ions like $K^+$, $Na^+$ $Ca^{2+}$ and $Mg^{2+}$ from the rock into solution.

**Hydration**

Evidence of hydration is seen in the supergene alteration of hematite to goethite.

$Fe_2O_3 + 3H_2O \leftrightarrow 2Fe(OH)_3$

Hematite Goethite

**Alkali Earth Metasomatism**

The most important reaction of this type involves the alteration of K-feldspar to chlorite according to the following equation:

$3KAlSi_3O_8 + 6.5\ Mg2^+ \leftrightarrow Mg_{6.5}(Si_3Al)O_{10}(OH)_8 + K^+ + 12H^-$

K-feldspar Chlorite

Alkali earth metasomatism is also responsible for the conversion of K-feldspar to albite during albitisation.

**Silicification**

Silicification involves the addition or production of a quartz-family member. This type of reaction is represented by the simple precipitation of quartz in open pore spaces, and as quartz veins. Several episodes of silicification occurred during the history of the Bushveld granites. The precipitation of late-stage, low temperature chalcedony veins at Grass Valley amongst earlier and later generations of quartz is unusual, and it is not clear what caused this change in the nature of silica.

**Oxidation-reduction**

Oxidation-reduction reactions are particularly important at Spoedwel since it is primarily an Fe-Cu deposit. These reactions affect ferrous-ferric iron and sulphur mineralogies. For example,

$4Fe_3O_4 + O_2 \leftrightarrow 6Fe_2O_3$

Magnetite Hematite

$2\ KFe_3AlSi_3O_{10}(OH)_2 + O_2 \leftrightarrow 2KAlSi_3O_8 + 2Fe_2O_3 + 2H_20$

Ferrous iron biotite K-feldspar Magnetite

**Sulphidation**

These reactions are also likely to have occurred at the deposits since the products of this reaction are abundant, although the reactants are absent.

$2\ KFe_3AlSi_3O_{10}(OH)_2 + 6S_2 \leftrightarrow 2KAlSi_3O_8 + 6FeS_2 + 2H_20 + 3O_2\ (g)$

Ferrous iron biotite K-feldspar Pyrite

## 4.7 CONCLUSION

Petrographic studies of the granites in the Leeufontein area, as well as in areas of mineralisation in the eastern lobe of the Bushveld Complex, have elucidated several key factors in understanding the development of the Lebowa Granite Suite and the localisation of mineralisation.

The association of mineralisation with subsolvus granites at Grass Valley, Spoedwel, and Albert is one of the most important points to come out of this petrographic study. In addition, the hypothesis proposed by Martin and Bonin (1976) to explain the hypersolvus-subsolvus granite association involves the concepts of water saturation of the magma, and the incursion of meteoric water. The significance of this is that it lends weight to the model of Kleemann (1985), in which he ascribes the development of the aplitic Klipkloof Granite to volatile enrichment of rest liquids.

Water enrichment probably occurred during the solidification of the Klipkloof Granite, when crystallisation of the pluton was well advanced (Kleemann and Twist, 1989). This statement is verified by mineralogical relationships at Spoedwel. The host granite at Spoedwel is the Nebo Granite, and the petrographical evidence suggests that water saturation occurred during the final stages of the crystallisation of this hypersolvus granite, coinciding with the onset of subsolvus granite crystallisation. Evidence for an influx of water is abundant at the deposits in the eastern lobe of the Bushveld Complex. Muscovitisation, local fusion of perthites, albitisation of feldspar, and precipitation of late albite, suggest that an increase in $P(H_20)$ occurred after partial solidification of the hypersolvus granite. Tensional fracturing resulted in the escape of volatiles, as well as the Klipkloof Granite, which occurs as dykes as sills occupying large scale regional faults. Thus, the fractures form the link between the subsolvus granite, and the metal charged hydrothermal fluids which deposited the complex paragenesis in the Bushveld granites.

The concept of water enrichment of the magma is supported by evidence from Ollila (1981), who conducted a study of the structural state and composition of the alkali feldspars in the Bushveld granites, and found that the alkali feldspars in the Bobbejaankop granite (coarse-grained Klipkloof Granite) exhibit the highest degree of ordering and are

maximum microcline, indicating the lowest thermal state. The alkali feldspars from the Lease Granite (fine-grained Klipkloof Granite) are intermediate microcline, indicating a higher thermal state, or less ordered state, which is due to the rapid cooling rate of this granite (Ollila, 1981). The Nebo (or "Main") Granite alkali feldspars are monoclinic, reflecting a state of greater disorder in the lattice. Ollila (1981) explained this phenomenon as the result of volatile deficiency during initial crystal growth stages, which may have prevented the later development of triclinic alkali feldspars. The variation in the structural state of the alkali feldspars is directly related to the availability of hydrothermal fluids during their cooling history (Parsons, 1978). Thus, the absence of volatiles during the crystallisation of the Nebo Granite is reflected in the monoclinicity of the K-feldspars, even though the rate of cooling was sufficiently slow for the formation of large interlocking crystals. As the degree of fractionation of the host rock increases, the water content of the residual melt increases, causing increased order in the younger K-feldspar crystals. Thus, the higher degree of order in the coarse-grained Klipkloof Granite reflects the increasing water content of the residual melt. This trend would have continued during the formation of the Lease Granite (Fine-grained Klipkloof Granite) were it not for the rapid cooling of this magma (Kleemann and Twist, 1989).

The overall paragenetic sequence suggests that mineralisation took place in three discrete episodes. The first episode of mineralisation resulted in the formation of cassiterite-scheelite-wolframite-molybdenite-specularite and possibly arsenopyrite. The mineralisation is disseminated and formed by processes related to fractional crystallisation of the magma. The second episode of mineralisation is represented by the sulphide paragenesis pyrite-galena-tetrahedrite/tennantite-sphalerite-chalcopyrite. The occurrence of this assemblage is fracture-related, with sizeable deposits located on the flanks of large-scale regional faults. These fracture systems presumably acted as conduits for mineralising fluids. The third episode of mineralisation resulted in the deposition of hematite, pitchblende and large amounts of fluorite. The introduction of this third assemblage along the same fracture systems which localised the sulphide assemblage, resulted in alteration of the sulphides, to secondary minerals such as bornite, chalcocite, digenite, covellite and limonite.

The comparison between granite-hosted mineralisation in the Bushveld and Olympic Dam granites indicates that the geological setting and paragenetic sequences are somewhat

similar. Although the siderite-bearing assemblage, which is recognised as the first association at Olympic Dam, has not been recognised at Houtenbek, Grass Valley, Spoedwel, Dronkfontein and Albert, it is preserved at the Boschhoek copper deposit and was described by Smits (1980). According to Smits (1980), the $CO_2$-rich magmatic gases reacted with $Fe^{2+}$ in the fluids, precipitating siderite and releasing $H^+$. This reaction resulted in a lowering of the fluid pH, which is reflected as a change to silica gangue minerals in the subsequent mineral assemblages.

The excess hydrogen ions caused pervasive sericitisation of the wall rock, liberating metals such as $K^+$, $Na^+$ $Ca^{2+}$ and $Mg^{2+}$ from the wall rock into solution, where they are transported and re-precipitated as alteration minerals such as chlorite, albite and K-feldspar in the propyllitc zone of alteration.

The alteration assemblages associated with the subsolvus granite, and the precipitation of the sulphide assemblage, indicate that the mineralising fluids were not particularly acidic and that high $K^+/H^+$ conditions prevailed at the time. Supergene enrichment of chalcopyrite, tourmalinisation, hematitisation of siderite veins and the presence of hematite veins were interpreted by Smits (1980) as being indicative of the introduction of oxygenated meteoric water along the fractures. In addition, the alteration of feldspar to chlorite and albite, and the oxidation and hydration of sulphides lowered the pH of the fluids considerably, favouring the transport of ferric iron (at pH less than 3). These late-stage fluids were strongly acidic and contained low $K^+/H^+$ and $Na^+/H^+$ ratios. The ferric oxides that form through hydrolysis of $Fe_2O_3$ are highly insoluble in the presence of oxygen and cannot be rehydrated. Thus, iron is transported by highly acidic fluids until it comes into contact with oxygenated ground waters, that are channelled along fractures, after which it is precipitated.

Thus, the alteration assemblages and stages in the paragenetic sequence in the granite-hosted deposits in the Bushveld are, in part, controlled by fluctuations in the pH of the hydrothermal fluids, caused by wall rock alteration, and the introduction of oxidising fluids. These fluids were channelled along fractures in the granite, which served to concentrate and localise polymetallic mineralisation in the Bushveld granites.

# CHAPTER 5

## FLUID INCLUSION PETROGRAPHY AND MICROTHERMOMETRY

The importance of hydrothermal fluids in granite-hosted mineralisation in the eastern Bushveld Complex was recognised during the petrographic study of the granites and selected ore deposits, discussed in Chapter 4. In order to test the hypothesis proposed in Chapter 1, a number of analytical techniques have been selected, the results of which are designed to shed light on the nature of hydrothermal fluids associated with granite crystallisation and mineralisation.

A detailed fluid inclusion study was undertaken in order to determine the nature of the fluids involved at each step of the paragenetic sequence, and, thus, to trace the evolution of the fluids associated with mineralisation. Fluid inclusions store a wealth of information regarding the physical and chemical conditions during the formation of the host minerals, as well as the conditions prevailing after crystallisation has ceased. For this reason, fluid inclusions have been chosen to form the basis of the analytical approach in this study. An outline of the research approach is shown in Figure 5.1. PIXE analysis, Raman spectroscopy and Quadrupole Mass Spectrometry were undertaken (see Chapter 6), in order to quantify the metal and volatile composition of the fluids more accurately than through conventional microthermometric analysis alone. The origin of the fluids was investigated through isotopic analysis of fluid inclusions and quartz (Chapter 7).

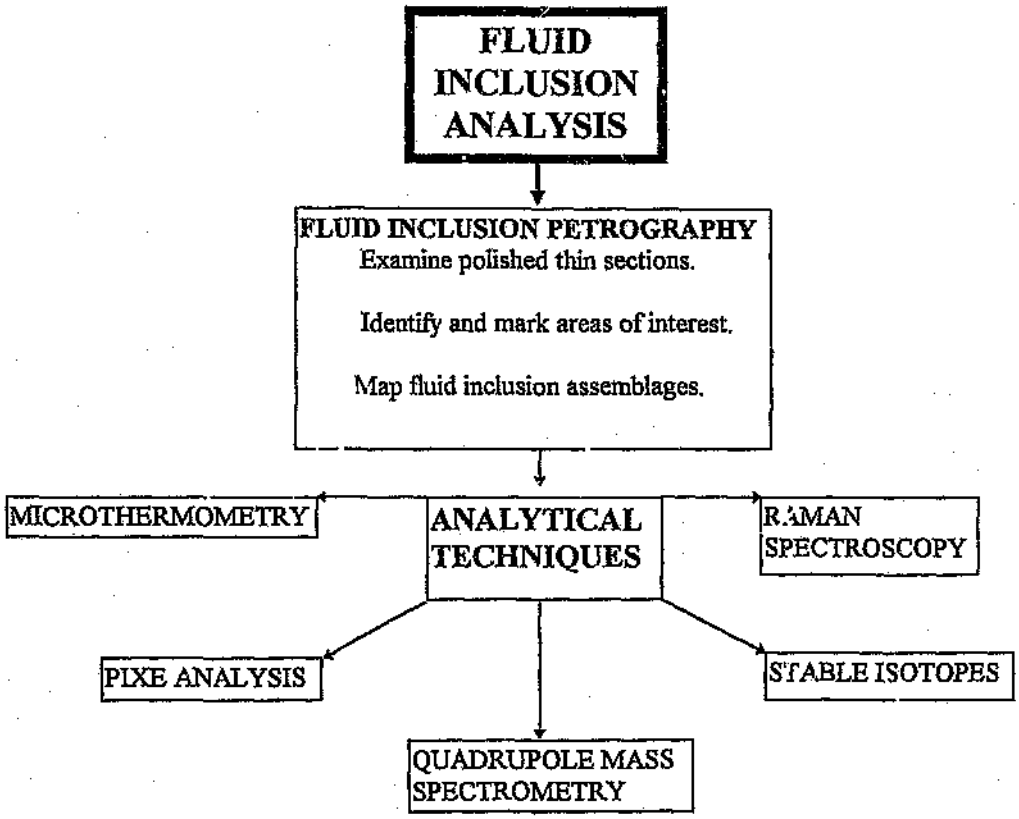


**Figure 5.1** Outline of research approach and analytical techniques employed in order to determine the physical and chemical conditions associated with mineralisation.

## 5.1 FLUID INCLUSIONS AND THEIR APPLICATIONS IN THE STUDY OF ORE DEPOSITS

During the crystallisation of most minerals, minute amounts of the fluid from which the crystal is growing are trapped in small imperfections in the crystal lattice, or along fractures within the crystal. These small fluid-filled cavities (generally smaller than 0.1mm) become sealed during subsequent crystal growth, forming what are referred to as fluid inclusions. Minerals are generally precipitated from hydrothermal fluids at elevated temperatures, and as the cooling proceeds, a number of changes in the fluid inclusion take place, the most obvious change being the appearance of a vapour bubble (Figure 5.2), which forms by differential contraction between the host crystal and the fluid. When the pressure of the inclusion drops below the saturation vapour pressure of the contained fluid at a particular temperature, the fluid splits into two phases - liquid and vapour. The relative amounts of these two [illegible] with the original fluid density. Any volatile species present (such as $H_2O$, $CO_2$ and $CH_4$) is partitioned into the bubble. In some instances, the fluids contain significant amounts of $CO_2$, which if, after being partitioned into the vapour bubble, is sufficiently dense, may split into two phases, i.e. liquid $CO_2$ and vapour $CO_2$. Thus, the fluid inclusion consists of three phases (Figure 5.3).

In addition to the formation of a vapour bubble, upon cooling the fluids often become saturated with respect to certain components, and precipitate solid phases. Since the trapped fluids are saturated with respect to the host mineral (Roedder, 1984), crystallisation of those components occurs on the walls of the inclusion. Other solid phases may also be crystallised within the inclusion, and are referred to as daughter crystals (Figure 5.4). These solids are distinguished from solids which were trapped along with the fluid, and were not precipitated from solution inside the fluid inclusion.

The size and shape of fluid inclusions is controlled by several factors; the crystallography, as well as the rate of cooling and precipitation of the host mineral, are among the most important. The shape of inclusions varies from well-defined euhedral negative crystal outlines which mirror the symmetry of the host crystal, to highly irregular, flattened, spheroidal, oblate or tabular shaped inclusions. Fluid inclusions are rarely observed with the naked eye due to their minute size. Some museum specimens of the largest inclusions

may be as large as a few millimetres, but the typical size range of fluid inclusions suitable for microthermometry is from 3 to 20 microns.

Often more than one generation of fluid may be trapped within a single crystal. Fluids trapped during progressive growth of a crystal are termed primary inclusions (Figure 5.5), whereas inclusions trapped along annealed fractures are referred to as secondary inclusions (Figure 5.6). A third category of inclusions, which occur as secondary trails which have been healed during crystal growth, are called pseudosecondary inclusions. The relationship between primary, secondary and pseudosecondary inclusions is shown in Figure 5.7.

**Figure 5.2** Microphotograph of several quartz-hosted fluid inclusions containing liquid and a vapour bubble, as well as a solid daughter crystal (Magnification X500).

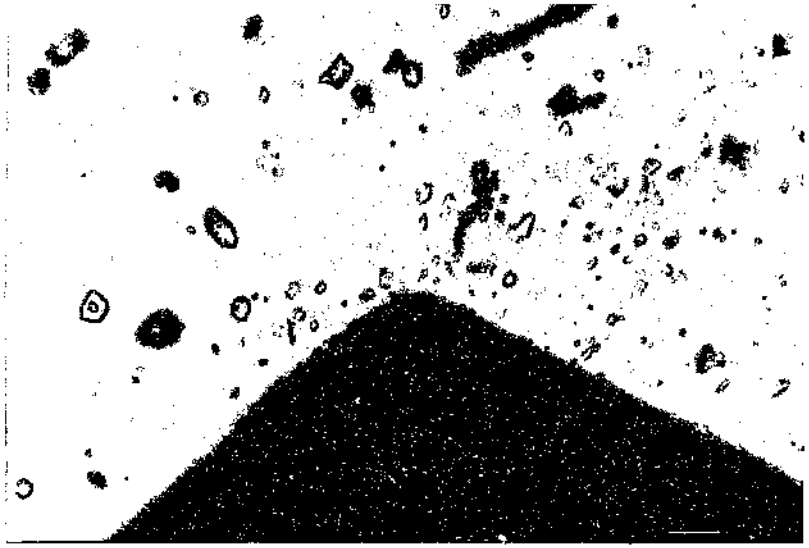

**Figure 5.3** Primary fluid inclusions trapped in quartz overgrowth on a pyrite crystal (Magnification X400).

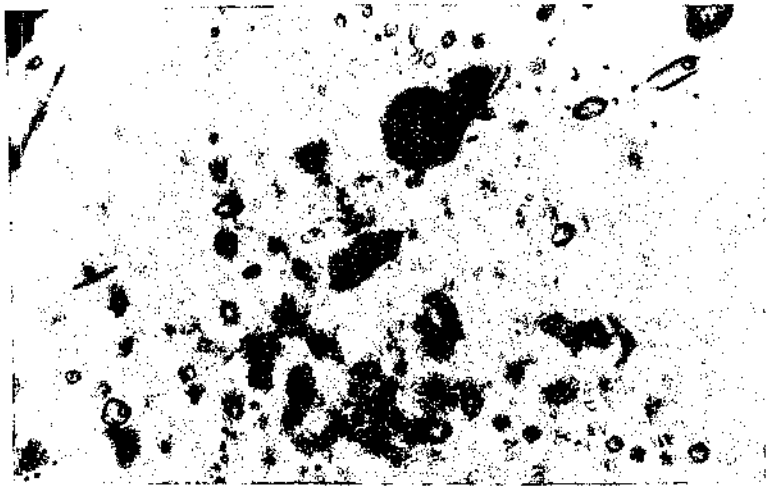

**Figure 5.5** Secondary fluid inclusions along cross-cutting fractures in fluorite (Magnification X400).

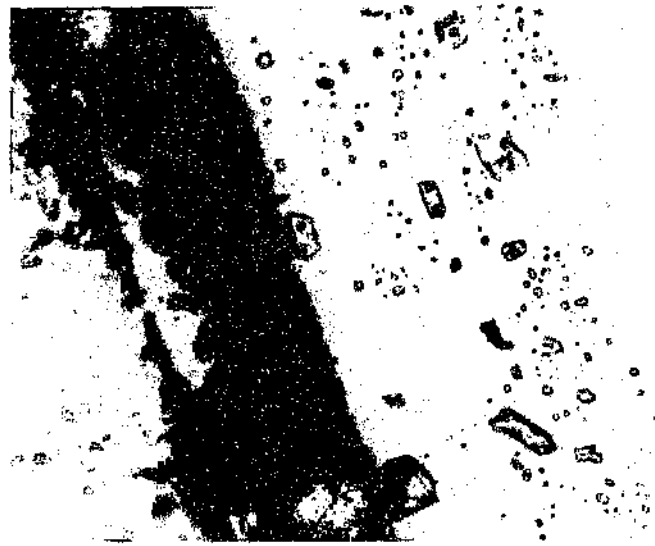

**Figure 5.4** Primary fluid inclusions along a growth zone in quartz. Note that the hematite crystals are not present in all fluid inclusions, and thus may be trapped solids rather than true daughter crystals. (Magnification X400).

**Figure 5.6** Pseudosecondary fluid inclusions trapped along a fracture emanating from the face of an earlier formed crystal and which was annealed during subsequent crystal growth (Magnification X100).

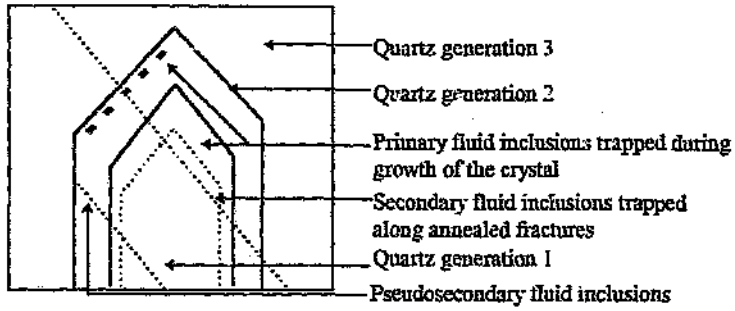


**Figure 5.7** Figure showing primary fluid inclusions (trapped during crystal growth), secondary and pseudosecondary fluid inclusions (trapped along annealed fractures in the crystal).

Fluid inclusions store a wealth of information about processes and conditions associated with mineralisation. Both gangue minerals and ore minerals within ore deposits contain fluid inclusions. Usually the transparent minerals, such as quartz, and fluorite are selected for microthermometry because the fluid inclusions and phase changes are readily visible; however, minerals like sphalerite and cassiterite are often useful. Although poor clarity of the crystal may impede recognition of phase changes, microthermometric measurements of primary inclusions within these minerals provides important information on the conditions during deposition of these ore minerals.

Fluid inclusion microthermometry involves the heating and freezing of the slices of rock with the aid of liquid nitrogen and a microscope, and the observation of phase changes as the inclusion contents respond to the different physical conditions (i.e. change in temperature, pressure and density). Fluid inclusion microthermometry is based on a number of assumptions (Roedder, 1984; Goldstein and Reynolds, 1994). These are listed below:

1) The fluid trapped when the inclusion was sealed was a single homogeneous fluid. If a heterogeneous fluid was trapped then interpretation of microthermometric data is difficult.
2) The cavity in which the fluid is trapped does not change in volume after sealing.
3) The host crystal is impermeable to chemical changes and the inclusion represents a chemically closed (isoplethic) system.

4) The effects of pressure are insignificant, or are known.

5) The origin of the fluid inclusion is known.

6) The determinations of $T_h$ (homogenisation temperature) are not only precise, but accurate.

The temperature, pressure, and density at the time of entrapment, and composition of the fluid are determined by measuring the temperatures of particular phase changes during heating and freezing of the fluid inclusion. These variables control the transitions between the three physical states (solid, liquid and gas), and are depicted in P-V-T diagrams (phase diagrams). The phase changes in the unary system pure $H_2O$ is the foundation on which the more complicated binary, ternary and multi-component systems are based. Figure 5.8 shows the relationship between pressure, volume and temperature, and the corresponding phase changes as cooling of the fluid inclusion proceeds. The natural cooling path of an inclusion may be reversed in the laboratory by heating the inclusion. From F to C, the bubble will gradually shrink and at C the bubble will disappear. The temperature at C is known as the homogenisation temperature ($T_h$).

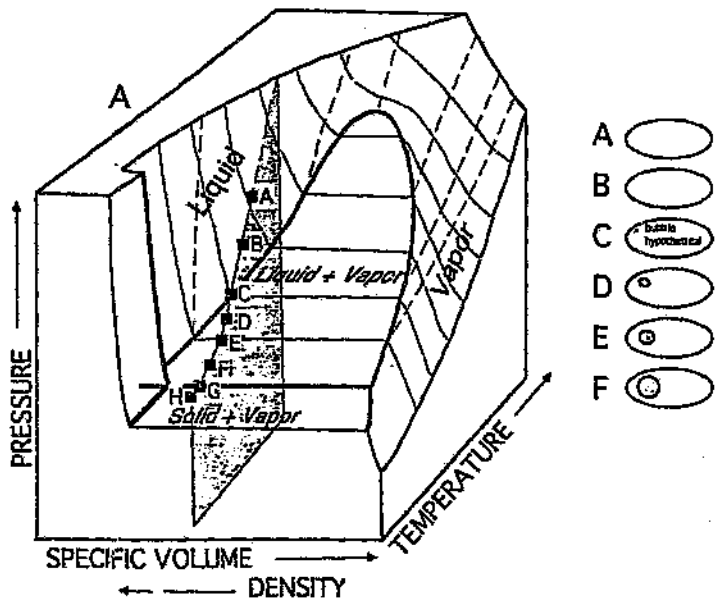


**Figure 5.8** Generalised a 1 schematic P-V-T diagram for the unary system $H_2O$ (from Goldstein and Reynolds, 1994).

In Figure 5.8, the intersections of planes of constant volume with the surface representing stable single-phase equilibria are shown as dashed lines. The intersections of planes of constant temperatures are shown as curved, light solid lines. The surface representing stable two-phase (liquid-vapour) equilibria is delimited by heavy solid lines. The intersection of these surfaces of stable equilibria with a plane of constant specific volume defines a curve known as an isochore. If an inclusion traps a fluid of specific volume (of that shown by the shaded plane) at the P-T conditions at point A, the inclusion will be constrained to the locus of points in P-V-T space by the intersection of the surface of the shaded (constant volume) plane with the surface of the stable equilibria (for cooling A-B-C-D-E-F-G-H is shown). The fluid inclusion sketches schematically show relative proportions of liquid (clear) and vapour (shaded) at the various labelled points shown on the phase diagrams (Goldstein and Reynolds, 1994).

The information obtained from the temperatures of phase changes pertinent to the determination of entrapment temperatures, pressure, density and composition is discussed below.

***TEMPERATURE***

The temperature of formation ($T_t$ or **trapping temperature**) of the host crystal, as well as the temperature of later fluids may be determined indirectly by measuring the **homogenisation temperature** ($T_h$) of primary and secondary fluid inclusion assemblages, respectively. The homogenisation temperature is an estimate of the minimum entrapment temperature of the fluid, and, by applying a pressure correction, the true trapping temperature may be inferred.

In two phase liquid/vapour inclusions, the homogenisation temperature is measured by heating the inclusion until the vapour bubble disappears. This temperature represents the minimum entrapment temperature of the fluid, and the true entrapment temperature may be determined by applying an appropriate pressure correction (see pressure and density).

In three phase inclusions, the temperature at which dissolution of the daughter crystal takes place provides important information of the composition of the fluids, as well as assisting in

the identification of daughter crystals. For example, KCl and NaCl may be distinguished by the temperature at which dissolution occurs. NaCl dissolves at lower temperatures than KCl. This temperature of dissolution is also useful in determining the salinity of the fluids (see Composition). However, some daughter crystals do not melt, even when heated to extremely high temperatures. This may be due to the fact that equilibration was not achieved in the time used to heat the sample, or that the melting point of the crystal was actually at higher temperatures than the temperature of homogenisation of liquid and gas phases. In addition, non-dissolution of daughter crystals may result from necking down, $H_2$ leakage, or the fact that the crystal may be a solid trapped within the inclusion.

The temperature at which the internal pressure of the fluid inclusion exceeds the tensile strength of the host crystal, is referred to as the decrepitation temperature (or $T_{decrepitation}$). At this point the fluid inclusion bursts, and it is assumed that $T_{decrepitation}$ coincides with $T_h$. However, this method of determining entrapment temperature is regarded with some scepticism due to its lack of theoretical basis, and the lack of agreement with actual $T_h$ data in some circumstances (Roedder, 1984).

*PRESSURE AND DENSITY*

Temperature, pressure and density are interrelated. Figure 5.8 shows the relationships between these variables. If a fluid is trapped from a homogeneous fluid along the boiling curve, $T_h = T_t$ and no pressure correction is needed. Such an inclusion would start to form a vapour bubble as soon as it cooled below $T_t$. However, most inclusions are not trapped on the boiling curve, but at some higher temperature and pressure, and a bubble does not form until the pressure and temperature have dropped to the boiling curve conditions. The density remains constant within the inclusion, and is represented by a straight line isochore. The isochore reflects the change in pressure and temperature inside the inclusion. The difference in temperature ($T_t$-$T_h$) is called the "pressure correction", and is actually a temperature correction as a result of pressure. It is calculated by dividing the difference between the pressure of trapping and the internal pressure at homogenisation, by the slope of the isochore originating at the measured temperature and pressure of homogenisation.

i.e. Pressure correction = $(P_t-P_h)/(\Delta P/\Delta T)$

Graphs of pressure corrections at particular temperatures, pressures, and salinities were published by Potter (1977), but are appropriate if the inclusions contain pure NaCl solutions, the salinity has been correctly determined, the estimate of pressure of formation is correct and the inclusion homogenises in the liquid phase. Highly concentrated solutions and those containing $CO_2$ or other gases result in significant errors.

*COMPOSITION*

Most geothermal fluids are not simple $H_2O$ systems, but are complex mixtures of a number of components. The effect of additional components is to shift the liquid phase equilibrium. The model $H_2O$-NaCl system is commonly used to evaluate the final melting temperature of ice and the salinity of the fluid is reported as NaCl salinity equivalent (or eNaCl). According to Goldstein and Reynolds (1994), this approximation is reasonable because comparisons of the cotectic surfaces, where ice melts for various systems, show relatively small variations.

The composition of the fluid may be estimated by measuring a number of phase changes. These are the freezing temperature ($T_{freeze}$), eutectic melting temperature ($T_e$), temperature of intermediate melting events, the final melting temperature ($T_{final\ melting}$), and the temperature of freezing, melting and homogenisation temperature of $CO_2$. The temperature at which the fluid freezes depends on the gaseous component and salinity of the fluids. Fluid inclusions containing methane and nitrogen, as well as high 'ine fluids, freeze at lower temperatures than fluid inclusions containing little in the way of dissolved solutes.

The temperature at which the liquid phase becomes frozen is recorded as the freezing temperature ($T_{freeze}$ or $T_f$). A sudden jerk in the inclusion is observed as the liquid expands on freezing and the vapour bubble becomes distorted. The temperature at which the liquid freezes depends to a large extent on the amount of dissolved solute and the nature of volatiles contained in the fluids. The greater the concentration of ions in solution, the lower the freezing temperature. In addition, the presence of $N_2$, $CH_4$ and $CO_2$ depress the freezing point further. The physical appearance of the frozen solid can also provide information on the fluid character. Fluids containing $CaCl_2$ and/or $MgCl_2$ develop a brown-coloured mosaic of crystals which is easily distinguished from the colourless mosaic produced by solutions containing NaCl, and KCl.

The eutectic, or initial melting temperature (Table 5.1), provides a good indication of the major ions in solution and, thus, the appropriate chemical system to be used in interpretation of microthermometric data. These phase changes are useful in identifying the phases involved in intermediate melting events, and thus assist in choosing a chemical system which includes most of the major ions in solution.

**Table 5.1** Eutectic temperatures for various chemical systems. (From Sheppard *et al.* (1985) and * Reynolds (1991).

| CHEMICAL SYSTEM | EUTECTIC TEMPERATURE ($^{o}$C) |
|---|---|
| NaCl | -21.2* |
| KCl | -10.6* |
| $CaCl_2$ | -49.8* |
| $MgCl_2$ | -33.6* |
| NaCl-KCl | -22.9* |
| NaCl-$CaCl_2$ | -52.0* |
| NaCl-$MgCl_2$ | -35.0* |
| $H_2O$-$MgCl_2$-$CaCl_2$ | -52.2 |
| $H_2O$-NaCl-$CaCl_2$ | -55 (-52) |
| $H_2O$-KCl-$CaCl_2$ | -50.5 |
| $H_2O$-$CaCl_2$ | -49.5 |
| $H_2O$-$Na_2CO_3$-$K_2CO_3$ | -37.0 |
| $H_2O$-$FeCl_2$ | -35.0 |
| $H_2O$-NaCl-$MgCl_2$ | -35.0 |
| $H_2O$-$MgCl_2$ | -33.6 |
| $H_2O$-NaCl-KCl | -23.5 (-22.9) |
| $H_2O$-NaCl-$Na_2SO_4$ | -21.7 |
| $H_2O$-NaCl-$NaHCO_3$ | -21.8 |
| $H_2O$-NaCl-$NaCO_3$ | -21.4 |
| $H_2O$-NaCl | -21.2 (-20.8) |
| $H_2O$-KCl | -10.6 |
| $H_2O$-$NaHCO_3$-$Na_2CO_3$ | -3.3 |
| $H_2O$-$NaHCO_3$ | -2.3 |
| $H_2O$-$Na_2CO_3$ | -2.1 |
| $H_2O$-$Na_2SO_4$ | -1.2 |

The temperature at which the last frozen solid melts is referred to as the final melting temperature ($T_{\text{final melting}}$). The phase changes in simple systems such as NaCl-$H_2O$ (Figure 5.9) or NaCl-KCl -$H_2O$, and in more complicated systems such as those in Table 5.1, are interpreted using phase diagrams which translate the final melting temperature into a salinity value. This phase change usually occurs at temperatures below 0°C, and is dependent on the composition of the fluids. In systems where $CO_2$ is a component of the fluid, gas hydrates (or clathrates) are formed, which resist melting until temperatures between 0 and 10°C. The final melting temperature of these clathrates is used to estimate the salinity of the fluids.

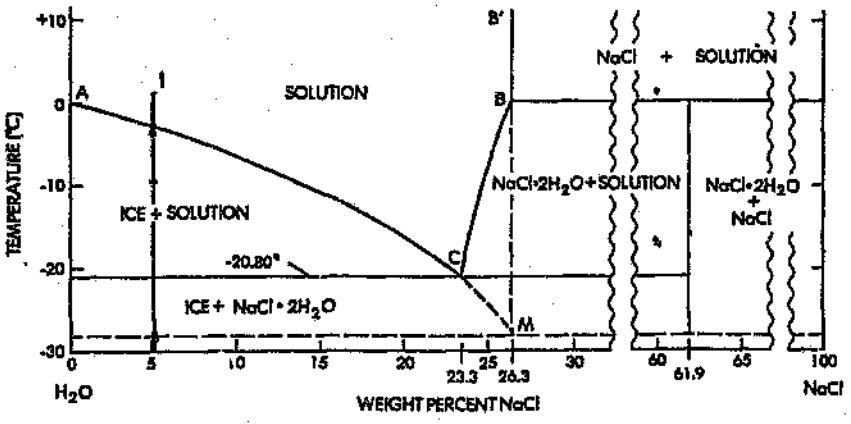


**Figure 5.9** T-X plot for the low temperature part of the NaCl-$H_2O$ system, in equilibrium with vapour at 1bar total pressure (Roedder, 1962).

## 5.2 FLUID INCLUSIONS IN THE BUSHVELD GRANITES

### *PREVIOUS WORK*

The description of a large moving bubble in a fluid inclusion within quartz by Robert Boyle (1672) sparked the interest of several naturalists in the eighteenth century, and resulted in numerous reports on the nature of trapped fluids. However, the first analytical work to establish the composition of specific inclusions was published only in the early nineteenth century. Among the pioneers in this field of study were Sorby (1858), Zirkel (1870) and Phillips (1875).

Advances in the understanding of the behaviour and significance of fluid inclusions has facilitated several in depth investigations into the nature of magmatic and hydrothermal fluids, as well as meteoric fluids, in a wide range of geological environments. The role of fluid phases in sedimentary, diagenetic, metamorphic and magmatic processes (Roedder, 1979a, 1984; Bodnar & Beane, 1980) has received considerable attention in recent years.

The study of fluid inclusions in the Bushveld granites is relatively new. In 1981, J.T. Ollila published a comparative study of the fluid inclusion data from three tin mining areas: 1) Zaaiplaats, 2) Rooiberg-Leeuwpoort, and 3) Union tin mines. Pollard *et al.* (1991) re-examined the fluids at the Zaaiplaats deposit, and Robb *et al.* (1994) analysed the fluids associated with mineralisation at the Albert Silver Mine. The results of these studies are briefly summarised below.

**Zaaiplaats**

At Zaaiplaats homogenisation temperatures were measured by Ollila (1981) for inclusions in quartz of the Bobbejaankop and Lease Granites, contact pegmatite and idiomorphic quartz, fluorite and calcite vuggy crystals. The results obtained by Ollila (1981) indicate that homogenisation temperatures for primary inclusions in the Bobbejaankop Granites were relatively high. The Bobbejaankop Granite yields $T_h$ values of between 480 °C and 719 °C, while those in the Lease Granite between 455 °C and 554 °C. Fluid inclusions in the contact pegmatite have homogenisation temperatures between 365 °C and 525 °C, and $CO_2$-rich fluid inclusions in vuggy quartz associated with cassiterite between 371 °C and

438°C. The results are summarised in Figures 5.10 to 5.13, which are taken directly from Ollila (1981). Figure 5.10 shows the distribution of homogenisation temperatures for primary and secondary inclusions in Bobbejaankop Granite, Lease Granite and contact pegmatite at Zaaiplaats. The combined results of primary and secondary fluid inclusions are shown in Figure 5.11.

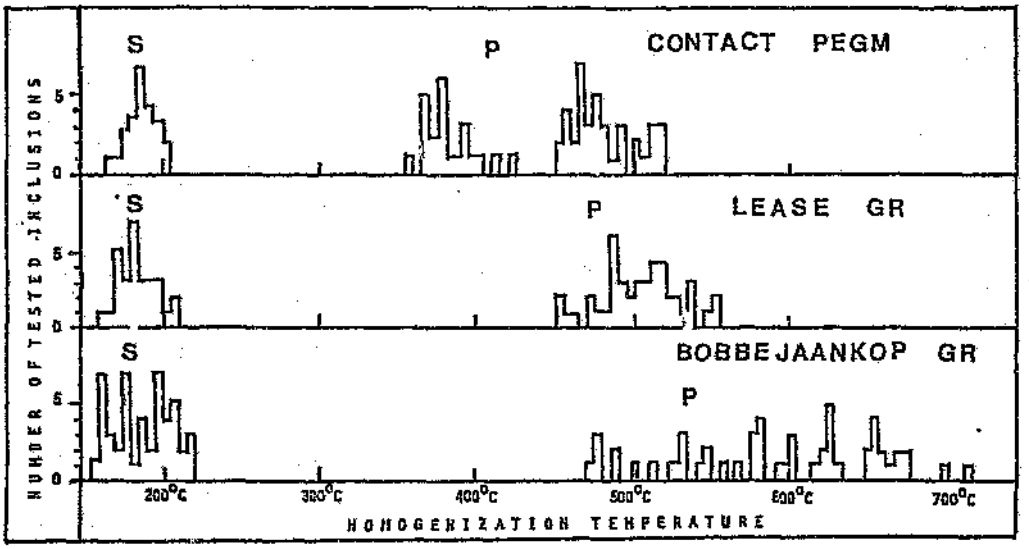


Figure 5.10 Frequency distribution of the homogenisation temperatures of primary (P) and secondary (S) fluid inclusions in the Bobbejaankop and Lease Granites and in the contact pegmatite. (From Ollila, 1981).

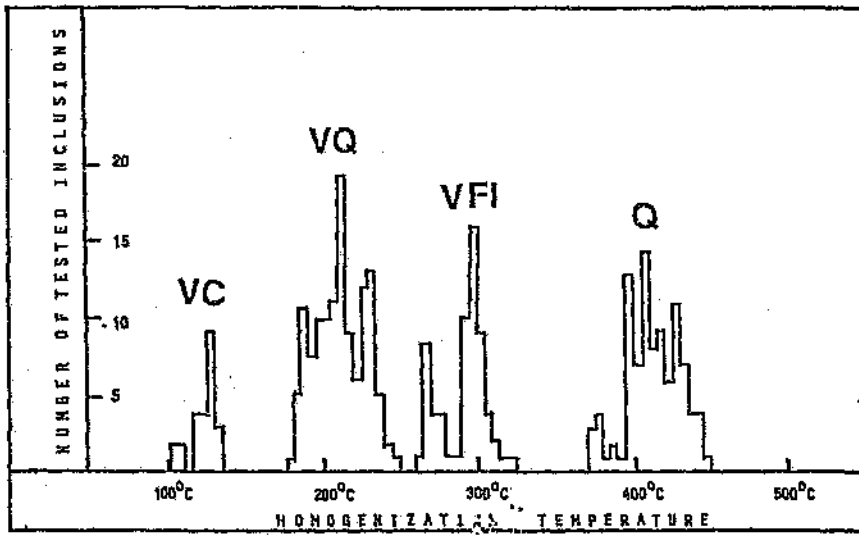


**Figure 5.11** Frequency distribution for homogenisation temperatures of the fluid inclusions of different origin in the vuggy minerals fluorite (VFl), quartz (VQ) and calcite (VC) in the Bobbejaankop Granite, and of vuggy quartz associated with cassiterite (Q) in the miarolitic cavities of the Lease Granite. (From Ollila, 1981).

Ollila (1981) maintained that the evidence for trapping of boiling fluids provided a good estimate of pressure conditions prevailing during crystallisation of the orthomagmatic cassiterite in the Bobbejaankop Granite. The orthomagmatic cassiterite crystallised at minimum total pressures of 600 bar in the Bobbejaankop Granite. The hydrothermal tin mineralisation in pipes and pockets and on the walls of the Lease Granite was due to dilute $CO_2$-$H_2O$ at partial pressures of $CO_2$ up to 750 bar. The low temperature vuggy minerals, fluorite, quartz and calcite, were deposited at pressures below 300 bar. The pressure and homogenisation temperature of fluids associated with the Bobbejaankop Granite, Lease Granite and quartz associated with tin mineralisation are plotted in Figure 5.12.

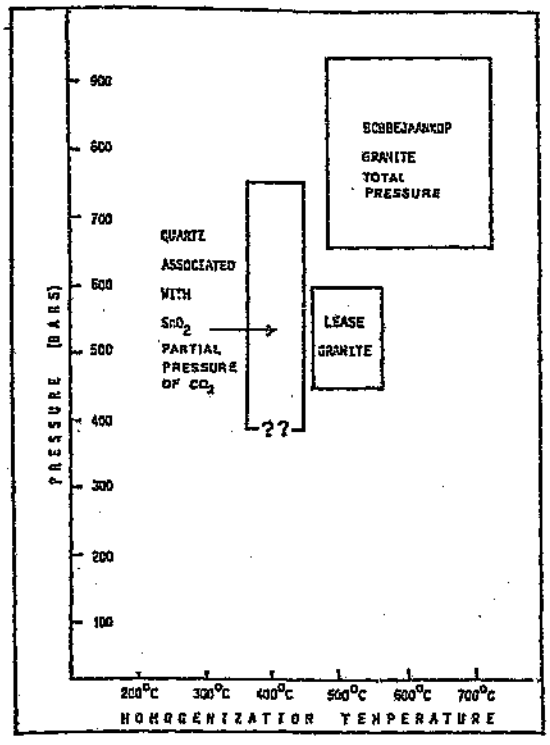


**Figure 5.12** Plot of pressures versus homogenisation temperatures for fluids at Zaaiplaats (From Ollila, 1981).

Ollila (1981) concluded that tin is soluble and may be transported in endogranitic environments in a low salinity and low density medium which is immiscible with the coexisting hydrosaline fluid. The compositions of the fluids at Zaaiplaats are summarised in Figure 5.13. The Bobbejaankop and Lease Granite have salinities (expressed as equivalent weight % NaCl) between 35 and 50 wt.% *eNaCl* . The vein fluorite and calcite, and the quartz associated with cassiterite, have lower salinites (>5 w..% eNaCl) than the host granites. The vein quartz, however, has salinities betw :en 20 and 35 wt.% eNaCl . Thus, with a decrease in temperature, there is a distinct increase in the salinity of the fluids at approximately 200°C in vein quartz.

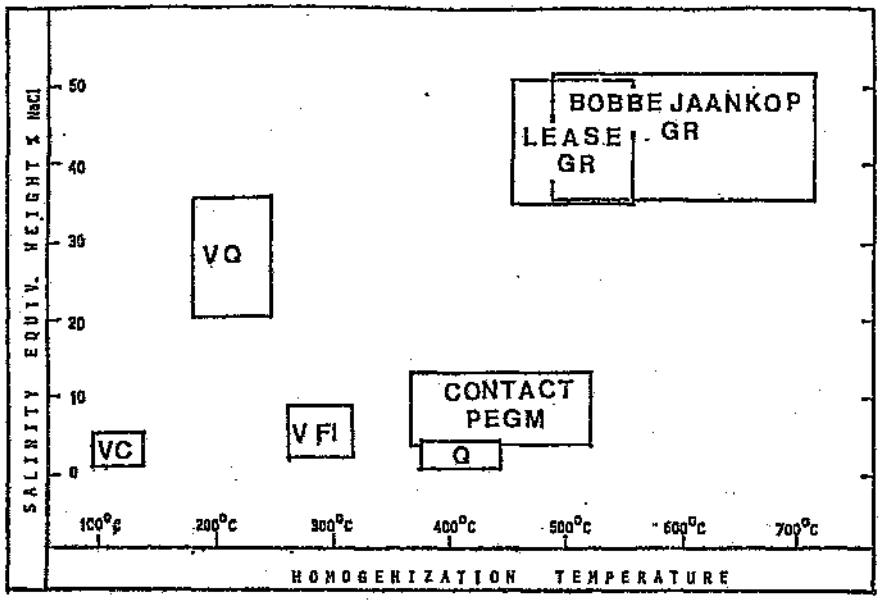


**Figure 5.13** Plot of salinities versus homogenisation temperatures for fluids at Zaaiplaats. Q= quartz associated with cassiterite, VFl= vuggy fluorite, VQ= vuggy quartz, VC= vuggy calcite. (From Ollila, 1981).

Pollard *et al.* (1991) re-examined the fluid inclusions at Zaaiplaats. They recognised three types of fluid inclusions. 1) Type 1a and b fluid inclusions: $H_2O$-NaCl-$CO_2$ inclusions occur as secondary inclusions. Type 1a inclusions contain $CO_2$ liquid (80-90 vol %) and $CO_2$ vapour (10-20 vol %), with $CO_2$ melting temperatures ranging from -56.7 to -57.7°C, and homogenisation to the liquid phase between 20 and 29.7°C. Type 1b inclusions contain $CO_2$ liquid and vapour and $H_2O$-rich liquid. The microthermometric data of Pollard *et al.* (1991) for Type 1b fluid inclusions are shown in Figure 5.14

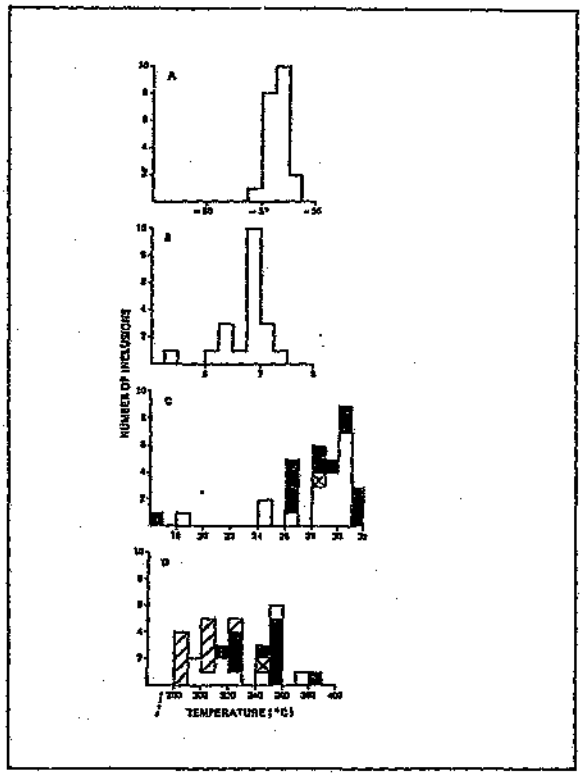


**Figure 5.14** Microthermometric data for Type 1b fluid inclusions from granite quartz, early cavity-filling quartz, and quartz from the Bobbejaankop pipe Zaaiplaats mine. A. $CO_2$ melting temperature. B. $CO_2$ clathrate melting temperature. C. Homogenisation temperature of $CO_2$ phase (to vapour = shaded, to liquid = unshaded), critical = cross-hatched. D. Final homogenisation temperatures (to $CO_2$ phase = shaded, to $H_2O$ phase = unshaded), cross hatched = critical, diagonal shading = decrepitated. (From Pollard *et al.*, 1991).

2) High salinity inclusions characterised by the presence of solid phases such as halite, sylvite and Fe-chloride which homogenise by dissolution of the solid phase in the range 160 °C to 600 °C ($T_{dissolution}$ for sylvite: 121 to 205°C, halite: 281 to 490°C). Type 2a inclusions contain a small vapour bubble and as many as six solid phases. Type 2b are similar to Type 1a inclusions, except that they lack Fe chloride daughter crystals, and Type 2c usually contain liquid, vapour and a halite crystal. The microthermometric data from quartz-, fluorite-, schelite- and cassiterite-hosted inclusions are summarised in Figure 5.15.

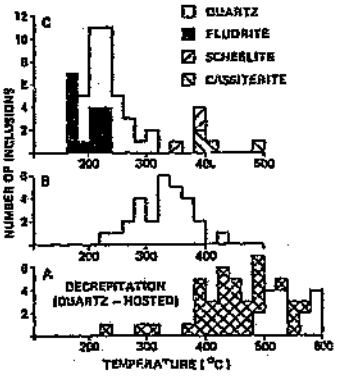


**Figure 5.15** Homogenisation temperatures for Type 2 fluid inclusions at Zaaiplaats. A. Type 2a inclusions (decrepitation temperatures = hatched). B. Type 2 b inclusions. C. Type 2c inclusions. (From Pollard *et al.*, 1991).

3) Type 3 inclusions are liquid-vapour inclusions which homogenise to the liquid phase between 88 °C and 240 °C while ice melting temperatures range from -11 °C to -30 °C. The microthermometric data of Pollard *et al.* (1991) for Type 3 inclusions are shown in Figure 5.16.

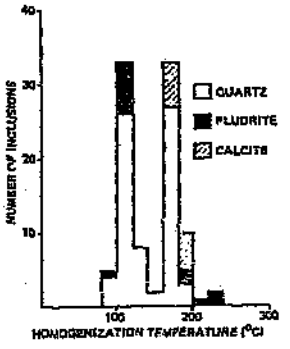


**Figure 5.16** Homogenisation temperatures of Type 3 inclusions from Zaaiplaats for quartz-, fluorite- and calcite-hosted fluid inclusions. (From Pollard *et al.*, 1991).

Pollard *et al.* (1991) conclude that early fluid inclusions contain solid phases (halite, sylvite and Fe chloride) and homogenise at temperatures up to 600 °C, and that fluid circulation occurred mainly via grain boundaries, microfractures, cavities and dissolution channel ways under lithostatic pressure of 1250 bars. They noticed a progressive decrease in temperature from 600 °C to 200 °C, which is accompanied by a decrease in salinity from 68 to 15 equivalent weight percent NaCl and a decrease in $\delta^{18}O_{fluid}$ values from 6.4 per mil. to 1.4 per mil. They maintain that the evolution of the fluid was dominated by interaction between granites and the magmatically derived fluid phase. The compositional range and homogenisation behaviour of the inclusions suggests immiscibility around 350 °C and 1000 bars. No mention was made of entrapment of boiling fluids or second boiling.

**Leeuwpoort**

Ollila (1981) studied fluid inclusions in gangue quartz at Leeuwpoort tin mine, which yielded homogenisation temperatures between 174 °C and 220 °C, and moderate salinities (between 13.9 and 22.0 mass % NaCl). In contrast with the inclusions at Zaaiplaats which commonly contain daughter crystals, no daughter crystals are found in the two phase inclusions at Leeuwpoort or the Union tin mines, indicating that the fluids were undersaturated with respect to the ore-forming constituents. A wide range of homogenisation temperatures are observed which may be due to mixing of the hydrothermal fluid with meteoric water. However, Ollila (1981) ascribes this variation as the interaction of the ore-forming fluid with the wall rocks. No evidence for boiling was found at Leeuwpoort.

**Albert**

A preliminary study of the fluids at Albert was carried out by Robb *et al.* (1994). The fluids were dominated by two phase aqueous inclusions ($H_2O$ liquid and vapour) with approximately 10% three-phase inclusions ($H_2O$ liquid and vapour, and solid). $CO_2$ was not detected as a separate phase in any inclusion. Two fluid populations were recognised, by final melting temperature at around -20°C (22 wt. % eNaCl) and between -5 and 0°C (<8 wt. % eNaCl). Homogenisation temperatures also indicate two fluid populations, one between 150±30°C and the other between 260 and 460°C. Eutectic melting temperatures

suggest the presence of $CaCl_2$ in the solutions. The microthermometric data of Robb *et al.* (1994) are shown in Figure 5.17.

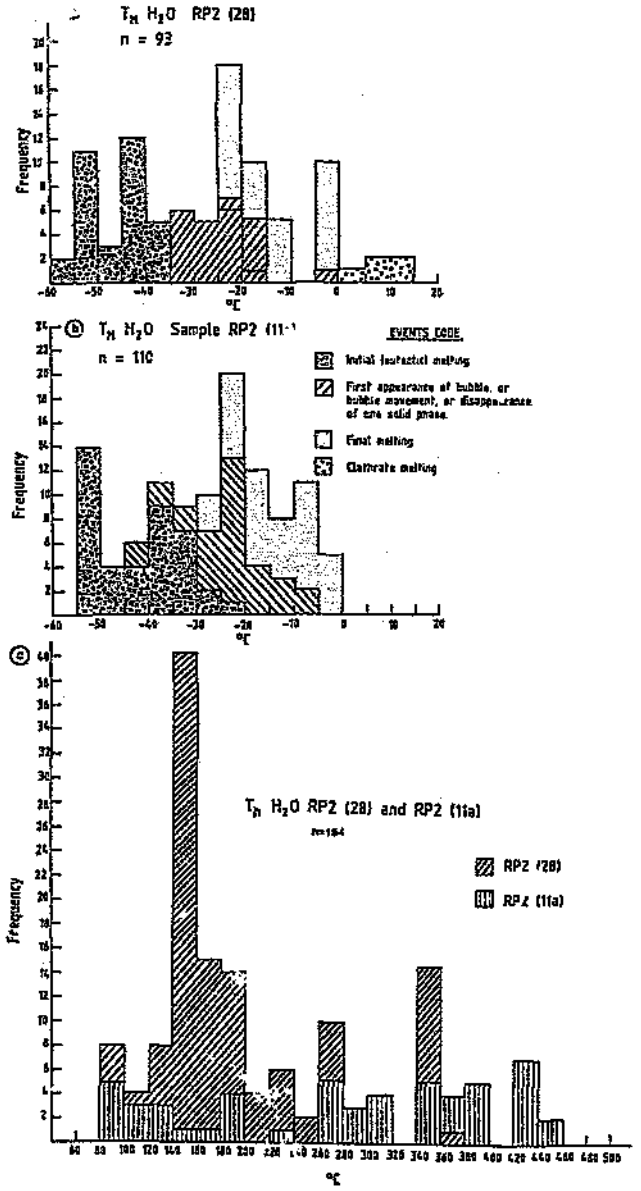


**Figure 5.17** Summary of fluid inclusion microthermometry from the Albert Silver Mine; a) and b) low temperature (melting) phase changes for samples RP2 (28) and RP2 (11a) c) homogenisation temperatures ($H_2O$ L to V) for the same two samples. (From Robb *et al.*, 1994).

The gangue minerals quartz and fluorite were targeted for petrographic and microthermometric analysis of fluids associated with mineralisation at Grass Valley, Houtenbek, Spoedwel and Albert, since they are the most common fluid inclusion-bearing minerals (Sheppard *et al.*,1985). Cassiterite and transparent sphalerite were also examined, but, except at Houtenbek, contained few inclusions generally too small to be suitable for microthermometric analysis. Sphalerite from Houtenbek contained several large primary and secondary fluid inclusions.

Transmitted light microscopy was undertaken to identify potential fluid inclusion-bearing grains of quartz, fluorite and sphalerite. The sections of interest were marked by engraving a circle around the appropriate grains with a diamond-tipped engraving tool, which is attached to the microscope and engraves a border around the field of view. This field of view is then transcribed on to paper, documenting the relationships between the host crystal and other minerals associated with it. The image on the microscope stage is projected through the drawing tube and onto the elevated pedestal, where light from the lamp, it is transcribed onto a piece of paper (Figure 5.9).

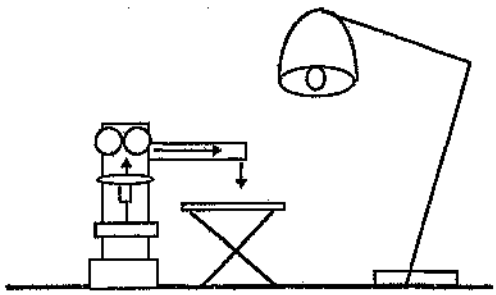

**Figure 5.18** Schematic diagram showing the set-up of the microscope, drawing tube and pedestal used for transcribing the field of view observed through the microscope onto a piece of paper.

At this low magnification, fluid inclusions may be visible as dots within the crystal. Increasing the magnification to a suitable power, say 2000X or 4000X (depending on the size on the inclusion), the fluid inclusion morphology may be recognised. Often, more than one fluid inclusion population or assemblage is present in a crystal, and the relationships between these are carefully mapped out as described.

**Fluid Inclusion Types and Assemblages**

It is important to note the difference between fluid inclusions types and assemblages (or populations). A fluid inclusion assemblage refers to a number of fluid inclusions occurring together, and in which the parental fluid is the same. Thus, a fluid inclusion assemblage can be composed of several fluid inclusion types, as a consequence of heterogeneous entrapment, leakage, necking-down and/or diffusion. In this study, fluid inclusions have been categorised according to the variation in the inclusion contents as proposed by Sheppard (1985) (Figure 5.19). These categories are not based on any microthermometric measurements or compositions, merely on appearance. These different types of fluid inclusions do not represent discrete populations of fluid inclusions. Several of these fluid inclusions types may be included in any one fluid inclusion assemblage (Figure 5.20).

*Type 1 inclusions:* These inclusions consist of two phases (liquid and vapour). The category is subdivided according to the degree of fill by the vapour phase.

*Type 1a inclusions*: These are liquid-rich where the liquid phase dominates and the vapour bubble occupies up to 40-50 % of the total volume (Figure 5.21).

*Type 1b inclusions*: These are vapour-rich and the vapour bubble occupies more than 50 % of the inclusion volume (Figure 5.22).

*Type 2 inclusions:* These inclusions contain both liquid and vapour phases, as well as one or more daughter crystals (solid phases) (Figure 5.23, 5.24, 5.25 and 5.26).

*Type 3 inclusions:* These are mono-phase liquid inclusions with no vapour bubble or solid phases (Figure 5.27).

*Type 4 inclusions:* These are mono-phase vapour inclusions where no liquid or solid phases are present (Figure 5.28).

*Type 5a inclusions*: These are aqueous, $CO_2$-rich inclusions where a separate $CO_2$ phase is present.

*Type 5b inclusions* - These are two phase (liquid and vapour), $CO_2$ inclusions.

**TYPE 1a fluid inclusions** - aqueous, two phase (liquid and vapour) fluid inclusions where the vapour bubble occupies up to 40-50% of the total volume.

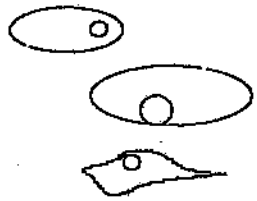

**TYPE 1b fluid inclusions** - aqueous, two phase (liquid and vapour) fluid inclusions where the vapour bubble occupies more than 50%of the inclusion volume.

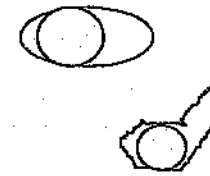

**TYPE 2 fluid inclusions** - aqueous, 3 phase (liquid, vapour and solid) fluid inclusions. The solid phases may be daughter crystals or trapped solids.

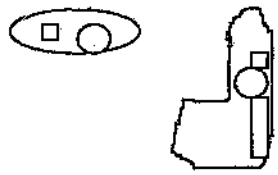

**TYPE 3 fluid inclusions** - Monophase liquid inclusions with no vapour bubble or solid phases

**Type 4 fluid inclusions** - Monophase vapour inclusions where no visible liquid or solid phases are present.

**TYPE 5a fluid inclusions** - aqueous, $CO_2$-rich inclusions where a separate $CO_2$ phase is present.

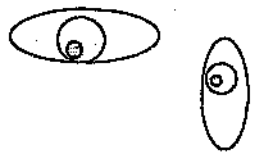

**TYPE 5b fluid inclusions** - two phase (liquid and vapour), $CO_2$ inclusions.

**Figure 5.19** Schematic representations of the five main fluid inclusion types recognised in the fluid inclusion assemblages of the Bushveld granites in the eastern lobe of the Bushveld Complex.

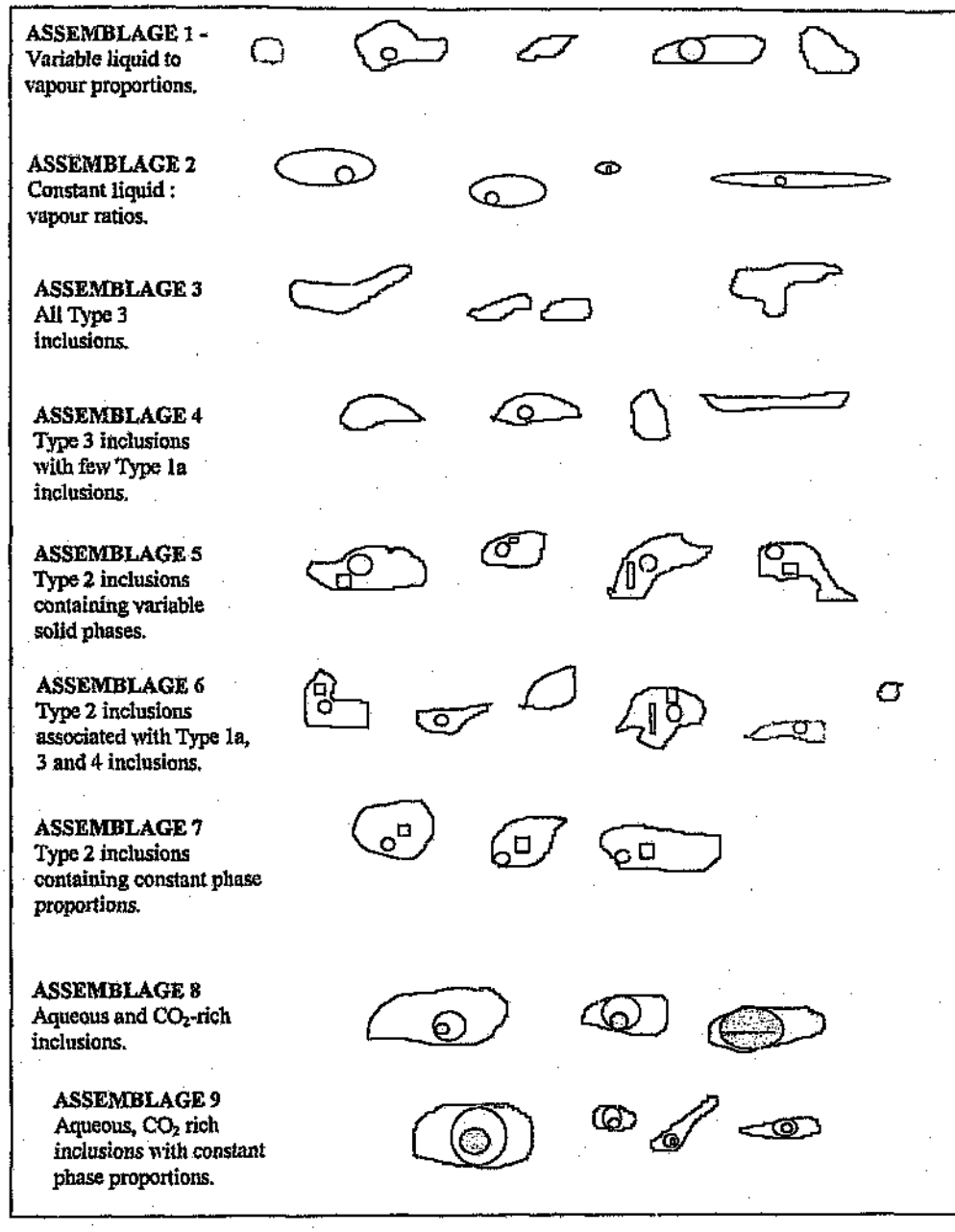


**Figure 5.20** Examples of types of fluid inclusion assemblages from this study.

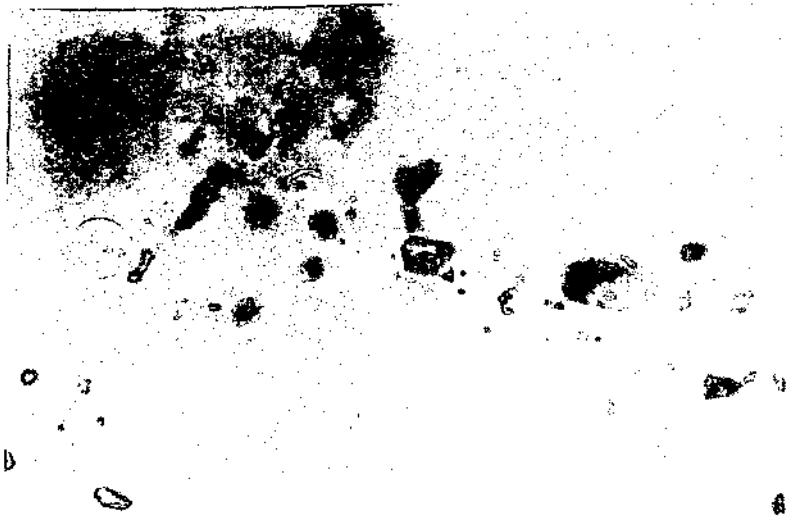

**Figure 5 .25** Primary fluid inclusion containing hematite solid phase.



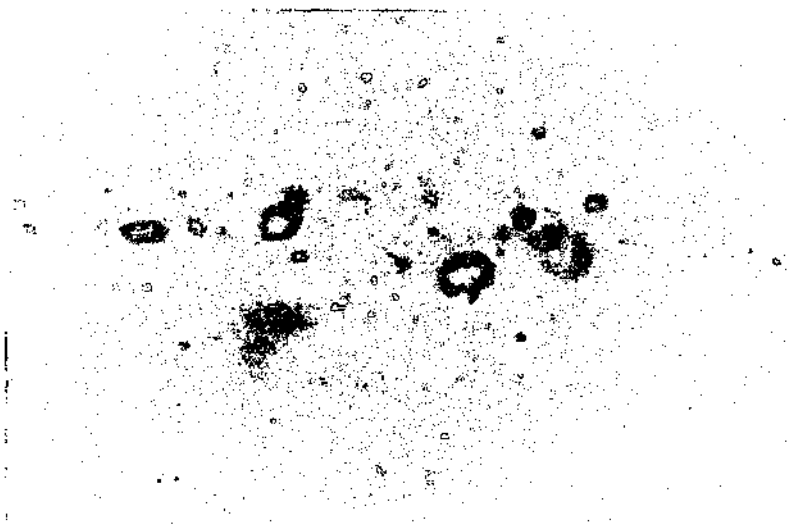

**Figure 5.27** Secondary trail containing Type 1a and Type 3 fluid inclusions.

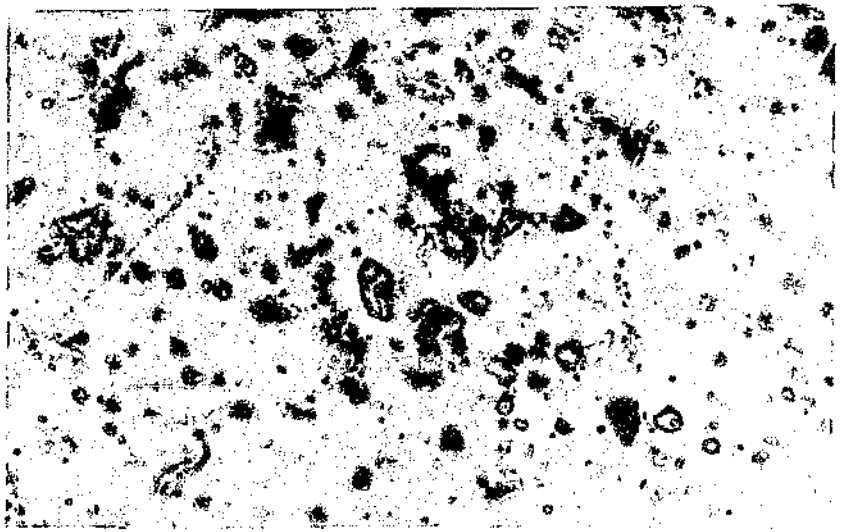

**Figure 5.26** Primary inclusions containing several solid phases, including a small opaque solid.

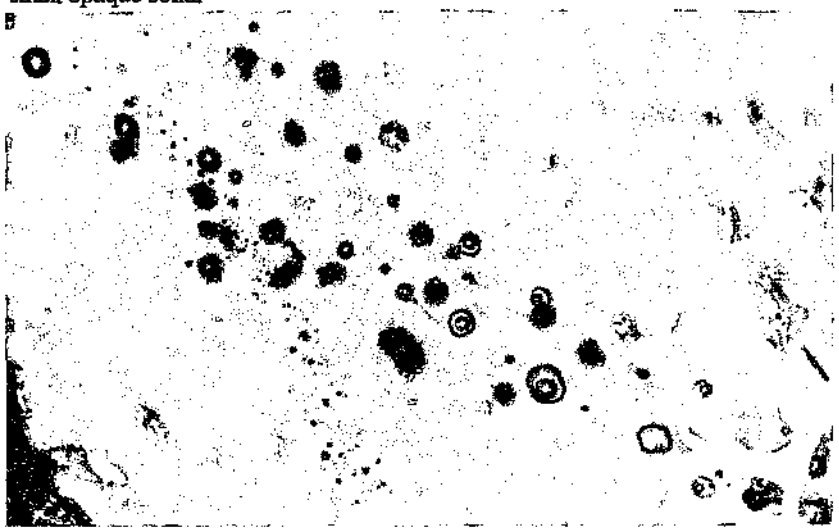

**Figure 5.28** Secondary trail containing Type 1a, Type 1b and Type 4 inclusions.

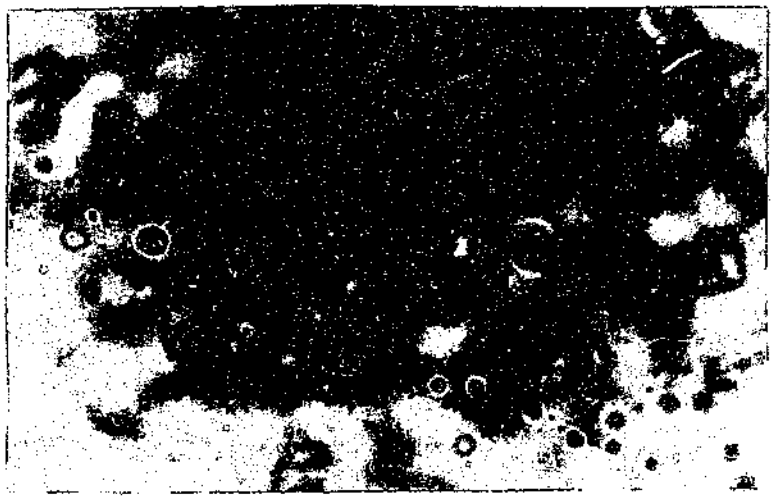

**Figure 5.21** Type 1a fluid inclusions along a fracture in fluorite.

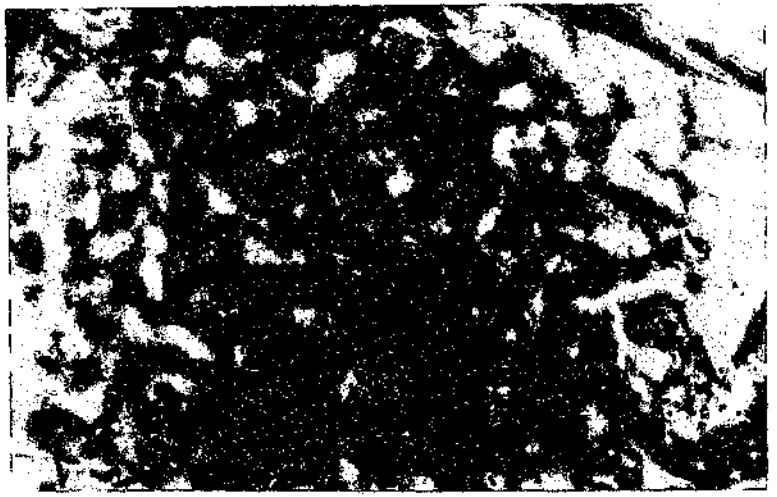

**Figure 5.22** Type 1b fluid inclusion in a secondary swarm of inclusion containing variable phase proportions.

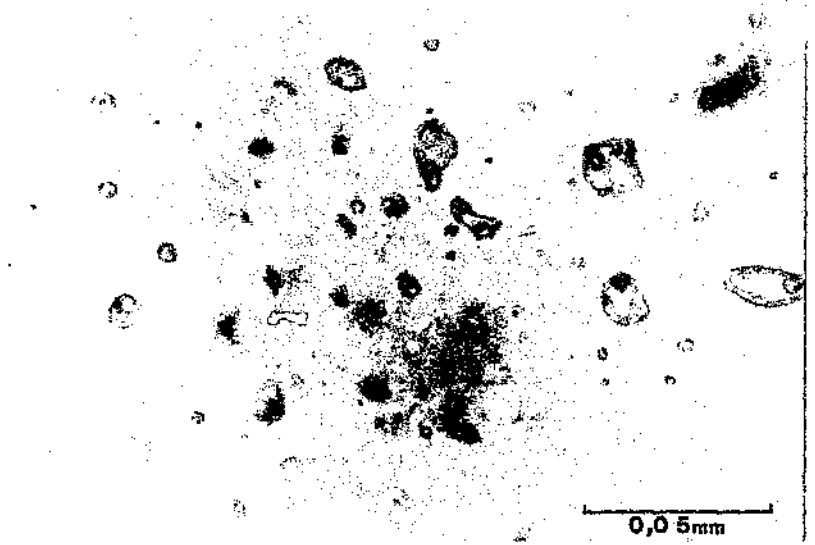


**Figure 5.23** Type 2 fluid inclusions containing a single daughter crystal and constant phase proportions.

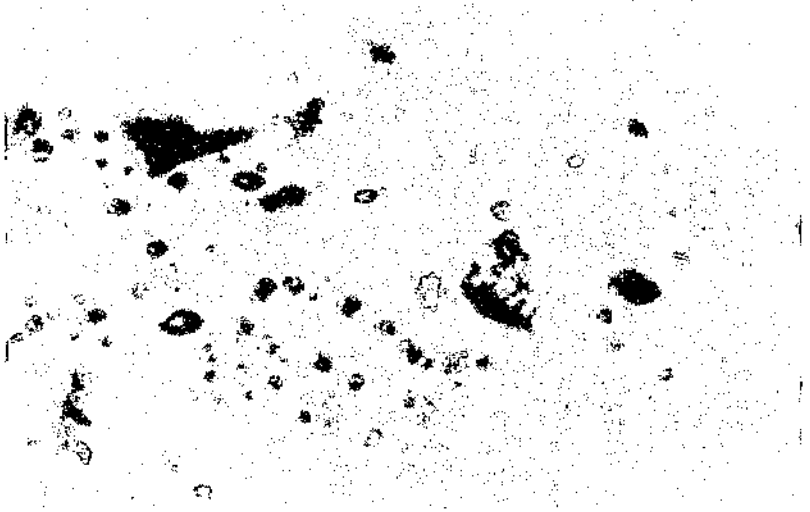

**Figure 5.24** Primary fluid inclusions containing muscovite as a solid phase.

**Microthermometry**

Microthermometric analyses were carried out at the University of the Witwatersrand, using both USGS and Linkam heating-freezing stages. The heating freezing stages were calibrated using synthetic fluid inclusions provided by Flincor® and the calibration was routinely checked during the study, in order to maintain uniform analytical conditions.

Once the fluid inclusions identified during the petrographical survey had been relocated on the heating-freezing stage, the sample was first supercooled to induce freezing of the fluid inclusion contents, and then gradually heated in order to record the temperatures at which first melting, final melting and intermediate melting events occurred. After these measurements were obtained, the sample was heated and the homogenisation temperature recorded. Wherever possible, all phase changes were recorded from each fluid inclusion assemblage studied.

The approach when measuring phase changes in fluorite-hosted fluid inclusions was slightly different to that employed when studying quartz-hosted fluid inclusions. Due to the weakness of the fluorite crystal lattice, the expansion of ice on freezing often causes stretching and leakage from the fluid inclusion, a situation not encountered with the strong quartz host crystal. Thus, fluorite-hosted fluid inclusions were heated before freezing was initiated, so that, in the event of stretching, at least reliable homogenisation temperatures were obtained from the inclusions. With the quartz hosted fluid inclusions, this approach was routinely adopted, for the purposes of cross checking.

***RESULTS***

Fluid inclusion maps of each fluid inclusion assemblage discussed in the following sections are shown in the Appendix. Selected maps are included in the presentation of results in order to illustrate salient points. These maps indicate the host mineral, the associated minerals, the grain size, the size of fluid inclusions, the types of fluid inclusions, their origins (primary or secondary), and the relationships of various assemblages within the field of view. For each field of view, a low magnification (40X) map showing mineral relationships

is given, as well as a high magnification (200X or 400X) map which shows the fluid inclusion petrography. In addition, hand specimen descriptions (and where possible, scanned images of the polished thin section), fluid inclusion petrography and microthermometry of selected samples from Spoedwel, Albert, Grass valley, Houtenbek, Dronkfontein and Leeufontein are presented separately, and the data integrated in the discussion and interpretation. Several terms and abbreviations (Table 5.2) are referred to repeatedly, and it should be clear at the outset what each of these mean.

**Table 5.2** List of microthermometric terms and abbreviations used (after Roedder, 1984).

| ABBREVIATION | TERM | EXPLANATION |
|---|---|---|
| $T_h$ | Homogenisation temperature | Temperature at which liquid and vapour phases homogenise. |
| $T_e$ | Eutectic melting temperature | Temperature at which melting begins. |
| $T_{freeze}$ | Freezing temperature | Temperature at which the liquid phase freezes to a solid. |
| $T_{final\ melting}$ | Final melting temperature | Temperature at which the last frozen solid melts. |
| $T_{dissolution}$ | Dissolution temperature of a solid phase | Temperature at which a daughter crystal melts completely. |
| $T_{decrepitation}$ | Decrepitation temperature | Temperature at which the internal temperature of the fluid inclusion exceeds the strength of the host crystal. |
| $T_h\ CO_2$ | Homogenisation temperature of $CO_2$ | Temperature at which $CO_2$ vapour homogenises into the $CO_2$ liquid phase. |
| Wt.% eNaCl | Weight percent equivalent NaCl | Unit of salinity. |

The samples from Grass Valley, Houtenbek, Spoedwel, Dronkfontein and Albert were selected with specific questions in mind. The questions were:

1) How do the fluids associated with the different quartz and fluorite generations in interstitial spaces compare with one another?
2) Are the fluids in vein quartz different to those in the interstitial spaces?
3) How do the fluids in vein quartz relate to the fluids associated with mineralisation?

4) How do the fluids associated with mineralisation compare with fluids in the un-mineralised host rock?
5) Can fluids associated with alteration be recognised?
6) How do the fluids of the sulphide paragenesis compare with those of the orthomagmatic cassiterite, remobilized cassiterite and hematite\fluorite assemblages.
7) Is there a difference in the nature of fluids which precipitated each mineral in the sulphide paragenesis.
8) How do the fluids at each of the ore deposits compare with one another?
9) Can evidence be found for boiling or fluid mixing?

The microthermometric results are presented according to the position of the primary ore assemblage at each deposit in the paragenetic sequence established in Chapter 4. Thus, the tin and molybdenite of the early paragenetic sequence represented at Grass Valley and Houtenbek are presented first, followed by the sulphide assemblage at Spoedwel and Dronkfontein, and the hematite-fluorite assemblage at Albert. Finally the fluids associated with unmineralised granites at Leeufontein are presented.

## GRASS VALLEY

The samples selected for microthermometry are listed in Table 5.3.

**Table 5.3** List of samples selected for microthermometry from Grass Valley and the reason for their selection.

| SAMPLE | Reason for selecting sample for microthermometry |
|---|---|
| GV01 | Sample contains quartz veins with $CO_2$-rich fluid inclusions associated with hematite precipitation. |
| GV02 | Sample contains three quartz generations, and remobilized cassiterite and sulphides. |
| GV04 | Sample contains fluids associated with sulphides and chlorite. |
| GV05 | Sample contains fluids associated with precipitation of fluorite, and quartz veins consisting of eight generations of quartz. |

**DEPOSIT:** GRASS VALLEY

**SAMPLE:** GV01

**HAND SPECIMEN**

Brecciated, medium-grained, red, hypersolvus granite, cut by veins filled with chalcedony, transparent quartz and hematite. Hematite precipitation is associated with the transparent quartz and postdates chalcedony precipitation. The hematite occurs as rosettes and spheroids within the transparent quartz.

**FLUID INCLUSIONS**

Fluid inclusions in the transparent quartz along the walls of the vein, preceding the precipitation of the microscopic hematite spheroids are predominantly secondary Type 1a and Type 3 inclusions (Figure 5.29 Field 1). No primary inclusions were recognised. Some trails contain both Type 1a and Type 3 inclusions, while others contain only Type 3 inclusions. In the quartz associated with and post dating the hematite, fluid inclusions consisting almost entirely of $CO_2$ are found (Figure 5.29 Fields 2). At first sight, some of these fluid inclusions appear to be normal Type 1a inclusions, but others contain the characteristic $CO_2$ "double bubbles". These $CO_2$- rich inclusions occur as secondary trails in the vein quartz, as well as in the interstitial quartz of the host rock.

In addition, secondary trails of a daughter-rich Type 2 fluid inclusion assemblages are trapped in the transparent quartz. Some inclusions contain hematite crystals, but it is impossible to determine whether they are true daughter crystals or trapped solids. The other solids are halite and sylvite.

## MICROTHERMOMETRY

Individual secondary trails of the Type 1a aqueous fluid inclusions, have been measured, and five groups of measurements have emerged.

The first group, consisting of Type 1a and Type 3 fluid inclusions, froze at -38.5 °C and developed clear, colourless mosaics. Eutectic melting could not be seen. The first signs of melting were visible at -33 °C when the edges of the frozen solid started becoming wavy. No other intermediate melting events were observed before final melting (between -5.5 °C and -4.7 °C). $T_h$ was not measured. The second group of Type 1a and Type 3 inclusions froze at -36 °C, and behaved exactly as the first group described, the only difference being that these fluid inclusions underwent final melting at -1.5 °C.

The third group consists of Type 3 inclusions only, which froze to a clear solid at -40 °C. No intermediate melting events were observed, and the frozen solid merely shrank away from the inclusion walls as melting proceeded. Final melting occurred at -2.1 °C.

The fourth group of aqueous inclusions are the daughter-rich, Type 2 inclusions which developed a brown solid on freezing (at -53 °C). Eutectic melting occurred at -48 °C. Intermediate melting events were observed at -44 °C when the mosaic appeared to disintegrate, at -35 °C when the mosaic became coarser, at-28 °C when the mosaic merged, and at -10 °C when round rafts developed. Final melting temperatures were variable in this assemblage. Some inclusions underwent final melting at +16 °C while others melted at -18 °C or underwent sublimation between -1 °C and 0 °C .

The $CO_2$-rich inclusions occur as crosscutting secondary trails. On cooling, the $CO_2$ vapour bubble expanded and freezing occurred at -97.7 °C. The liquid $CO_2$ froze to an irregular spiky shell around the gaseous $CO_2$, and started melting at -67 °C. Final melting of the liquid $CO_2$ took place between -57.4 °C and -57.8 °C. Within individual trails, homogenisation of the liquid and gaseous $CO_2$ occurred at different temperatures, ranging from 22.5 °C to 27.8 °C.

**Figure 5.29** Petrographic maps of fields 1 and 2 in sample GV01.

**DEPOSIT: GRASS VALLEY**

**SAMPLE: GV02**

**HAND SPECIMEN**

Pegmatitic, euhedral quartz, over grown by milky-quartz and cassiterite. Cassiterite is intergrown with calcite. Minor amounts of galena, sphalerite, and chalcopyrite post date the cassiterite. Chalcopyrite is partially altered to chalcocite.

**FLUID INCLUSIONS**

Fluid inclusions associated with the three major quartz generations have been studied, and some of the fluid inclusion populations show unusual behaviour .

Fluid inclusions in quartz generations 1 and 2 are secondary in nature, and no definite primary inclusions were found. Three categories of inclusions were identified in terms of their visual properties/morphology (Figure 5.30 Field 1 a, b and c). Firstly, zones/planes of Type 1a and Type 3 inclusions are present in the early quartz generations. The second category contains Type 2 and Type 3 inclusions as secondary trails. The solid phases identified are $FeCl_2$ and an opaque crystal. One blue needle-like crystal (prism)(possibly anhydrite or rutile), and two small anhedral crystals were also observed. Finally, secondary trails of $CO_2$-rich fluid inclusions are present. Some of these inclusions are Type 5b inclusions, consisting of liquid $CO_2$ and a vapour bubble (gaseous $CO_2$), while others contain water, liquid $CO_2$ and gaseous $CO_2$, and showing the characteristic $CO_2$ double bubble (Type 5a inclusions).

Fluid inclusions in the third quartz generation are predominantly primary and are so numerous that they cloud the quartz. The fluid inclusions show extremely variable phase proportions and are Type 1a, Type 1b, Type 3 and Type 4 inclusions. $CO_2$ double bubbles (Type 5a) are present, as well as Type 5b $CO_2$ inclusions.

**MICROTHERMOMETRY**

The most convenient way to present the icrothermometric data for this sample is as individual fluid inclusion trails, beginning with those presumed to be trapped first.

*Fluid inclusion population 1:* These inclusions froze to a colourless mosaic at -46 °C. Possible eutectic melting occurred at -43 °C and round rafts were formed by -40 °C. On heating, the rafts gradually shrank until they disappeared altogether at -0.4 °C. Homogenisation temperatures ranged from 194 °C to 201 °C.

*Fluid inclusion population2*: Freezing occurred at temperatures between -35 °C and -40 °C, and a colourless mosaic was formed. Eutectic melting was not observed, and, by -44 °C, round rafts were already visible. At -19 °C, these rafts merged to form larger ones, and at -10 °C some of the rafts melted. Final melting occurred between -4.4 °C and -3.1 °C. Homogenisation of the two phase inclusions occurred between 134 °C and 167 °C, with the mean $T_h$ at 143 °C.

*Fluid inclusion population 3*: Freezing occurred at -54 °C, and a brown mosaic formed. Eutectic melting may have occurred before -48 °C. An intermediate melting event at -23 °C was recorded. Final melting took place at -16 °C and homogenisation occurred between 149 °C and 160 °C.

*Fluid inclusion population 4:* This trail froze at -64 °C and developed a moderately brown mosaic. Eutectic melting occurred at -50 °C. Intermediate melting events at -39 °C (coarsening of mosaic), at -24 °C ( mosaic merged into round rafts), and at -23 °C (many rafts disappeared rapidly). Final melting temperatures and homogenisation of the liquid and vapour phases were constant, at -14 °C and 134 °C, respectively.

*Fluid inclusion population 5*: This assemblage behaved in a similar manner to populations 3 and 4, except that final melting occurred at -6.8 °C. A brown mosaic was produced on freezing. Eutectic melting occurred at -50 °C, and intermediate melting events were observed at -37 °C, -27 °C and -23 °C. Homogenisation took place between 120 °C and 130 °C.

*Fluid inclusion population 6*:

The $CO_2$-rich inclusions: The carbon dioxide froze between -92 °C and -94 °C. Final melting of the liquid $CO_2$ occurred at -57.4 °C. In the inclusions containing no visible water, homogenisation of the liquid and gaseous $CO_2$ occurred between 29 °C and 30 °C. In inclusions containing water as well as the $CO_2$, final melting occurred at 7.5 °C. Homogenisation of the gaseous $CO_2$ into the aqueous phase occurred at temperatures above 250 °C. The exact value is not known, because stretching of the inclusions became visible and the heating run was abandoned.

The aqueous inclusions: The aqueous fluid inclusions, with no visible $CO_2$ present, froze to a colourless mosaic at unusually high temperatures (-29 °C to -34 °C). Eutectic melting and intermediate melting events were difficult to recognise. Final melting occurred between -1.7 °C and 1.8 °C in most inclusions, but a few were melted by -4 °C. Simultaneous melting of large rafts and the appearance of a full-sized vapour bubble occurred in several inclusions. Homogenisation of the liquid and vapour phase occurred between 214 °C and 233 °C.

**Figure 5. 30** Petrographic maps of GV02 showing quartz generations 1, 2 and 3 and fields 1a, b and c referred to in the text.

**DEPOSIT:** GRASS VALLEY

**SAMPLE:** GV04

**HAND SPECIMEN**

Late stage, massive, pegmatitic vein quartz associated with muscovite, chlorite, and pyrite.

**FLUID INCLUSIONS**

Only one fluid assemblage is preserved in this sample. The fluid inclusions are Type 1a and Type 3 inclusions which occur as trails and planes, as well as scattered throughout the quartz. No solid phases occur in any of the inclusions.

**MICROTHERMOMETRY**

The fluid inclusions froze at -35.2 °C and produced a colourless mosaic. Eutectic melting could not be seen, and by -30 °C, the mosaic had merged into a clear solid. This solid rafi receded from the inclusion walls as melting proceeded. Final melting occurred in the range -2.8 °C to 0.6 °C. Sublimation was observed in several inclusions. Homogenisation of the vapour bubble into the liquid phase occurred between 83 °C and 128 °C.

**DEPOSIT:** GRASS VALLEY

**SAMPLE:** GV05

**HAND SPECIMEN**

Fused and albitised, medium-grained host granite with minor interstitial quartz and fluorite, cross cut by a quartz vein which contains at least eight discrete generations of quartz (Figure 4.18).

**FLUID INCLUSIONS**

*In vein quartz*: Fluid inclusions occur in eight stages of quartz growth in vein quartz (Figure 5.31 ). The inclusions in the early generations are predominantly Type 1a inclusions, while those associated with quartz generations contain $CO_2$ and are Type 1a, Type 5a and Type 5b inclusions.

*In interstitial fluorite*:

Clusters and trails of aqueous Type 1a inclusions, as well as secondary trails of $CO_2$ - rich Type 5b inclusions are present in the interstitial fluorite.

*In interstitial quartz*: Fluid inclusions with $CO_2$ double bubbles occur along crosscutting secondary fractures. Aqueous Type 1a and Type 3 inclusions occur along growth zones.

## MICROTHERMOMETRY

*Fluid inclusions in interstitial fluorite:*

Primary inclusions along growth zones froze to a brown mosaic between -38 °C and -44 °C. First melting was observed at -43 °C. At -33 °C, many round rafts formed and at -22.3 °C, rapid clearing of the rafts (hydrohalite) took place. Final melting occurred between -14 °C and -10 °C.

The aqueous inclusions along annealed fractures froze between -49 °C and -55 °C, and developed a colourless mosaic. Melting was first observed at -45 °C when the mosaic became coarser. At -36 °C, the mosaic merged into bigger rafts, some of which melted at -16 °C. Final melting values between -8.9 °C and -4.4 °C were recorded.

The $CO_2$ -rich inclusions contain no visible water, and are Type 5b inclusions. The $CO_2$ liquid froze at -96 °C and underwent final melting at -57.4 °C. Homogenisation of the liquid and gaseous occurred at 27.1°C in some trails and at 25.4 °C in others.

*Fluid inclusions in interstitial quartz:*

The secondary, $CO_2$ -rich inclusions froze at -96 °C. Final melting of the $CO_2$ occurred at -57.1 °C and final melting of the clathrate occurred at 7.3 °C. Homogenisation of the liquid and vapour $CO_2$ took place at 30 °C for the one trail and at 28.4 °C for a crosscutting trail.

The aqueous fluid inclusions fall into two groups according to their final melting temperatures. These inclusions are anomalous because they produced a colourless mosaic on freezing (at -42 °C), but underwent final melting at relatively low temperatures. One group melted between -4 °C and -5 °C, and the other group melted at -17 °C. In both groups, intermediate melting events were observed at -38 °C (merging of the mosaic) and -24 °C (some rafts melted).

*Fluid inclusions in quartz vein:*

Quartz generations were labelled from 1 to 8, with quartz 1 being the oldest generation occurring against the vein walls, and quartz 8 being the youngest generation, occurring in the central portions of the vein (Figure 5.31). Primary inclusions in each quartz generation were sought for microthermometry, in order to trace the evolution of the fluids with time. Quartz generations 1, 2, 3 and 5 contained no fluid inclusions suitable for microthermometry.

Quartz generation 4 contained numerous Type 1a and Type 3 fluid inclusions which froze to a dark brown mosaic between -49 °C and -52 °C. First melting was observed at -45 °C. Definite coarsening and rounding into rafts had taken place by -43 °C. Intermediate melting events were observed at -21 °C and -16 °C when several rafts disappeared. Final melting temperatures fall in the range -8.7 °C to -6.8 °C. Homogenisation of all the two phase inclusions occurred at 101 °C.

The fluids associated with quartz generations 6,7 and 8 are rich in carbon dioxide. Only quartz 7 contains fluid inclusions which were undoubtedly primary in origin. Type 5b $CO_2$-rich inclusions and Type 1a aqueous inclusions coexist in quartz 7. The $CO_2$-rich inclusions froze at 95.3 °C and underwent final melting at -57 °C Homogenisation of the liquid and vapour $CO_2$ occurred at temperatures from 25.8 °C to 29.8 °C. A few $T_h$ $CO_2$ values of 30.4 °C were recorded.

The aqueous inclusions developed a brown mosaic on freezing (at -44 °C). First melting had occurred by -39 °C. Final melting of most inclusions occurred between -6.5 °C and 7 °C. However, some $T_{final\ melting}$ values of -1.5 °C were recorded. Homogenisation temperatures between 146 °C and 195 °C were measured.

**Figure 5. 31** Petrographic maps of vein quartz with multiple episodes of quartz growth in sample GV05.

**DEPOSIT:** GRASS VALLEY

**SAMPLE:** GV06


**HAND SPECIMEN**

Medium-grained, hypersolvus granite consisting of perthite, quartz, muscovite, with hematite and goethite alteration minerals. The quartz is interstitial to the perthite, and muscovite occurs locally filling entire interstitial cavities. Localised hematite patches are present. There is evidence for two quartz generations.

**FLUID INCLUSIONS**

The second quartz generation is full of fluid inclusions with variable phase proportions (Figure 5.32 Field 1). There are Type 1a, Type 1b, Type 2 (halite and 1 unidentified crystal), Type 3 and Type 4 fluid inclusions which appear to be primary with respect to the second quartz generation. The aqueous fluid inclusions occur in patches and zones of hundreds of inclusions; some containing only liquid and vapour phases, and other containing solid phases in addition . The solids recognised are halite, sylvite, and $FeCl_2$, and one other low relief, anhedral, green crystal. Secondary crosscutting trails of aqueous and $CO_2$-rich fluid inclusions are also present (Figure 5.32 Field 2).

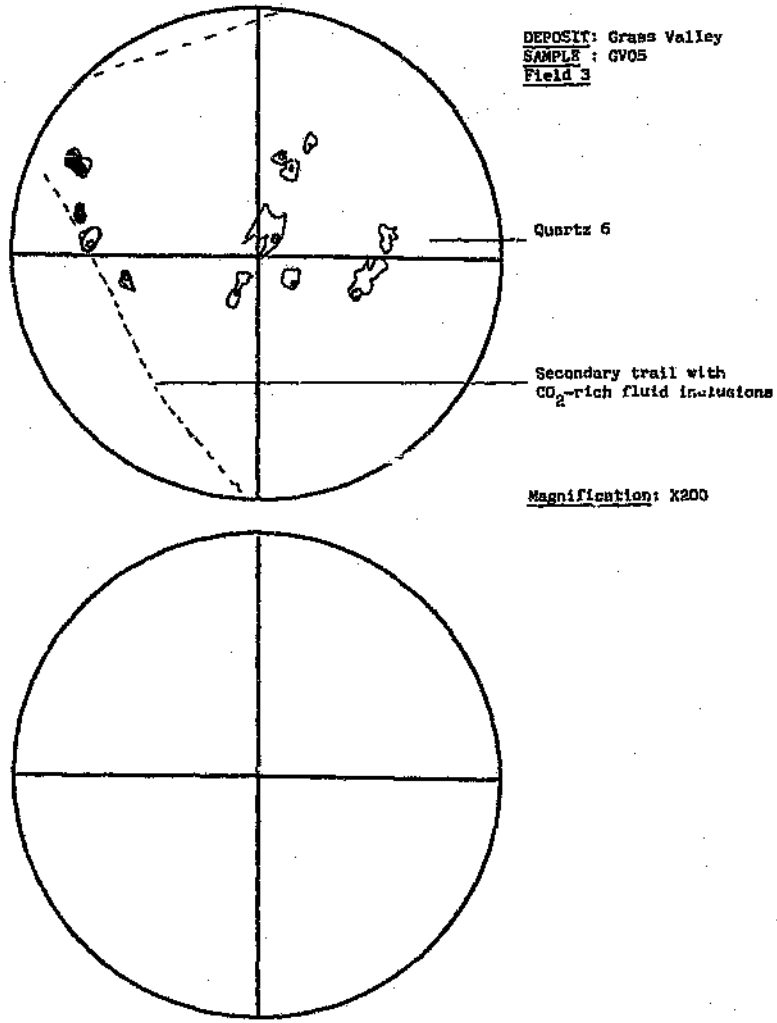


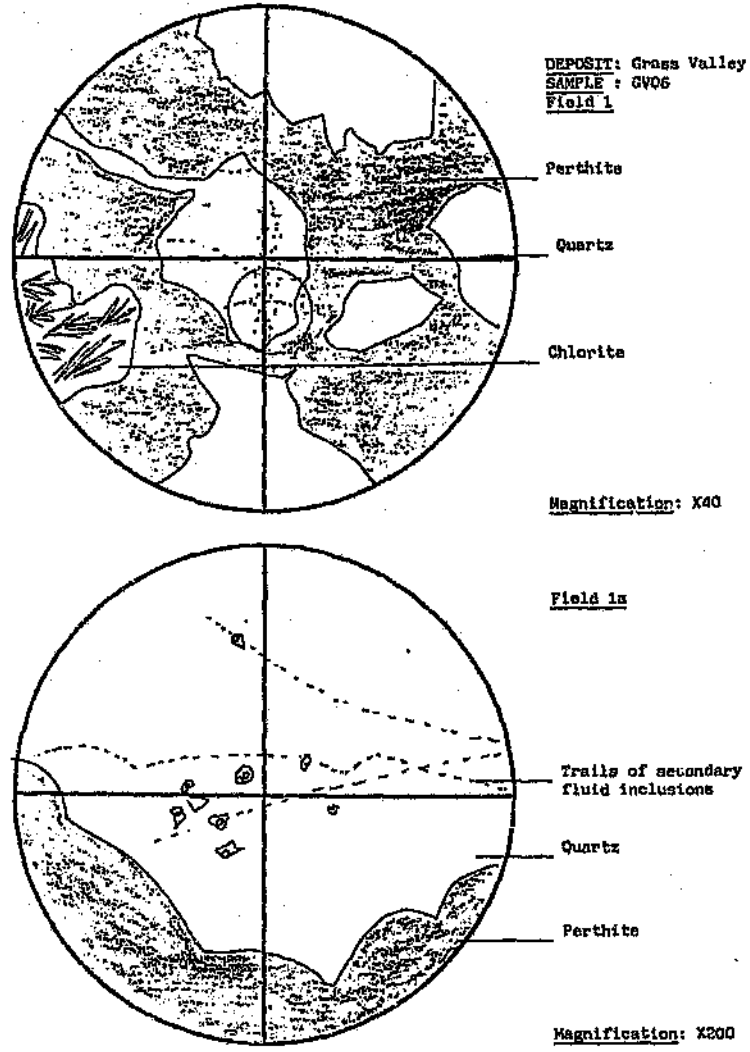


**Figure 5. 32** Left: Petrographic map of interstitial quartz with secondary $CO_2$-rich inclusions from sample GV05. Right: Petrographic map of inclusions in two interstitial quartz generations in sample GV06.

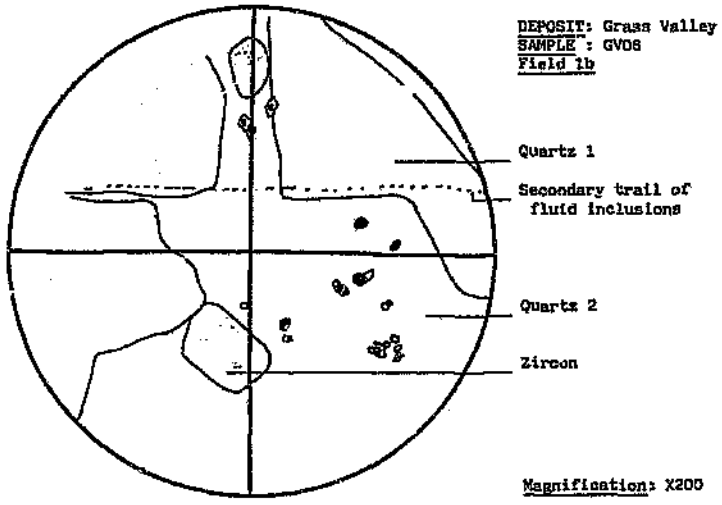


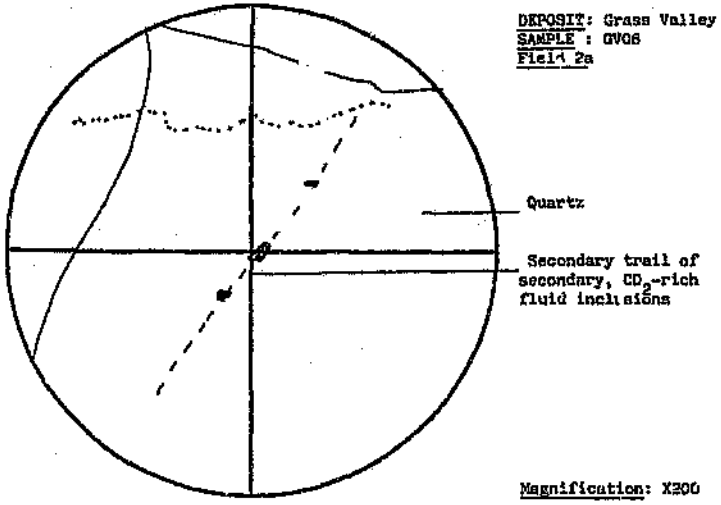


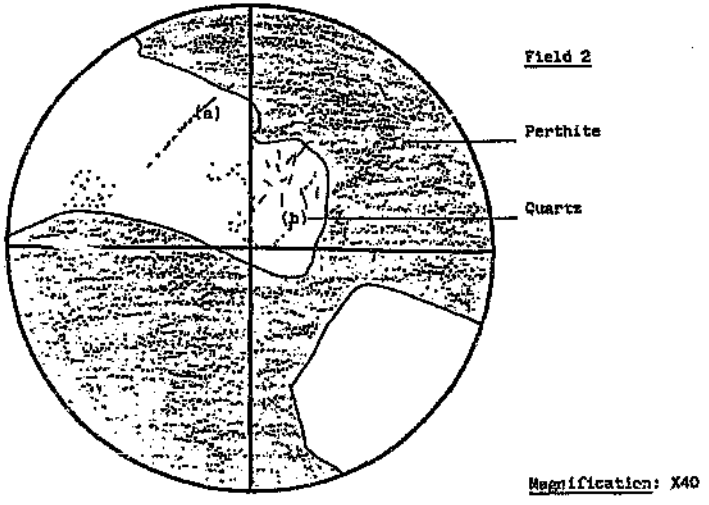


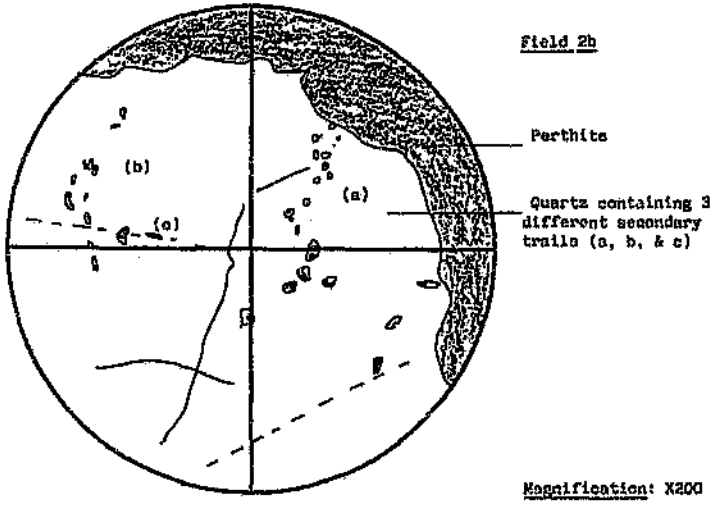




**Figure 5.32 Continued** Petrographic map showing $CO_2$-rich inclusions associated with zircon in quartz generation two (Field 1b) and as secondary trails in quartz 1 (Field 2a and b).

**MICROTHERMOMETRY**

The secondary trails of $CO_2$-rich inclusions consist of Type 5b fluid inclusions (i.e. $CO_2$ liquid and vapour), as well as Type 5a fluid inclusions containing an aqueous phase, and $CO_2$ (liquid and vapour). $T_{freeze}$ for the $CO_2$ is -95.9 °C and $T_{final\ melt}$ of $CO_2$ is -57.4 °C. Final melting of the clathrate in the water-bearing inclusions is at 8.4 °C. Homogenisation of the liquid $CO_2$ and the aqueous phase occurs at temperatures above 200 °C.

The aqueous inclusions developed a dark brown mosaic on freezing over a range from -45 °C to -57 °C. The first signs of melting were observed at -46 °C. Intermediate melting events were observed at -35 °C, when the mosaic coarsened slightly, at -33 °C when round rafts developed, and at -24 °C when the brown colour faded and some rafts melted. Final melting was observed at -22.9 °C for one inclusion, but the bulk of the values recorded fell in the range -19 °C to -15 °C. Homogenisation temperatures for the inclusions with $T_{final\ melting}$ near -22 °C and -19 °C have higher $T_h$ values (198 °C to 176 °C) than the ones with $T_{final\ melting}$ at -15 °C, in which $T_h$ is 113 °C.

**DEPOSIT: GRASS VALLEY**

**SAMPLE: GV10**

**HAND SPECIMEN**

Albitised, hypersolvus granite consisting of perthite, quartz, muscovite and sericite. Hematite occurs in patches. The perthite crystals have been partially to completely altered to albite.

## FLUID INCLUSIONS

The fluid inclusion populations in this sample all belong to the same assemblage of fluids associated with the alteration of the granite. The phase proportions are variable, and fluid inclusions containing $CO_2$ double bubbles (Type 5a inclusions) (Figure 5.33 Field 1) are found associated with Type 1a, Type 2 and Type 3 inclusions (Figure 5.34 Field 2 and 3).

## MICROTHERMOMETRY

Freezing occurred between -53 °C and -5 °C, and a brown mosaic developed. First melting was observed at -49 °C in some inclusions and at -46 °C in others. At -42 °C, the mosaic coarsened considerably, and merged at -22 °C. Final melting occurred between -17 °C and -18 °C. A group of about 30 inclusions within this assemblage underwent final melting at 13.3 °C. Homogenisation of the liquid and vapour phases occurred between 157 °C and 180 °C. Homogenisation of the liquid and vapour $CO_2$ occurred at 25.3 °C.

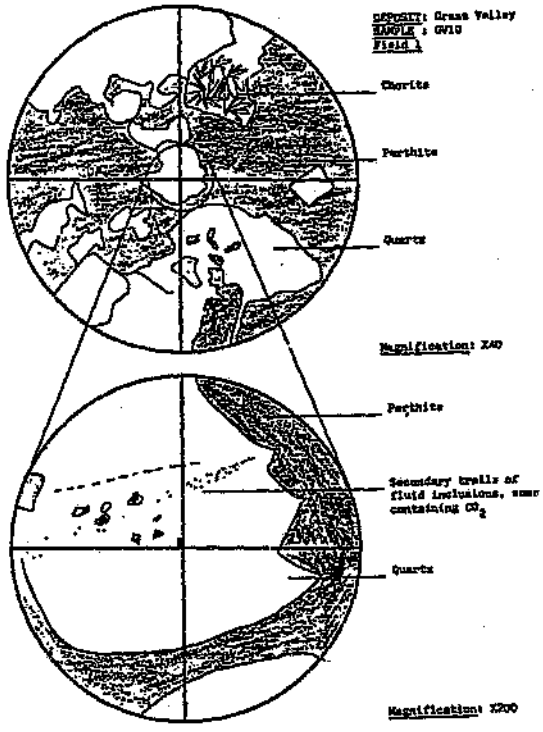


**Figure 5. 33** Petrographic map showing $CO_2$-rich inclusions associated with Type 1a, Type 2 and Type 3 inclusions.

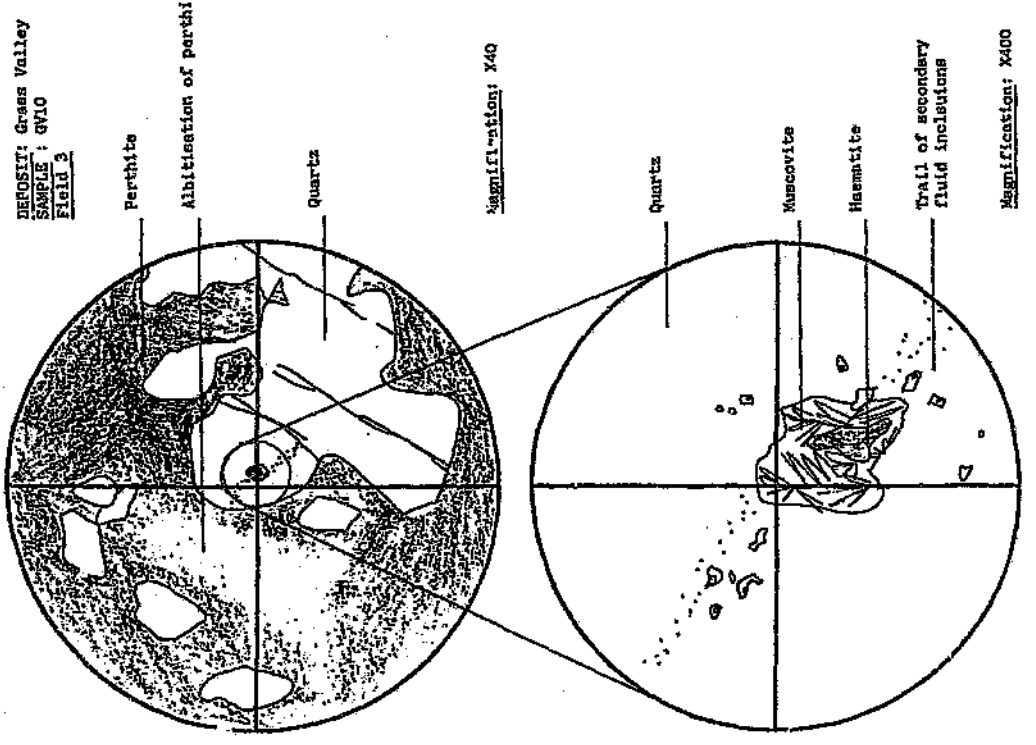


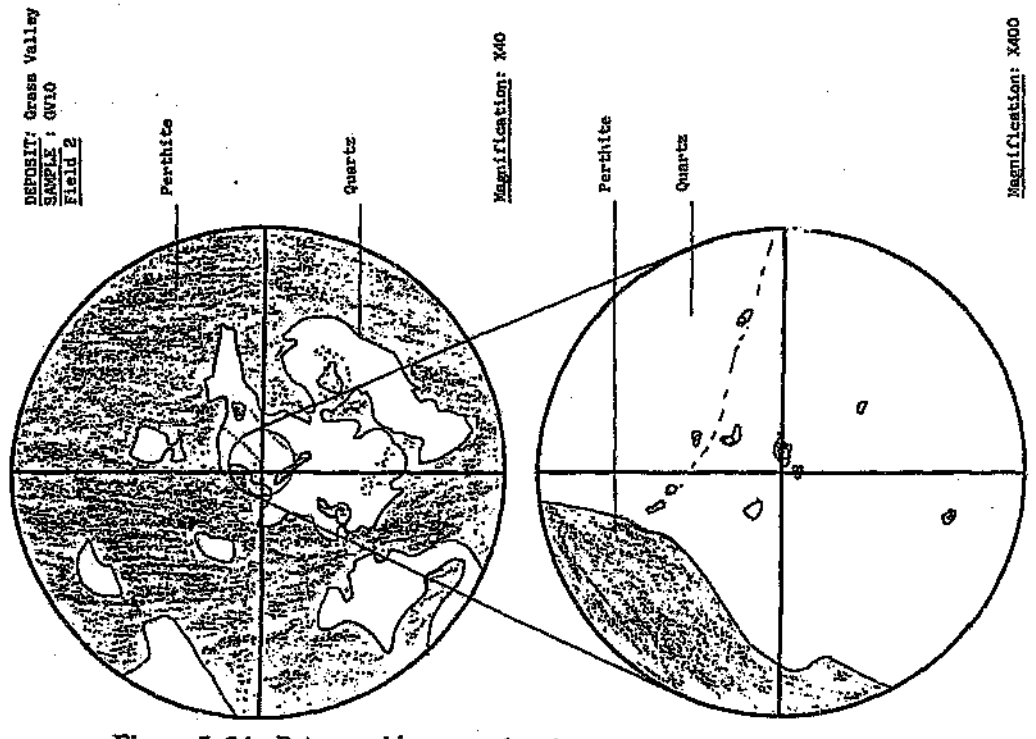


**Figure 5. 34** Petrographic maps showing secondary trails of inclusions associated with alteration of the granite.

## HOUTENBEK

Systematic microthermometry of specifically chosen samples was not undertaken at the Houtenbek deposit. A preliminary investigation of fluids associated with the precipitation of quartz, purple fluorite and transparent sphalerite was undertaken and the results are presented below. It should be noted that these minerals appear to post-date molybdenite precipitation, and if this is indeed the case, should contain no early fluids associated with molybdenite precipitation.

***Fluid inclusions in transparent sphalerite***

Colour banding in the sphalerite indicates that precipitation occurred in several stages and that slight fluctuations in the nature of the fluids occurred. The sphalerite contains primary (Figure 5.35) and secondary (Figure 5.36) fluid inclusions which are predominantly Type 1a inclusions. Primary fluid inclusions in growth zones demarcated by colour banding in the sphalerite were studied. The sketch in Figure 5.37 shows the relationships between sphalerite 1 and sphalerite 2. The primary fluid inclusions hosted by sphalerite 1 are Type 1a inclusions in which the vapour bubble is easily visible. The fluid inclusions in sphalerite 2 are also Type 1a inclusions, but it is very difficult to see the vapour bubble due to the dark discol ration of the inclusion walls. At first sight these inclusions looked like Type 4 vapour inclusions, but on closer inspection it appears that the inclusion walls have been partially altered to an opaque Fe-rich variety of sphalerite.

**Figure 5.35** Primary Type 1a fluid inclusion in sphalerite from Houtenbek.

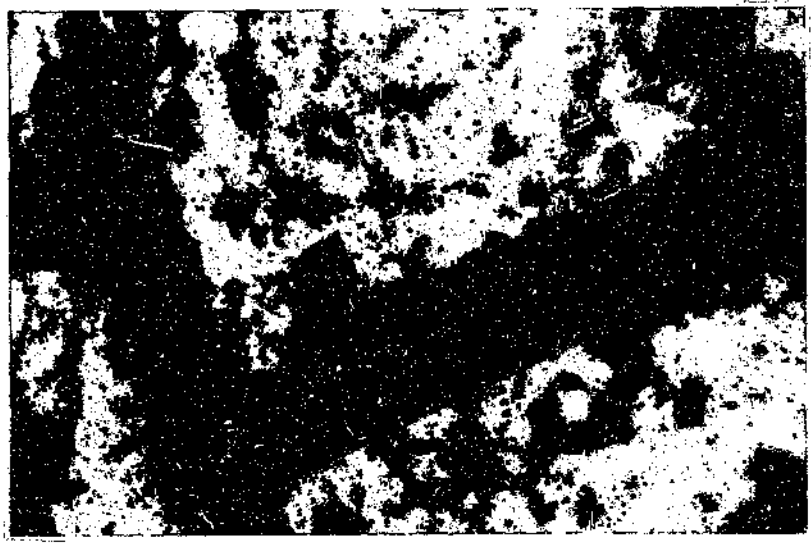

**Figure 5.36** Secondary inclusions in fractures cutting across zoned sphalerite from Houtenbek.

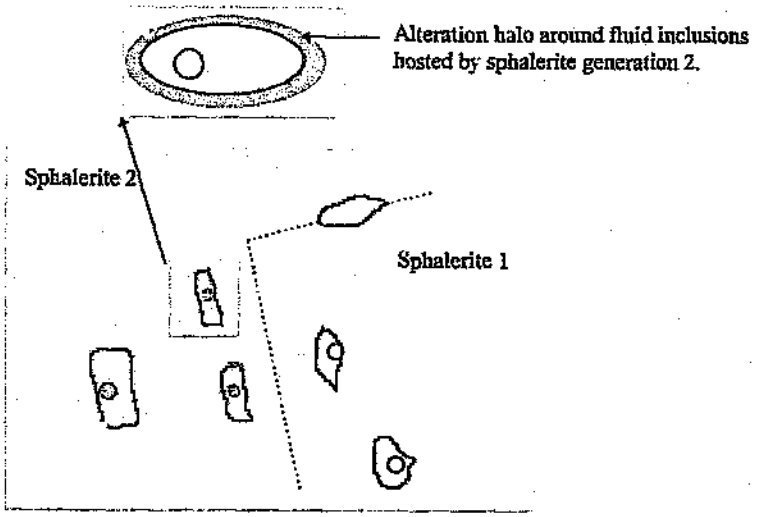


**Figure 5.37** Sketch showing primary fluid inclusions in parallel growth zones in sphalerite generations 1 and 2. The fluid inclusion walls in the second generation have been altered and the resulting opacity makes it difficult to observe phase changes during microthermometry.

The fluid inclusions in sphalerite 1 froze at -47 °C and in sphalerite 2 at -50 °C. In both cases, the vapour bubble collapsed and the inclusions darkened. In sphalerite 1, a mosaic became visible at -39.1 °C, and no change was visible in the inclusions in sphalerite 2. At -27 °C and -26 °C round rafts became visible in sphalerite 1 and 2 respectively. Final melting occurred at -12 °C in inclusions in sphalerite 1 and at -10 °C in sphalerite 2. In both cases, the vapour bubbles chased the ice rafts around the inclusions until they disappeared completely. Homogenisation temperatures for fluid inclusions in sphalerite 1 ranged from 188 °C to 204 °C, and in sphalerite 2 from 200 °C to 215 °C. Decreptitation occurred at temperatures higher than 215 °C.

Fluid inclusions in brown-coloured sphalerite which was precipitated toward the end of the mineralisation event, homogenised at approximately 100 °C and had final melting temperatures between -1.6 °C and 1.4 °C. The inclusions froze at -35 °C and eutectic melting was observed at -33 °C. Intermediate melting events were not recognised due to the poor clarity of the samples.

*Fluid inclusions in purple fluorite:*

The purple fluorite contains many secondary populations of fluid inclusions, as well as a few primary assemblages associated with growth zonation. The inclusions are predominantly Type 1a, and Type 4 fluid inclusions, but rarely, secondary trails containing Type 2 and Type 3 inclusions are also present. Some assemblages contain fluid inclusions with highly variable phase proportions, while others are relatively uniform.

*Fluid inclusions associated with growth zonation*

Growth zones, highlighted by dark purple bands and numerous fluid inclusions outlining crystal faces, contain two fluid inclusion assemblages. Fluid inclusions trapped during the early stages of growth contain populations in which the phase proportions are highly variable consisting of Type 1a, Type 1b, Type 4 and Type 5b ($CO_2$ double bubble) inclusions. They did not develop a brown mosaic on freezing, but rather froze to a clear or cloudy colourless mass. Eutectic melting was not observed. The first obvious signs of melting were visible at -16 °C when coarsening began. At -10.2 °C, an intermediate melting event was observed. Final melting occurred at temperatures slightly above 0 °C (i.e. 0.1 °C to 0.7 °C). Homogenisation of the liquid and vapour phases occurred between 193 °C and 210 °C.

The fluid inclusions trapped in subsequent fluorite growth, froze to a dark brown mosaic at low temperatures (-80 °C). Rearrangement and a slight colour change occurred at -56.6 °C and eutectic melting was observed at -43 °C. Large rafts were visible by -37 °C and final melting took place from -15 °C to -24 °C. Homogenisation temperatures ranged from 231 °C to 250 °C.

Secondary fluid inclusion trails of the fluids associated with the later stages of growth also occur as secondary trails in the earlier formed fluorite. They are slightly lower temperature ($T_h$ 151 °C), but show all same the characteristics.

An intermediate category of fluids, which is intermediate between the fluids associated with the early and late fluorite growth stages were only observed as secondary trails, containing Type 1a and Type 2 inclusions (generally halite and sylvite daughter

crystals). They froze to a brown mosaic at approximately -75 °C. Eutectic melting was observed at -50 °C when the brown coloration began to fade and the relief of the mosaic increased. By -25 °C the mosaic had merged into round rafts, which gradually shrank in size until they were completely melted. The temperature of final melting for this category of fluid inclusions ranges from -4 °C to -7 °C, and homogenisation of the liquid and vapour phases occurred between 150 °C and 240 °C.

The lowest temperature fluids ($T_h$ >100 °C) occur as secondary trails of predominantly Type 3 inclusions. These inclusions produce a colourless solid on freezing. Eutectic melting and intermediate melting events were difficult to recognise before final melting occurred. At -25 °C areas of higher relief became visible, and may represent the eutectic melting event. In many instances, the vapour bubble simply expanded and the cloudiness inside the inclusion disappeared on final melting, and in other cases, sublimation (i.e. the frozen solid melted and the vapour bubble sprang back simultaneously) was noticed. This behaviour was observed at temperatures slightly above 0 °C. In some inclusions clathrates could be seen, but in general they were not visible.

*Fluid inclusions in fluorite post-dating sphalerite*

Primary fluid inclusions in fluorit, post-dating sphalerite and associated with green chlorite, are predominantly Type 1a and Type 3 inclusions, with a few Type 2 inclusions containing chlorite as solid phases. The fluorite partially fills a vug formed by sphalerite crystals, and an open cavity is present in the centre. Fluid inclusions occur in growth zones, with the fluids trapped last occurring towards the central cavity, and those trapped earlier are closer to the vug walls. On freezing ($T_{freeze}$ -45 °C), the vapour bubble disappeared and a colourless mosaic developed. Eutectic melting was observed at -35.8 °C, and intermediate melting events were observed at -29 °C (mosaic merged into round rafts), at -20 °C (the round rafts merged into bigger rafts) and at -12 °C (some rafts melted). Final melting occurred between -2.4 °C and -2.0 °C for the early fluid inclusions, and at -0.8 °C for those fluid inclusions trapped in the late stages of fluorite deposition. Homogenisation temperatures range from 134 °C in the early fluid inclusions to less than 100 °C in the late fluid inclusions, which corresponds with the increase in $T_{final\ melting}$ temperatures from -2.4 °C to -0.8 °C.

***Fluid inclusions in quartz***

The fluid inclusions hosted by the pegmatitic quartz at Houtenbek are predominantly Type 1a inclusions, but several Type 1b, Type 2 and Type 3 inclusions do occur. Phase proportions within assemblages are variable and any combination of the above mentioned fluid inclusion types is possible.

The change in the nature of the fluids was studied in fluid inclusions in four consecutive growth stages in a crystal. The earliest fluids were trapped at relatively high temperatures ($T_h$ approx. 250°C), and the late stage fluids were trapped at temperatures below 100 °C. A change in the fluid character was also observed. The early fluids underwent final melting between -24 °C and -20 °C. The fluids trapped in the last quartz growth stage melted at -2 °C and progressive decrease was observed between the two extremes. A considerable number of $T_{final\ melting}$ data points fell in the range -10 °C to -15 °C. Freezing temperatures for the fluid inclusions trapped in the early quartz growth stages are not as low as was observed in fluid inclusion assemblages at the other deposits. At Houtenbek, freezing took place between -33°C and -41 °C, despite indications that the solute content was considerable (i.e. $T_{final\ melting}$ as low as -24 °C). On freezing, a pale brown mosaic developed and eutectic melting was observed between -38 °C and -34 °C. Intermediate melting events for those inclusions melting below -20 °C were observed at -29 °C and -24 °C.

## SPOEDWEL

The samples selected for microthermometry from Spoedwel are listed in Table 5.4, and the reasons for their selection are given. Hand specimen descriptions, fluid inclusion petrography and microthermometry for each sample are presented in the following sections.

**Table 5.4** List of samples selected for microthermometry from Spoedwel, and the reasons for selection.

| SAMPLE | REASONS FOR SELECTING SAMPLE FOR MICROTHERMOMETRY |
|---|---|
| SP1 | Sample contains fluid inclusions in interstitial quartz that are not necessarily associated with mineralisation, as well as fluids introduced along fractures (quartz veins) which are associated with chalcopyrite precipitation. |
| SP2 | Sample contains fluids associated with the three major quartz generations present in interstitial cavities, including the fluids associated with disseminated sulphide precipitation. |
| SP3 | Sample contains primary fluid inclusions which are associated with the precipitation of fluorite. |
| SP7 | Sample contains fluids associated with quartz vein containing sphalerite crystals. |
| L1 | Sample contain quartz vein with two quartz generations and is associated with chalcopyrite |

**DEPOSIT: SPOEDWEL**

**SAMPLE: SP1**

**HAND SPECIMEN**

This is a fine-grained, pinkish-red granite. The grain size is less than 1mm for the largest quartz grains and 0.1mm for the smallest grains. The rock consists of equal proportions of secondary quartz and hematitised feldspar (perthite). No interstitial fluorite is present. Fluorite and quartz occur as veins from 5mm to a few micrometers in width. The fluorite is colourless to pale purple, the darker coloured fluorite occurring in fine veinlets. The wall rock of the larger quartz veins has been hydrothermally altered. A zone extending approximately 3cm into the host consists of very fine-grained (0.01mm) material. This

zone contains tiny specks of chalcopyrite (0.01mm) which are not present in the host rock. Minor amounts of muscovite are found against the walls of the quartz vugs. Altered cassiterite crystals and euhedral zircon crystals are disseminated throughout the quartz and feldspar host rock. Euhedral monazite is disseminated in the granite. This is a sample of chilled hypersolvus (Nebo) granite, which has been invaded by secondary quartz and fluorite.

## FLUID INCLUSIONS

*In interstitial quartz :*

Two generations of quartz are present in the interstitial spaces between perthite crystals. Fluid inclusions are scarce in the first quartz generation, and extremely abundant in the second generation (Figure 5.38 ). These inclusions are predominantly Type 2 inclusions, containing several solid phases. A total of six different solid phases have been observed in this fluid inclusion assemblage, as many as five solids occurring in any one inclusion. The solids that have been identified by optical methods are halite, hematite, and $FeCl_2$, while the others (a pinkish cube, a blueish cube and an opaque phase) remain unidentified. The degree of fill by the vapour bubble is typically between 10% and 20 %. However, a few inclusions contain no vapour bubble or solid phases (Type 3 inclusions).

## MICROTHERMOMETRY

Fluid inclusions in the interstitial quartz froze on cooling between -50 °C and -80 °C. No super-cooling was required to nucleate ice particles during re-heating. A brown mosaic developed on freezing, which masked the halite crystals and no others. At the eutectic melting temperature, the relief of the mosaic became enhanced and coarsening took place. Eutectic melting occurred at -52 °C. Final melting of the majority of these inclusions occurred between -28 °C and -34 °C. A few inclusions showed an intermediate melting event at these temperatures and final melting occurred at temperatures above 0 °C. Homogenisation temperatures for this FIA were in the range 149 °C to 164 °C, the maximum $T_h$ being 173 °C. Dissolution of daughter crystals did not occur before decreptitation of the fluid inclusions.

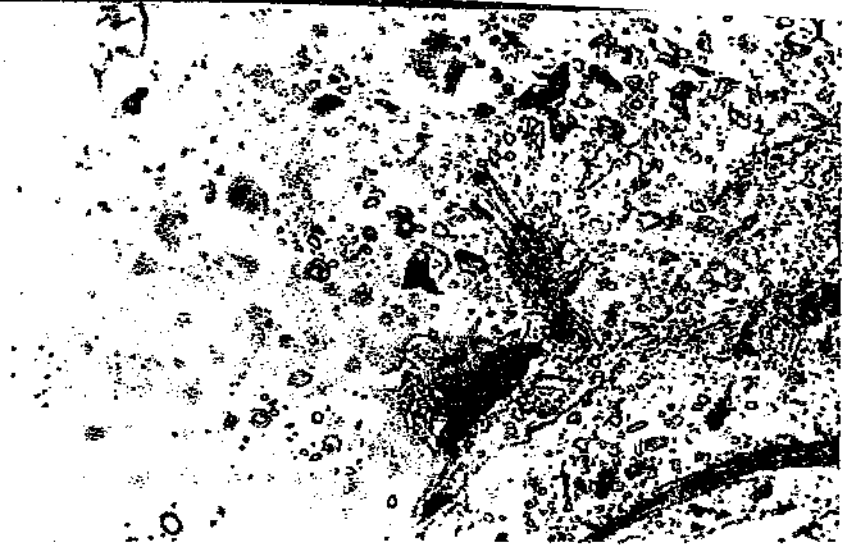

**Figure 5.38** Microphotograph showing the abundance of fluid inclusions in quartz generation 2 (on the right hand side of the picture) compared with quartz generation 1 (on the left). (X 200).

**DEPOSIT: SPOEDWEL**

**SAMPLE: SP2**

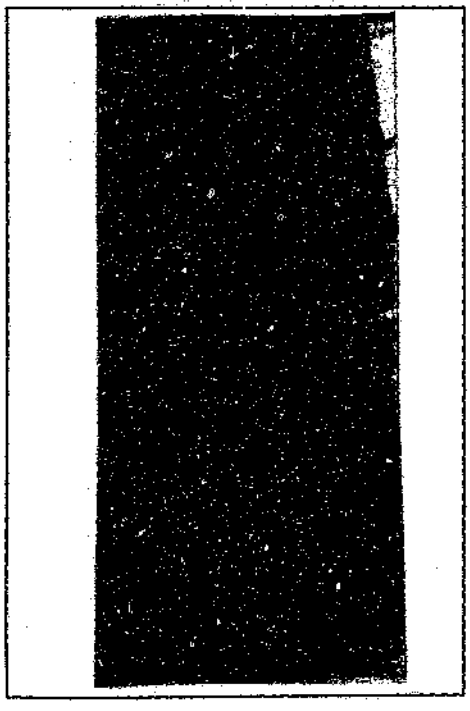

**HAND SPECIMEN**

Medium-grained, red, hypersolvus granite (average grain size 1.2mm) with sulphide specks disseminated throughout the rock, and numerous cross-cutting quartz veins. The vein walls are not hydrothermally altered. The vein material (fluorite) is white and sugary with a purple tint towards the centre of the veins. Chalcopyrite, cassiterite and monazite are scarce. The chalcopyrite is associated with a greenish-yellow alteration mineral that has been identified as chlorite.

## FLUID INCLUSIONS

Fluid inclusions hosted by three generations of quartz occur in the interstitial quartz in this sample (Figure 5.39). The image shows that the early quartz (pale grey), is overgrown by a second generation of quartz (intermediate grey), displaying internal growth lamellae/zonation. A third generation of quartz occurs as secondary trails cutting across the earlier generations. Quartz generation 3 is associated with zircon formation. The zircon crystals have alteration halos that are visible on Figure5.39, but that are invisible to the naked eye. Fluids associated with each of these episodes of quartz deposition have been recognised. The inclusions associated with Quartz 1 are Type 1 and Type 3 inclusions. They contain no daughter crystals and have highly irregular liquid : vapour ratios. In contrast, the fluid inclusions associated with Quartz 2 are Type 2 inclusions, consisting of small vapour bubbles (10% vapour fill), liquid and the occasional small halite daughter crystal. The inclusions associated with Quartz 3 are also Type 2 inclusions, but halite daughter crystals are present in all inclusions, and the crystals are larger. In addition, hematite and several other small solid phases have also been observed in these inclusions. Quartz generation 1 contains few inclusions and is relatively clear, while Quartz 2 is speckled with abundant fluid inclusions (Figure 5.40).

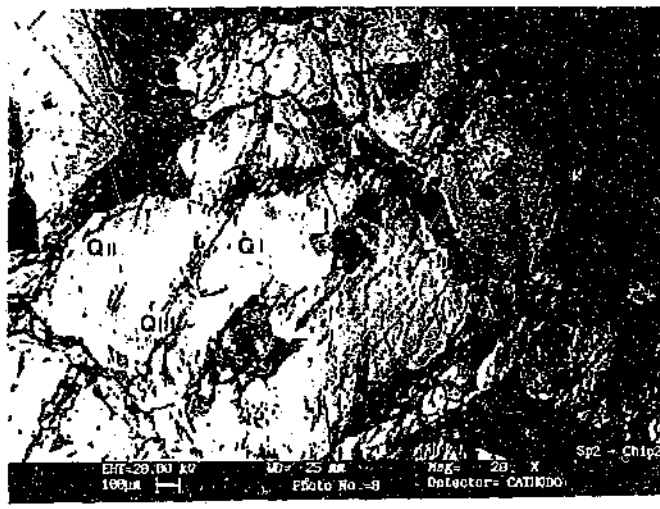


**Figure 5.39** Cathodo-luminescence image showing three generations of quartz in interstitial spaces between feldspar crystals.

**MICROTHERMOMETRY**

*Fluid inclusions in Quartz 1*: This FIA froze at temperatures between -40 °C and -50 °C. The fluid inclusions developed a white cloudy texture, and no brown mosaic was observed. First melting was difficult to observe, the first signs of obvious melting appearing at ~-35 °C, when round rafts developed. Two intermediate melting events were recorded, at -22 °C and at -9 °C. Final melting occurred at temperatures close to, or at, 0 °C. A few fluid inclusions had melted by -2 °C, but most melted at temperatures higher than 0 °C, the highest value recorded being 10 °C. Homogenisation of the liquid and vapour phases generally occurred at temperatures between 225 °C and 250 °C, but the upper and lower limits were not determined.

*Fluid inclusions in Quartz 2:*

These inclusions froze at lower temperatures (-50°C to -60°C) than those in Quartz 1, and they developed a brown mosaic of high relief. Eutectic melting occurred at -36 °C. In some inclusions, intermediate melting events were not observed before final melting at -17.2 °C. Several inclusions melted in the range -12 °C to -15 °C, but melting over a wide range of temperatures has been recorded for this FIA. Fluid inclusions situated near the contact between Quartz 1 and Quartz 2, in the early growth zones, froze at temperatures similar to those of Quartz 1, and underwent final melting at approximately -7 °C. Before final melting occurred, two intermediate melting events were observed, at -31 °C when melting of the clear mosaic became pronounced, and at -24 °C, when the remainder of the mosaic merged into round rafts.

Determining minimum entrapment temperature was difficult for this FIA. Fluid inclusions with small vapour bubbles, which homogenised at approximately 170 °C, are associated with inclusions with larger vapour bubbles, which homogenised at temperatures as high as 378 °C. These inclusions belong to the same FIA, but show extremely large differences in homogenisation temperatures. The average $T_h$ for fluid inclusions in Quartz 2 is 230 °C. Thus, both homogenisation temperatures and final melting temperatures vary considerably in this FIA.

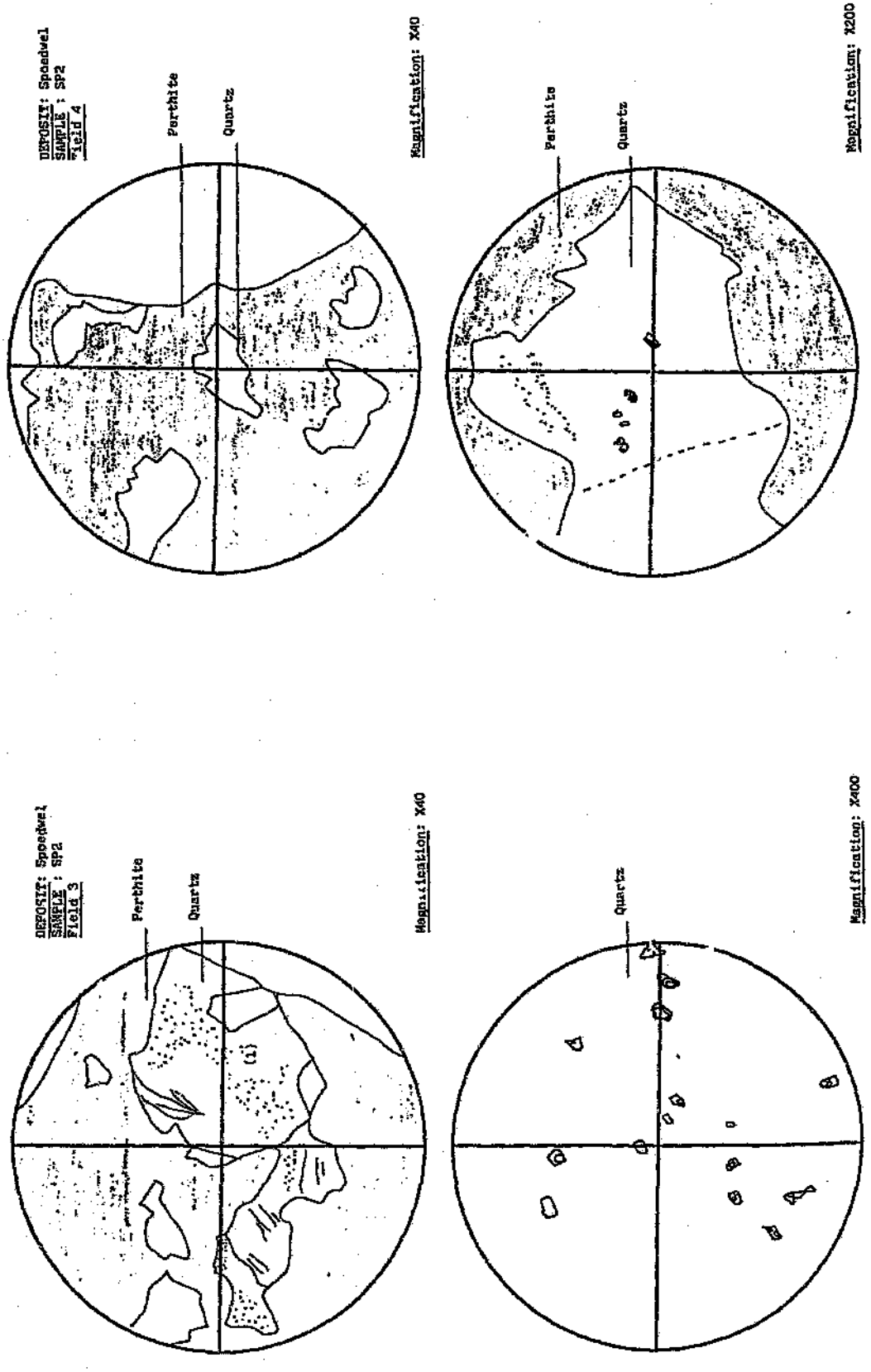


**Figure 5.40** Petrographic maps showing fluid inclusions associated with quartz generations 1 and 2.

*Fluid inclusions in Quartz 3:*

These inclusions froze at even lower temperatures (~-80 °C) than those in Quartz 2, and developed a dark brown mosaic. Eutectic melting occurred between -50 °C and -60 °C, when the mosaic disintegrated and coarsened. Final melting occurred between -30 °C and -38 °C. Homogenisation of the vapour and liquid phases occurred between 93 °C to 107 °C.

**DEPOSIT: SPOEDWEL**

**SAMPLE: SP3**

**HAND SPECIMEN**

A coarse-grained, brick red, hypersolvus granite with little interstitial quartz. The interstitial spaces are generally filled with purple fluorite and dark green chlorite which is partially replaced by hematite. Rosettes of hematite occur as overgrowths on cassiterite and zircon. The hematite rosettes are pseudomorphs after chlorite. Perthite crystals are large (<7mm) and the interstitial quartz and fluorite is minor. No veins or sulphides are present. Small disseminated cassiterite grains are associated with zircon crystals.

**FLUID INCLUSIONS**

*In quartz:*

At least two different fluid inclusion assemblages (FIA's) are recognised in this sample. The one FIA is composed of Type 1 fluid inclusions with approximately 10 % vapour fill, and is associated with monazite. The other consists of predominantly Type 3 (monophase liquid inclusions) with few Type 1 fluid inclusions (less than 5 % vapour fill), and occurs as primary inclusions in quartz overgrowing hematite crystals.

*In fluorite:*

Several FIA's with different characteristics have been trapped in the two fluorite generations at Spoedwel. FIA's with uniform liquid to vapour ratios, as well as FIA's with variable liquid to vapour ratios, have been observed. However, variability in the degree of vapour fill is more often the case. Primary inclusions occurring along growth zones, as well as secondary trails of fluid inclusions, display this variability (Figure 5.39). Solid phases are

extremely rare, and where present, are most likely to represent trapped solids rather than true daughter crystals.

## MICROTHERMOMETRY

*Fluid inclusions in quartz:*

The fluid inclusions associated with hematite precipitation froze at temperatures between -50 °C and -60 °C and developed a brown mosaic. Melting was first observed at -38 °C and by -34 °C the mosaic had disappeared, and only rafts remained. Intermediate melting events were observed at -21°C and -14 °C. Final melting for this FIA occurred between -9 °C and -10 °C. Homogenisation temperatures for the few two phase inclusions occurred below 100 °C.

Within the Type 1a fluid inclusions, two FIA's have been recognised with different microthermometric behaviour. The assemblage with the highest $T_{final\ melting}$ (-13 °C to -17 °C) also had the highest temperatures for homogenisation of the liquid and vapour phases (average 190°C; max. 259°C), and lowest freezing temperatures (-59 °C). The other assemblage had very low $T_{final\ melting}$ (approximately 0°C). This assemblages did not develop a dark brown mosaic on freezing ($T_{freeze}$ between -42°C and -46°C). Homogenisation of vapour into the liquid phase occurred at 158°C.

*Fluid inclusions in fluorite*:

At least four different categories of fluid inclusions have been measured in the fluorite, and are discussed in order of increasing final melting temperatures.

The fluid inclusions with the lowest $T_{final\ melting}$ (-13°C), and lowest freezing temperatures (-60 °C), developed a brown mosaic on freezing and appeared to be secondary in origin. First melting was observed by -42 °C when the relief of the mosaic became enhanced. By -27 °C, the mosaic had merged into rafts which began rounding off. No other obvious intermediate meting events were recorded for this assemblage. Homogenisation occurred between 128 °C and 150 °C.

The FIA with the second lowest $T_{final\ melting}$ (-8 °C to -9 °C), showed very similar microthermometric behaviour to the above mentioned assemblage. First melting occurred

at -52°C, and intermediate melting events were observed at -44 °C (mosaic coarsened), at -37 °C (mosaic merged into rafts), at -28 °C (rafts began rounding), at -23 °C (vapour bubbles sprang back) and at -14 °C (several rafts disappeared). Homogenisation temperatures were slightly lower (123 °C to 128 °C).

A primary FIA occurring along a euhedral growth zone contained fluids that froze at approximately -50 °C and developed no dark brown mosaic. Instead, a pale, cloudy mosaic was produced. Coarsening occurred at -40 °C and then no further changes were observed until -23 °C when round rafts developed. At -21 °C, the individual rafts merged into one large raft, which disappeared at final melting (-4.3 °C). $T_h$ for these fluid inclusions was 150 °C.

The last discrete FIA recognised underwent final melting between -1 °C and 0 °C. On freezing (-42 °C) no brown mosaic developed. $T_e$ was observed at -37 °C. At -30 °C the mosaic merged. No intermediate melting events were observed before final melting. The two phase inclusions underwent homogenisation of the vapour into the liquid phase over a broad range of temperatures, beginning at 130 °C and continuing until 270 °C. The inclusions with small vapour bubbles homogenised at the low end of the range, while those with larger bubbles persisted until higher temperatures.

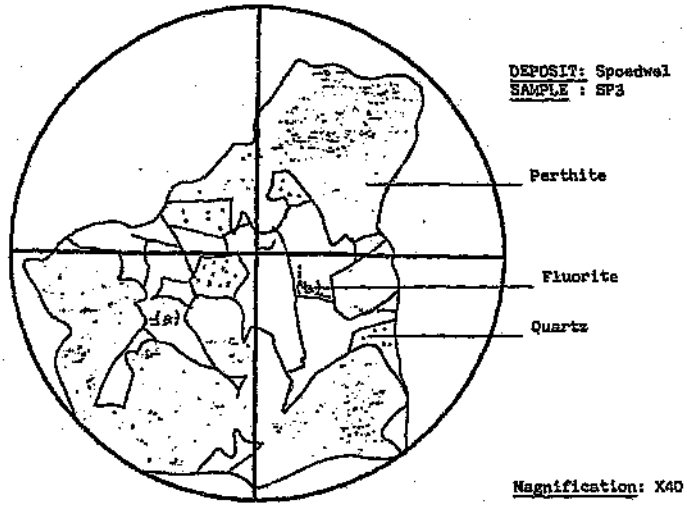


**Figure 5.41** Petrographic map of interstitial quartz and fluorite showing secondary trails of inclusions (a) and growth zone containing primary inclusions (b).

**DEPOSIT:** **SPOEDWEL**

**SAMPLE:** **SP7**

**HAND SPECIMEN**

A medium-grained, hypersolvus granite with local fusion of perthite. Quartz veins with hematite staining along the central seam are present. Interstitial material is minor, and is mostly fluorite with minor quartz. Some quartz contains perthite fragments. Transparent sphalerite occurs against the quartz vein walls. Monazite and a black pitted mineral (identified as hematite by Raman Spectroscopy) are present in this sample.

**FLUID INCLUSIONS**

*In quartz vein material:*

The quartz veins in this sample contain small specks of sphalerite on the walls. The fluid inclusions hosted by the surrounding quartz of the vein show variable phase proportions, being Type 1, Type 2 and Type 3 inclusions. The Type 2 inclusions contain one or two solid phases, which are probably halite and sylvite. The degree of fill of the Type 1 inclusions also varies, from less than 5% to 20 % fill.

**MICROTHERMOMETRY**

The majority of fluid inclusions measured belong to an assemblage which froze to a brown mosaic at temperatures between -50 °C to -55 °C. However, a few inclusions did not show this behaviour, and developed a colourless solid on freezing at approximately -40 °C.

The melting behaviour of these two assemblages differs. The former assemblage displayed rather variable melting temperatures with $T_e$ observed at -52 °C in some inclusions and at -44 °C in others. An intermediate melting event was observed between -24 °C and -26 °C. Final melting temperatures, however, showed the greatest variation, ranging from -14 °C to 5 °C, where clathrate formation retards final melting. Furthermore, homogenisation of liquid and vapour phases also occurred over a wide range of temperatures (173 °C to 288 °C).

Melting in the second assemblage first became obvious at -30 °C, when subtle changes in the mosaic occurred. The formation of round rafts occurred at -25 °C and final melting of the entire assemblage occurred at -5 °C. Homogenisation in this assemblage occurred at slightly lower temperatures (190 °C to 225 °C) than in the FIA described above.

**DEPOSIT: SPOEDWEL**

**SAMPLE: L1**

**HAND SPECIMEN**

A coarse-grained, hypersolvus granite with quartz veins. The feldspars are fused, and interstitial quartz is minor. Most of the quartz in the sample is related to the introduction of the quartz veins. Disseminated cassiterite is present in the host rock. Sulfides are not present in the host rock, but occur as tiny specks of chalcopyrite in the quartz veins. The vein material consists of two generations of quartz. The first generation lines the walls of the veins, projecting as euhedral crystals into the vein center. The second quartz generation occurs in the center of the veins, overgrowing the first euhedral quartz generation.

**FLUID INCLUSIONS**

*Fluid inclusions in vein quartz generation 1:*

This quartz contains few primary inclusions, but mostly secondary and pseudo-secondary fluid inclusions. The primary fluid inclusions are generally located in the central portions of the crystals and may either be isolated or associated with several other inclusions in clusters not related to any linear trend. They also occur as zones parallel to crystal faces corresponding to the consecutive growth stages of the crystal. The shapes of the inclusions range from small spheroids to larger more irregularly

shaped inclusions. The smaller inclusions tend to be monophase liquid (Type 3) inclusions, while the larger inclusions generally contain up to 20% vapour fill. True daughter crystals or trapped solids are rare. Isolated instances of halite and sylvite crystals have been observed.

*Fluid inclusions in vein quartz generation 2:*

The fluid inclusions are highly irregular in shape and are generally necked and faceted. The phase proportions are variable. Many of these inclusions contain a dark solid phase which has been identified as hematite by Raman Spectroscopy. The number of Type 3 inclusions present is greater than the number of Type 1 inclusions. There are no solid phases.

**MICROTHERMOMETRY**

*Fluid inclusions in vein quartz generation 1:*

Freezing occurred between -80 °C and -85 °C , and a fine-grained mosaic of brown-coloured solids developed. Rearrangement of the crystals was observed at -63 °C, and eutectic melting was recognized at approximately -52 °C. Several intermediate melting events were recorded. At -44 °C a change in the mosaic was observed. The mosaic developed wavy edges at approximately -35 °C and the whole mosaic coarsened at -30 °C. The development of round rafts began, and by -15 °C only a few large rafts remained. Final melting of almost all fluid inclusions in this assemblage occurred between -4 °C and -5 °C. Homogenisation temperatures range from 203 °C to 244 °C.

*Fluid inclusions in vein quartz generation 2:*

Freezing occurred between -32 °C and -40 °C, and no brown discoloration of the mosaic was observed. Eutectic melting could not be determined with certainty, but the first obvious signs of melting were visible at -22 °C Two intermediate melting events were observed before final melting. At -10 °C the cloudiness of the mosaic faded, leaving a single clear raft, which then began to shrink at -5 °C. Final melting occurred between [illegible] °C and 0.3 °C. Homogenisation occurred between 160 °C and 193 °C.

## DRONKFONTEIN

The samples from Dronkfontein were selected from diamond drill core, and are listed in Table 5.5 , along with the reasons for their selection.

**Table 5.5** List of samples selected for microthermometry from Dronkfontein, and the reasons for selection.

| SAMPLE | REASONS FOR SELECTING SAMPLE FOR MICROTHERMOMETRY |
|---|---|
| GC600 | Sample contains fluids associated with three generations of interstitial quartz and contains fluids responsible for precipitating disseminated low grade chalcopyrite. |
| GC406 | Sample contains minor disseminated sulphides, and numerous zircon crystals. |

**DEPOSIT: DRONKFONTEIN**

**SAMPLE: GC406**

### HAND SPECIMEN

Medium- to coarse-grained, pink granite composed of quartz, perthite and green chlorite. Some sulphide specks occur in the mafic specks. The average grain size is 3-6mm. Cathodo-luminescence images have shown the same number of quartz generations as in GC600: i.e., there are at least three distinct generations of quartz (Figure 5.42) The first generation consists of euhedral crystals with minor internal growth zonation. The second quartz generation has overgrown the first and is commonly marked by zircon crystals at the contact. The third quartz generation is minor and occurs as secondary trails cutting across quartz 1 and 2. A fourth quartz generation has been observed in some sections where the fractures in which quartz 3 was precipitated were re-utilized, and another (fourth) quartz generation was deposited.

### FLUID INCLUSIONS

The quartz in this sample is full of secondary fluid inclusion trails. Two fluid inclusions assemblages are recognized in this sample, both of which occur as secondary trails. The first assemblage consists of Type 2 inclusions which contain halite daughter

crystals and rarely sylvite crystals. The second assemblage consists of Type 1a (>5% vapour fill) and Type 3 inclusions.

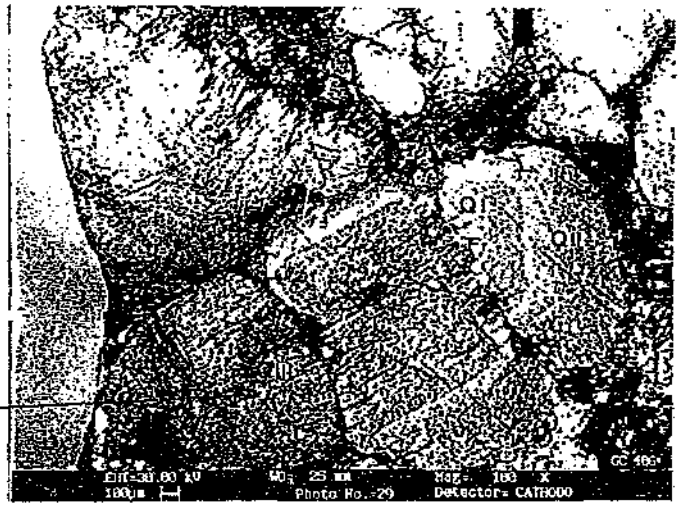


Figure 5.42 Cathodo-luminescence image showing three quartz generations, and the association between zircon precipitation and quartz generations 1, 2 and 3.

MICROTHERMOMETRY

The Type 2 halite-bearing inclusions develop a brown mosaic on freezing at temperatures below -66 °C. A rearrangement of the mosaic was obse d at -64 °C and first melting occurred at -51 °C. At temperatures between -42 °C and -46 °C, the vapour bubble expanded and the last of the frozen solids disappeared. No further melting events could be seen, and the inclusions appeared to be completely melted. Homogenisation temperatures between 116 °C and 125 °C were recorded

The Type 1a and Type 3 inclusions of the second assemblage froze (at -59 °C) to a clear colorless solid and developed no brown mosaic. First melting was observed at -43 °C when a low relief mosaic formed. Coarsening of the mosaic occurred at -35 °C and merging took place at -22.5 °C. Final melting occurred in the range -8 °C to -2 °C. Homogenisation of the vapour bubble into the liquid phase occurred at temperatures below 100 °C.

**DEPOSIT: DRONKFONTEIN CORE -Nebo Granite**

**SAMPLE: GC600**

**HAND SPECIMEN**

Medium-grained granite with disseminated chalcopyrite specks. Cathodo-luminescence images have shown that there are at least three distinct generations of quartz. The first generation consists of euhedral crystals with minor internal growth zonation. The second quartz generation has overgrown the first. The third quartz generation is minor and occurs as secondary trails cutting across Quartz 1 and 2. A fourth quartz generation has been observed in some sections where the fractures in which Quartz 3 was precipitated were re-utilized, and another (fourth) quartz generation was deposited.

**FLUID INCLUSIONS**

Primary fluid inclusions in each of these quartz generations have been studied. The fluid inclusions in quartz 1 are Type 1a, Type 1b, Type 3 and Type 4. The fluid inclusions in quartz 2 are very abundant and show a wide range of characteristics. The fluid inclusions types in this assemblage are Type 1 a, Type 2, Type 3 and Type 4. The Type 2 inclusions contain several daughter crystals, including halite, sylvite, hematite, one opaque crystal, $FeCl_2$ and a small blue cube. e are as many as five of these solids in any one inclusion. However, not all inclusions contain all of these crystals. For example, some contain only hematite and $FeCl_2$, while others contain only halite crystals. Thus, the inclusion contents are highly variable.

The fluid inclusions in quartz 3 are mostly Type 1a, but a l.. Type 2 inclusions containing small halite daughter crystals are present. The inclusions in quartz 4 are Type 1a and Type 3 inclusions and contain no solid phases.

**MICROTHERMOMETRY**

*Fluid inclusions in quartz 1*: On freezing, the vapour bubble became distorted and a clear solid was formed. First melting was observed at -45 °C when a high relief mosaic developed. No further melting events were observed until final melting at -1°C.

Homogenisation of the vapour bubble into the liquid phase occurred between 231°C and 296°C.

*Fluid inclusions in quartz 2*: This assemblage is extremely complex. Freezing occurred between -60 and -70 °C and a brown mosaic was formed. Heating was required in order to induce freezing in some inclusions. Eutectic melting generally occurred between -48 °C and -52 °C. Intermediate melting events were observed at -35 °C (coarsening of mosaic and brown colour fading), at -27 °C (merging of mosaic into round rafts), and at -24 °C (several rafts melted). Final melting occurred over a very wide interval (from -25 °C to 12 °C), but three modes were evident between -25 °C and -22 °C, between -4 °C and -2 °C, and at positive values between 1.7 °C and 12 °C. Homogenisation of the vapour bubble into the liquid phase in Type 1 inclusions occurred between 142 °C and 200 °C, but the bulk of the values recorded were in the range 160 °C to 170 °C.

*Fluid inclusions in quartz 3:* These inclusions froze at -72 °C and developed a clear solid. At -68 °C a brown mosaic developed. First melting was observed at -54 °C and at -26 °C the mosaic began rounding into large rafts. At -24 °C the vapour bubble sprang back and several rafts melted. Final melting values of 0.1 °C were recorded for most of the inclusions, but some fluid inclusions melted at -1.2 °C and 8 °C. Homogenisation occurred between 126 °C and 127 °C.

*Fluid inclusions in quartz 4*: These inclusions froze on heating at -70 °C and became slightly discoloured. Since the inclusions were so small, no mosaic or melting behaviour could be recorded with confidence. Values of melting events at -37 °C and -40 °C were recorded but their siguificance is uncertain. Homogenisation of the small vapour bubbles occurred between 78 °C and 85 °C.

## ALBERT

The sample material was selected from diamond drilled cores and is listed in Table 5.6.

**Table 5.6** List of samples selected for microthermometry from Albert and the reason for their selection.

| SAMPLE | REASONS FOR SELECTING SAMPLE FOR MICROTHERMOMETRY |
|---|---|
| RP1 11 | Sample contains sulphide-bearing quartz veins with associated chlorite. |
| RP1 11a | Sample contains three generations of cross-cutting quartz veins. The second vein contains sulphides and chlorite, and the third is associated with sericitsation. |
| RP2 20B | Sample contains fluids associated with sulphide assemblage and with hematite/fluorite assemblage. |
| AS26.10C | Sample contains fluids associated with the precipitation of arsenopyrite, sphalerite and chalcopyrite. |
| RP2 27A | Sample contains no mineralisation, but is hematitised and chloritised adjacent to a quartz vein. |
| RP2 29 | Sample of unmineralised subsolvus host granite which has been mildly hematitised. |

**DEPOSIT: ALBERT**

**SAMPLE: RP1 11**

**HAND SPECIMEN**

Three quartz veins, two parallel and one cross-cutting, are hosted by a fine-grained, porphyritic transsolvus granite. The average grain size of the host rock is approximately 0.3mm. The original quartz, perthite, albite, and K-feldspar are chloritised and sericitised. First the milky-white quartz vein was intruded, followed by the intermediate milky/clear quartz vein. Both of these vein were cross-cut by the clear quartz vein. Chloritic alteration precedes sericitic alteration, since sericite is associated with the youngest vein only.

## FLUID INCLUSIONS

*Vein 1: Milky-quartz vein*

The vein is made up of many euhedral, terminated quartz crystals. Green chlorite occurs along the vein walls. At least four episodes of quartz precipitation are recognized in the vein, and fluid inclusions associated with each episode have been studied (Figure 5.43). The fluid inclusions are so abundant that they cloud the crystals. Type 1a and Type 3 inclusions are present in primary and secondary populations. No daughter crystals are visible.

*Vein 2: Intermediate- milky/clear quartz vein*

The vein is made up of euhedral crystals that are not as perfectly interlocked as those described in the milky quartz vein. Dark green chlorite fills the interstitial spaces. Many secondary fluid inclusions, which parallel the youngest vein (vein 3 described below), are present in this vein. The phase proportions are variable, and Type 1a, Type 2 and Type 3 fluid inclusions coexist within single populations. Hematite crystals are present in some inclusions. The Type 2 inclusions typically contain halite and sylvite daughter crystals.

*Vein 3: Clear quartz vein with chlorite booklets*

This vein contains quartz crystals with few fluid inclusions. Those present are secondary, with variable phase proportions. Sericite and chlorite are associated with this vein, the wall rocks being highly sericitised and the chlorite occurring within the vein.

## MICROTHERMOMETRY

**Vein 1**

*Quartz generation 1:* Freezing occurred on cooling to -44 °C, and no brown mosaic formed. Eutectic melting was observed at -40 °C. An intermediate melting event was observed at approx. -34 °C. Final melting occurred between - 6 °C and -7.5 °C. Primary inclusions in the center of this quartz generation indicate homogenisation temperatures of approximately 200 °C, while those in growth zones near the crystal faces indicate $T_h$ values of approximately 170 °C.

*Quartz generation 2:* Fluid inclusions in this quartz generation behaved similarly to those in quartz generation 1. However, final melting occurred between -10 °C and -5 °C, and a concentration of $T_{final\ melting}$ values at -5 °C and -6 °C was recorded. Homogenisation temperatures were between 160 °C and 165 °C for primary inclusions.

*Quartz generation 3*: For this population final melting occurred between -4.9 °C and -5.9 °C and homogenised between 120 °C and 140 °C. All other features are the same as in quartz generations 1 and 2.

*Quartz generation 4:* This quartz generation contained the greatest number of Type 3 fluid inclusions. Final melting occurred from -3.1°C (at the beginning of quartz growth) to -0.4°C (at the end of quartz growth).

**Vein 2:**

Freezing occurred between -40 °C and -50 °C, and no brown mosaic developed. Eutectic melting was observed at -47 °C when merging of the colorless mosaic began. At -32 °C, round rafts were visible. Final melting occurred at approximately -5 °C for most inclusions, but a few $T_{final\ melting}$ values at -2 °C were recorded, indicating two different fluid inclusion populations. Homogenisation temperatures in the former assemblage are higher (150 °C to 170 °C) than in the latter assemblage (104 °C to 114 °C). This vein correlates with quartz generations 2 and 3 in vein 1.

**Vein 3:**

Freezing occurred between -37 °C and -40 °C and no brown mosaic formed. Eutectic melting must have occurred at some temperature below -36 °C and was not observed. The first melting event visible occurred at -36 °C when round rafts started developing. At -25°C the small round rafts began merging into single large rafts. Final melting occurred between -7.8 °C and -6.4 °C. Homogenization of these inclusions occurred at approximately 152 °C. A single inclusion underwent final melting at -24 °C, and homogenised at 103 °C.

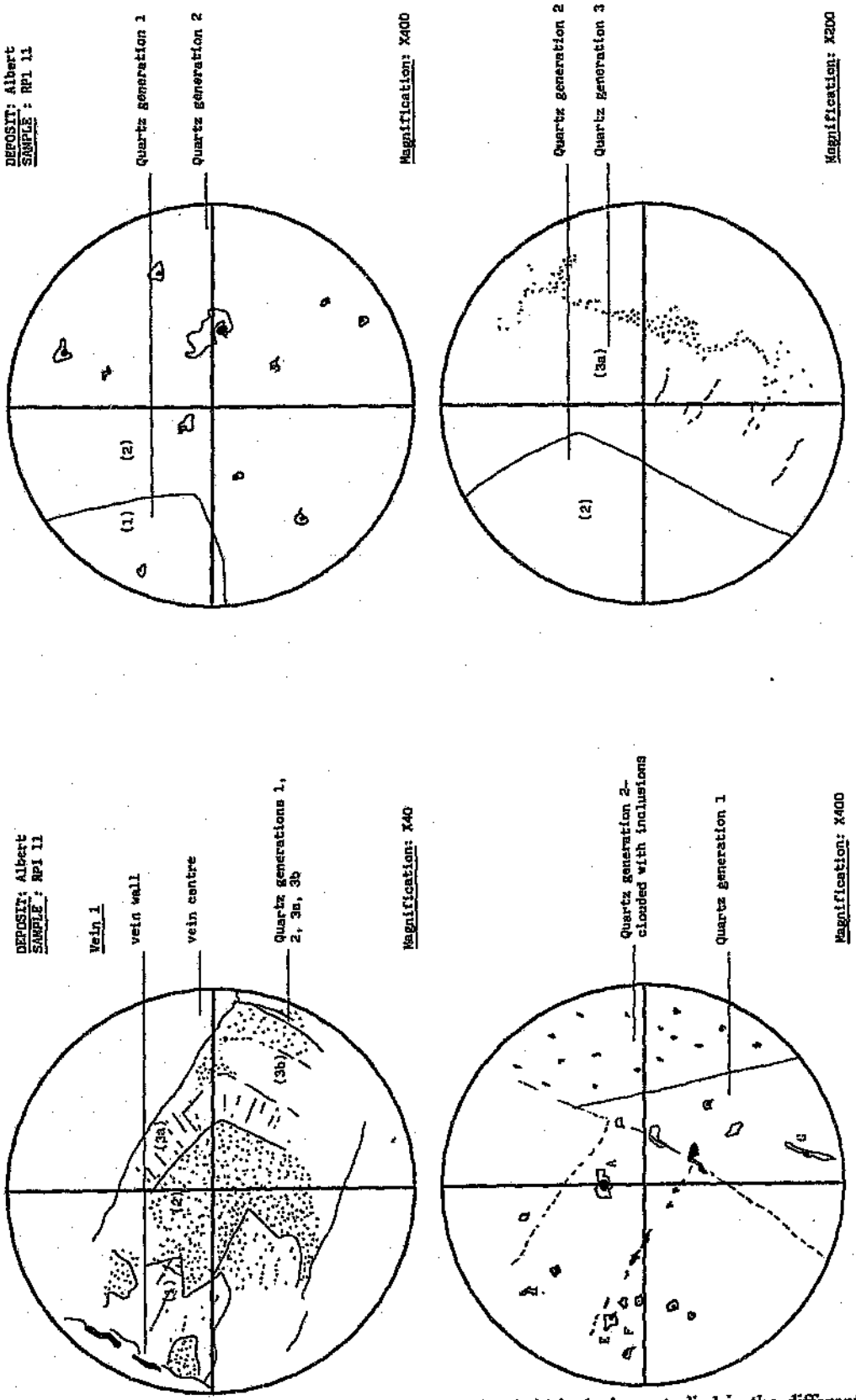


**Figure 5.43** Petrographic maps showing the fluid inclusions studied in the different quartz generations in vein 1, and in veins 2 and 3 in sample RP1 11 from Albert.

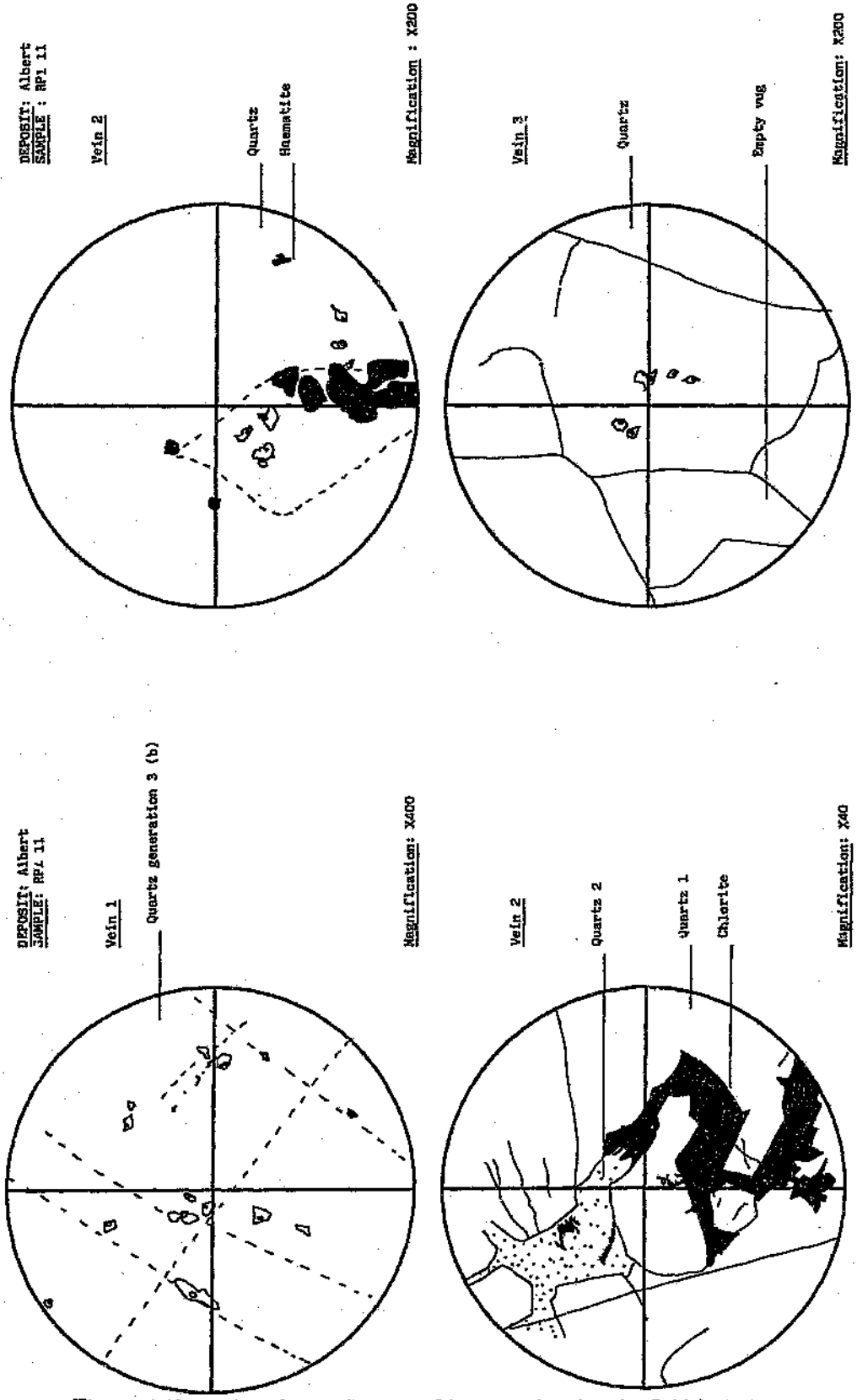


**Figure 5.43 continued** Petrographic maps showing the fluid inclusions studied in the different quartz generations in vein 1, and in veins 2 and 3 in sample RP1 11 from Albert.

**DEPOSIT: ALBERT**

**SAMPLE: RP1 11A**

**HAND SPECIMEN**

Three parallel quartz veins cutting across fine-grained subsolvus granite.

*Vein 1: Clear quartz containing sulphides and chlorite*

The vein walls are composed of fine-grained, crypto-crystalline quartz which has been chloritised. The central portions of the vein consists of coarse-grained, euhedral quartz intergrown with pyrite. Grass green chlorite fills cavities in the middle. Hematite specks occur on the crystal faces of the quartz. The pyrite crystals are generally large (2-5mm), but smaller crystals (0.3mm) do occur. Minor tetrahedrite, galena and chalcopyrite are present.

*Vein 2: Milky-white quartz*

Many small, euhedral crystals fill this vein. The milky appearance of the quartz is due to the abundance of fluid inclusions in the crystals. The wall rock is sericitised and chloritised (pale, olive green chlorite).

*Vein 3: Intermediate- milky/clear quartz*

The vein is composed of small quartz crystals. The center of the vein contains massive quartz. No alteration minerals are associated with this quartz vein.

**FLUID INCLUSIONS**

*Vein 1: In clear quartz containing sulphides and chlorite*

Fluid inclusions in the quartz vein containing sulphides and chlorite are Type 1a and Type 2 inclusions. Type 4 inclusions (monophase vapour) are abundant in certain patches and Type 3 inclusions are scarce. Phase proportions are constant. Daughter crystals are common. Halite, sylvite and $FeCl_2$ daughter crystals have been identified by

optical methods. Daughter crystals are rarely vary large, filling more than 50% of the inclusion volume.

*Vein 2: Milky-white quartz*

Fluid inclusions are irregular and many dark solids (hematite?) cloud the clarity of the crystals. Most inclusions are Type 1a inclusions.

*Vein 3: Intermediate- milky/clear quartz*

Type 1 and Type 3 fluid inclusions are present. Phase proportions are generally variable. Secondary trails with constant phase proportions do occur.

**MICROTHERMOMETRY**

*Vein 1: In clear quartz containing sulphides and chlorite*

Fluid inclusions in this sample are extremely complex. It was not possible to categorize them according to their microthermometric behavior and they have been grouped as one assemblage with highly variable compositions. This variability may be the result of fluids associated with veins 2 and 3 being trapped as secondary inclusions within primary populations of inclusions associated with vein 1.

All fluid inclusions froze at temperatures between -50 °C and -82 °C, and developed a brown mosaic. Eutectic melting was observed at a number of different temperatures, ranging from -52 °C to -44 °C. The majority of values recorded were at approximately -44 °C, but a group of values between -39 °C and -36 °C were also recorded. This temperature range corresponds to an intermediate melting event in inclusions in which eutectic melting was observed from -52 °C to -44 °C. Intermediate melting events were observed at -36 °C and -23 °C in both primary and secondary populations. At -36 °C coarsening of the mosaic was observed, whereas at -23 °C rapid clearing of the mosaic took place, and a few small round rafts remained. In some inclusions, final melting occurred almost immediately (-22.3 °C) afterwards. Final melting of fluid inclusions continued until 10 °C when the last inclusions underwent final melting. However, within this continuum, many $T_{final\ melting}$ values were recorded at -16 °C, from -10 °C to -6 °C, and from 9 °C to 13 °C. The average temperature for homogenisation of liquid and vapour phases was 168 °C, but values as low as 96 °C and as high as 214 °C

have been recorded. Dissolution of daughter crystals was not achieved before the vapour phase had disappeared. A temperature for dissolution of one halite daughter crystal was measured at 168 °C. There is no considerable difference in homogenisation temperatures in the primary and secondary populations, although the few high $T_h$ values recorded are from primary populations.

**DEPOSIT: ALBERT**

**SAMPLE: RP2 20B**

**HANDSPECIMEN**

Pegmatitic vein quartz and fluorite, with associated chalcopyrite and grass green chlorite. Euhedral quartz crystals and chalcopyrite are overgrown by massive fluorite and chlorite. Hematite occurs along grain boundaries and in interstitial cavities.

**FLUID INCLUSIONS**

*Fluid inclusions in fluorite:*

The fluorite contains numerous fluid inclusions, mostly Type 1a and Type 3, but a few Type 1b (with more than 50% vapour fill) inclusions are present. Daughter crystals are scarce. Both primary and secondary assemblages have been recognized, the secondary assemblages containing smaller vapour bubbles than those appearing to be primary in origin. In general, there is a variation in phase proportions. Figure 5.44 shows the petrographic relationships of fluid inclusions selected for study in this sample

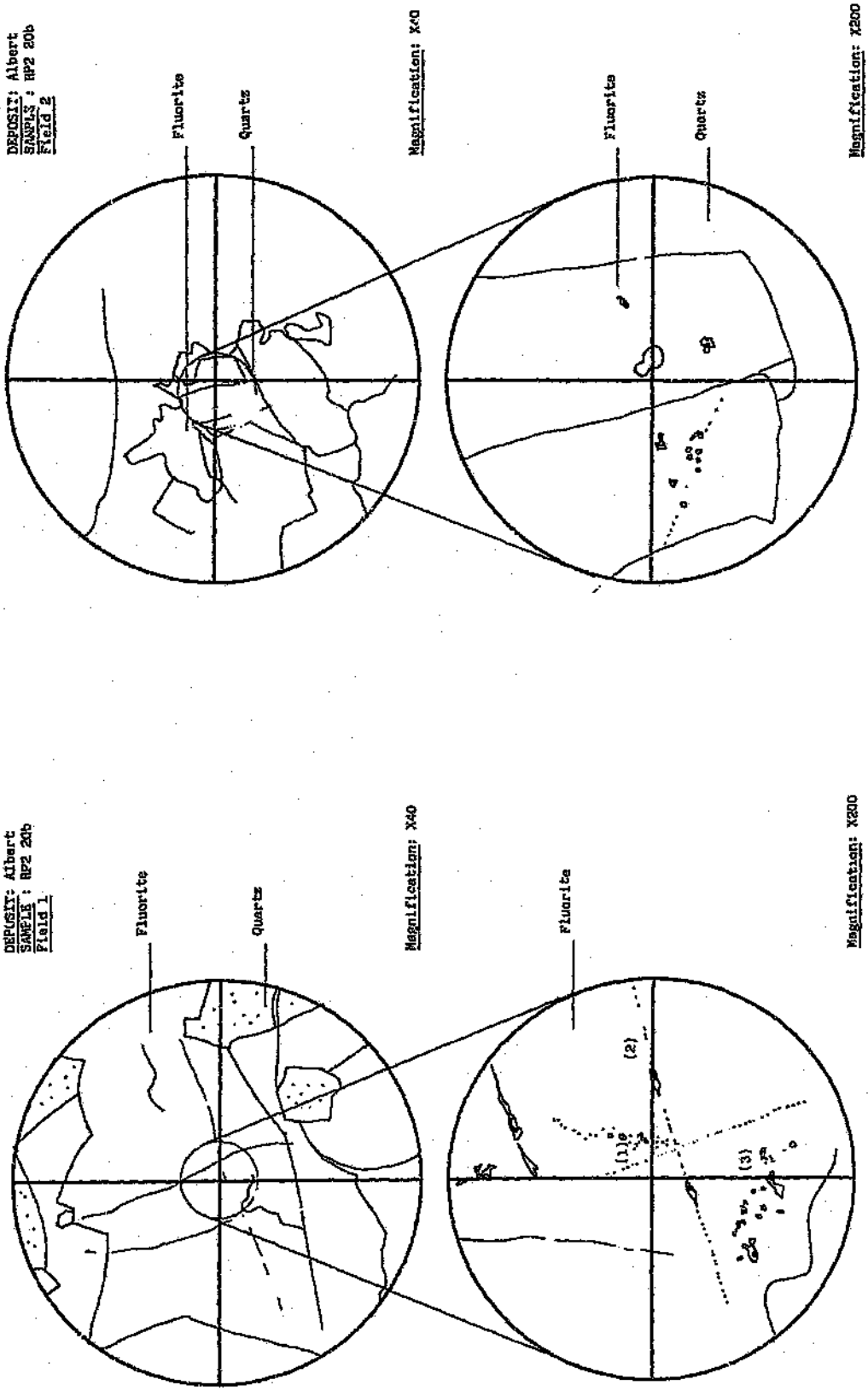


**Figure 5.44** Petrographic maps showing fluid inclusions in fluorite in sample RP2 20B.

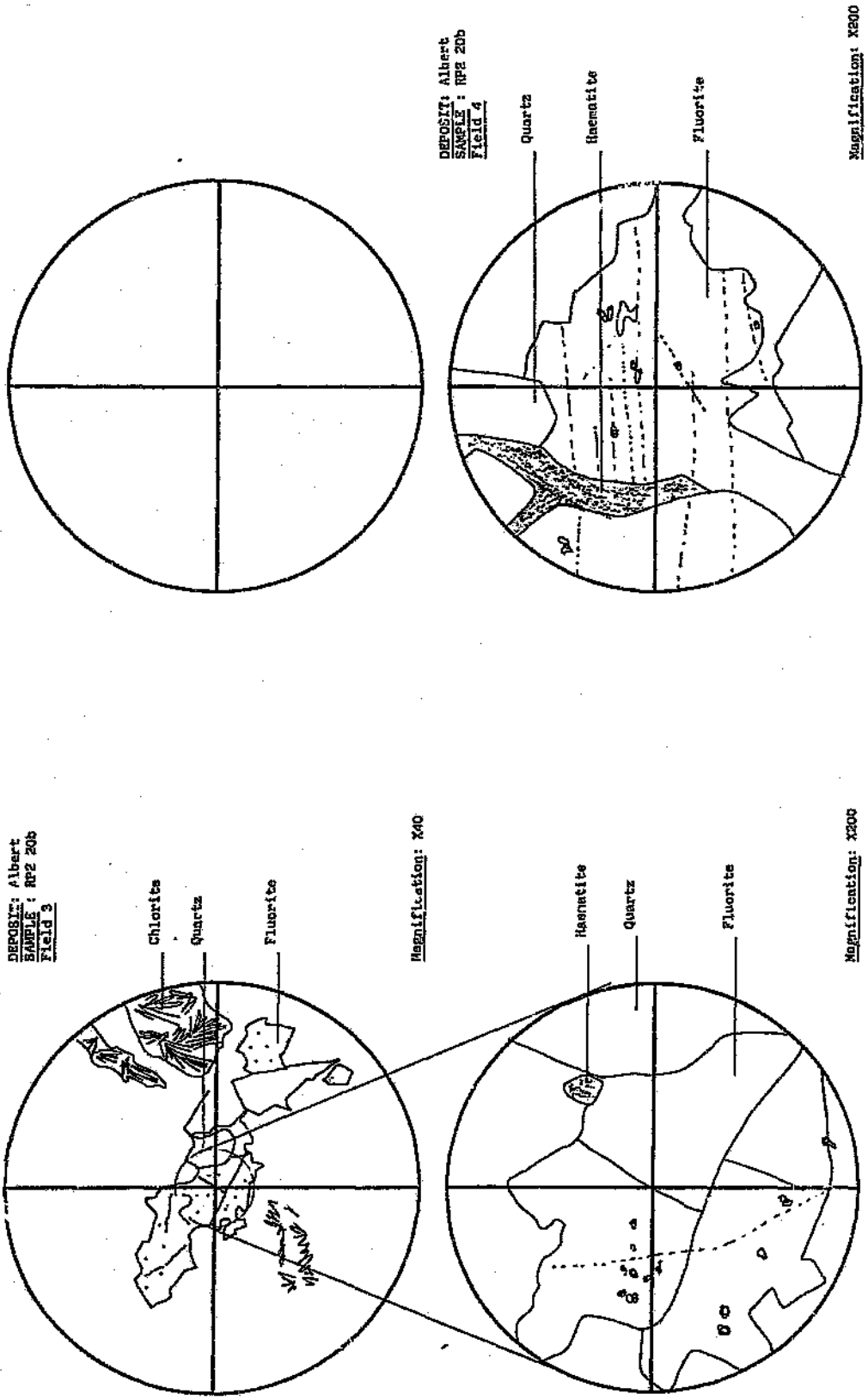


**Figure 5.44 continued** Petrographic maps showing fluid inclusions in fluorite in sample RP2 20B.

**MICROTHERMOMETRY**

At least three different fluid inclusion assemblages are present in the fluorite in this sample. At the one extreme, the assemblage with the lowest final melting temperature range (between -16 °C and -10 °C) occur as primary and pseudo-secondary inclusions, which froze between -57 °C and -78 °C, and developed a brown mosaic. Eutectic melting occurred at approximately -49 °C, and the mosaic began to disintegrate. At -29 °C, the mosaic became coarser and rafts became visible. Some rafts melted at -23 °C and others at -16 °C. Final melting temperatures ranged from -16 °C to -10 °C. $T_h$ for this assemblage was between 171 °C and 200 °C.

An intermediate category of fluid inclusions, which froze by -48 °C and developed a colorless mosaic, has been observed. Eutectic melting occurred at or before -39 °C. One intermediate melting event at -30 °C was observed before final melting (at -6 °C to -8 °C). Entrapment of the fluids occurred at temperatures below 200 °C (decrepitation occurred at temperatures higher than 200°C).

The bulk of the fluid inclusions measured belong in the category of inclusions which underwent final melting between -4.8 °C and -3.2 °C. These fluid inclusions occur in secondary trails, and clearly belong to the same fluid inclusion assemblage. On freezing, a colorless mosaic formed, which underwent eutectic melting at -33 °C. By -27 °C, the mosaic had merged to form rounded rafts, and, in general, only one large round raft remained in each fluid inclusion. This raft became progressively smaller as final melting temperatures were approached. The wide variation of final melting temperatures within single fluid inclusions assemblages is mirrored in the measured homogenisation temperatures, which range from 218 °C and 273 °C.

At the other extreme is a fluid inclusion assemblage displaying the same characteristics as the assemblage described immediately above, but in which final melting occurred between -2.6 °C and -1.7 °C, and homogenisation of the liquid and vapour phases occurred at low temperatures ( 93 °C to 112 °C).

**DEPOSIT:** **ALBERT**

**SAMPLE:** ***A*S26.10C**

**HAND SPECIMEN**

Massive cryptocrystalline quartz, associated with quartz and fluorite. Patches and veins of sulphide occur along grain boundaries, and are associated with green chlorite. The sulphide paragenesis is arsenopyrite-sphalerite-chalcopyrite. Veins of a later quartz generation (which is optically clear) cut across earlier formed milky-white quartz crystals.

**FLUID INCLUSIONS**

Fluid inclusions occur in quartz which contains solid inclusions of chlorite and arsenopyrite, as well as in the fluorite post-dating these phases (Figure 5.45). The fluid inclusions in the quartz are Type 1a and Type 2 inclusions. Small pale blue cubic daughter crystals are present in some of the fluid inclusions. The fluid inclusions selected for microthermometry are primary and negative crystal outlines are relatively common. The fluorite contains many fluid inclusions, most of which are secondary Type 1a inclusions, and Type 3 inclusions. A few Type 2 inclusions were observed, but the solid phases are probably trapped solids and not true daughter crystals.

**MICROTHERMOMETRY**

*Fluid inclusions in quartz associated with arsenopyrite and chlorite:*

$T_{freeze}$ was between -46 °C and -56 °C, and a pale brown mosaic formed. Eutectic melting occurred at -41°C, and by -27 °C round rafts were visible. An intermediate melting event occurred at -12 °C, when some rafts disappeared. A broad range of melting temperatures was observed in this FIA. Fluid inclusions containing the blue

cubes melted at -8.8 °C, and those without daughters underwent final melting between -4.2 °C and 0.2 °C. Homogenisation temperatures were not recorded.

*Fluid inclusions in fluorite post-dating arsenopyrite and chlorite:*

A population of possibly primary Type 1a fluid inclusions froze to a colorless solid at -37 °C, and underwent eutectic melting at -31°C. At -23 °C, the mosaic rapidly disintegrated into rafts. Final melting of some inclusions began at -3.5 °C and continued until -1.4 °C when all fluid inclusions were melted. The first inclusions to homogenise did so at 123 °C, while the rest homogenised between 140 °C and 145 °C. The highest temperature recorded for homogenisation in this assemblage was 243 °C.

A secondary trail of Type 3 inclusions with a few Type 1a (degree of vapour fill approx. 2%) froze to a pale mosaic which darkened at -40°C ($T_e$?). At -25 °C, coarsening of the mosaic began, and by -?3°C, round rafts had developed. Final melting occurred in the range -3.9 °C to 1.6 °C. Homogenisation temperatures for the two phase inclusions were between 100 °C and 120 °C.

**Figure 5. 45** Petrographic maps showing the relationship of quartz-hosted fluid inclusions with arsenopyrite and fluorite-hosted fluid inclusions with chlorite.

**DEPOSIT:** **ALBERT**

**SAMPLE:** **RP2 27A**

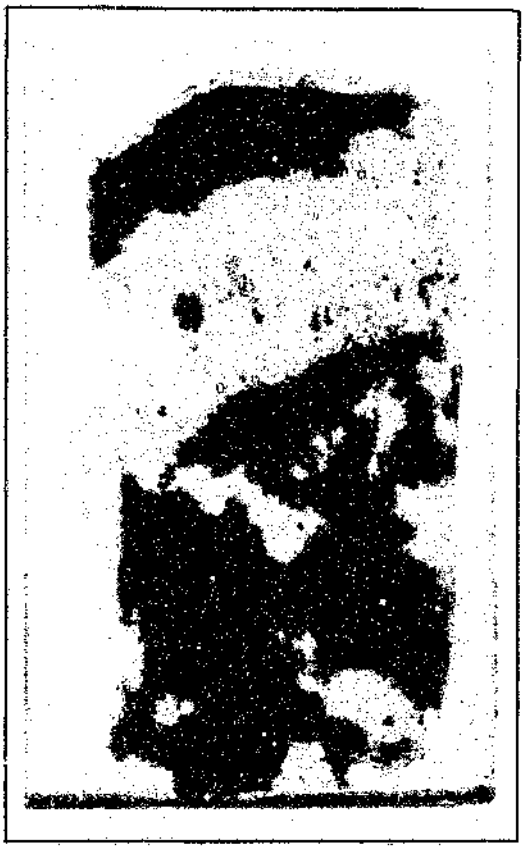

**HAND SPECIMEN**

Quartz vein cutting across a chloritised, hematitised and sericitised subsolvus granite host rock. Epidote is present in some portions of the sample. The quartz vein is composed of many small euhedral crystals and a very fine-grained cryptocrystalline quartz variety. Hematite is associated with the quartz vein.

**FLUID INCLUSIONS**

Fluid inclusions in the quartz vein are too small to be useful for microthermometry. However, the interstitial quartz material of the granite host contains two fluid inclusion assemblages, which are associated with the granite itself, and as secondary trails, parallel to the quartz vein (Figure 5.46). The one assemblage contains no solid phases, and consists of Type 1a and Type 3 inclusions. The other assemblage contains Type 1a and Type 2 inclusions.

**Figure 5. 46** Petrographic maps of interstitial quartz containing numerous cross-cutting secondary trails of inclusions.

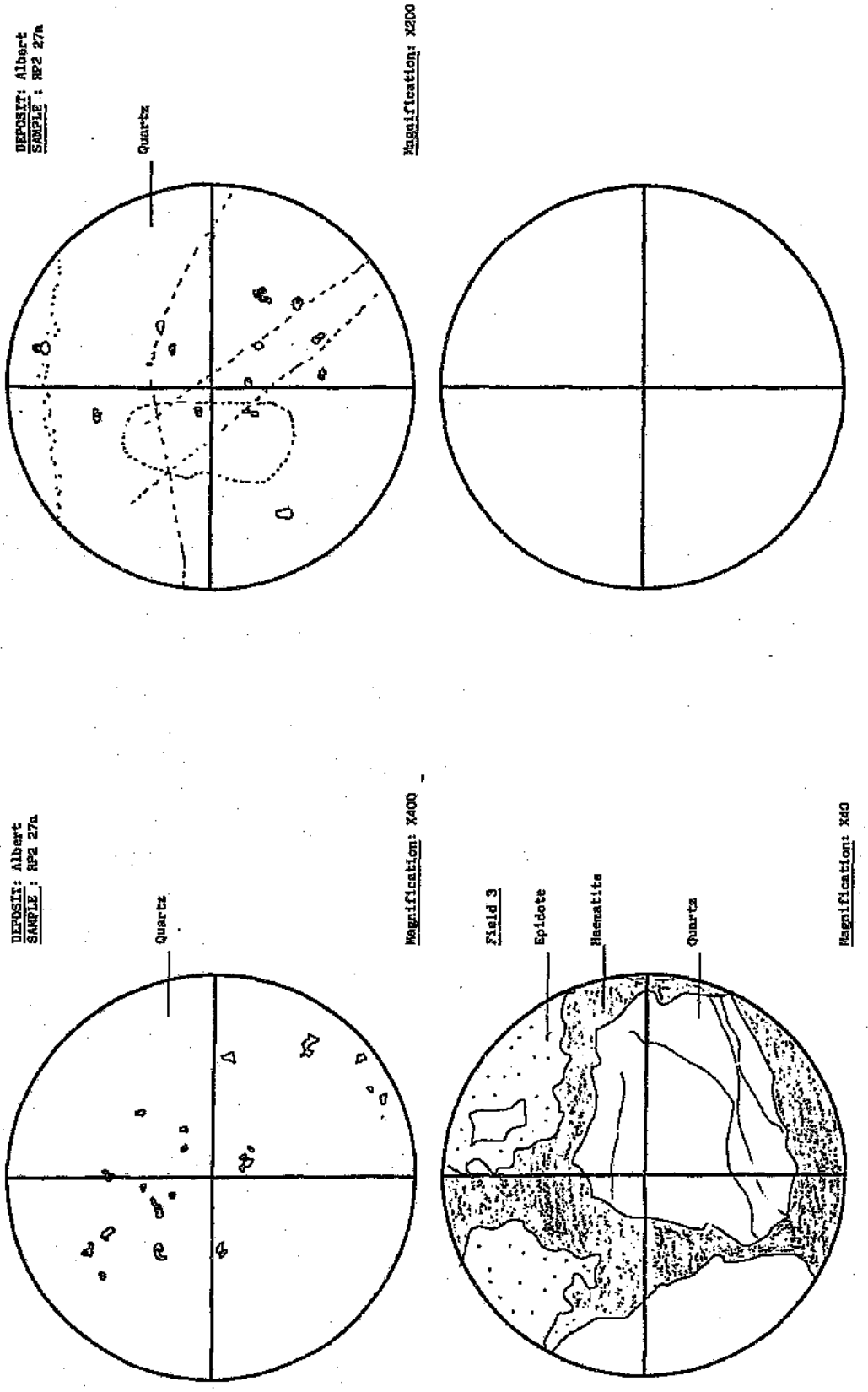


**Figure 5. 46 continued** Petrographic maps of interstitial quartz containing numerous cross-cutting secondary trails of inclusions.

## MICROTHERMOMETRY

Two distinct fluid inclusion assemblages are recognizable in terms of their microthermometric behavior. They are distinguished by the different ranges of freezing temperatures and the presence or absence of a brown mosaic.

The assemblage that showed no brown discoloration of the mosaic on freezing (between -44 °C and -48 °C), underwent eutectic melting at approximately -40 °C and is present as primary and secondary inclusions. Intermediate melting events were observed at -34 °C when the coarsened mosaic merged to form larger rafts. At -21°C and -16 °C several rafts in each inclusion melted. The ice melted over a broad temperature range (-4.4 °C to 4.3°C). Eutectic and intermediate melting events were not visible in some fluid inclusions. At final melting, the vapour bubble sprang back and solids disappeared simultaneously. $T_h$ values were between 128 °C and 173 °C.

The second fluid inclusion assemblage contains several daughter crystals ($FeCl_2$, halite and sylvite) and developed a very pronounced brown mosaic on freezing, which took place at considerably lower temperatures (-66 °C to -75 °C) than the first assemblage described. Eutectic melting occurs between -50 °C and -52 °C. Intermediate melting events were observed at -40 °C when the mosaic became coarser, at -33 °C , at -28 °C when the mosaic merged to form rafts, and at -24 °C when several rafts melted. Final melting occurred over a wide range of temperatures (-4.8 °C to 15 °C). However, two modes of values are apparent, one between -4 °C and -5 °C, and the other, at the unusually high range from 8.6 °C to 15.3 °C. Homogenisation occurred between 76 °C and 160 °C, but the majority of fluid inclusions homogenised at approximately 130 °C. Dissolution of daughter crystals did not occur before homogenisation of the vapour bubble into the liquid phase.

**DEPOSIT:** ALBERT

**SAMPLE:** RP2 27/9

**HAND SPECIMEN**

A coarse-grained porphyritic, subsolvus granite containing large, pink, perthite phenocrysts which are partially chloritised and sericitised. Euhedral albite crystals occur with partially albitised perthite and quartz. Mafic patches of hematite, biotite and zircon are present. Hematite liberated from the perthite occurs as rims of red material around the grains.

**FLUID INCLUSIONS**

In terms of appearance, two distinct assemblages are recognizable. The most obvious fluid inclusion assemblage contains as many as six unidentifiable daughter crystals, which occur as primary inclusions along growth zones towards the end of the crystallization history of the quartz, and as secondary trails cutting across earlier formed crystals (Figure 5.47 Field 3) They are all Type 2 inclusions and are rather unusual in appearance. The difference in refractive index between the host quartz and the fluid inclusion liquid is small, and, thus, there is little contrast in optical properties between the two media. The vapour bubble and solids appear to be suspended in the quartz, and it is only on freezing that the outline of the fluid inclusions becomes visible. The other group of inclusions are normal Type 1a and Type 2 (with one halite daughter crystal) and Type 3 inclusions which tend to be secondary in origin (Figure 5.47 Field 1 and 2).

## MICROTHERMOMETRY

Four FIA's have emerged from the microthermometric data. Two groups exist within the daughter-rich assemblage which are distinctly different from the Type1a fluid inclusions in terms of microthermometric behavior. The Type 1a inclusions are separated into three categories depending on their final melting temperatures.

The daughter-rich assemblage froze at temperatures between -63 °C and -72 °C, and a slight brown discoloration of the mosaic was visible. These inclusions are among the few that require heating after super-cooling to induce freezing. At -66°C the brown mosaic developed, and rearrangement took place at -59°C, after which the brown began to fade. Eutectic melting was not recorded. Intermediate melting events were observed at -40 °C, when the mosaic started merging, and at -31°C when round rafts developed. Final melting of some inclusions occurred at -24.5 °C and -18.1°C. These inclusions are associated with another group that generally have final melting temperatures above 0 °C. In fact most of these Type 2 inclusions melted completely between 3.7 °C and 9.2 °C. Homogenisation temperatures were relatively high ( >225 °C), and the solid phases tended to resist melting. Dissolution temperatures (180 °C to 184 °C) were recorded for an unidentifiable solid phase.

Microthermometric behavior in the Type 1a assemblage was relatively constant except for the final melting temperatures. They all froze at -63 °C, developed no brown mosaic and underwent eutectic melting between -46 °C and -48 °C. Intermediate melting events occurred at -45 °C, when coarsening occurred, at -36 °C when round rafts developed, and at -30 °C and -24 °C when several rafts disappeared. Three different secondary trails each with different final melting temperatures were measured. One group melted between -15 °C and -11 °C, another at approximately -10 °C, and the last between -8 °C and -5 °C. However, it is clear that these measurements form part of a continuum from -5 °C to -15 °C. The corresponding ranges of homogenisation temperatures are 130 °C to 147 °C, 155 °C and 190 °C to 200 °C.

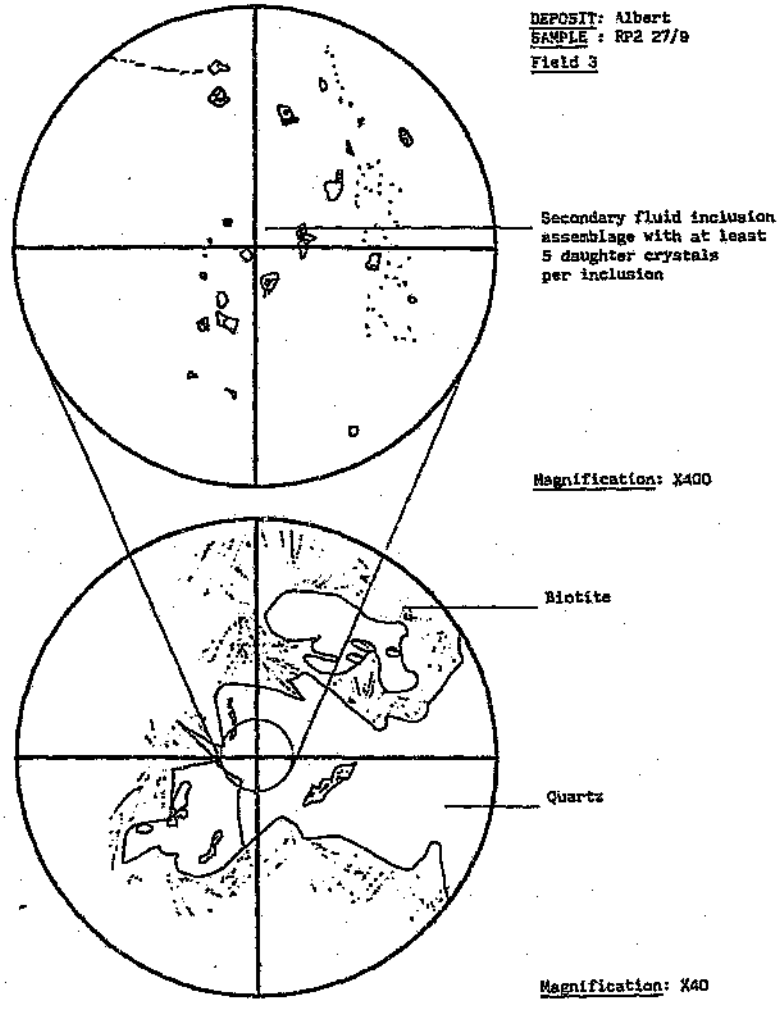


**Figure 5.47** Petrographic maps of the daughter crystal-rich fluid inclusion assemblage in quartz associated with biotite in sample RP2 27/9.

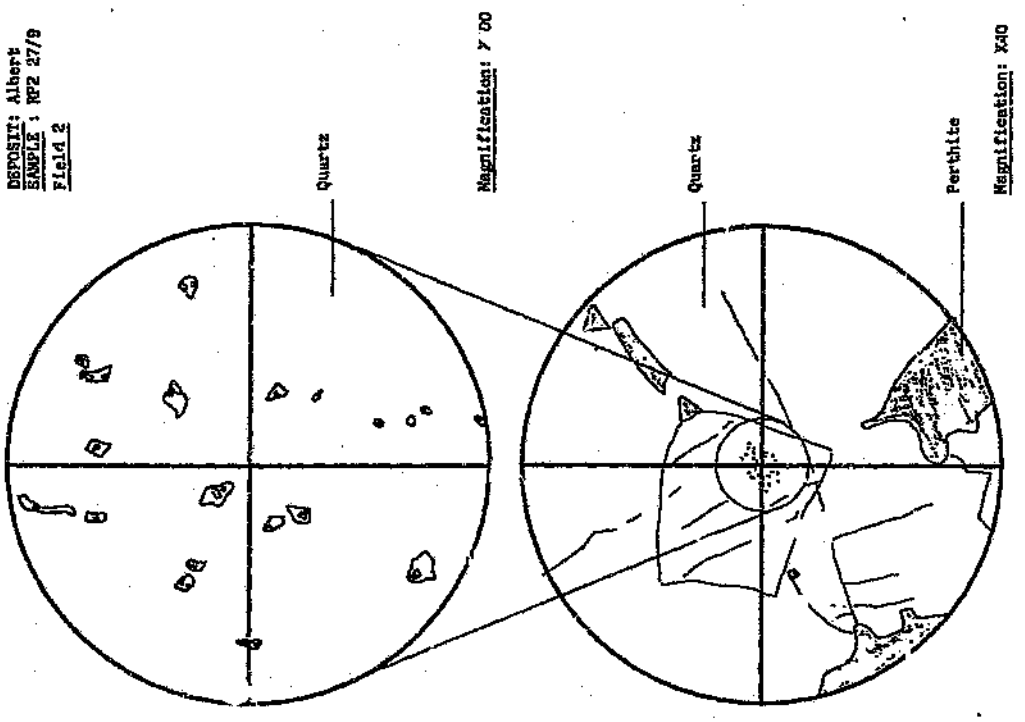


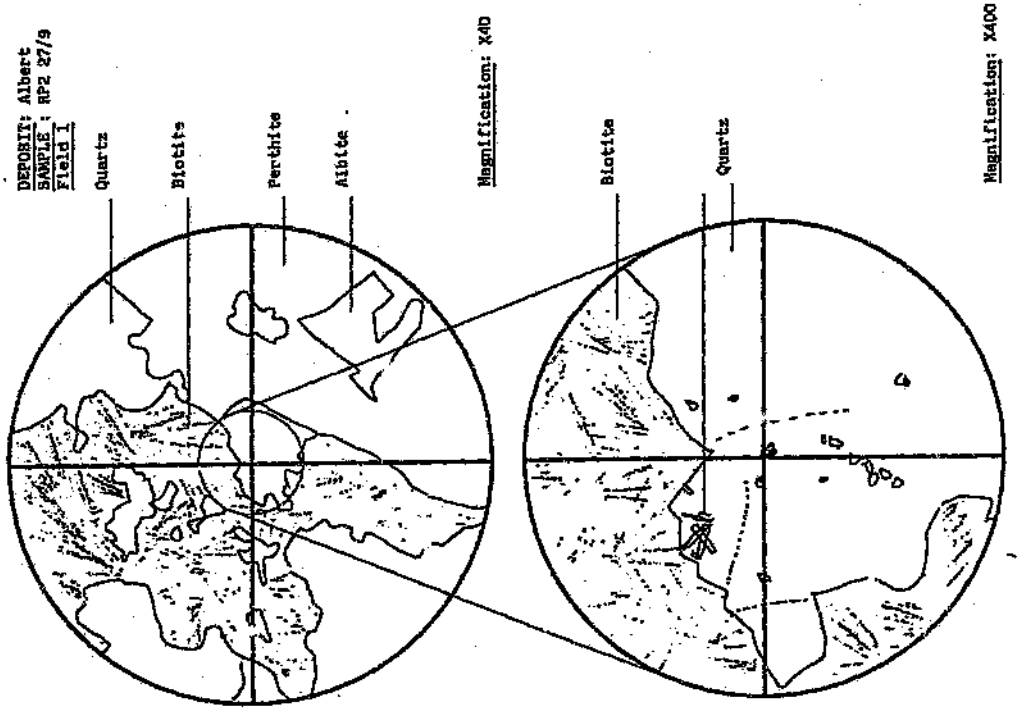


**Figure 5.47 continued** Petrographic maps showing secondary trails of Type 1a, Type 2 and Type 3 inclusions in sample RP2 27/9.

## LEEUFONTEIN

Sample material of unmineralised granite was collected from surface outcrop in the mapping area east of Marble Hall (Leeufontein). The samples selected for microthermometry are listed in Table 5.7, and the reasons for their selection given.

**Table 5.7** List of samples selected for microthermometry from Leeufontein, and the reasons for selection.

| SAMPLE | REASONS FOR SELECTING SAMPLE FOR MICROTHERMOMETRY |
|---|---|
| WG35 | Sample contains no fluids associated with mineralisation and hematitisation |
| WGA35 | Sample contains fluids associated with hematitisation. |
| WG03 | Sample contains fluids associated with albitisation. |
| TB01 | Sample contains fluids responsible for albitisation and tourmalinisation. |

**ROCK TYPE:** FINE-GRAINED KLIPKLOOF GRANITE

**SAMPLE:** WG35

**HAND SPECIMEN**

A creamy-brown hand specimen with few (>5%) mafic specks (>2mm in size). The average grain size is 0.4mm. Argillic alteration of feldspars (albite and K-feldspar) is evident, and they show no twinning or albitisation. Portions of the sample contain granophyric intergrowths. Hematite patches (>1mm) occur within the feldspar. No fresh K-feldspar or albite is visible.

## FLUID INCLUSIONS

Three fluid inclusion assemblages are present in the quartz. The one assemblage consists almost entirely of Type 2 fluid inclusions which all contain halite daughter crystals. The second assemblage consists of Type 1a inclusions and the third assemblage consists of Type 3 inclusions. No primary inclusions were found, and all measurements were made on secondary trails of hundreds of inclusions (Figure 5.48 ).

## MICROTHERMOMETRY

Anomalous microthermometric behaviour was observed in the fluid inclusion assemblage containing halite daughter crystals. No freezing was observed, even at temperatures of -196 °C. No melting behaviour whatsoever could be observed in any of the hundreds of inclusions studied. Homogenisation of liquid and vapour phases occurred at temperatures between 71 °C and 92 °C.

The two phase inclusions froze at -73 °C (on warming the inclusions from -110 °C). The vapour bubble collapsed and a clear solid was produced. At -58 °C, a brown mosaic developed. Coarsening of the mosaic was observed at -51 °C, and at -44 °C the relief of the mosaic increased. At -23 °C rapid clearing of rafts (hydrohalite) was observed. Final melting was observed at temperatures above 0 °C, when clathrate melting was observed. Values between 2.9 °C and 6.1 °C for clathrate melting were recorded. Homogenisation of liquid and vapour phases occurred between 123 °C and 128 °C.

The Type 3 inclusions froze at -42 °C and developed clear round solids. At -35 °C, merging of the solids was observed, and -24 °C several of the solids melted. Final melting occurred at -5. °C. Homogenisation of liquid and vapour phases at temperatures below 100 °C are inferred from the absence of vapour bubble at room temperature and the fact that one did not appear on cooling.

**Figure 5. 48** Petrographic maps showing secondary trails of fluid inclusions in interstitial quartz in Klipkloof granite (sample WG35).

**ROCK TYPE:** HEMATITISED FINE-GRAINED KLIPKLOOF GRANITE

**SAMPLE:** WGA35

**HAND SPECIMEN**

Hematitised, fine-grained Klipkloof granite composed of quartz perthite and minor secondary albite. The perthite is fused and mildly albitised in patches. Specks (0.3mm - 0.5mm) of hematite are dispersed throughout the rock. No fresh primary albite is present, but altered remnants are visible.

**FLUID INCLUSIONS**

Primary fluid inclusions are scarce in this sample. Patches and trails of Type 1a, Type 2 and Type 3 inclusions appear to be secondary in origin. The Type 2 inclusions contain several daughter crystals, all of which are not present in each fluid inclusion. Those recognised include hematite, halite, an orange coloured crystal, a blue cube and a pale green anhedral solid (Figure 5.49). In some sections, most of the inclusions contain several of these solids, while, in others, only a few solids (or none at all) are present in selected inclusions. It was not possible to separate these inclusions in terms of microthermometric behaviour, and thus only one fluid inclusion assemblage is recognised in this sample.

**MICROTHERMOMETRY**

This assemblage required supercooling to induce freezing during the warming cycle. Temperatures were cooled to -100 °C and freezing took place between -63 °C and -60 °C. The frozen solid was colourless in some inclusions and had a pale brown tint in others.

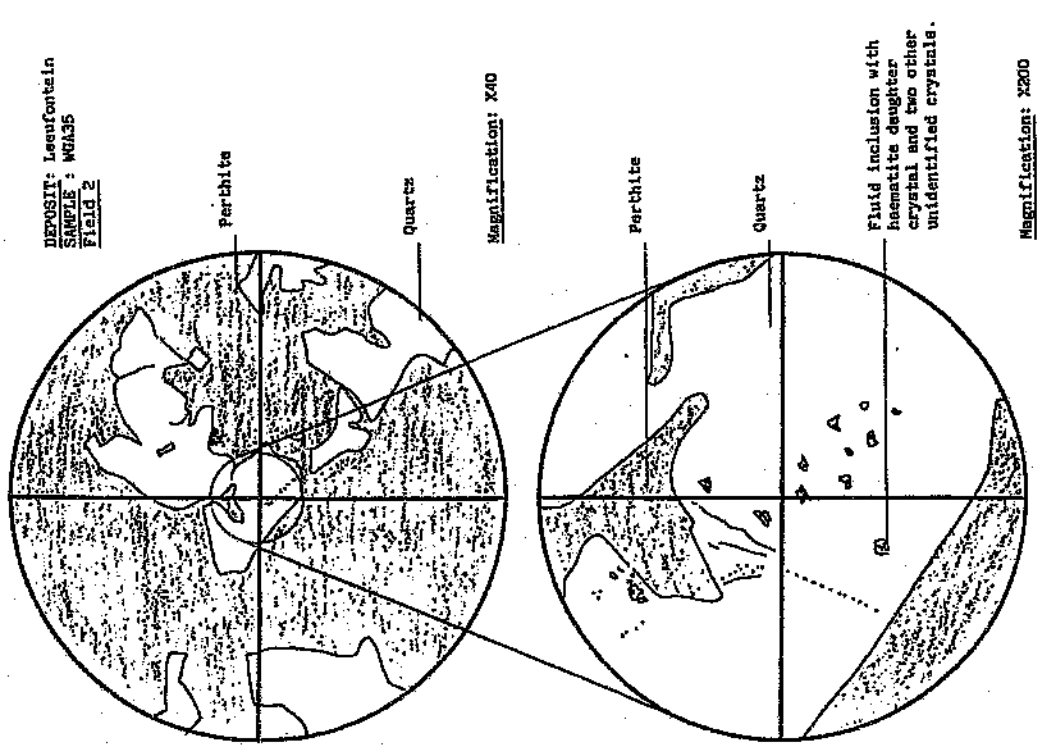


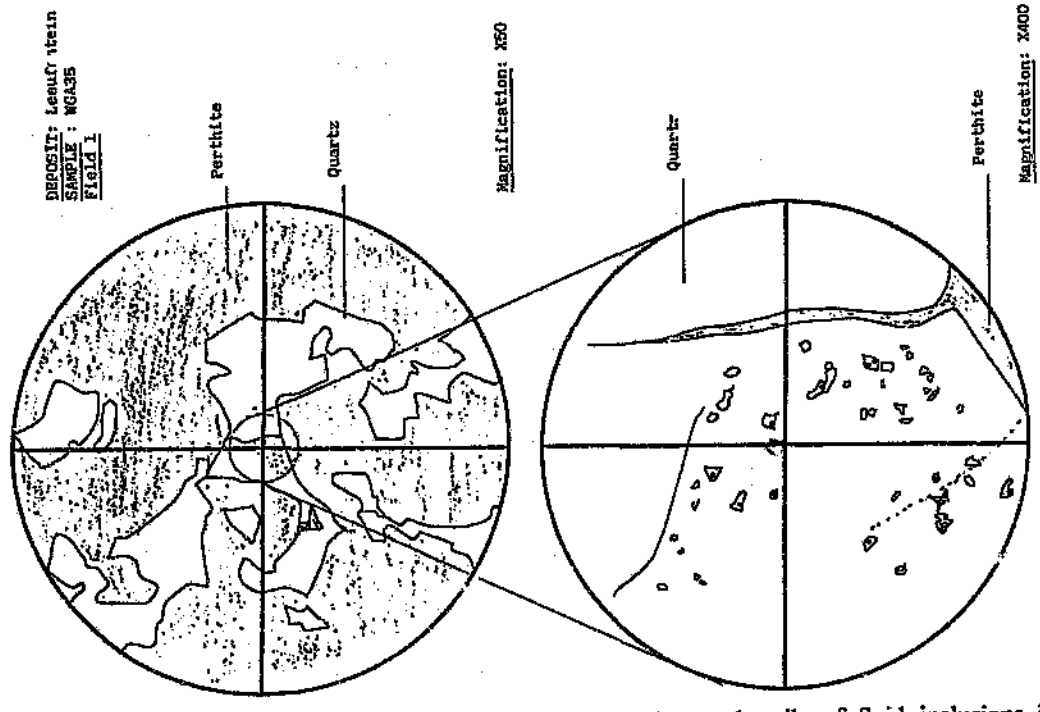


**Figure 5.49** Petrographic maps showing patches and trails of fluid inclusions in WGA35.

First melting was observed at -54 °C, the mosaic developed higher relief at -44 °C, and coarsening of the mosaic took place at -36 °C. Final melting behaviour in this assemblage is extremely variable. Simultaneous, instant melting of large ice rafts, and the appearance of the full-size vapour bubble at -20 °C, was observed in one inclusion. By -25 °C, most inclusions contained only one large raft, which melted at between -24.7 °C and -10.1 °C. Clathrate melting was observed in one inclusion at 5.9 °C. Homogenisation of the liquid and vapour phases occurred between 78 °C and 164 °C.

**ROCK TYPE:** **FINE-GRAINED KLIPKLOOF GRANITE**

**SAMPLE:** **WG03**

**HAND SPECIMEN**

Fine-grained, pale creamy-white sample with disseminated biotite specks. Chloritisation and minor albitisation of the feldspar has occurred. Minor fluorite is present. Argillic alteration of the feldspars is pronounced.

**FLUID INCLUSIONS**

Two fluid inclusion assemblages are present in this sample (Figure 5.50). Both occur as secondary trails. The one consists of Type 3 inclusions only, and the other consists of Type 2 inclusions which contain two small solids (possibly halite and sylvite).

**Figure 5.50** Petrographic maps showing secondary trails of fluid inclusions in fine-grained Klipkloof granite (sample WG03).

**ROCK TYPE:** TOURMALINE SPHEROID IN ALBITISED KLIPKLOOF GRANITE

**SAMPLE:** TB01

**HAND SPECIMEN**

The tourmaline spheroids are hosted by fine-grained Klipkloof Granite which has been intensely albitised, and hence is called albitised Klipkloof Granite. The spheroids are composed of albite, quartz, tourmaline and, rarely, minor fluorite. Two generations of quartz are present. The order of formation of these secondary minerals is : albite, quartz 1, tourmaline1?, quartz 2, tourmaline 2?. The tourmalinisation is not restricted to spheroids, but also occurs along fractures, and as irregular blebs.

**FLUID INCLUSIONS**

Fluid inclusions associated with quartz 1 and quartz 2 have been recognised. Fluid inclusion assemblages containing Type 1a, Type 1b and Type 2 and Type 3 inclusions have been observed. Two morphologically distinct groups of inclusions have been linked to different minerals. A group of predominantly Type 2 inclusions, commonly with halite and sylvite daughter crystals, and few Type 1a inclusions have been linked to the first quartz generation. Three groups of Type 1a fluid inclusions are associated with tourmaline and quartz 2 generation. Type 1a and Type 1b inclusions are preserved as primary and secondary inclusions in the tourmaline (Figure 5.51 ).

**MICROTHERMOMETRY**

*Fluid inclusions in quartz 1*: The primary fluid inclusions in quartz 1 are predominantly Type 2 with a few Type 1a inclusions. They froze to a clear solid at -66 °C, and the mosaic developed at -36 °C. Merging of the mosaic occurred at -22 °C and final melting took place between -15 °C and -16 °C. Clathrate melting at 6 °C and 16 °C was observed in a few inclusions. Homogenisation of the liquid and vapour phases occurred between 140 °C and 187 °C.

*Fluid inclusions in quartz 2*: Primary inclusions in quartz 2 contain very few solid phases, and are predominantly Type 1a and Type 3 inclusions. They froze between -47 °C and -50 °C, and developed a colourless mosaic. Eutectic melting was observed -51 °C and coarsening of the mosaic took place at -47 °C. At -22 °C, some rafts melted and the vapour bubble enlarged. Final melting occurred at -10 °C and homogenisation of liquid and vapour between 122 °C and 149 °C.

*Fluid inclusions in tourmaline*: One assemblage of primary fluid inclusions has been found in the tourmaline. The assemblage freezes at temperatures below -85 °C. No intermediate melting events were observed before -13 °C when the vapour bubble reappeared and final melting occurred between -9.7 °C and -12.7 °C. Homogenisation of the vapour bubble into the liquid phase occurred between 80 °C and 90 °C. This assemblage is also preserved as secondary trails in the quartz. Instantaneous melting of large rafts and appearance of a vapour bubble is common in the quartz-hosted inclusions of this assemblage.

**Figure 5.51** Petrographic maps of quartz-hosted and tourmaline-hosted fluid inclusions in a tourmaline spheroid (sample TB01).

*DISCUSSION*

The petrography and microthermometry of quartz-hosted and fluorite-hosted fluid inclusions, in interstitial spaces and in veins, has revealed some very interesting information concerning the evolution and character of fluids associated mineralisation in the granites of the eastern lobe of the Bushveld complex. The salient points shall be discussed according to the scheme are (Figure 5.52).

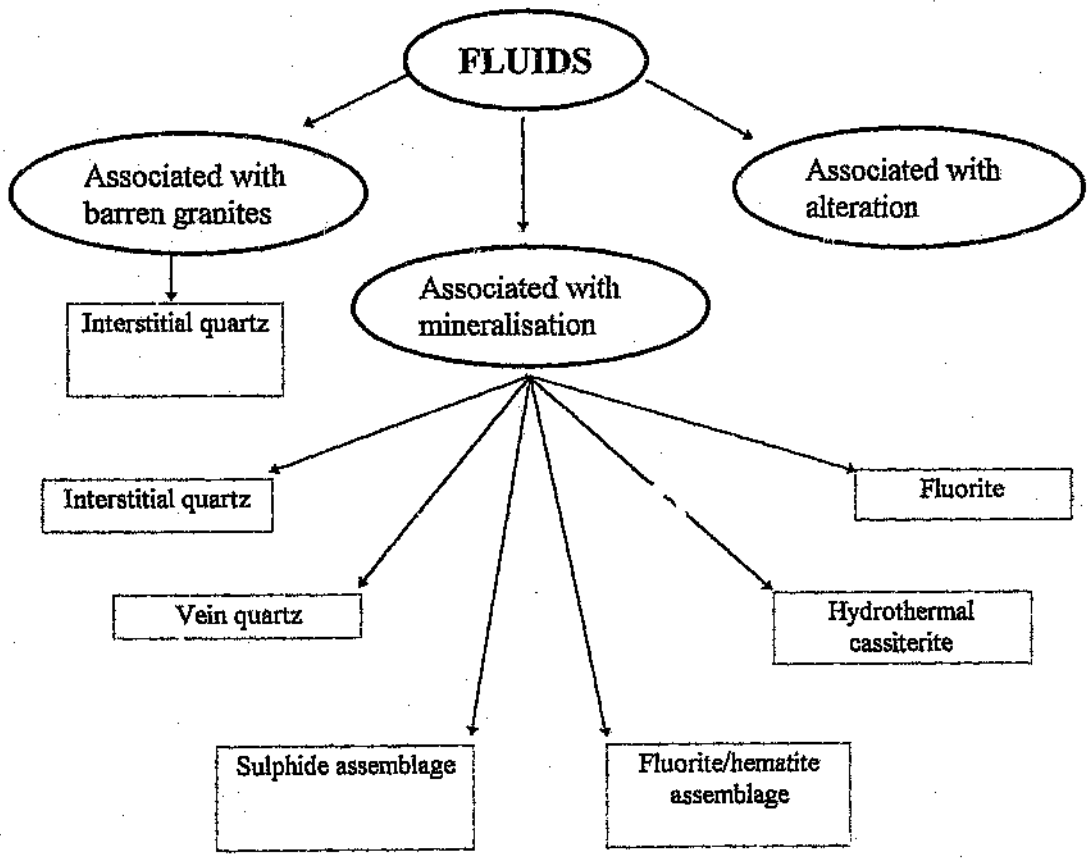


**Figure 5. 52** Schematic representation of fluid categories discussed in terms of their microthermometric behaviour and significance.

The microthermometric data presented in the preceding sections highlight certain characteristics that are significant. In the paragraphs that follow, these characteristics will be discussed and their relevance in determining the composition, entrapment temperature, pressure and density of the fluids associated with the different stages in the paragenetic sequence, considered.

**Composition**

The temperature of freezing and the characteristics of the frozen solid are not aspects which are usually used to distinguish between different fluid inclusion assemblages. However, these characteristics were particularly useful as first order tools in estimating the composition of the fluid inclusions in this study.

It has been found that the fluid inclusions associated with quartz generations 2 and 3 in the interstitial quartz from each study area freeze at low temperatures, develop a brown ice mosaic on freezing, and commonly contain several solid phases. In contrast, the fluids associated with quartz generation 1 and the very late stage fluids post-dating quartz 2 and 3, freeze at moderate temperatures, produce a colourless solid on freezing, and seldom, if ever, contain daughter crystals. The brown mosaic is also observed in certain fluid inclusion assemblages in vein quartz. Thus, without recording any microthermometric data, the origin of the fluids and position within the evolutionary history of the granite may be deduced, simply by observing the freezing behaviour of the fluid inclusions.

In addition, a number of inferences can be made about the composition of the fluid inclusions in which the brown ice mosaic develops. The brown discoloration indicates the presence of the divalent ions $Ca^{++}$ and $Mg^{++}$ (Goldstein and Reynolds, 1994), and the low freezing point suggests a relatively high solute content of the fluid. Furthermore, the presence of daughter crystals implies that the fluids were saturated with respect to one or more elements. Fluid inclusion assemblages containing solid phases fitting the criteria for being true daughter crystals and which were positively identified through optical methods, i.e. halite (NaCl), sylvite (KCl), hematite ($Fe_2O_3$), iron chloride ($FeCl_2$), muscovite ($K_2Al_4(Si_6Al_2)O_{20}(OH)_4$), and calcite ($CaCO_3$),

suggest that the fluids contained $Na^+$, $K^+$, $Fe^{++/+++}$, $Ca^{++}$, and $Cl^-$ at saturation levels. Salinity estimates are usually based on the assumption that fluid compositions can be represented in terms of two or three component systems, such as $NaCl-H_2O$ or $NaCl-KCl-H_2O$ or $NaCl-H_2O-CO_2$. The presence of additional ions in olution hampers the determination of salinity of the fluids by lowering the liquidus and eutectic temperatures below those for pure $NaCl-H_2O$ inclusions. The amount of lowering of the $NaCl-H_2O$ liquidus is much greater when divalent chlorides are added than when KCl is added (Roedder, 1984). However, the density and thermal coefficient of expansion of multi-component fluids can be estimated to within 1% from that of a simple NaCl solution having the same freezing point (Clynne and Potter, 1977).

The problem of estimating salinity is amplified by the presence of gases such as $CO_2$, $CH_4$ and $N_2$. Murphy and Roberts (1996) have shown that the occurrence of clathrates (solid gas hydrates) complicates the use of microthermometry in the estimation of composition and density of aqueo-carbonic fluids. Murphy and Roberts (1996) suggest that there is a problem with the use of predictive thermodynamic models based on final clathrate melting temperatures and the assumption of equilibrium within aqueo-carbonic inclusions. Numerous clathrate melting temperatures were recorded for fluid inclusions in this study, and values above 10°C were not uncommon. In fluid inclusions with $CO_2$ double bubbles, freezing temperatures were suppressed by as much a 1°C, and this is indicative of the presence of gases such as $N_2$ and $CH_4$ in solution.

The dissolution temperature of daughter crystals is often used in order to determine the salinity of saturated solutions. According to Sheppard (1985) knowledge of the solubility of each salt in the mixed system is required, and it is rarely possible to express the composition of the fluid phase in terms of more than two or three simple salts. Attempts to dissolve daughter crystals were made, but no instances were recorded where dissolution of the daughter crystals occurred before homogenisation of the liquid and vapour phase, or before the inclusion decrepitated. Reasons for the non-dissolution of the solid phases may include the fact that the solids were not true daughter crystals but merely trapped solids, or that changes in the fluid inclusion has occurred, such as necking down, and $H_2$ leakage. Some minerals require several hours

of heating for dissolution to occur, and it is possible that equilibrium was not achieved in the short time the samples were heated before decrepitation took place. Decrepitation data were obtained during thermal decrepitation of fluid inclusions for quadrupole mass spectrometry, and the reader is referred to Chapter 6 for more details.

Intermediate melting temperatures were recorded in great detail in this study, and provide some insights into the fluid phase composition. At the eutectic temperature for experimentally determined chemical systems, rapid melting of one phase takes place, and which is often observed as an intermediate melting event in the fluid inclusions. The temperatures of these events can be correlated to eutectic temperatures of known systems listed below (refer to Table 5.1). Intermediate melting events, corresponding to several eutectic melting temperatures for the chemical systems, were recorded. The intermediate melting events suggest the presence of a combination of NaCl, KCl, and $FeCl_2$ in the fluids. Melting of phases in the ranges for the eutectic melting temperatures for the $H_2O$-$NaHCO_3$, $H_2O$-$Na_2CO_3$-$K_2CO_3$, and $H_2O$-NaCl-$Na_2SO_4$ systems alludes to the presence of some of these components, but, in the absence of supporting evidence, no emphasis has been placed on them. The intermediate melting events are plotted in histograms in the following sections which compare the fluids in minerals at the different deposits, and with the host granites.

**Temperature, pressure and density**

Determination of the entrapment temperature ($T_{true}$) and pressure is problematic. According to Reynolds and Goldstein (1994), a prerequisite for the determination of pressures of entrapment is the presence of FIA's that produce consistent reproducible data and that contain no other gases, such as methane and carbon dioxide. The only gas present in the bubble must be water vapour. The chemical system and salinity of the fluids must be accurately determined, and homogenisation temperatures recorded. Isochores (lines of equal density) are then plotted on a graph of pressure versus temperature, and the point of intersection of the measured homogenisation temperature with the isochore yields the unique pressure of entrapment. Clearly, this method of determining entrapment pressure is inappropriate for the fluid inclusions measured in this study, since complex gas mixtures are present in most FIA's, the

microthermometric data from single FIA's are variable, and the salinity cannot be determined accurately. Thus, an alternative method of determining entrapment temperature and pressure is required.

**Boiling versus fluid mixing**

The variability in phase proportions in fluid inclusions belonging to the same fluid inclusion assemblage could be interpreted in two ways, namely, boiling or fluid mixing. Evidence for boiling (homogenisation to the liquid phase as well as to the vapour phase at the same temperature in different inclusions within a single FIA) was not observed in any fluid inclusion studied from any of the study areas. This, in addition to the sequence of halite and vapour bubble disappearance, confirms that boiling did not take place. By contrast, abundant evidence for fluid mixing was observed. Fluid mixing has been discussed in previous chapters in connection with petrographic observations, and is confirmed by fluid inclusion microthermometry. The evidence for fluid mixing includes variable salinities and homogenisation temperatures for fluid inclusions in the same FIA, as well as the recognition of two discrete fluids coexisting at similar temperatures.

Furthermore, the order of disappearance of halite daughter crystals and the vapour bubble on heating, is also related to the formation conditions of fluid entrapment (Reynolds, 1991). In cases where the temperature of melting of the halite crystal is equal to or less than the temperature of homogenisation of the liquid and vapour phases, boiling of the fluid is a possibility. However, in cases where dissolution of the halite crystal occurs at higher temperatures than homogenisation of the liquid and vapour phases, boiling is not possible. The sample material in this study contained no halite-bearing fluid inclusions in which dissolution of the halite crystal occurred before homogenisation of the liquid and vapour phases. Thus, boiling can be ruled out as a possible mechanism for mineralisation.

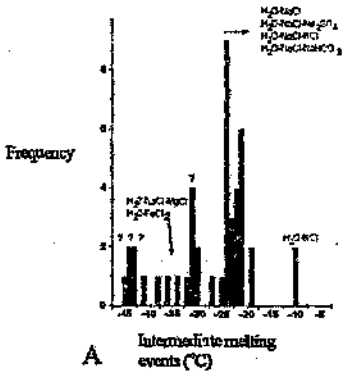


**Figure 5.53** Histograms of temperatures of intermediate melting events, final melting temperatures and homogenisation temperatures in barren granites at Leeufontein.

**Fluids associated with barren Klipkloof Granite**

***Intermediate melting events***

The temperatures of intermediate melting events in quartz samples of barren granite from Leeufontein are shown in Figure 5.53A. The peaks corresponding with eutectic melting temperatures in the systems listed in Table 5.1 are indicated. A number of chemical systems have eutectic temperatures in the range -21°C to -24°C. From these phase changes, the presence of KCl, NaCl, $NaHCO_3$, $NaCO_3$, and $Na_2SO_4$ is possible. Several peaks do not correspond with those in Table 5.1, but are in the general range for fluids containing $MgCl_2$ and $FeCl_2$. The events in the range -45°C to -40°C may be linked to the presence of $CaCl_2$ in the fluids.

***Final melting temperatures***

The final melting temperatures of fluid inclusions in quartz in the Klipkloof Granites are shown in Figure 5.53B. The majority of values fall in the range -10 to -26°C, with peaks at -10 °C, -13 °C and from -22 °C to -26 °C. Clathrate melting at temperatures above zero were recorded in several inclusions. Note that values above 10 °C cannot be explained by the presence of $CO_2$ alone, and indicate the presence of other volatiles.

*Homogenisation temperatures*

Primary fluid inclusions in unaltered fine-grained Klipkloof Granite were not found, and thus, only homogenisation temperatures of secondary trails could be measured. The maximum $T_h$ value obtained in altered and unaltered samples was 200°C and provides a minimum estimate for crystallisation of Klipkloof dykes. Primary inclusions in late stage tourmaline indicate that tourmalinisation occurred at low temperatures (below 100°C).

The microthermometric data from fluid inclusions in the fine-grained Klipkloof Granites and in quartz and tourmaline in the tourmaline spheroids are plotted in Figures 5.54 and 5.55, respectively.

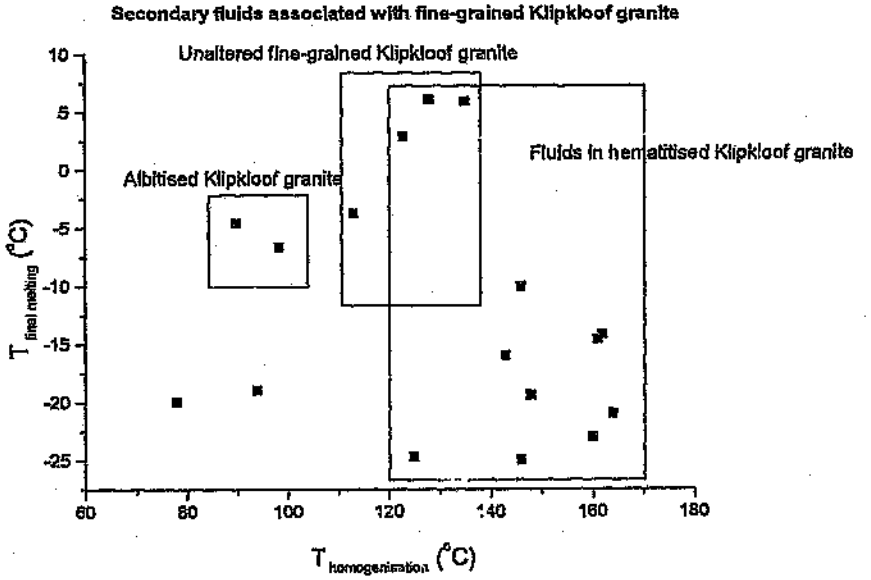


**Figure 5.54** Plot of final melting temperatures and homogenisation temperatures of fluid inclusions in the fine-grained Klipkloof Granites at Leeufontein.

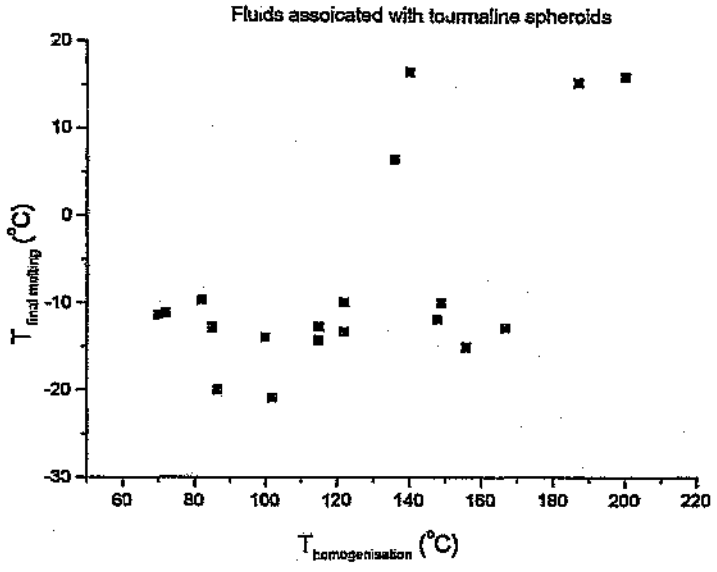


**Figure 5.55** Plot of final melting temperatures and homogenisation temperatures of fluid inclusions in tourmaline spheroids in Albitised Klipkloof Granite at Leeufontein.

The hematitised Klipkloof Granites contain a highly saline assemblage of inclusions which homogenise between approximately 120 °C and 165°C, and have final melting temperatures ranging from -10 °C to -26 °C (14 to >21.2 wt. % eNaCl). The unaltered granites and the hematitised granites share a common fluid inclusion assemblage which is moderately saline and contains $CO_2$. Clathrates which melted between 2 and 6.5 °C suggest salinities of 14 to 8 wt. % eNaCl. The fluids associated with the Albitised Klipkloof Granites are moderately saline (8 to 11.5 wt. % NaCl), and were trapped at lower temperatures. Thus, hematitisation is considered to be a higher temperature alteration phenomenon than albitisation. This deduction is supported by textural evidence, where hematite liberated from the feldspar lattice during subsequent albitisation, occurs as rims around individual grains and along fractures within the grains.

The fluids in the tourmaline spheroids hosted by Albitised Klipkloof Granite contain fluids with salinity equivalents of between 14.5 to 22.6 wt. % eNaCl. The temperature range for these fluids ranges from 200°C to 72°C. Two generations of quartz and tourmaline were recognised in the spheroids, the early generation of quartz has salinity of 18.5 wt. % eNaCl while the youngest low temperature fluids trapped in the second generation of tourmaline have salinities of 13 to16 wt.% eNaCl.

**Fluids in hypersolvus and subsolvus granites associated with mineralisation**

The fluid inclusions in interstitial quartz from the hypersolvus granites at Spoedwel and Dronkfontein, and the subsolvus granites at Albert, were studied. At Spoedwel and Dronkfontein, three generations of quartz were recognised by means of cathodo-luminescence imagery. The characteristics of fluids associated with these three interstitial quartz generations in the altered hypersolvus granites containing minor disseminated mineralisation at Spoedwel, and the implications of the observed phenomena are tabulated below (Table 5.8)

Table 5.8 Table summarising the characteristic features of the fluids associated with quartz generations 1, 2 and 3 at Spoedwel.

| OBSERVATION | IMPLICATION |
|---|---|
| QUARTZ GENERATION 1 | |
| No brown mosaic | No Ca in solution |
| $T_e$ -35°C | $H_20$-NaCl-$MgCl_2$ eutectic and $H_20$-$FeCl_2$ eutectic |
| Intermediate melting events: | |
| -22°C | NaCl eutectic (-22.3 °C?) |
| -9°C | KCl eutectic (-10.7°C) |
| $T_{final\ melting}$ -2°C to 0°C and up to 10°C | Almost pure water. Low concentration of dissolved constituents. Clathrate melting at temperatures above 0°C indicates the presence of $CO_2$. Salinity up to 3 wt % e NaCl. |
| $T_h$ >250°C | Moderate temperature of entrapment |
| QUARTZ GENERATION 2 | |
| Brown mosaic | Ca present |
| Low freezing temperature (-50°C to-60°C) | -significant amounts of dissolved constituents. -possibly $N_2$ and/or $CH_4$ |
| $T_e$ -36°C | $H_20$-NaCl-$MgCl_2$ eutectic and $H_20$-$FeCl_2$ eutectic |
| Daughter crystals: | Saturation with respect to components. |
| halite | NaCl |
| sylvite | KCl |
| hematite | $Fe_2O_3$ |
| Iron chloride | $FeCl_2$ |
| Intermediate melting events: | |
| -31°C | ? $MgCl_2$ |
| -24°C | ? melting of hydrohalite ($NaCl.H_2O$) |
| $T_{final\ melting}$ -20 °C to -17 °C | Salinity 22.5 to 20 wt. % eNaCl. |
| $T_h$ 170°C-378°C average $T_h$ 230°C | |
| QUARTZ GENERATION 3 | -significant amounts of dissolved constituents. |
| Very low $T_{freeze}$ -80°C | -possibly $N_2$ and/or $CH_4$ |
| Dark brown mosaic | Ca in solution |
| $T_e$ -50 °C to -60 °C | $CaCl_2$ Eutectic (melting of antarcticite) |
| $T_{final\ melting}$ -30 °C to -38 °C | Extremely low. Abundant dissolved solutes. Salinity cannot be determined using $H_20$-NaCl system. |

The characteristics of the fluids associated with the subsolvus Verena Granite, which hosts the quartz veins associated with mineralisation at Albert, are shown in Table 5.9. Two distinct fluids are recognised by their microthermometric behaviour.

**Table 5.9** Tabulation of fluid characteristics associated with the subsolvus Verena Granite hosting mineralisation at Albert silver deposit.

| OBSERVATION | IMPLICATION |
|---|---|
| FLUID 1 | |
| Colourless mosaic | No Ca |
| Tf -44 °C to -48 °C | |
| Te -40 °C | ? |
| Intermediate melting events | |
| -34 °C | $H_2O$-$FeCl_2$ (-35°C) |
| -21 °C | $H_2O$-NaCl |
| -16 °C | |
| Final melting -4.4 °C to 4.3 °C | Clathrates indicate presence of $CO_2$. Salinity 6.6 to 10.5 wt % eNaCl. |
| Th 128 °C -173°C | |
| FLUID 2 | |
| Brown mosaic | Ca Present |
| Tf -60 °C to-75 °C | |
| Te -50 °C to -52 °C | $H_2O$-$MgCl_2$-$CaCl_2$ eutectic |
| Intermediate melting events | |
| -40 °C | |
| -33 °C | $H_2O$-$MgCl_2$ eutectic |
| -28 °C | |
| -24 °C | $H_2O$-NaCl-KCl eutectic -23.5°C |
| Daughter crystals | |
| $FeCl_2$ | |
| Halite | |
| Sylvite | |
| $T_{final\ melting}$ -4.8 °C to 15 °C (average -5 °C) | Clathrate melting above 10°C indicates volatiles other than $CO_2$ are present. Salinity 7.6 wt. % eNaCl. |

The fluid inclusion $T_h$ and $T_{final\ melting}$ data points for hypersolvus and subsolvus granites are shown in Figure 5.56. The fluids in the host rock at Spoedwel and Dronkfontein represent the hypersolvus granite fluids, and the fluids in the host rock at Albert represent the subsolvus granite fluids. The fluids in subsolvus granites are less saline than the hypersolvus granite fluids, and contain none of the high salinity and high temperature fluids at Spoedwel and Dronkfontein. However, fluids with similar characteristics to the fluids associated with subsolvus granites do also occur in the hypersolvus granites. The reason suggested for this is that fluids associated with the subsolvus granites at Spoedwel, (and possibly at Dronkfontein), were trapped as secondary inclusions within the previously crystallised hypersolvus granites in the area.

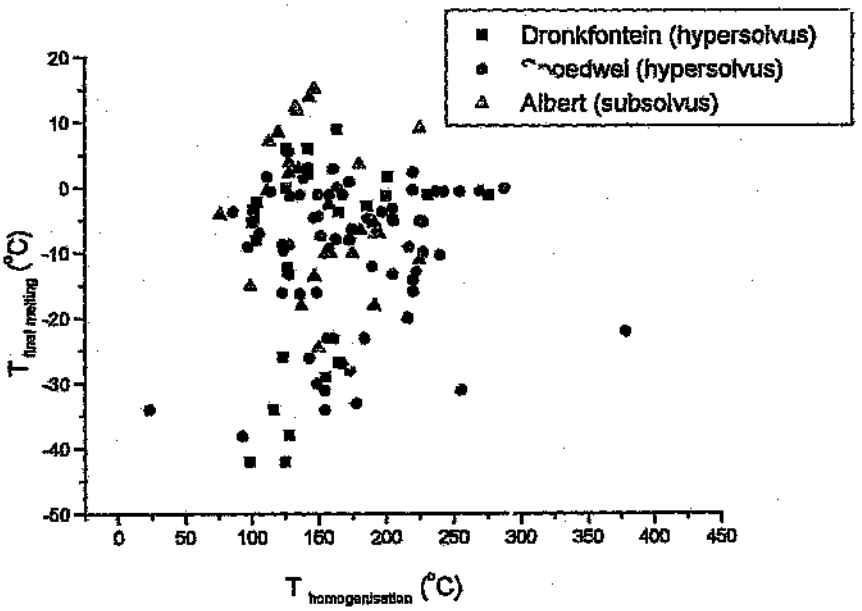


**Figure 5.56** Diagram plotting $T_{final\ melting}$ versus $T_{homogenisation}$ for the fluids in hypersolvus (Spoedwel and Dronkfontein) and subsolvus granites (Albert).

*Intermediate melting events*

The intermediate melting events from fluid inclusion in each deposit are summarised in the histograms in Figure 5.58 A-E. At Albert, peaks in the ranges indicating the presence of NaCl, $MgCl_2$, $FeCl_2$ and $CaCl_2$ are recognised. Peaks in the range for $Na_2CO_3$ and $Na_2$[illegible] are also observed.

A

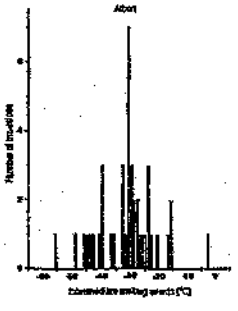

B

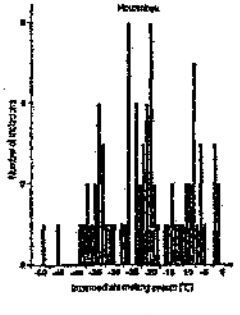

C

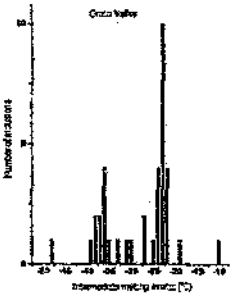

D

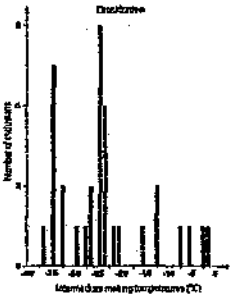

E

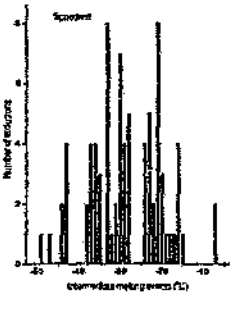

**Figure 5. 57** Histograms of temperatures of intermediate melting events at Albert (A), Houtenbek (B), Grass Valley ( C), Spoedwel (D), and Dronkfontein (E).

At Houtenbek, the presence of $MgCl_2$, $FeCl_2$, NaCl, KCl, $CaCl_2$, $Na_2CO_3$ and $Na_2SO_4$ is suggested by the temperatures at which melting of intermediate phases occurred. However, as mentioned above, without supporting evidence, the presence of $Na_2CO_3$ and $Na_2SO_4$ is dubious. At Spoedwel, Dronkfontein, Grass Valley and Albert, the intermediate melting events suggest that the fluids are essentially the same, only having better pronounced peaks in the eutectic ranges of $FeCl_2$-$H_2O$ and $MgCl_2$-$H_2O$.

***Homogenisation and final melting temperatures***

The homogenisation temperatures and final melting temperatures of fluids associated with mineralisation at Grass Valley, Houtenbek, Spoedwel, Dronkfontein and Albert are plotted in Figure 5.58.

The most saline fluids are associated with the hypersolvus granites hosting mineralisation at Spoedwel and Dronkfontein. It is not possible to determine the percentage eNaCl for these fluids because their final melting temperatures are too low to be interpreted in terms of the $H_2O$-NaCl chemical system. The bulk of the fluids directly associated with mineralisation from all deposits plot fairly closely together. The fluids associated with late stage hematite-fluorite at Albert tend to be lower temperature and salinity fluids, and contain volatiles in addition to $CO_2$ (indicated by high temperature clathrate melting). Although there is some scatter in the data points, the fluids at each of the deposits appears to plot in particular fields in Figure 5.58.

The fluids identified as being associated with the precipitation of certain minerals in the sulphide paragenesis, with hydrothermal cassiterite and with the hematite-fluorite assemblage are tabulated in Table 5.10. The data in Table 5.10 are from primary inclusions in vein quartz associated with each of the minerals listed. These fluids are plotted in Figure 5.59, which clearly shows the differences in the fluids in the various stages of the paragenetic sequence.

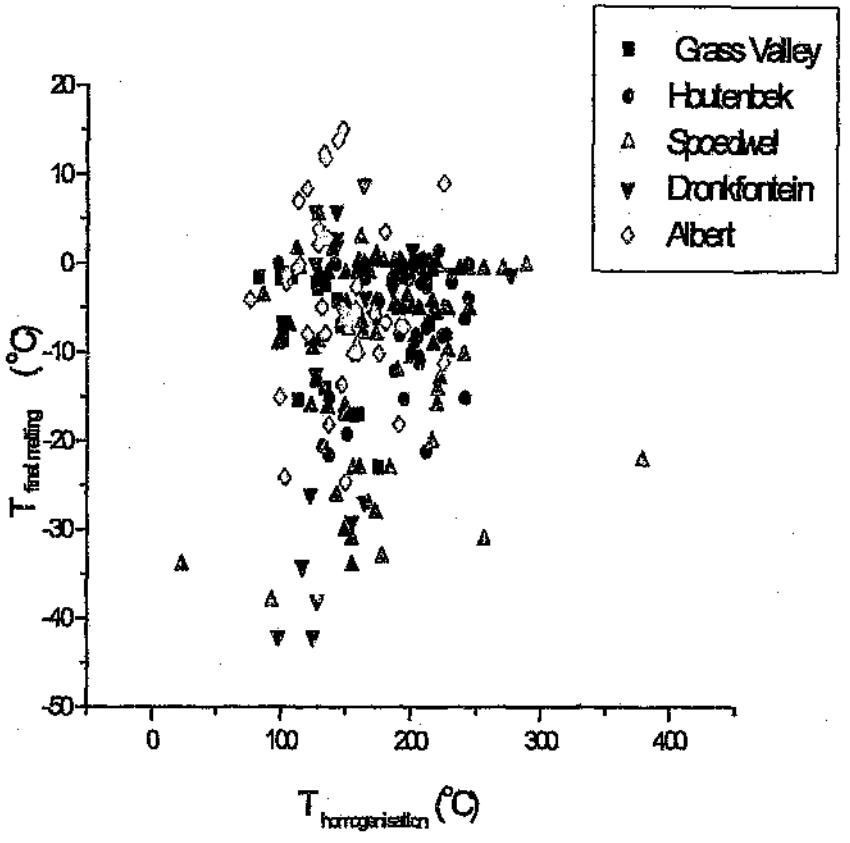


**Figure 5.58** Plot of final melting temperatures versus homogenisation temperatures for fluids associated with mineralisation at Grass Valley, Houtenbek, Spoedwel, Dronkfontein and Albert.

**Table 5.10** Table comparing the fluids associated with deposition of minerals in each of the mineral assemblages, as determined from fluid inclusions in synchronous quartz.

| ASSEMBLAGE | MINERAL (DEPOSIT) | $T_{final\ melting}$ (°C) | $T_h$ |
|---|---|---|---|
| Sn-W | Hydrothermal cassiterite (Grass Valley) | -0.4 | 194 -201 |
| | | (-4.4; -3.1) | 134 -167 |
| | Arsenopyrite (Albert) | -8.8 | ? 168 - 214 |
| | Sphalerite (Grass Valley) | -16 | 149 - 160 |
| | Galena (Grass Valley) | -14 | 134 |
| | Chalcopyrite (Spoedwel) | -5 | 203 - 244 |
| | Chalcopyrite (Albert) | -4.2 | ? |
| | Chalcopyrite (Grass Valley) | ? -4.4 | ? 143 |
| Fluorite/hematite | Quartz (Spoedwel) | -10 | >100 |
| | Fluorite | -16 to -6 | 200 to 150 |
| | (Albert) | -2.6 to -1.7 | 112 to 93 |

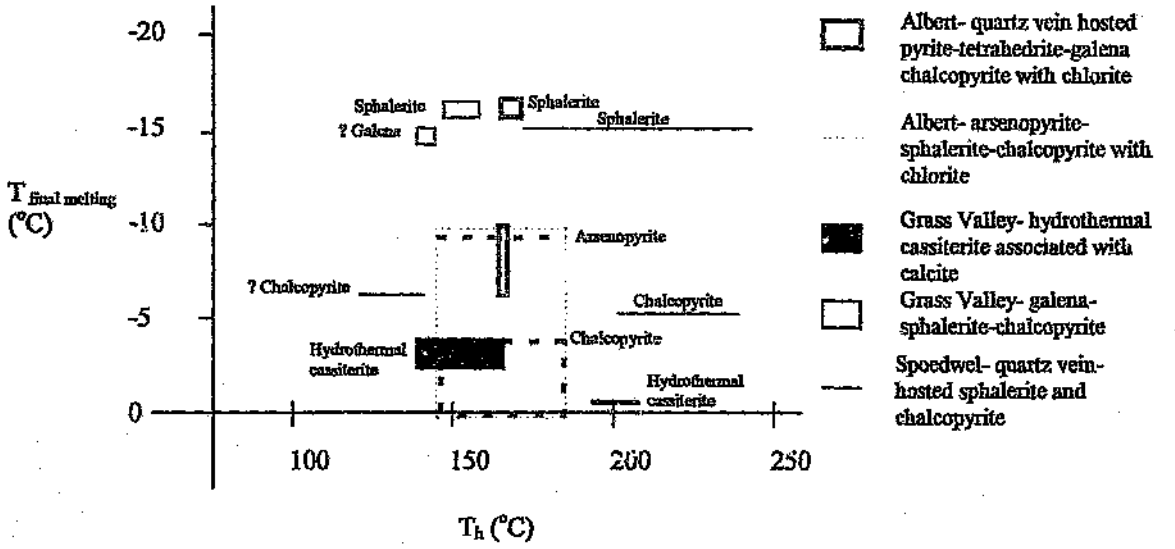


**Figure 5.59** Diagram showing the fluids associated with mineralisation in the eastern lobe of the Bushveld granites.

The fluids identified as being responsible for precipitating cassiterite at Grass Valley, and associated with chalcopyrite, arsenopyrite, sphalerite and galena, are shown in Figure 5.59. The fluids associated with cassiterite deposition contain few dissolved solutes, and, thus, have relatively high final melting temperatures compared with the fluids that precipitated the sulphide minerals. On the diagram, the ranges for fluids associated with the minerals from Spoedwel (blue), Albert (green), and Grass Valley (red), suggest that the fluids that deposited the minerals at each of these deposits were similar. The similar compositions of the fluids associated with sphalerite indicates that precipitation occurred at different temperatures at each deposit. Assuming that mineralisation was triggered by mixing of two fluids, the similar fluid compositions associated with sphalerite deposition suggests that fluid mixing occurred at different stages in the paragenetic sequences. A similar trend is observed in the fluids associated with chalcopyrite precipitation. The order of decreasing temperature, from Spoedwel to Albert to Grass Valley, is observed in the fluids associated with sphalerite and chalcopyrite precipitation. However, at Albert, two fluid inclusion assemblages are associated with chalcopyrite deposition, at similar temperatures. The implication of

this is that mixing of different proportions of fluid occurred at different locations within the pluton. A trend in the salinity of the fluids has emerged which can be linked to the paragenetic sequence. In Figure 5.60 it is clear that the fluids became progressively more saline, peaking with the deposition of sphalerite, and then decreasing in salinity with the precipitation of chalcopyrite.

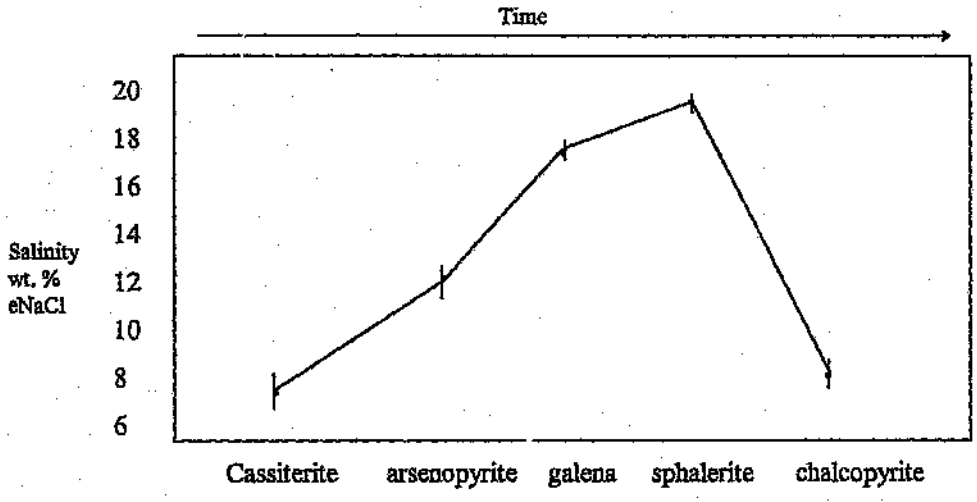


**Figure 5.60** Diagram showing the variation in the salinity of fluids associated with different stages in the paragenetic sequence.

This variation in salinity may be ascribed to the increasing solute ontent ( in particular Ca, and Fe) of the fluids as the external, connate fluid became more dominant. The fluids associated with the precipitation of Stage 1 in the paragenetic sequence became progressively more saline with time, peaking with the precipitation of the sphalerite in the second stage of the paragenetic sequence. The decline in salinity after sphalerite precipitation occurred as a consequence of the extraction of the components of albite, K-feldspar, muscovite and chlorite from the fluids, as the subsolvus granite was crystallised. Thus, the character of the fluids was governed not only by a progressive increase in the salinity, but also by the solute composition, which evolved as interaction of the magmatic and connate fluids proceeded.

**Fluids associated with vein quartz**

Quartz veins are abundant at Spoedwel, Albert and Grass Valley. The homogenisation temperatures and final melting temperatures of fluids from vein quartz at these deposits are plotted in Figure 5.61.

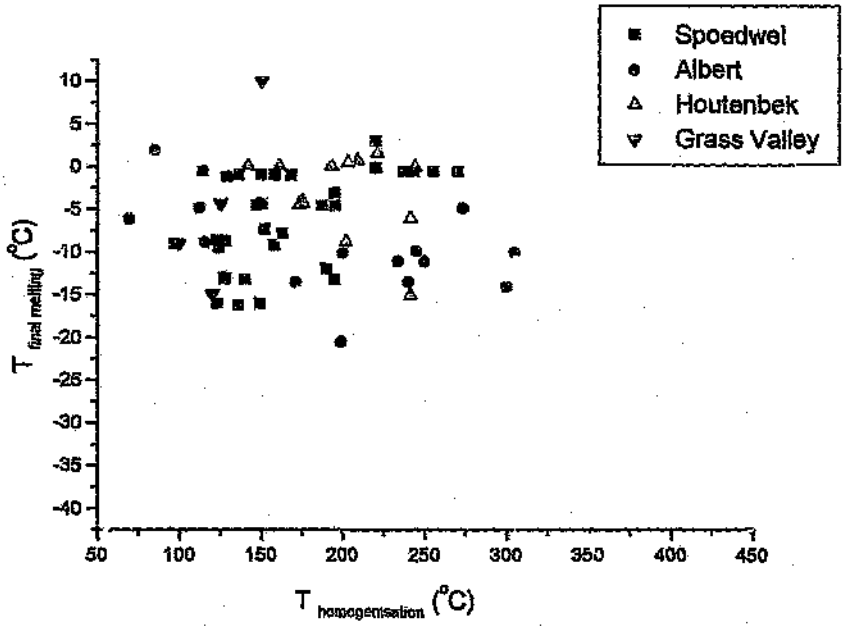


**Figure 5.61** The homogenisation temperatures and final melting temperatures of fluids from vein quartz at Spoedwel, Albert and Grass Valley.

The fluids at Spoedwel and Grass Valley are similar in terms of composition, although, homogenisation temperatures at Spoedwel are higher than those at Grass Valley. The fluids at Albert show a wide range of homogenisation temperatures and final melting temperatures, and this is a result of the multiple episodes of quartz precipitation which span the entire paragenetic sequence. At Spoedwel, quartz veining is largely confined to the major mineralising event associated with the intermediate stages of the paragenetic sequence (i.e. the sulphide assemblage), while, at Grass Valley, the quartz veining post-dates the sulphide assemblage and is associated with late stage quartz-

hematite veins. The fluids associated with several cross-cutting quartz veins from Spoedwel, Albert and Grass Valley are summarised in Figure 5.62.

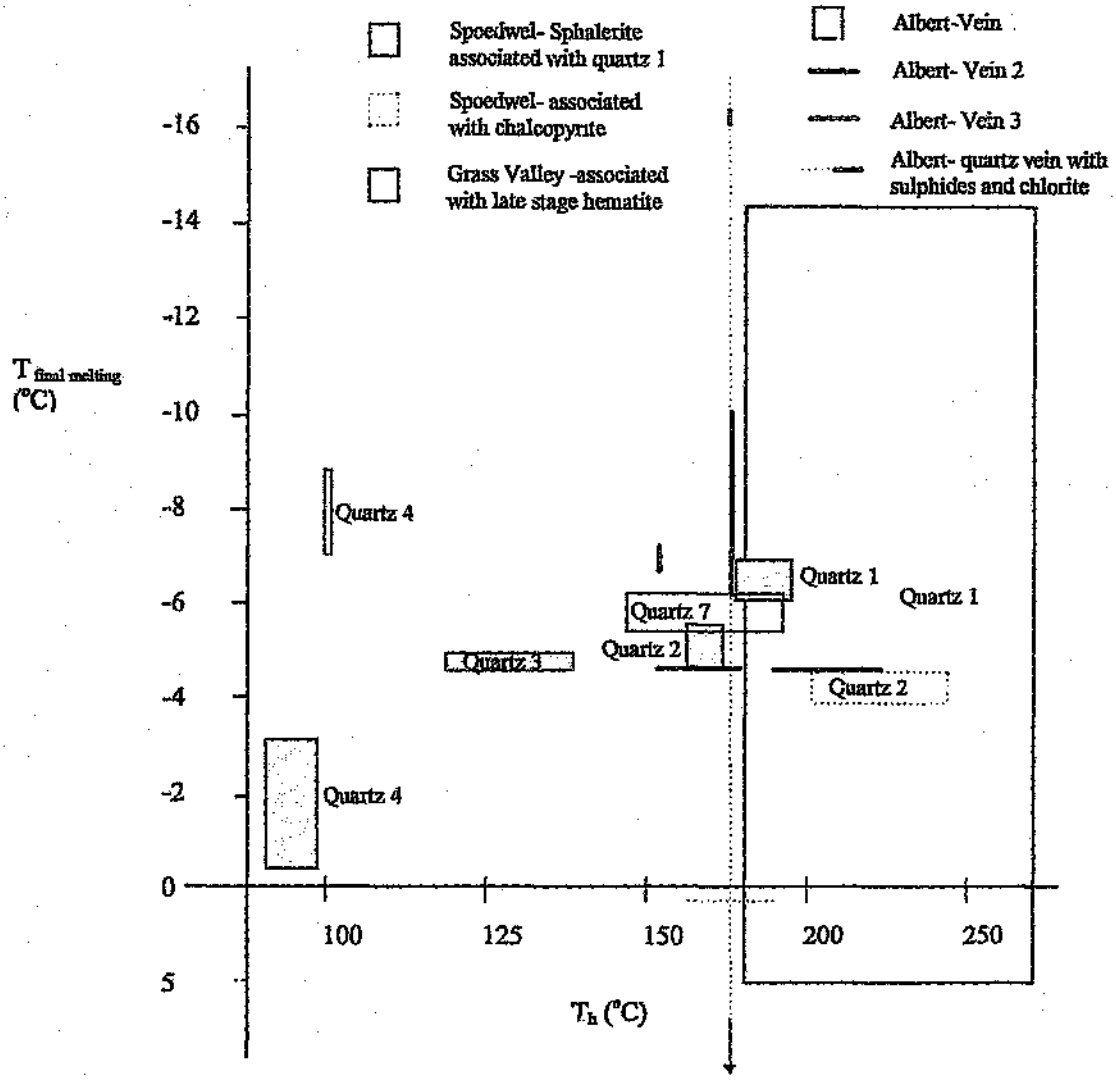


**Figure 5.62** Diagram plotting fluids from Spoedwel, Albert and Grass Valley.

The basic trends in the fluids from these deposits indicate that the earliest quartz veins were associated with the precipitation of the sulphide assemblage. With time, the fluids cooled and became less saline (inferred from lower $T_{final\ melting}$ temperatures).

In addition, the quartz veins at Spoedwel were formed at higher temperatures than those at Albert and Grass Valley. The $CO_2$-rich fluids at Grass Valley post-date and are superimposed on the aqueous fluids in the earlier quartz generations in the veins. These fluids have higher salinities (lower final melting temperatures), and were trapped at higher temperatures than the last of the aqueous fluids (see quartz 4 on Figure 5.62). Thus, the carbonic fluids associated with hematite precipitation at Grass Valley are different to those responsible for precipitation of the hematite/fluorite assemblage at Spoedwel and Albert.

**Fluids associated with fluorite**

Fluorite containing primary and secondary fluid inclusions is present at Spoedwel, Albert, Grass Valley and Houtenbek. Cathodo-luminescence imagery has shown that the fluorite can be divided into two growth stages, and fluid inclusions in each of these growth stages have been examined. The data points for fluorite-hosted fluid inclusions from Spoedwel, Albert, and Grass Valley and Houtenbek are plotted in Figure 5.63

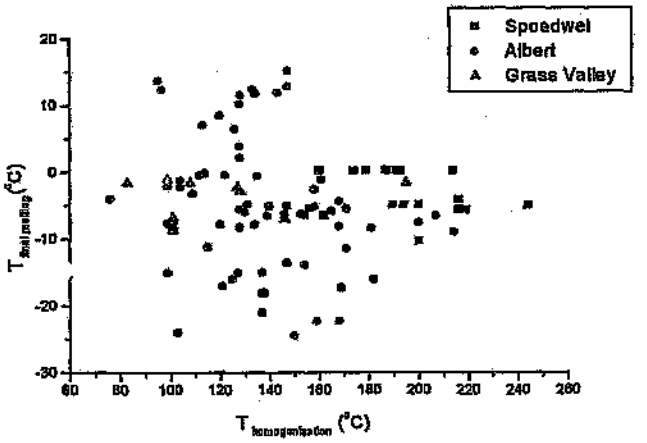


**Figure 5.63** Plot of homogenisation temperature versus final melting temperature for fluorite hosted fluid inclusions from Spoedwel, Albert, Grass Valley and Houtenbek.

Primary fluid inclusions along growth zones in two generations of fluorite have been recognised at Spoedwel. The first generation of fluorite contains fluids that are not particularly saline (between 0 and 6.5 wt. % eNaCl)) and trapped at relatively high temperatures (above 200°C). The highest temperature for minimum entrapment is 270 °C, but the majority of data points fall within the range 130°C to 150 °C. The fluid inclusions with the lower final melting temperatures (i.e. -4 °C) have higher homogenisation temperatures. These fluids are also present in the fluorite at Houtenbek. The most saline fluids (17 wt. % eNaCl; $T_{final\ melting}$ -13°C; $T_h$ 128 °C to 200 °C) occur in the second generation of fluorite at Spoedwel. These fluids contain Ca (producing a brown mosaic on freezing and with Te -52 °C). A higher-temperature fluid inclusion assemblage with similar salinites is present at Houtenbek. Houtenbek fluorite does not contain any of the lower-temperature fluid inclusion assemblages recognised at Albert, and Grass Valley.

The fluids have been categorised and are represented in Figure 6.64 which plots the different fluids in fluorite-hosted fluid inclusions from Spoedwel, Albert and Grass Valley. Note the overlap of temperature ranges of the saline fluids and the non-saline fluids, implying that both fluids were circulating at the same time and that interaction between them probably took place. Supporting evidence for the interaction between magmatic and connate fluids in similar temperature ranges which are associated with two generations of fluorite was also recognised by Plumlee *et al.* (1995) in the genesis of the Illinois-Kentucky fluorite deposits.

At the Albert silver deposit, three main fluid populations have been recognised in the fluorite. The fluids associated with the first fluorite generation are high temperature ($T_h$ 218 °C to 273 °C), and contain little or no Ca (no brown mosaic was produced and $T_e$ -33 °C). Eutectic melting temperatures suggest that $MgCl_2$ may be present in the fluids. Final melting temperatures (-4.8 °C to -3.2 °C) and salinities (7.2 to 5 wt. % eNaCl) fall in the range of values recorded for the fluids associated with fluorite 1 at Spoedwel. The fluids associated with the second generation of fluorite correlate with those in the second generations of fluorite at Spoedwel.

They contain Ca (producing a brown freezing mosaic and $T_e$ -49 °C), and are relatively saline (16 to 19.5 wt. % eNaCl) ($T_{final\ melting}$ -16 °C to -6 °C). The maximum $T_{final\ melting}$ and $T_h$ values are slightly higher than those recorded at Spoedwel; however, it is clear that they are related fluids. A third, late stage, low temperature (93 °C to 112 °C) and low salinity (4.3 to 2.6 wt. % eNaCl) fluid occurs in secondary trails and is unrelated to fluorite precipitation.

Fluid inclusions belonging to the early, high temperature fluid assemblage recognised at Spoedwel and Albert, are not present in the fluorite at Grass Valley. The fluids occurring in primary inclusions correlate with the fluids associated with the second fluorite generation at Spoedwel and Albert. They share all the same characteristics, and plot in similar positions on a graph of $T_{final\ melting}$ and $T_h$. Trails of lower temperature and salinity (11.8 to 6.5 wt. % eNaCl), secondary fluid inclusions, are trapped along annealed fractures, and post-date the primary fluid inclusion assemblage. Except for the high salinity fluids ($T_{final\ melting}$ -17 °C to -38 °C ), the fluids trapped in interstitial fluorite in all deposits are the same as those trapped in interstitial quartz.

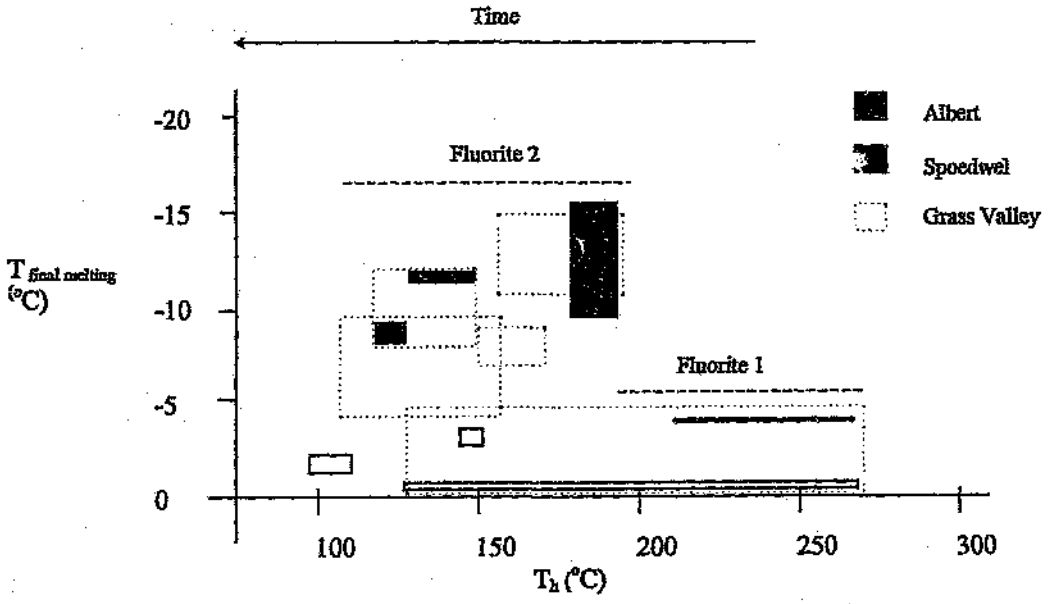


**Figure 5. 64** Diagram comparing fluid populations in fluorite from Spoedwel, Albert and Grass Valley

## 5.3 CONCLUSION

Fluid inclusion petrography and microthermometry have revealed that mixing between magmatically derived fluids, and an external fluid of connate origin, played an important role in the evolution of the granites and the localisation of mineralisation in the eastern lobe of the Bushveld Complex. The stage at which the magmatic and externally derived fluids dominated the system are shown in Figure 5.65.

The salinity and composition of the fluids evolved with time, being moderately saline and containing few divalent cations (Ca, Mg and Fe) at Stage 1 in the paragenetic sequence when cassiterite, scheelite, wolframite, molybdenite, specularite and arsenopyrite were deposited. The influence of the external fluid was minimal at this stage, but with time, the external fluid component became more dominant and interacted with the magmatically derived fluids. At this stage the fluids reached their peak salinity, and crystallisation of the subsolvus granites and associated sulphide assemblage took place. Towards the waning stages of magmatic activity, the magmatic fluids were diluted substantially by the incursion of the external fluid, leading to the deposition of the hematite-fluorite-pitchblende assemblage in the third episode of mineralisation

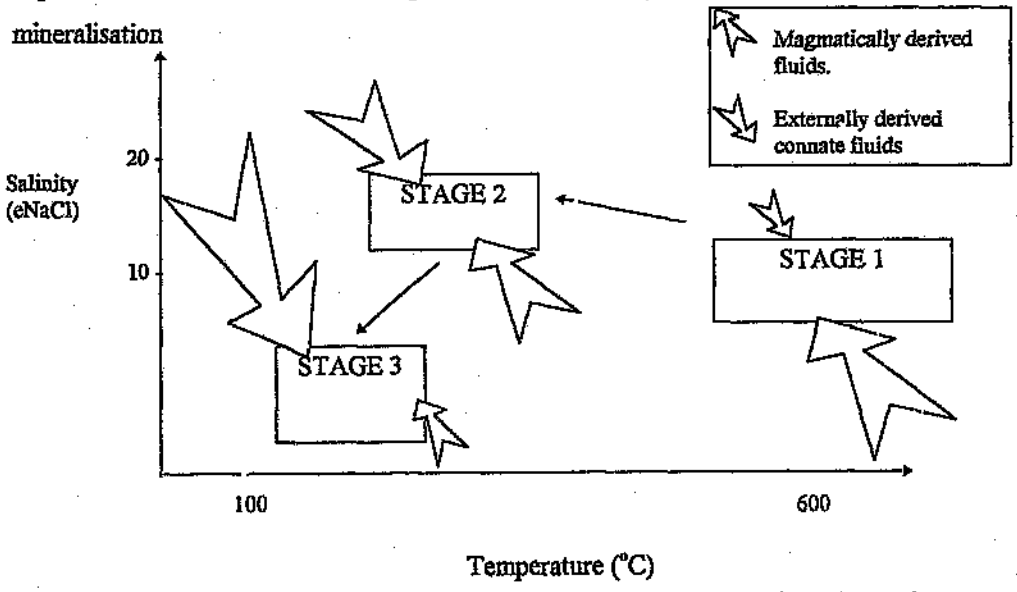


**Figure 5.65** Schematic diagram showing the change in salinity with time, decreasing temperature and increasing external fluid component.

# CHAPTER 6

# QUANTITATIVE FLUID INCLUSION ANALYSIS

Fluid inclusion microthermometry does not provide conclusive quantitative data regarding the composition of the fluids associated with mineralisation. It is possible only to presume the presence of certain elements on the basis of the eutectic melting temperatures and the intermediate and final melting temperatures. This technique does not adequately solve the question of exactly which metals/elements are present in the fluids, and in what concentrations. For this reason, PIXE analysis, Raman Spectroscopy and Quadrupole Mass Spectrometry were undertaken. The results of these analytical techniques are presented within the paragenetic framework established in Chapter 4, and linked to the major fluids recognized during microthermometry (Chapter 5).

## 6.1 PIXE ANALYSIS

PIXE analysis of selected fluid inclusions was carried out at the National Accelerator Center in Faure, South Africa. At present, this technique provides an accurate assessment of most of the elements present in the fluid inclusions (see following paragraphs).

### *OVERVIEW*

Proton-Induced X-Ray Emission (PIXE) analysis on individual fluid inclusions was first attempted by Horn (1983) and Horn and Traxel (1985, 1987). This method of spectroscopic analysis enables *in situ* analysis of unopened fluid inclusions, being non-destructive, and provides qualitative and semi-quantitative data on the fluid inclusion contents.

The application of this method to fluid inclusions has been investigated by Anderson *et al.*. (1989), Ryan *et al.* (1991), Heinrich *et al.* (1992), Ryan *et al.* (1993), Ryan *et al.* (1995) and others.

PIXE analysis involves bombarding the atoms of the subject, in this case the fluid inclusion, with protons, causing the ejection of inner shell electrons and emission of the characteristic X-rays of the elements in the fluid (Anderson *et al.*, 1989). Ryan *et al.* (1993) have described the four main steps entailed in quantitative PIXE microanalysis of fluid inclusions. Firstly, theoretical X-ray yields must be calculated for a) the layered structure representing the inclusion, b) the overlying mineral overburden and c) the underlying mineral matrix (Figure 6.1). Secondly, the yields expected for simple layers need to be modified to correct for the details of the overlap of the proton beam envelope with the detailed geometry of a particular inclusion. Thirdly, the PIXE spectrum must be analysed using accurate element line shapes with X-ray relative intensities which reflect these integrated X-ray yields. Fourthly, the contributions of X-rays originating from the elements in the host mineral must be subtracted from the observed peak areas. Details of the procedure are given in Ryan *et al.*, (1993).

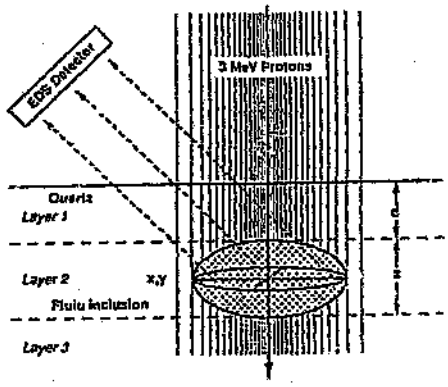


**FIGURE 6.1** Model geometry for PIXE analyses of fluid inclusions, schematically indicating the proton beam, sample and detector arrangement, and the geometric parameters used to quantify PIXE microprobe spectra. The dimensions x, y and z are determined by optical microscopy; d is determined using the Cl $K_\alpha/K_\beta$ ratio and/or optical measurement. (From Heinrich *et al.*, 1992)

All elements heavier than Si (Anderson *et al.*, 1989) or where the atomic number (Z) >16 (Ryan *et al.*, 1991) are detected using this method. The lighter elements of interest to geologists, such as Li and Na, are not detected even though their concentration may be significant. The heavier elements are detected at concentrations as low as a few ppm. The detection and quantification of sulphur is difficult and unreliable (Heinrich *et al.*, 1992).
There are several limitations or restrictions to PIXE analysis. The energy loss of the protons penetrating the mineral host affects the yield of the X-rays from the fluid inclusion. The absorption of the induced X-rays by the host mineral also influences the sensitivity of the method. The degree of absorption is a function of the depth of the inclusion below the mineral surface, the take-off angle, the composition and density of the host mineral and the energy of the emitted X-rays (Anderson *et al.*, 1989). Thus, the depth below surface is a critical consideration when selecting suitable inclusions for PIXE analysis, since the quality of the results deteriorates with increasing depth.

The size and shape of the inclusions also influences the sensitivity of the method. Large euhedral inclusions (>10microns in diameter) at depths between 5 and 15 microns are the most suitable for optimal PIXE sensitivity (Ryan *et al.*, 1991).

The fluid inclusion geometry and the depth below surface are critical factors when it comes to quantification of PIXE yields. Deviations from the model's ideal conditions are not accounted for. Since fluid inclusions are rarely perfectly euhedr ıd errors in the estimation of geometrical parameters are unavoidable, a degree of uncertainty in the extracted elemental concentrations is introduced. In addition, the nature of fluid inclusion (vapour bubble and solid phases) further compounds the degree of uncertainty in the quantitative analysis of the inclusion contents.

***EQUIPMENT***

A preliminary investigation of selected fluid inclusion using the PIXE technique was undertaken at the National Accelerator Centre (NAC), Faure, South Africa. A focused raster-scanned proton beam of 3 micron diameter spot size was applied to the individual inclusions bathing the entire inclusion in an even dose of protons. In cases where the inclusions are smaller than the spot size, the surrounding quartz matrix is also excited.

Using a beam of 3 MeV protons, each part of the inclusion was exposed to a uniform dose of protons, thus improving the accuracy and reproducibility of the results. The beam current was set between 250 and 700 pA. The beam incidence was normal to the sample surface and the detector take-off angle was 45°.

*SAMPLE MATERIAL*

Fluid inclusions were specifically selected from Grass Valley, Spoedwel, Albert and Leeufontein in order to obtain information on the fluids associated with each of the major stages in the paragenetic sequence. The fluid inclusions selected from Grass Valley are associated with quartz growth in two generations of quartz preceding cassiterite precipitation. The fluids associated with the second generation of interstitial quartz material at Spoedwel, which contains highly saline fluids and numerous solid phases, as well as fluids associated with quartz vein-hosted sulphides at Albert, were selected as representatives of later fluids associated with the sulphide assemblage. The fluids associated with albitisation and tourmalinisation, which post-date the sulphide assemblage, were selected from Leeufontein. More detailed accounts of the fluid inclusions are given below. Sketches of the inclusions and their characteristics are shown in Table 6.1.

**Grass Valley**

Fluid inclusions hosted by the two quartz generations preceding cassiterite precipitation have been probed. They are secondary inclusions and microthermometry suggests that they are not particularly saline, melting between -2°C and -4°C. They were trapped at low temperatures (homogenisation between 130°C and 160°C). These fluids are not the same as the high temperature (600 °C) fluids at Zaaiplaats. Rather, these fluids may be associated with tin remobilization, thus accounting for the low temperature ranges measured.

**Spoedwel**

The inclusions probed are hosted by the second generation of interstitial quartz and belong to the population of inclusions containing hematite daughter crystals. Microthermometry of this fluid population suggests the presence of $CaCl_2$, NaCl, KCl, and $H_2O$. The phase relationships in the simple $CaCl_2$-NaCl-$H_2O$ system, which does not take into account all known solutes, suggest salinities of between 18 and 24 wt. %.

At least six daughter crystals from eleven possible solid phases have been observed in any one inclusion in this population, including hematite, two opaque phases, $FeCl_2$, halite, sylvite, and smaller unidentified crystals.

**Albert**

These inclusions are primary, occurring in vein quartz which contains euhedral pyrite crystals and minor sphalerite. During microthermometry, these inclusions freeze at moderate temperatures and do not suggest the presence of $CaCl_2$. However, eutectic melting is in the range -40°C to -50°C, suggesting the presence of divalent cations in solution. Final melting temperature for this inclusion is -17°C, but the other fluid inclusions in the assemblage show wide ranges of melting temperatures. Homogenisation of liquid and vapour occurs between 128°C and 214°C.

**Leeufontein**

These are quartz-hosted fluid inclusions in a tourmaline spheroid. The fluid is moderately saline, which is indicated by final melting temperatures between -10°C and -20°C. Daughter crystals commonly include halite and sylvite. Homogenisation occurs at relatively low temperatures (85 to 115°C). Two categories of fluid inclusions have been recognised, those with liquid and vapour, and those with liquid, vapour and solid phases.

**Synthetic fluid inclusions**

Synthetic quartz-hosted fluid inclusions containing NaCl and KCl solutions of eutectic compositions (23.2 wt % NaCl and 19.6 wt % KCl) were used for comparison in the quantification of PIXE yields. Sketches of the inclusions are shown in the following table and in the appendix.

**Table 6.1** Table of sample material selected for PIXE analysis from Spoedwel, Albert, Grass Valley and Leeufontein.

| DEPOSIT | SAMPLE NO. | SKETCH | COMMENTS |
|---|---|---|---|
| Spoedwel | SP2 | A  | Fluid inclusions in interstitial quartz of medium- to fine-grained hypersolvus granite. The fluid inclusion assemblage is associated with the second episode of quartz precipitation at Spoedwel, as well as the sulphide assemblage. |
| | | B  | |
| Spoedwel | OF | OFA  | As above. |
| | | OFB  | |
| Albert | RP11A |  | Fluid inclusion in pyrite- and sphalerite-bearing quartz vein hosted by fine-grained granite. |
| Grass Valley | GV02 | A  | Aqueous inclusions in pegmatitic quartz preceding cassiterite precipitation. Fluid inclusions A and B are from consecutive growth stages in the crystal. |
| | | B  | |
| Leeufontein | TB01 | TB01B1  | Fluid inclusions in quartz intergrown with tourmaline in late stage spheroids hosted by fine-grained Klipkloof granite. |
| | | TB01B13  | Primary fluid inclusion in tourmaline. |
| | TB01A |  | |
| Synthetic fluid inclusions | NaCl |  | Fluid inclusions hosted by synthetic quartz produced by FLUID INC., and used for calibration purposes. The composition of these inclusions is known to be 23.2wt % NaCl and 19.6 wt % KCl. |
| | KCl |  | |

***METHODS***

Doubly polished rock wafers (150 microns in thickness) were surveyed for large inclusions (10-20 microns) located at shallow depths (less than 20 microns) beneath the sample surface. The relationship between fluid inclusions were carefully mapped in three dimensions to allow easy relocation of the inclusion of interest when in the sample chamber of the microprobe.

Alphabetically marked copper and nickel Maxtaform Finder Grids (200 mesh, 127 microns pitch) were glued on to the sample with UHU-stic® or Pritt® to assist in easy relocation of the appropriate field of view and the selected inclusions (Figure 6.2).The sample was then mounted onto metal (Al) sample holders by evaporating de-ionised water from the 0.4

micron Formvar® film on the sample holder. The depth below surface, as well as the vertical dimensions of the inclusion, were measured using a graduated ocular.

The sample holder was then mounted on to an X-Y mobile stage at an angle normal to the beam path. The location of inclusions using a transmitted light petrographic microscope with a 45° take-off angle proved unreliable. Instead, finder grids were mounted onto the sample surface and the co-ordinates of inclusions with reference to the grids were first measured off-line using a transmitted light petrographic microscope. During microprobe measurements, a preliminary, short raster scan (about 30s) was necessary to obtain a total X-ray map with dominant signal coming from the finder grid. This allowed selection of the longer raster scan in the right area above a selected fluid inclusion, using true elemental imaging (Ryan *et al.*,1995; Ryan and Jamieson, 1993). Ideally, the inclusions were positioned in the middle of grid holes in order to minimise the signal from the grid from interfering with the PIXE spectrum from the sample. Such ideal positioning was usually difficult to achieve. The presence of these peaks in the PIXE spectrum from fluid inclusion was the only drawback of this procedure, which was otherwise rather fast and reliable.

The data were collected during two separate visits to NAC. On the first occasion, copper finder grids were pasted on with Uhu-stic®, and the samples were not carbon coated. On the second visit, nickel grids were used instead of copper grids, because Cu is known to be present in the mineralising system. Thus, contamination of the Cu values obtained from the fluid inclusions by an external source was avoided. Carbon coating was necessary to prevent charging of the nickel grid, a situation not encountered with the copper grid.

The calculation of PIXE yields was done in generic form using the GeoPIXE software package (Ryan *et al.*, 1990). The yields of each X-ray line for each major and trace element were integrated to include contributions along the slowing down path of the proton beam including secondary X-ray fluorescence and absorption effects in the fluid and surrounding mineral along the X-ray path to the detector (Heinrich *et al.*, 1992). The PIXE spectra were analysed using element line shapes constructed using X-ray relative intensities deduced directly from the individual X-ray yields for a particular inclusion geometry and corrected for the efficiency of the EDS detector and the attenuation caused by X-ray absorbers used to reduce the intensity of Si X-ray lines from the quartz matrix and to stop

back-scattered protons entering the detector. A 125 μm thick Be filter was used for this purpose.

As a control measure, synthetic fluid inclusions with known composition (i.e. 23.2 wt % NaCl and 19.6 wt % KCl) were analysed, in order to assess the accuracy of the instrument in providing quantitative data.

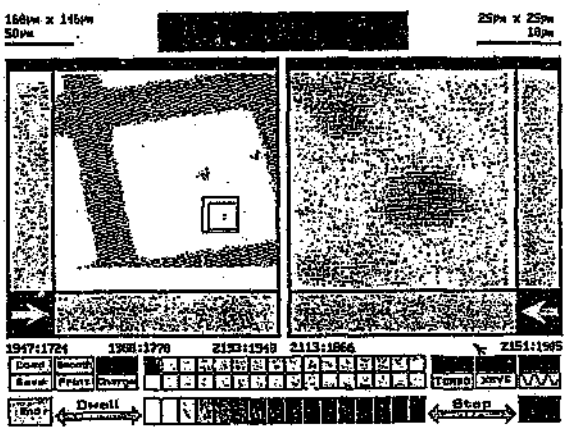

**Figure 6.2** Screen printout showing how finder grids assist in relocation of fluid inclusions once in sample holder.

*RESULTS*

**Maxtaform® Finder Grids**

The only peak produced by the copper grid is that of Cu. No other components are detected. The spectrum produced by the nickel grid shows that it too contains no impurities. It appears that the use of Ni finder grids instead of the Cu grids is not advantageous. Nickel peaks appear in almost all the spectra and, since Ni-bearing minerals do not feature in the parageneses of the deposits, it is assumed that contamination from the finder grid is the source. This situation was not encountered with the Cu finder grids since analysis of quartz well removed from the grid shows no Cu peak. Therefore, the copper detected in the fluid inclusions is an actual component of the fluid and not a result of contamination by the grid.

**Inclusion-free quartz**

The inclusion-free quartz some distance from the Maxtaform® grid produces only the Si peak (Figure 6.3). Spectra of quartz nearer the grids show the Cu or Ni peaks, depending on which type of grid was used, as well as the Si peak (Figure 6.4).

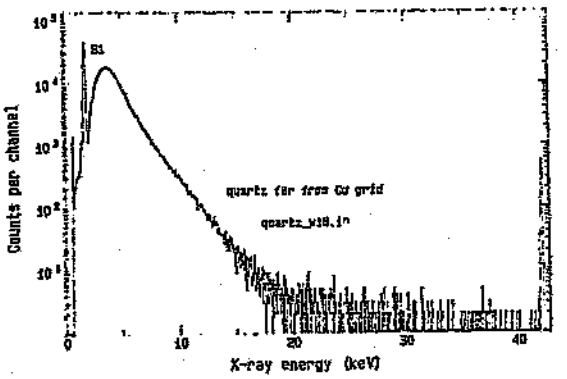


**Figure 6.3** PIXE microprobe spectrum of quartz some distance from the finder grids showing that only Si peaks are detected.

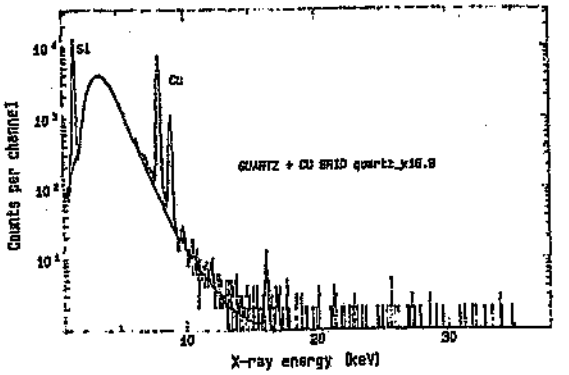


**Figure 6.4** PIXE microprobe spectrum of quartz near the finder grid, showing that excitation of the grid (in this case Cu), creates interference with the spectrum for pure quartz.

**Synthetic fluid inclusions**

Sketches of the synthetic NaCl and KCl fluid inclusions probed are shown in the Appendix. The PIXE spectra generated by the synthetic fluid inclusions showed that the NaCl standard contained no impurities, and that the KCl standard contained very small amounts of Ti, Cu and Zn. These impurities, however, had no effect on the element of interest (K), and were disregarded. The quantitative PIXE yields (see Table 6.2) for these inclusions are extremely low in comparison with the known concentrations. The shapes of these inclusions are not ideal for calculating the concentrations of elements, since the assumption of the model is that fluid inclusions are ellipsoidal in shape. Furthermore, estimates of depth, thickness and dimensions of these inclusions may be inaccurate, causing additional error in the calculations.

**Table 6.2** Expected and observed values for Cl and K from synthetic fluid inclusions.

| | Cl (wt. %) | | K (wt %) | |
|---|---|---|---|---|
| | Expected | Observed | Expected | Observed |
| **NaCl (23.2 wt. % NaCl)** | ±14 | 1.34 | | |
| **KCl (19.6 wt. % KCl)** | ±9.5 | 0.594 | 10.5 | 0.386 |
| | | | | |

The attempt to quantify the data was rather discouraging. The data are included as a matter of interest, but it should be borne in mind that the concentrations of elements are inaccurate. Taking the 23.2 wt % NaCl synthetic fluid inclusion standard as an example, the Cl content should be ~14 wt % but is only 1.34 wt %. The KCl standard also shows enormous errors between expected and observed yields; Only 0.594 wt % Cl is detected instead of the 9.5 wt % expected, while 0.386 wt % of K is observed compared with the 10.5 wt % expected. Clearly these discrepancies are unacceptable, and thus, at this stage, the data should only be considered as being qualitative. The major factors responsible for the discrepancy appear to be related to the inaccurate determination of the fluid inclusion dimensions, the deviation of these dimensions from the ideal model geometry and the difficulty in determining the true depth below surface of the sample at which the fluid inclusion is situated.

**Fluid inclusions**

Petrographic maps and PIXE spectra for each of the inclusions probed are shown in the Figures 6.5 to 6.10. In each of these figures, a petrographic map indicating fluid inclusion relationships and microthermometry, as well as the PIXE spectrum produced by probing the selected inclusion(s), is shown. The quantitative results are shown in Table 6.3. The table indicates the concentration (in parts per million) of elements present in each sample. The samples are arranged in deposits, starting from the earliest fluids in the Grass Valley samples, through to the latest fluids associated with albitisation and tourmalinisation at Leeufontein.

The concentrations of K, Ca and Cl are shown in the bar chart in Figure 6.11. The fluids at Grass Valley are depleted in these elements in comparison with Spoedwel, Albert and Leeufontein. The Spoedwel fluids contain the highest concentration of K and Ca. At Albert K is more abundant than Ca, while the opposite is observed at Spoedwel. The fluids in the tourmaline ball are enriched in Ca. The elements associated with the sulphide assemblage are shown in Figure 6.12. As with Cl, Ca and K, the Grass Valley fluids do not contain significant amounts of these elements. However, the Spoedwel fluids contain significant amounts of these components. The abundance of the elements progressively decreases at Albert and Leeufontein. A similar pattern is observed in the Fe content of the fluids (Figure 6.13). Spoedwel fluids contain the greatest amount of dissolved Fe, and lesser amounts are present at Albert and Leeufontein. The early fluids at Grass Valley contain virtually no Fe. S was not easily detected, with Grass Valley fluids containing the only significant amounts (Figure 6.14). The concentration of REE's (Ga, Br and Rb) are plotted with S and Cl in Figure 6.15. The abundance of these elements at Spoedwel is noteworthy, compared to the total absence at Albert and Grass Valley. The tourmaline spheroids contain small amounts of Br and Rb. Manganese and titanium were also detected in the fluids, but at lower concentrations than Fe (Figure 6.16). The Fe, K and Ca content of the fluids are plotted on a ternary diagram (Figure 6.17), which shows two clusters of data points. The data points at the Fe apex are from Spoedwel, Albert, and Leeufontein tourmaline, while the points in the centre of the diagram are from Grass Valley and Spoedwel.

Table 6.3 Quantitative PIXE yields (ppm)

| | Sample | Cl (ppm) | K (ppm) | Ti (ppm) | Mn (ppm) | Ga (ppm) | Br (ppm) | Rb (ppm) |
|---|---|---|---|---|---|---|---|---|
| Grass Valley | GV022A | | 2230 ±876 | 1773 ±365 | | | | |
| | GV022C | | 972 ±650 | 981 ±395 | | | | |
| | GV022c? | 503 ±110 | 467 ±91 | | | | | |
| Spoodwel | OFB | 4892 ±358 | 21091 ±464 | 6128 ±164 | 9434 ±301 | | | 8071 ±579 |
| | OFA | 8679 ±672 | 5833 ±485 | 9713 ±429 | 17017 ±869 | | | 3092 ±569 |
| | OFA | 10336 ±552 | 5660 ±120 | 353 ±75 | 2550 ±102 | | | 276 ±112 |
| | OFA | 577 ±125 | 935 ±129 | 1001 ±154 | 19577 ±347 | | | 2237 ±220 |
| | OFA | 985 ±430 | 1613 ±356 | 2524 ±245 | 13228 ±562 | | | 1984 ±408 |
| | OFA2 | 6347 ±209 | 2044 ±124 | 1111 ±115 | 1547 ±101 | | | |
| Leenfontein | TB01B1 | 680 ±218 | 1357 ±183 | 1466 ±153 | 1364 ±96 | | | 319 ±118 |
| | TB01B13 | 6238 ±703 | 2879 ±480 | 9006 ±413 | 219 ±204 | | 592 ±200 | 549 ±247 |
| | TB01A | | 436 ±20 | 2073 ±16 | 526 ±22 | 76 ±5 | | |
| Albert | RP11A | | 5692 ±313 | 618 ±195 | 318 ±117 | | | |
| | RP11A | | 3338 ±272 | 813 ±192 | 222 ±109 | | | |
| | RP11A | | 6180 ±387 | 765 ±165 | 5365 ±193 | | | |

Table 6.3 Quantitative PIXE yields (ppm)

| Sample | S (ppm) | Ca (ppm) | Fe (ppm) | Cu (ppm) | Zn (ppm) | Mo (ppm) | Pb (ppm) | As (ppm) |
|---|---|---|---|---|---|---|---|---|
| GV022A | | 3178 ±572 | 2504 ±293 | 671 ±231 | | | | |
| GV022C | 2116 ±822 | 2191 ±351 | 1419 ±229 | 1172 ±263 | | | | |
| GV022c? | 553 ±214 | 489 ±118 | 2562 ±113 | | 140 ±74 | | | |
| OFB | | 2662 ±648 | 534202 ±3459 | 667 ±235 | 11592 ±508 | | | 14100 ±498 |
| OFA | | 9524 ±1035 | 56264 ±1472 | 2423 ±372 | 9793 ±693 | 3331 ±1060 | 7034 ±1425 | |
| OFA | | 7952 ±107 | 95039 ±632 | | 4337 ±132 | | | |
| OFA | | 1550 ±154 | 19383 ±290 | | 2240 ±101 | | 4785 ±943 | |
| OFA | | 2270 ±256 | 21218 ±510 | | 1988 ±329 | 1395 ±666 | 3407 ±1033 | |
| OFA2 | | 3472 ±120 | 24585 ±319 | | 1565 ±140 | | | |
| TB01B1 | | 526 ±132 | 12296 ±264 | | 1124 ±129 | | | |
| TB01B13 | | 1191 ±280 | 5263 ±197 | | 837 ±170 | | | |
| TB01A | | 827 ±154 | 127736 ±321 | | 214 ±7 | | | |
| RP11A | | 7367 ±255 | 7890 ±176 | 301 ±125 | 1089 ±155 | | | |
| RP11A | | 4963 ±313 | 7094 ±157 | 303 ±110 | 841 ±110 | | | 395 ±143 |
| RP11A | | 5195 ±232 | 130095 ±988 | | 890 ±118 | | | |

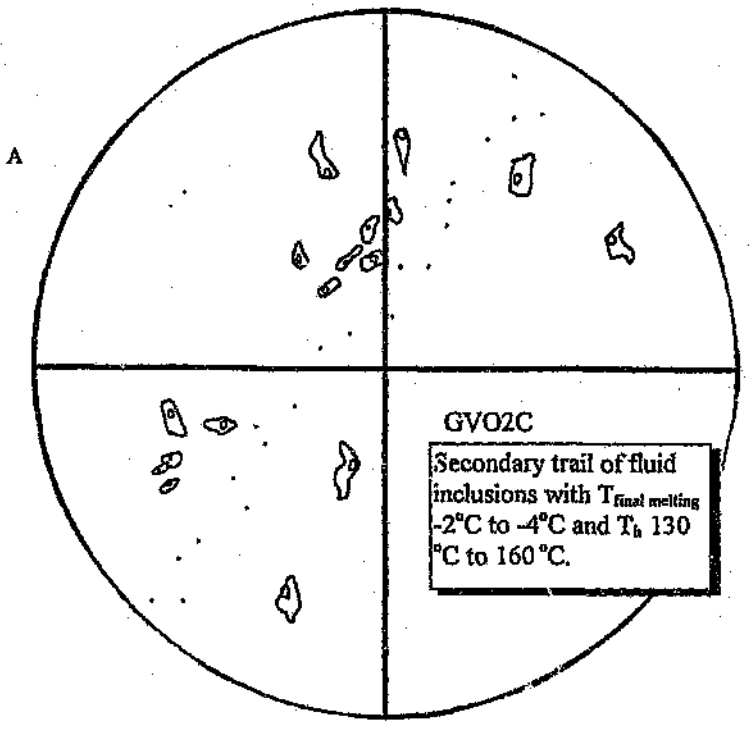


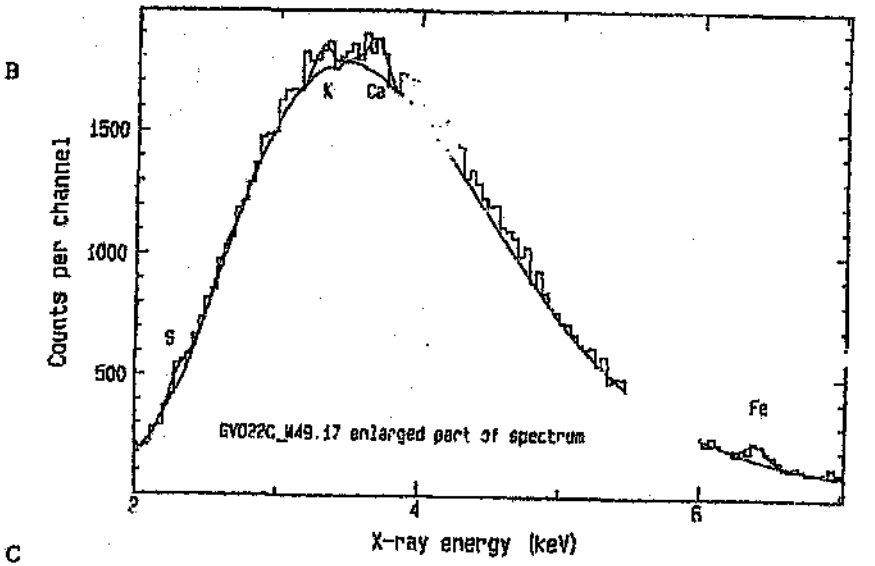


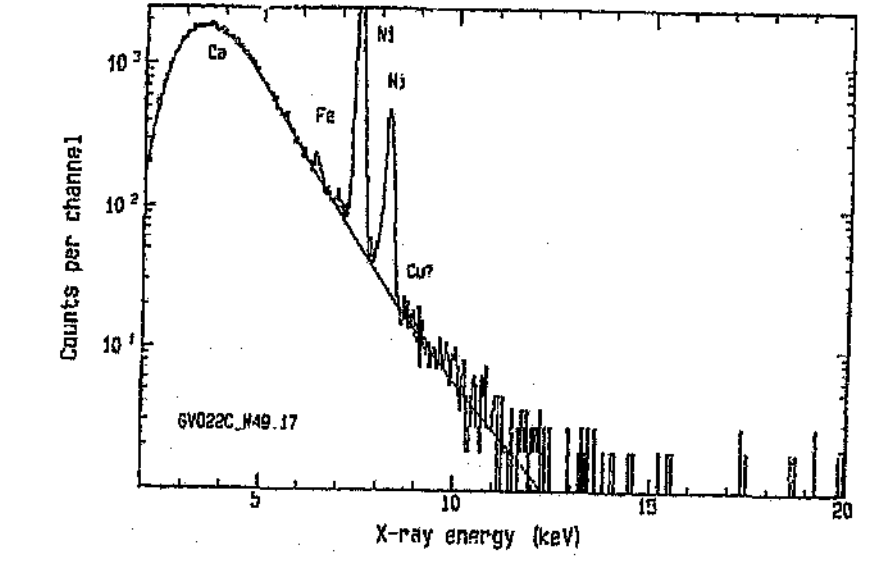


**Figure 6.5** A) Petrographic map of quartz-hosted fluid inclusions from the Grass Valley Sn deposit. The inclusions occur along the border between quartz generations 1 and 2, both of which precede cassiterite precipitation.

B) PIXE microprobe spectrum (Q = 115 nC, I = 250 pA) of inclusion C (depth 0.57μm, thickness 2.28μm, dimensions 16μm X 12μm) in sketch A), indicating the presence of Ca, Fe and Cu.

C) Enlargement of portion of B) in which S, K and Ca peaks become more obvious.

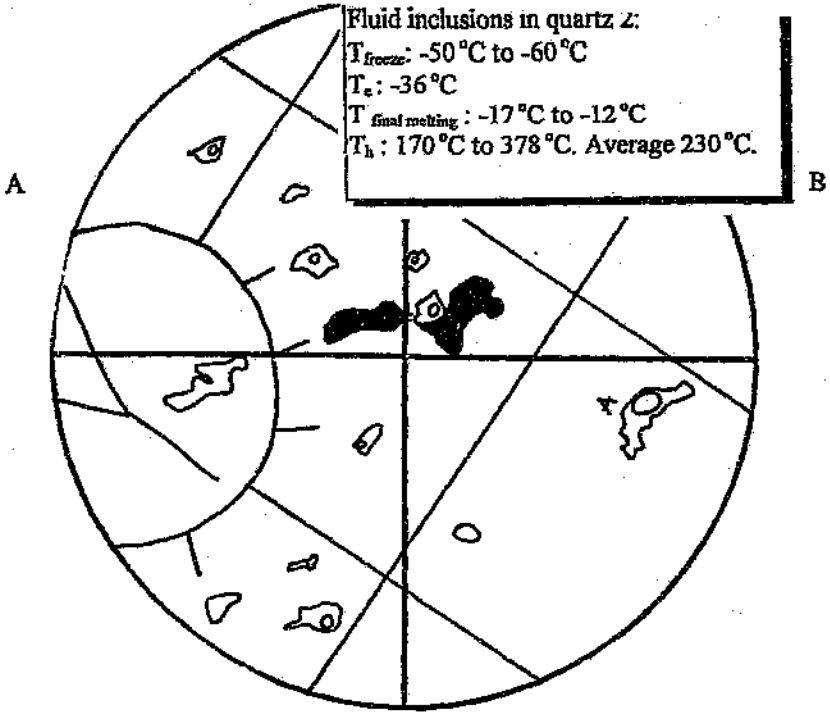


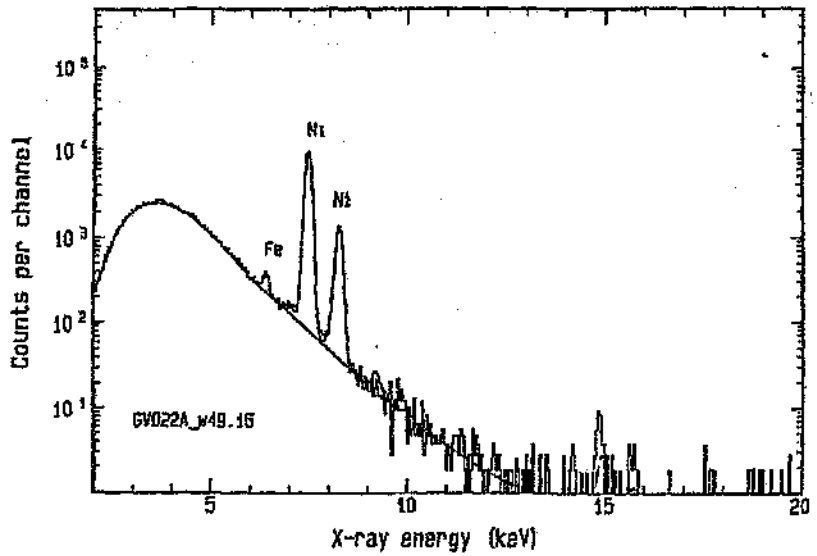


**Figure 6.6** A) Petrographic map of quartz-hosted fluid inclusions from the Grass Valley deposit. The inclusions occur in euhedral, pegmatitic quartz associated with calcite and cassiterite. The inclusion probes occurs in a secondary trail of inclusions in quartz generation 1 preceding cassiterite precipitation.

B) PIXE microprobe spectrum of fluid inclusion A in A), indicating the presence of Fe and Ni. Only Fe is derived from the inclusion, Ni peaks are caused by excitation of the Ni finder grid.

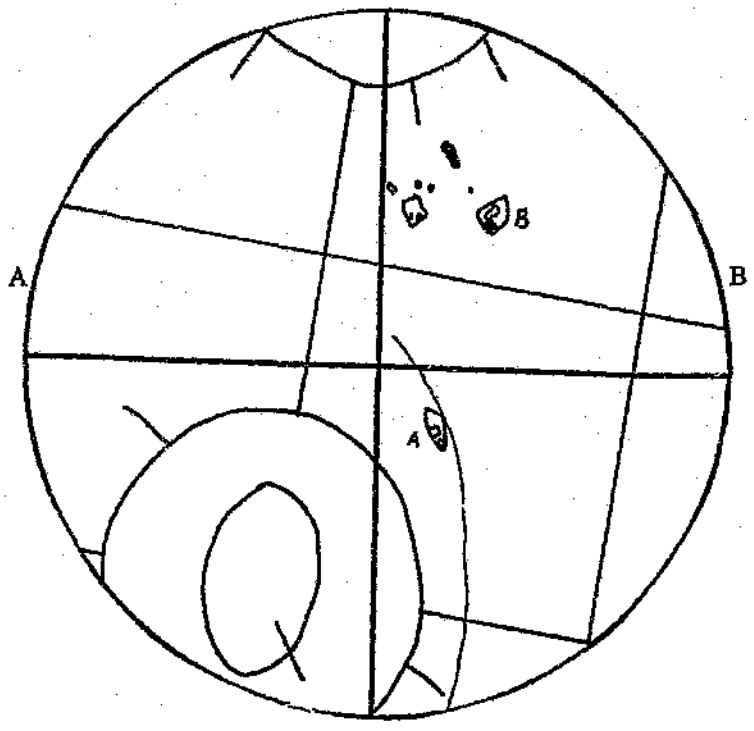


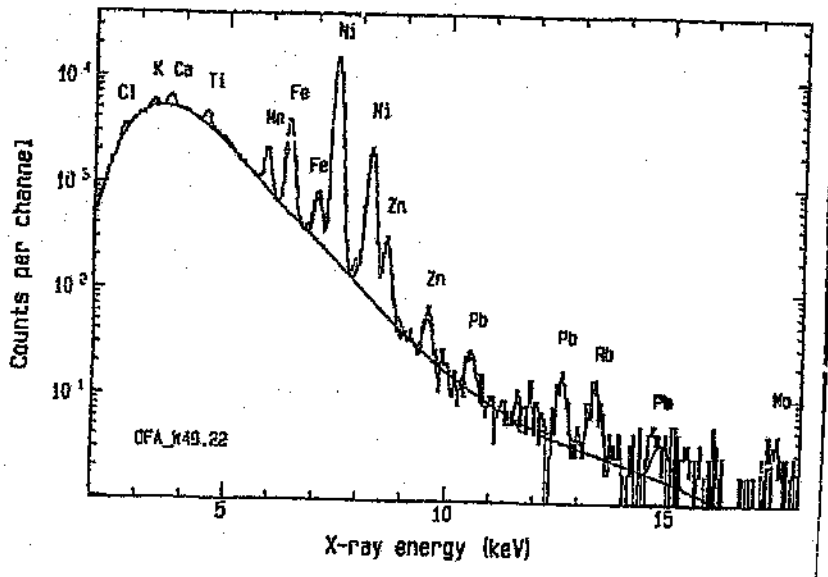


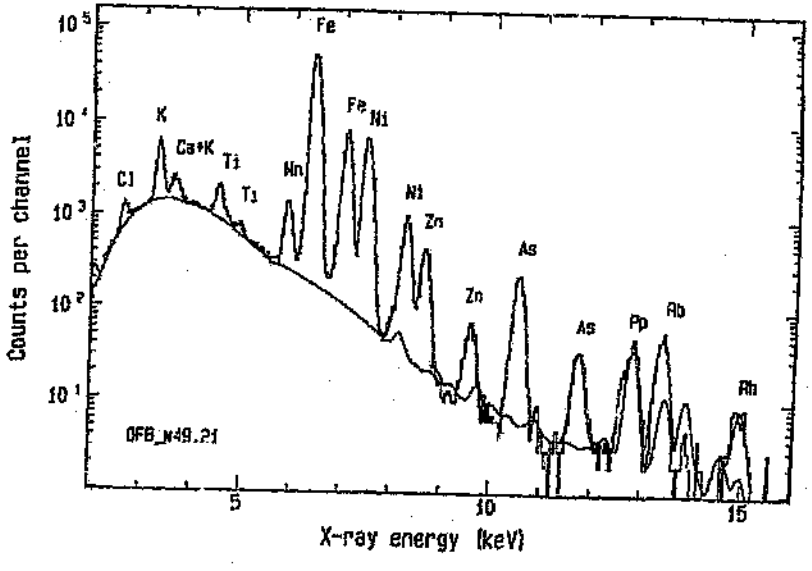


**Figure 6.7** A) Petrographic map of quartz-hosted fluid inclusions from the Spoedwel Cu deposit. These fluid inclusions are primary with respect to the second generation of quartz precipitated at the deposit, and have variable phase proportions. Inclusion A is a Type 2 inclusion consisting of liquid, vapour and a halite daughter crystal. Inclusion B contains no visible vapour phase, only liquid and 2 solids (hematite and one unidentified crystal). B & C) PIXE microprobe spectra (Q =213 nC, I = ~500 pA) of inclusions A (depth 0.5μm, thickness 1.57μm, dimensions 14μm X 6μm) and B (depth 0.57μm, thickness 2.28μm, dimensions 16μm X 12μm), indicating the presence of Cl, K, Ca, Ti, Mn, Fe, Zn, Pb, As, Rb and Mo in the inclusions.

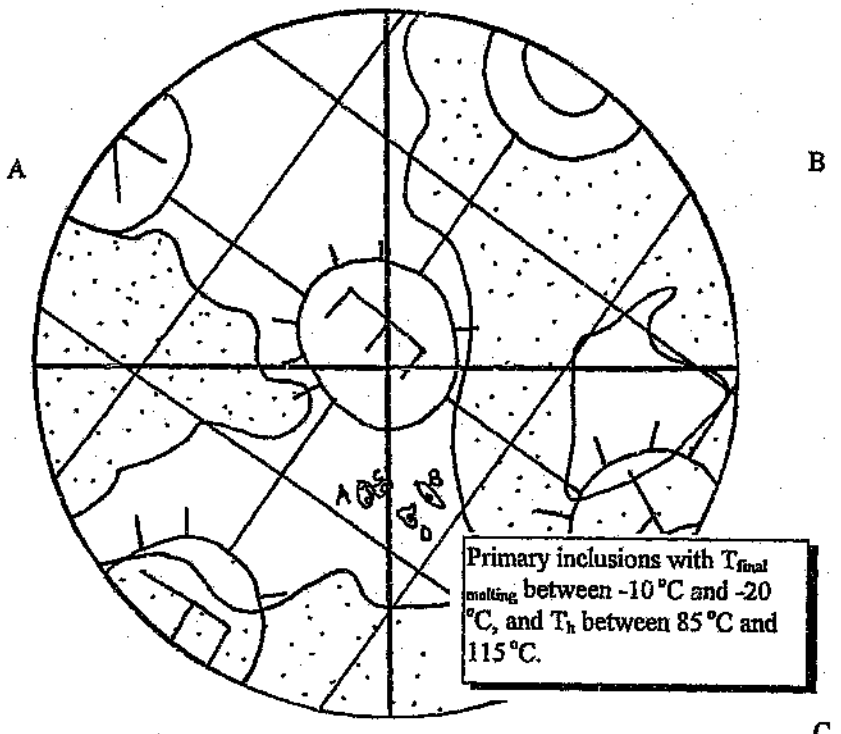


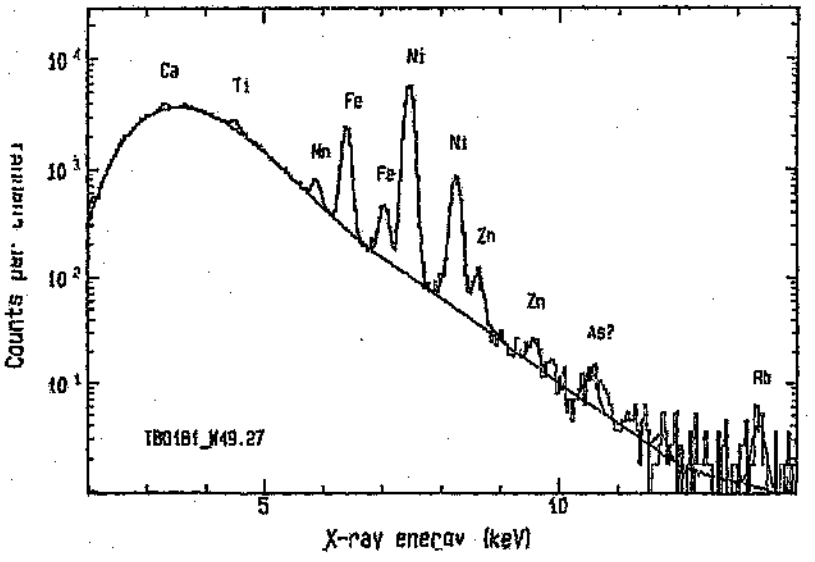


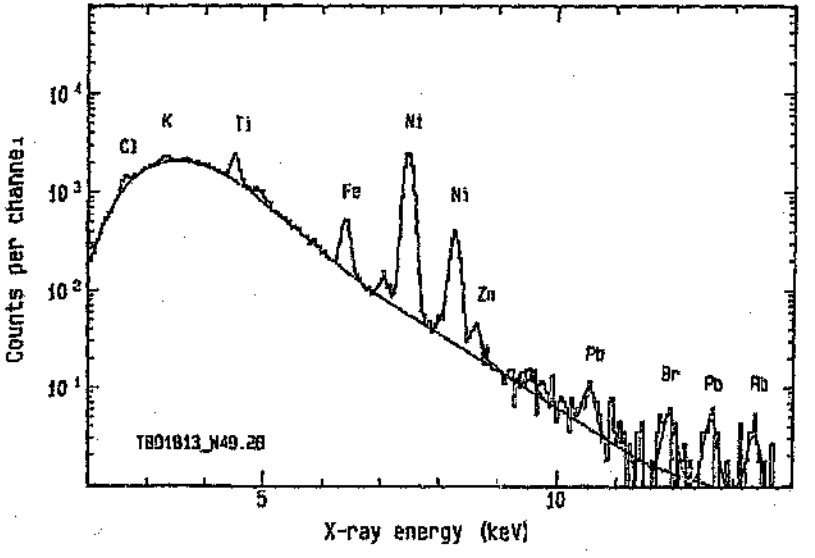


**Figure 6.8** A) Petrographic map of quartz-hosted primary fluid inclusions occurring in tourmaline spheroids from Leeufontein.
B) PIXE microprobe spectrum (Q =487 nC, I =500 pA) of inclusion A (depth 0.57μm, thickness 2.28μm, dimensions 18μm X 16μm), indicating the presence of Ca, Ti, Mn, Fe, Zn, As? And Rb in the fluids.
C) PIXE microprobe spectrum (Q =283 nC, I = 500 pA) of inclusion C (depth 2.14μm, thickness 1.71μm, dimensions 20μm X 8μm), indicating the presence of Cl, K, Ti, Fe, Zn, Pb, Br and Rb in the fluids.

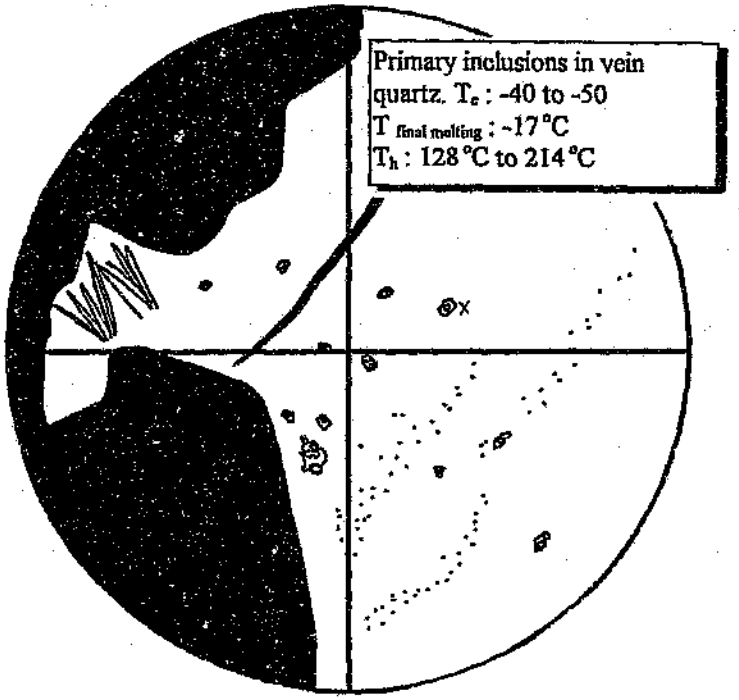


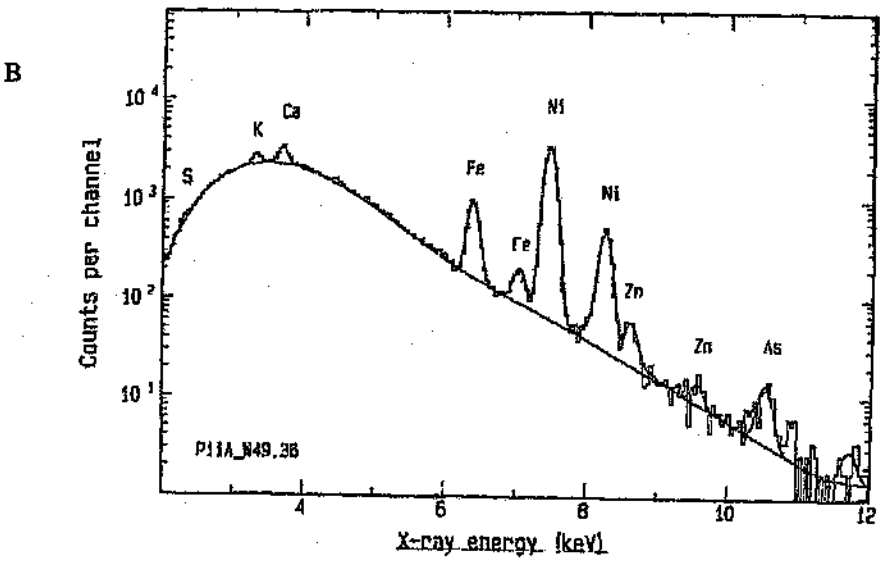


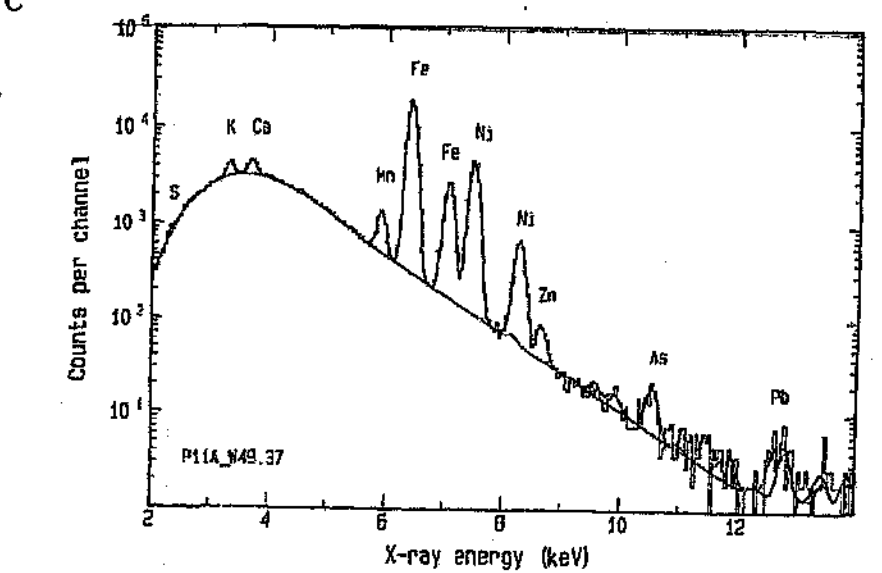


**Figure 6.9** A) Petrographic map of a quartz-hosted fluid inclusion assemblage that is associated with pyrite and sphalerite mineralisation in a vein from Albert silver deposit. The inclusion probed appears to be primary in origin, however, secondary trails are also present. Magnification: X400.
B) PIXE microprobe spectrum (Q =325 nC, I = ~500 pA) of inclusion A (depth 3.99μm, thickness 0.0856μm, dimensions 12μm X 10μm) in A), indicating the presence of S, K, Ca, Fe Zn and As in the inclusion. The components detected in the inclusion reflects those of the associated minerals.
C) PIXE microprobe spectrum of the same inclusion A, but where Q = 458 nC and I =~500pA. The Fe response is enhanced and Mn and Pb are detected.

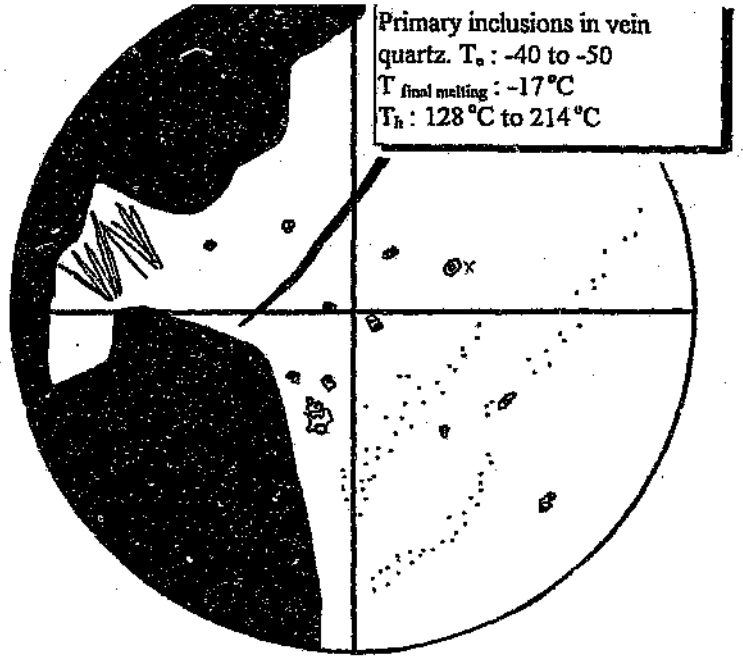


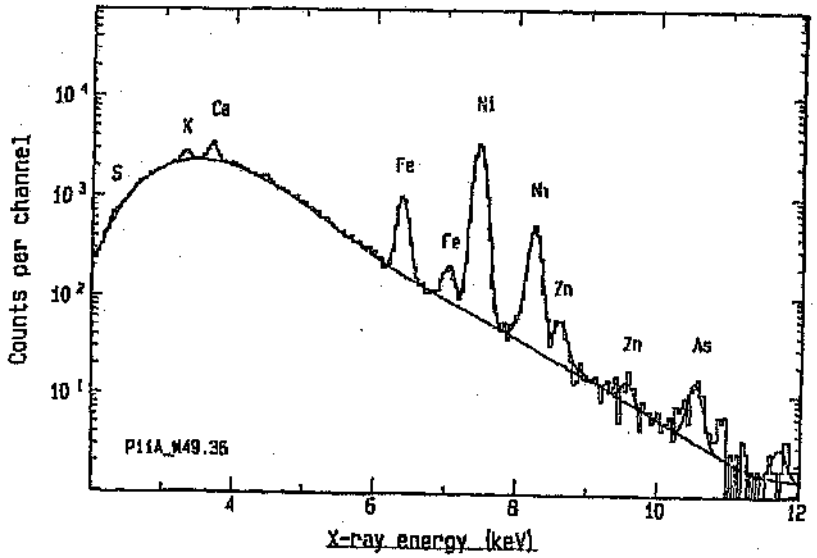


C

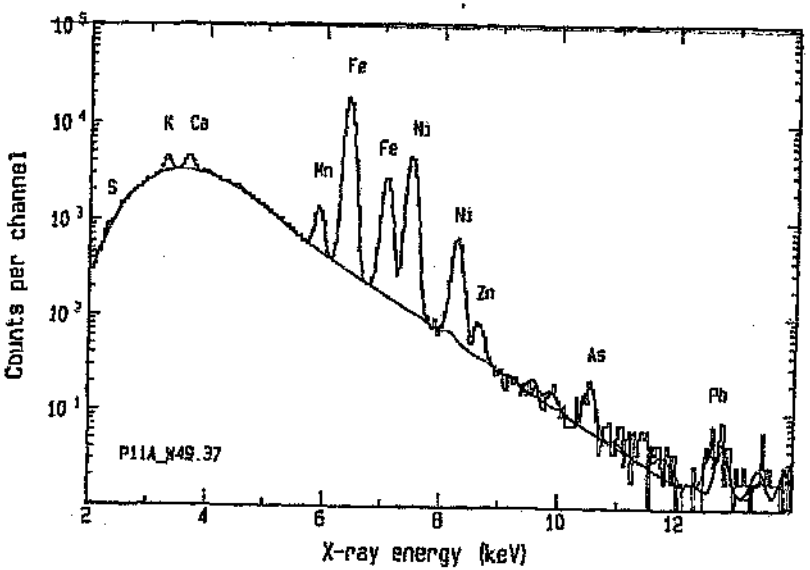


**Figure 6.9** A) Petrographic map of a quartz-hosted fluid inclusion assemblage that is associated with pyrite and sphalerite mineralisation in a vein from Albert silver deposit. The inclusion probed appears to be primary in origin, however, secondary trails are also present. Magnification: X400.
B) PIXE microprobe spectrum (Q =325 nC, I = ~500 pA) of inclusion A (depth 3.99μm, thickness 0.0856μm, dimensions 12μm X 10μm) in A), indicating the presence of S, K, Ca, Fe Zn and As in the inclusion. The components detected in the inclusion reflects those of the associated minerals.
C) PIXE microprobe spectrum of the same inclusion A, but where Q = 458 nC and I =~500pA. The Fe response is enhanced and Mn and Pb are detected.

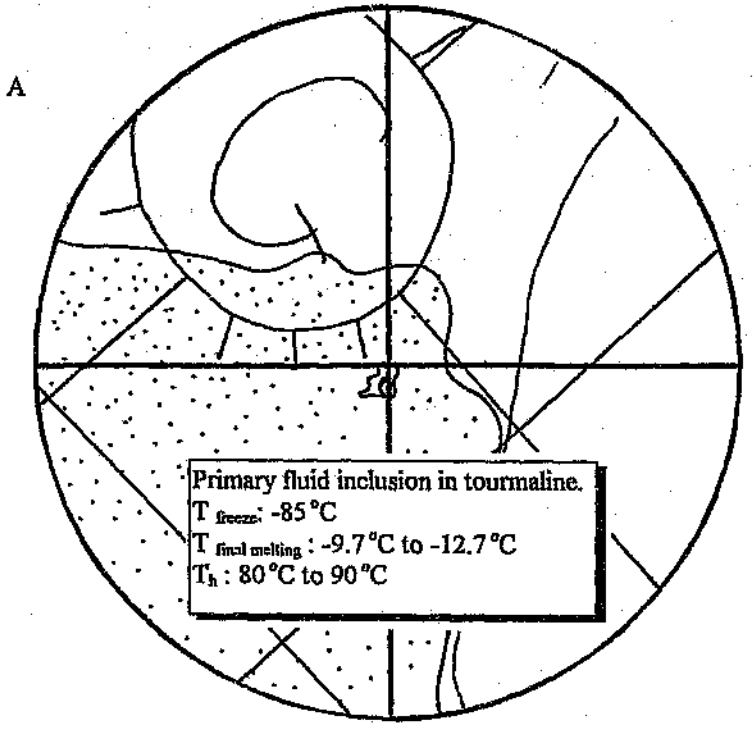


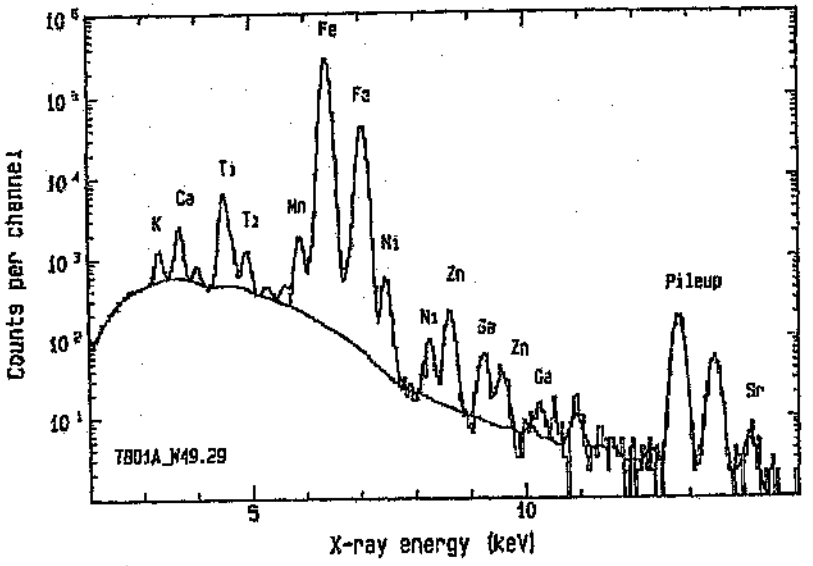


**Figure 6.10** A) Petrographic map of tourmaline-hosted primary fluid inclusion occurring in a tourmaline spheroid from Leeufontein. Magnification: X400.

B) PIXE microprobe spectrum (Q =72 nC. I =100 pA) of inclusion (depth 0.85μm, thickness 2.85μm, dimensions 20μm X 20μm) in A). The fluid inclusion contents cannot be distinguished from the elements in the tourmaline lattice.

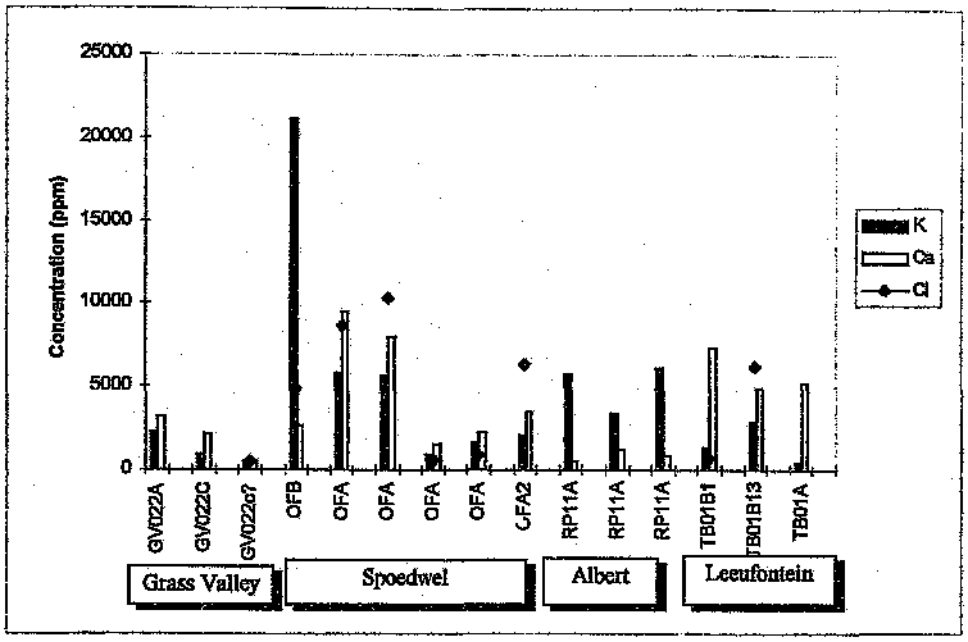


**Figure 6.11** Bar chart showing the concentrations (ppm) of K, Ca and Cl in the fluids from Grass Valley, Spoedwel, Albert and Leeufontein.

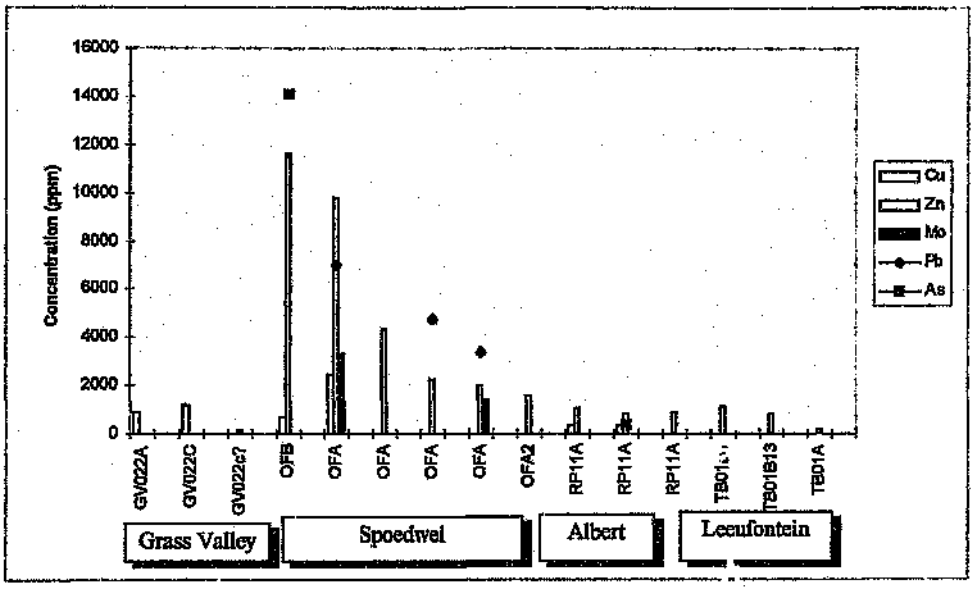


**Figure 6.12** Bar chart showing the concentrations (ppm) of Cu, Zn, Mo, Pb, and As in the fluids from Grass Valley, Spoedwel, Albert and Leeufontein.

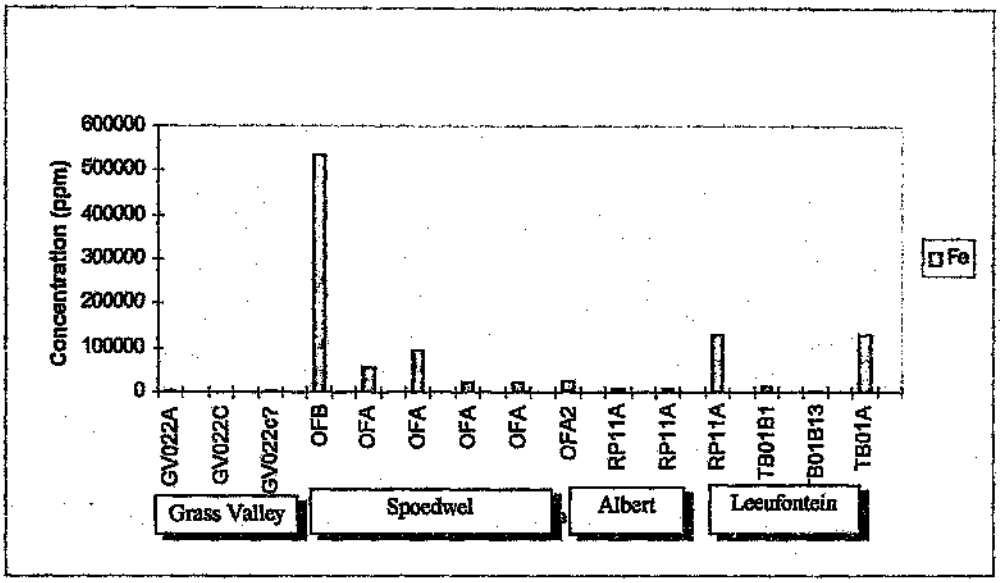


**Figure 6.13** Bar chart showing the concentration (ppm) of Fe in the fluids from Grass Valley, Spoedwel, Albert and Leeufontein.

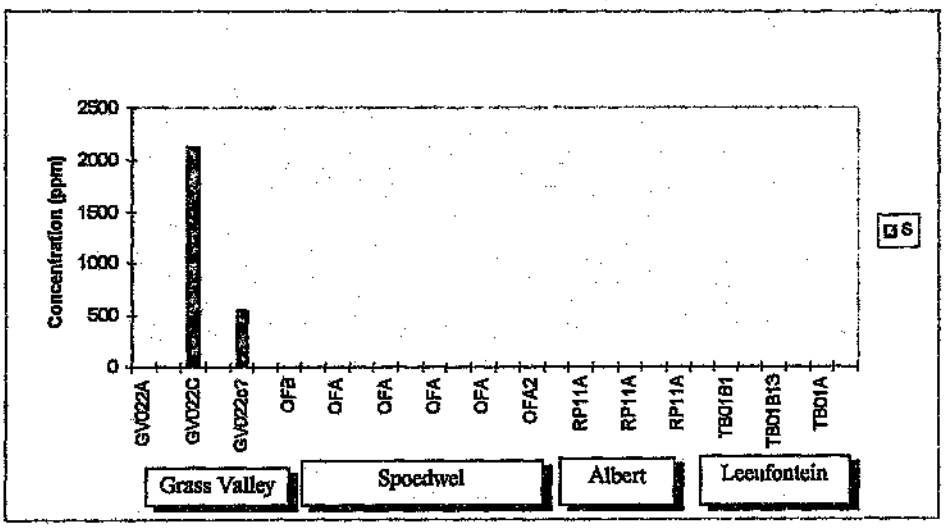


**Figure 6.14** Bar chart showing the concentration (ppm) of S in the fluids from Grass Valley, Spoedwel, Albert and Leeufontein.

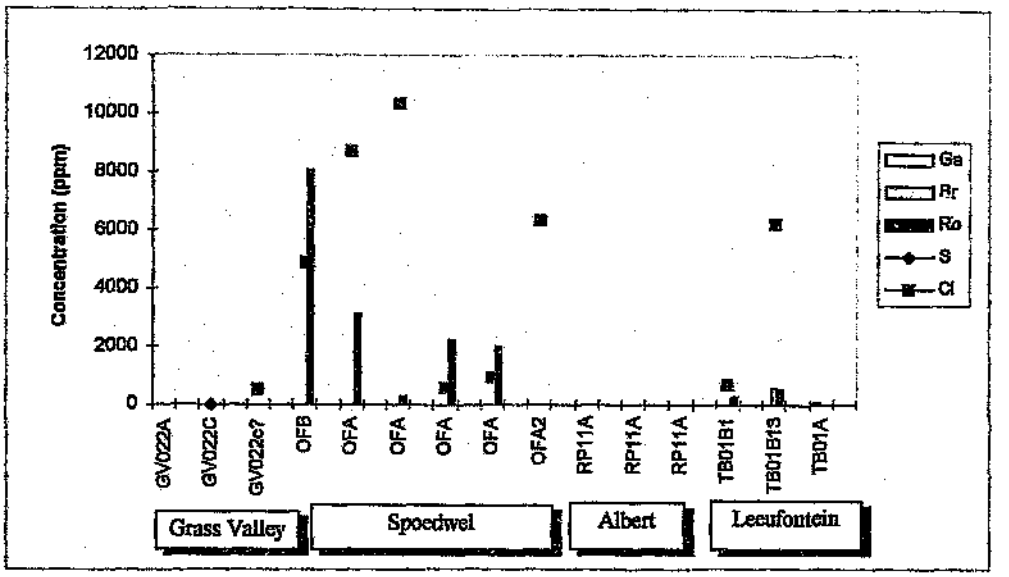


**Figure 6.15** Bar chart showing the concentrations (ppm) of Ga, Br, Rb, S and Cl in the fluids from Grass Valley, Spoedwel, Albert and Leeufontein.

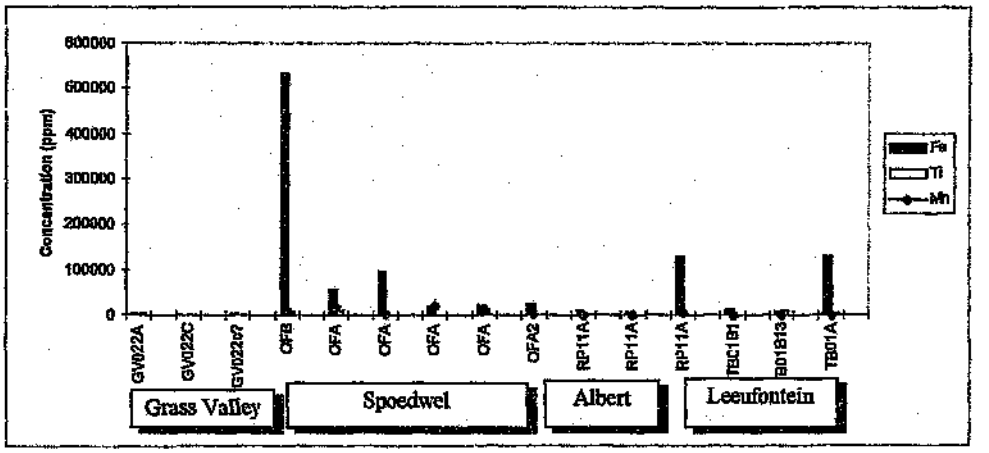


**Figure 6.16** Bar chart showing the concentrations (ppm) of Fe, Ti and Mn in the fluids from Grass Valley, Spoedwel, Albert and Leeufontein.

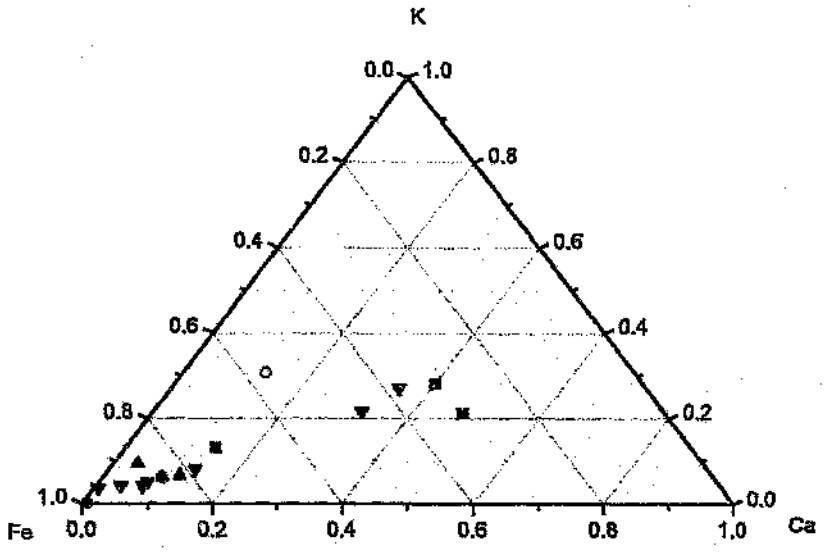


**Figure 6.17** Ternary diagram (K-Fe-Ca) of fluids from Grass Valley (black square), Spoedwel (red downwards triangle), Albert (blue upwards triangle) and Leeufontein tourmaline (green dot).

## *DISCUSSION*

The use of PIXE microanalysis is particularly useful in detecting the presence of a number of elements such as S, Ti, Mn, Fe, Zn, Ga, As, Br, Rb, Sr, Mo and Pb, which are not easily detected by microthermometric methods. The presence of these components in the fluids has several implications for the interpretation of microthermometric measurements, particularly the salinity. Phase relationships in such multi-component systems are not well understood, and estimates of salinity should be made with caution. In general, the elements with the highest concentration are Fe and K, followed by Ca, Cl, Zn, Rb and Pb. However, the major elements in solution vary depending on the stage in the paragenetic sequence.

The fluid inclusions were chosen to represent samples of the fluid at each stage of the evolving paragenesis in the Bushveld granites (discussed in Chapter 4). Fluids associated with the early, orthomagmatic (600°C) Sn-W assemblage at Zaaiplaats are not preserved at the deposits chosen for this study. The compositions of fluids associated with the lower temperature (>300°C), hydrothermal cassiterite assemblage observed at Grass Valley, the sulphide assemblage preserved at Spoedwel (and, to a lesser extent, at Albert), and the late stage fluids responsible for tourmalinisation and albitisation (Leeufontein), have been determined by this method. Unfortunately, fluids associated with the third major episode of mineralisation, which led to the formations of the hematite-fluorite-pitchblende assemblage, could not be assessed because the fluorite hosting the fluid inclusions interfered with the analysis.

The aqueous and gaseous inclusions from Grass Valley contain minor amounts of Ca, K, and Cl. The gaseous, $CO_2$-rich inclusions contain small amounts of S and Cu, which is consistent with the theory that Cu is transported in the vapour phase (Lowenstern *et al.*, 1992; Heinrich *et al.*, 1992). In determining salinity for these early fluids, a chemical system including NaCl-KCl-$CaCl_2$-$H_2O$-$CO_2$ would be appropriate.

In contrast, the fluids at Spoedwel contain significant amounts of (in order of abundance) Fe, Mn, Pb, Zn, Cu, Ca, K, Mo, Ti, Rb and Cl. These fluids have the highest Cl content of all the deposits. Thus, in order to determine salinity meaningfully, the phase relationships between all these components should be taken into account. At the very least, a chemical system with Fe and Mn as the major solutes should be used. A simple chemical system such as the one appropriate for the early fluids at Grass Valley would be inappropriate for the fluids associated with quartz generation 2 at Spoedwel. The fluids associated with quartz-sulphide veins at Albert contain K, Ca and Fe as the major elements, and minor amounts of Cu, Zn, and As. No REE's were detected at Albert.

The fluids associated with tourmalinisation and albitisation in the fine-grained Klipkloof granite dykes in the Leeufontein area contain significant amounts of Ca, K and Fe, and lesser amounts of Zn, K, Cl, Br, Ga and Rb. Br and Ga were not detected in the fluids at the other deposits.

Even though the quantitative data are not accurate, valuable information regarding the

transport of ions in solution has been obtained, and has shown that the evolution of the fluids in terms of their ion content can be traced from one deposit to another. Furthermore, the detection of so many elements within single inclusions confirms that the ore forming components of the sulphide paragenesis were transported by one fluid, which was progressively modified by the addition of, and mixing with, an external connate fluid.

Two distinct fluid types have been detected in terms of their solute composition. These fluid types may be correlated with the two end-member fluids recognised during microthermometry. The fluids with the lowest salinity and highest temperature, are those which PIXE analysis has shown to be relatively barren with respect to ore-forming components. These fluids are represented by the early fluids at Grass Valley which precede cassiterite precipitation. In contrast, the highly saline, lower temperature fluid preserved in primary inclusions hosted by a second generation of quartz at Spoedwel contain significant amounts of all the ore-forming components. The sample material from Albert represents the intermediate category of fluids recognised by microthermometry, where the temperature and solute content is moderate, reflecting partial interaction between the two fluid types.

The fluids post-dating the major episodes of mineralisation, and which are associated with alteration of the host granites and the ore deposits themselves, contain small amounts of the components of the sulphide assemblage. Furthermore, the fluid inclusions hosted by quartz and tourmaline in the tourmaline spheroids show that Fe, Zn and Pb (as well as trace elements- Br, Ga, Rb, Sr) are present in the late stage fluids. The presence of these elements in the fluids at such a late stage in the system suggests that, in addition to enrichment of the residual fluid in incompatible elements, some of these components may have been in continuous supply and transported into the complex by an external fluid.

## 6.2 LASER RAMAN SPECTROSCOPY

Laser Raman Microprobe (LRM) Spectroscopy provides quantitative information on the composition and concentration of solutes in fluid inclusions, and is able to detect the presence of geologically significant, covalently bonded gas species such as $CO_2$, CO, $N_2$, $CH_4$, $H_2S$, $H_2$ and $O_2$. The presence of several of these components in the fluid inclusions from Grass Valley, Houtenbek, Albert, Spoedwel and Dronkfontein have been indicated during microthermometry by features such as $CO_2$ double bubbles, clathrate formation, low freezing temperatures and eutectic melting temperatures. For this reason, LRM spectroscopy was employed in order to determine exactly which gaseous species where responsible for the observed microthermometric behaviour. Furthermore, this technique complements the PIXE microanalysis in that it detects the presence of the lighter elements such as C, H, and N which are not detected by PIXE microanalysis, thereby providing a more comprehensive representation of the nature of hydrothermal fluids associated with mineralisation.

### *OVERVIEW*

LRM spectroscopy is applicable to solid, liquid and gaseous samples. Samples as small as 1-3 microns in diameter can be analysed non-destructively, *in situ* (in thin sections), and with good spatial resolution, while being microscopically viewed in the context of their surrounding matrix (Pasteris, 1996). Thus, it is ideal for examining fluid inclusions in transparent minerals such as quartz and fluorite.

This method of analysis is based on the principle of Raman scattering of light, in which the energy of an incident beam of light is slightly raised or lowered by inelastic interaction with the vibrational modes (Mc Millan and Hofmeister, 1988).

In a Raman scattering experiment, visible light usually emitted from a monochromatic laser beam, is passed through the sample. Most of the light exits from the sample unchanged, but a small fraction ($\sim 10^{-3}$ of the incident intensity) is scattered by the atoms. Of this scattered light, a small portion ($\sim 10^{-6}$ of the incident light) interacts with the sample, inducing a vibrational mode. When this occurs, the energy of the scattered light is reduced by an

amount corresponding to the vibrational transition. This type of inelastic scattering is referred to as Raman scattering, in contrast with the elastic (Rayleigh) scattering of light with no energy change.

In addition to the Raman and Rayleigh scattered radiation produced when an intense beam of light of given wavelength is passed through an optically transparent substance, a third type of scatter is often encountered, which is referred to as fluorescence. When the incident radiation is absorbed by the substance and emitted as a new radiation of longer wavelength, the substance is displaying fluorescence. The wavelength of the emitted radiation is characteristic and does not shift if the exciting radiation is shifted (Roedder,1984).

The most common application of LRM spectroscopy to fluid inclusion analysis is in the identification and quantification of covalently bonded gases such as $CO_2$, CO, $CH_4$, $H_2S$, $N_2$, $O_2$ and $H_2$. Once an LRM machine has been calibrated against gas standards, quantitative compositional analyses of the molar proportions of gas species in multi-component inclusions can be accomplished to an accuracy of ~1mole%. Moreover, the specific positions and shapes of the Raman bands are functions of the bulk composition of the gas and the gas pressure (Pasteris, 1996).

One limitation of this method is that simple ionic electrolytes (e.g. $Na^+$, $K^+$, $Cl^-$, $Br^-$) cannot be detected from their own vibrational signatures. These components may be detected by freezing the inclusions to approximately -180°C, and taking Raman spectra of the various hydrated solids that form, e.g. chloride hydrates which can be distinguished from each other (Dubessy *et al.*, 1982, 1992).

For dissolved species that are Raman-active (e.g. complex ions consisting of covalently bonded groups, such as $SO_4^{2-}$ and $HCO_3^{2-}$), LRM calibration on solutions of known concentration enables the quantitative analysis of those solutes. Furthermore, LRM also provides information on speciation e.g.$S^{2-}$, $H_2S$, $(SO_4)^{2-}$ of Raman-active solutes (Dubessy *et al.*, 1983).

Laser Raman Spectroscopy involves focusing a monochromatic laser beam through a microscope objective into a fluid inclusion or into an individual solid, liquid or gas phase within the inclusion. The Raman scattered light is collected through the same objective, passes through a double monochromator, and is detected by a photon counting device (Seitz *et al.*, 1987). This information is then converted into a set of absorption or scattering peaks as a function of energy. These peaks are represented as a vibrational spectrum, in which individual peaks correspond to the energies of vibrational transitions within the sample (Roedder, 1984).

Raman spectra are plots showing intensity of the scattered photons (on y-axis) as a function of the shift in the frequency of the scattered light (on x-axis), with respect to the frequency of the laser source. The frequency term used is $cm^{-1}$ and the x-axis units are $\Delta\ cm^{-1}$ (Raman shift). The Raman spectrum of a compound is a unique fingerprint that distinguishes it from all other compounds with different crystalline structure and/or composition (Pasteris, 1996).

***EQUIPMENT***

Laser Raman Spectroscopy was conducted at the University of Pretoria, and at the University of the Witwatersrand. The system at the University of Pretoria comprised an argon laser directed through the objectives of an Olympus Microscope fitted with 10X,50X and 100X magnification lenses. The data collected by the Dilor XY multichannel instrument was processed by the Dilor XY software package installed on a computer connected to the spectrometer.

***SAMPLE MATERIAL***

In selecting fluid inclusions to be analysed by the Raman microprobe, the parameters suggested by Pasteris *et al.* (1988) were followed. Suitably sized inclusions with high optical clarity, at a shallow depth below the sample surface, were sought.

Polished thin sections and doubly polished rock wafers were made at the University of the Witwatersrand using Superglue as a mounting medium. The doubly polished rock wafers were cut thick enough to be removed from the supporting glass slide by immersion in the solvent acetone. Fluid inclusions in the polished thin sections were analysed *in situ*, and hence some Raman response from the Superglue is to be expected.

Samples from Spoedwel, Grass Valley and Houtenbek selected for Raman analysis are tabulated in Table 6.4. Three of the samples (SF02, SD52, SD35) from Spoedwel were polished thin sections which had been mounted with epoxy glue. The others were doubly polished thin sections on which microthermometry was to be carried out.

**Table 6.4** Samples selected for Raman analysis from Spoedwel, Grass Valley and Houtenbek.

| DEPOSIT | SAMPLE | COMMENTS |
|---|---|---|
| Spoedwel | SF02 | Fluid inclusions hosted by interstitial quartz in intensely chloritised granite. |
| | SD52 | Fluid inclusions hosted by interstitial quartz in hematitised hypersolvus granite with disseminated chalcopyrite mineralisation. |
| | SD35 | Fluid inclusions hosted by interstitial quartz in intensely chloritised granite. |
| | L2 | Fluid inclusions in a quartz vein in medium-grained hypersolvus granite. |
| | SP3 | Fluid inclusions hosted by interstitial fluorite in coarse-grained hypersolvus granite with minor quartz. |
| | SP6 | Fluid inclusions hosted by interstitial fluorite in graphic granite. |
| Houtenbek | HB2 | Fluid inclusions hosted by sphalerite. |
| Grass Valley | GV02 | Vapour-rich fluid inclusions in quartz preceding cassiterite precipitation. |

***METHODS***

All Raman scans taken at the University of Pretoria were conducted at room temperature and at atmospheric pressure with the following analysis parameters: 100 seconds integration time (counting time per step), excitation by a 514.50nm continuous wave argon

laser, 100mW laser power (at surface of sample), using either 50X or 100X objectives, 2.99$cm^{-1}$ spectral slit width, 800$cm^{-1}$ Spectro, 100 slit width (Im), detector 1024, number of accumulations 1, and a grating of 1800 on the monochromator. At the University of the Witwatersrand, single spectrographs were generated using a 514nm argon laser, with 400mW laser power, 100X microscope objectives, slit width of 20microns, 600g/mm grating, and 0.2mm pinhole.

Several scanning intervals were chosen. Most fluid components in geological systems have Raman responses at wavelengths between 500$cm^{-1}$ and 4000$cm^{-1}$ and therefore, scanning intervals were generally limited to this range. Daughter crystals likely to be present in the inclusions have Raman peaks below 500$cm^{-1}$ and are often masked by peaks of the host crystal and therefore identified with difficulty.

Control spectra of the mounting media, namely the epoxy-based glue and Superglue, were produced by focusing the laser beam directly onto the rim of the sections. Therefore, by a process of elimination, glue peaks could be discarded and any other peaks assumed to belong to the fluid inclusion or the host material. Raman spectra were obtained for each of the following host crystals: quartz, sphalerite and fluorite.

## *RESULTS*

### Raman spectra generated by the mounting media:

#### *Superglue*

The spectrum obtained from pure Superglue is shown in Figure 6.18. The spectral range is broad and spans the wavelengths between 200 and 3400 $cm^{-1}$. It is chiefly composed of carbon compounds. The peak of greatest intensity occurs at the methane position (~2912 $cm^{-1}$). On the left flank of this broad peak another sharp peak is present at ~3069 $cm^{-1}$. These two peaks always occur together and are indicative of Superglue contamination of the sample. The wavelength range from approximately 600 to 1600 $cm^{-1}$ is crowded with 11 discrete peaks of similar intensity. Of these peaks the Fermi diad (1279 and 1383$cm^{-1}$) is sandwiched between the other peaks. No nitrogen or sulphur complexes have been recognised as constituents of the Superglue.

*Epoxy Glue*

The spectrum obtained from the epoxy glue (Figure 6.18) is remarkably similar to that obtained from the Superglue. Between 1100 and 3310 $cm^{-1}$ the number of peaks and peak positions are almost perfectly matched. However, the intensity of the epoxy glue is double that of the Superglue.

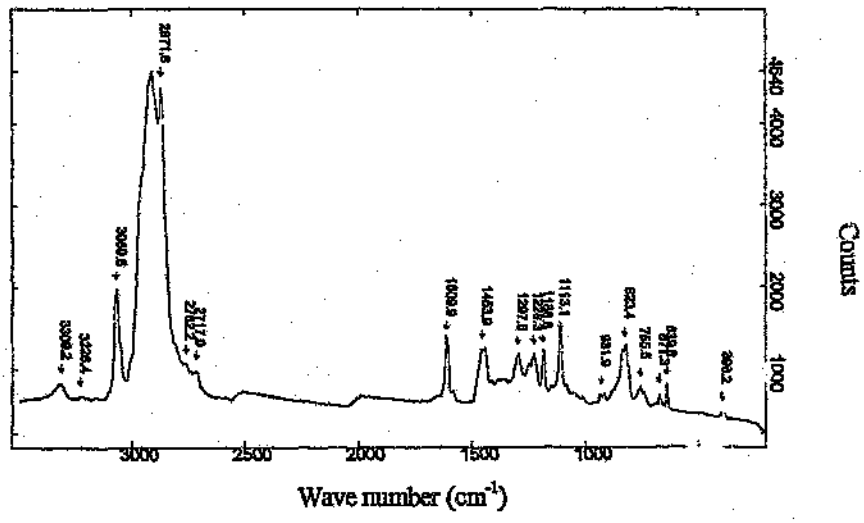


**Figure 6.18** Raman spectrum of Superglue.

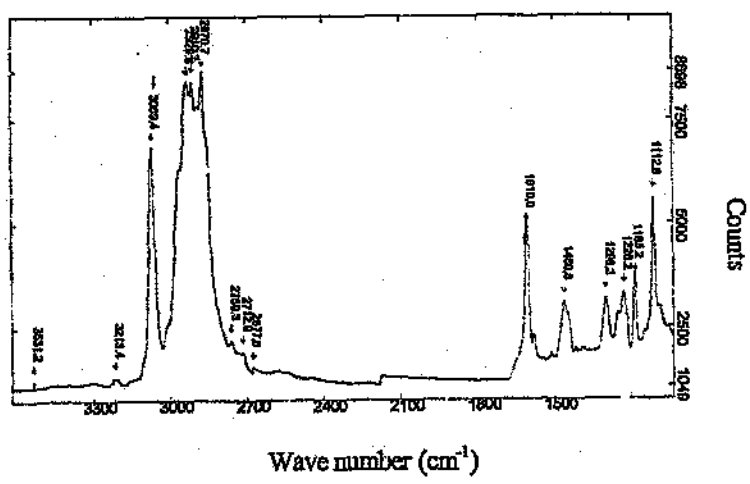


**Figure 6.19** Raman spectrum of epoxy glue.

**Raman Spectra generated by the host minerals**

***Sphalerite*** (Figure 6.20)

Peaks are confined to the lower wavelengths below 700 $cm^{-1}$. The spectrum consists of several low intensity peaks, the highest peak intensity occurring at 349,8 $cm^{-1}$. No peaks are found above 800 $cm^{-1}$ and hence any peaks observed in this region when focusing on inclusions cannot be contributed to the host crystal.

***Quartz*** (Figure 6.21)

Pure quartz has a strong Raman response of 10 discrete peaks in the range 205 to 1161 $cm^{-1}$, the peak with the highest intensity occurring at 464 $cm^{-1}$. These peaks cause no overlap with the $N_2$, $CH_4$ or Fermi diad ($CO_2$) peak positions. However, the response of $HCO_3^-$ and the monatomic ions $Na^+$, $K^+$, $Ca^{2+}$ and $Mg^{2+}$ are masked or even obliterated by the strong quartz peaks.

**Fluorite** (Figure 6.22)

The fluorite spectrum is confined to those wavelengths below ~1586 $cm^{-1}$ and consists of a broad based peak which stretches from ~800 to~1500 $cm^{-1}$. Superimposed on this are several other sharp peaks and bell-shaped curves. The peak of greatest intensity occurs at 808$cm^{-1}$, and 3 minor undulations 646, 547 and 321 $cm^{-1}$ are found in the lower spectral region.

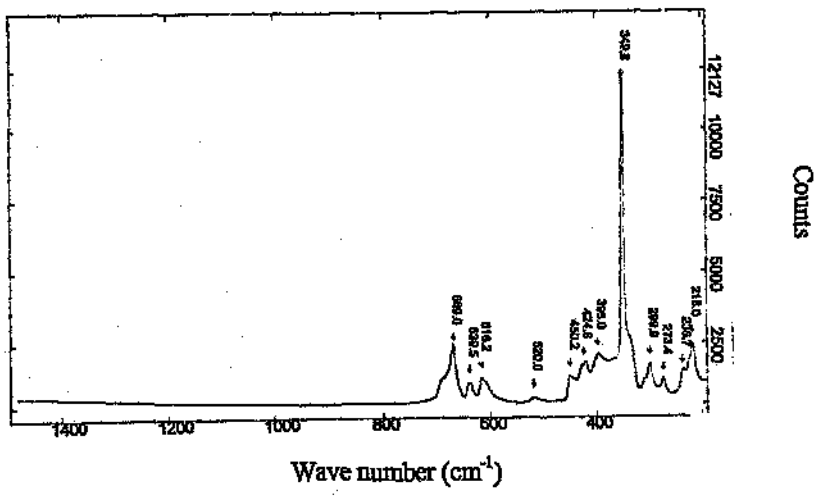


Figure 6.20 Raman spectrum of sphalerite from Houtenbek.

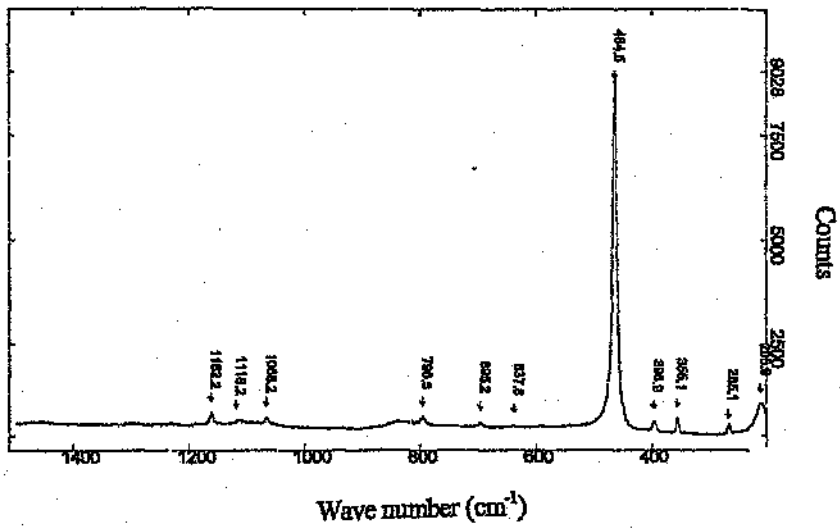


**Figure 6.21** Raman spectrum of quartz from Spoedwel.

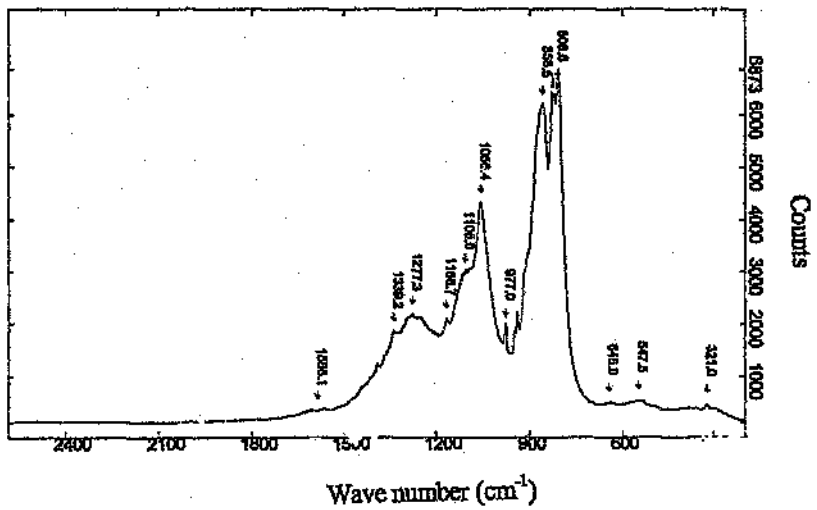


**Figure 6.22** Raman spectrum of fluorite from Houtenbek.

**Raman Spectra generated by fluid inclusions**

The components detected in the fluid inclusions are shown in Table 6.5. The Raman responses from the polished thin sections were masked by the strong peaks generated by the epoxy glue. The spectra from the doubly polished thin sections indicated the presence of $N_2$, $CH_4$, $CO_2$ and $H_2O$ in the fluids. Of the fluid inclusions examined, only those in which the components undoubtedly originate from the fluid inclusions, and not from the air or surficial contamination, are presented.

**Table 6.5** Table showing components of each fluid inclusion analysed.

| SAMPLE NO. | HOST MINERAL | COMPONENTS | COMMENTS |
|---|---|---|---|
| SF02 | quartz | | Epoxy masked Raman response-no data obtained. |
| SD52 | quartz | $N_2$ | Hematite daughter crystal |
| SD35 | quartz | $H_2O$ | Epoxy peaks mask all other peaks. |
| HB2 | sphalerite | $H_2O$, ($N_2$ $CO_2$) | Unidentified peak at 1600.9cm$^{-1}$. $N_2$ and $CO_2$ peaks very small. Sphalerite fluorescence interferes with peaks from fluid inclusion components. |
| L2 | quartz | $N_2$ | Sharp, high intensity peak. No other components (see Figure 6.23). |
| SP3 | fluorite | $H_2O$, ($CH_4$), $N_2$ | Large peaks for all three components. $CH_4$ is not from the fluid inclusion but from the surface (see Figure 6.24). |
| SP6 | fluorite | $CH_4$ | Broad, high intensity peak for methane (see Figure 6.25). |
| GV02 (MM2-c) | quartz | $CO_2$, $N_2$, $CH_4$ | Large $CO_2$ peaks, minor $N_2$, $CH_4$ peaks (see Figure 6.26a). |
| GV02 (MM1-a) | quartz | $CO_2$, $CH_4$ | No $N_2$ detected (see Figure 6.26b). |
| GV02 (MM3-a2) | quartz | $CO_2$, $N_2$ ($CH_4$) | $CH_4$ came from the surface of the sample (see Figure 6.26c). |

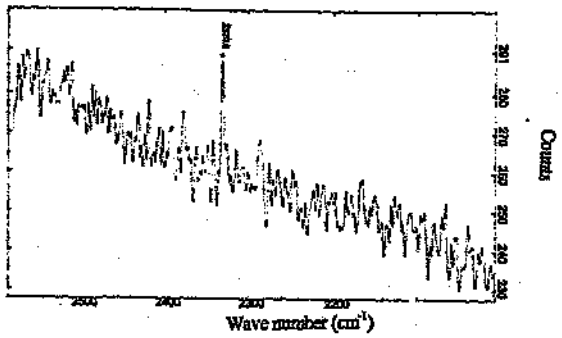


**Figure 6.23** Raman spectrum showing nitrogen peak in sample of vein quartz from Spoedwel.

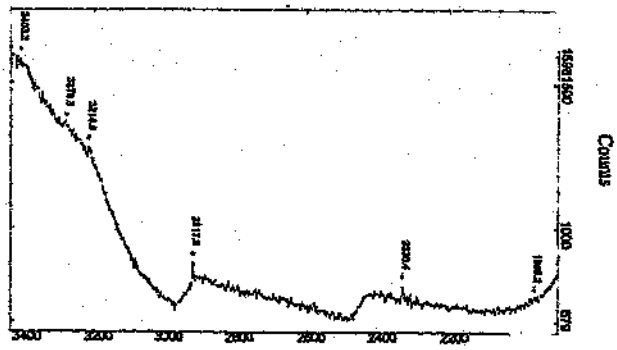


**Figure 6.24** Raman spectrum showing nitrogen and methane peaks, as well as a broad bell-shaped water curve in fluorite from Spoedwel.

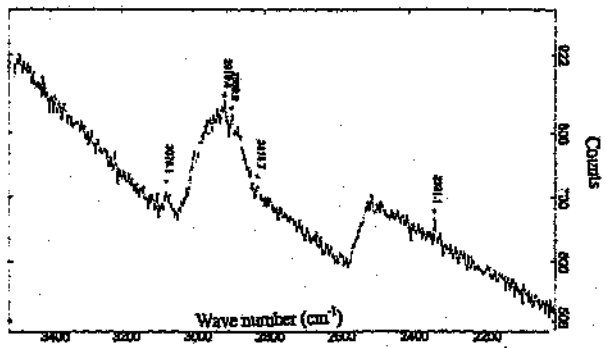


**Figure 6.25** Raman spectrum showing nitrogen and methane peaks in late stage quartz associated with hematite precipitation at Spoedwel.

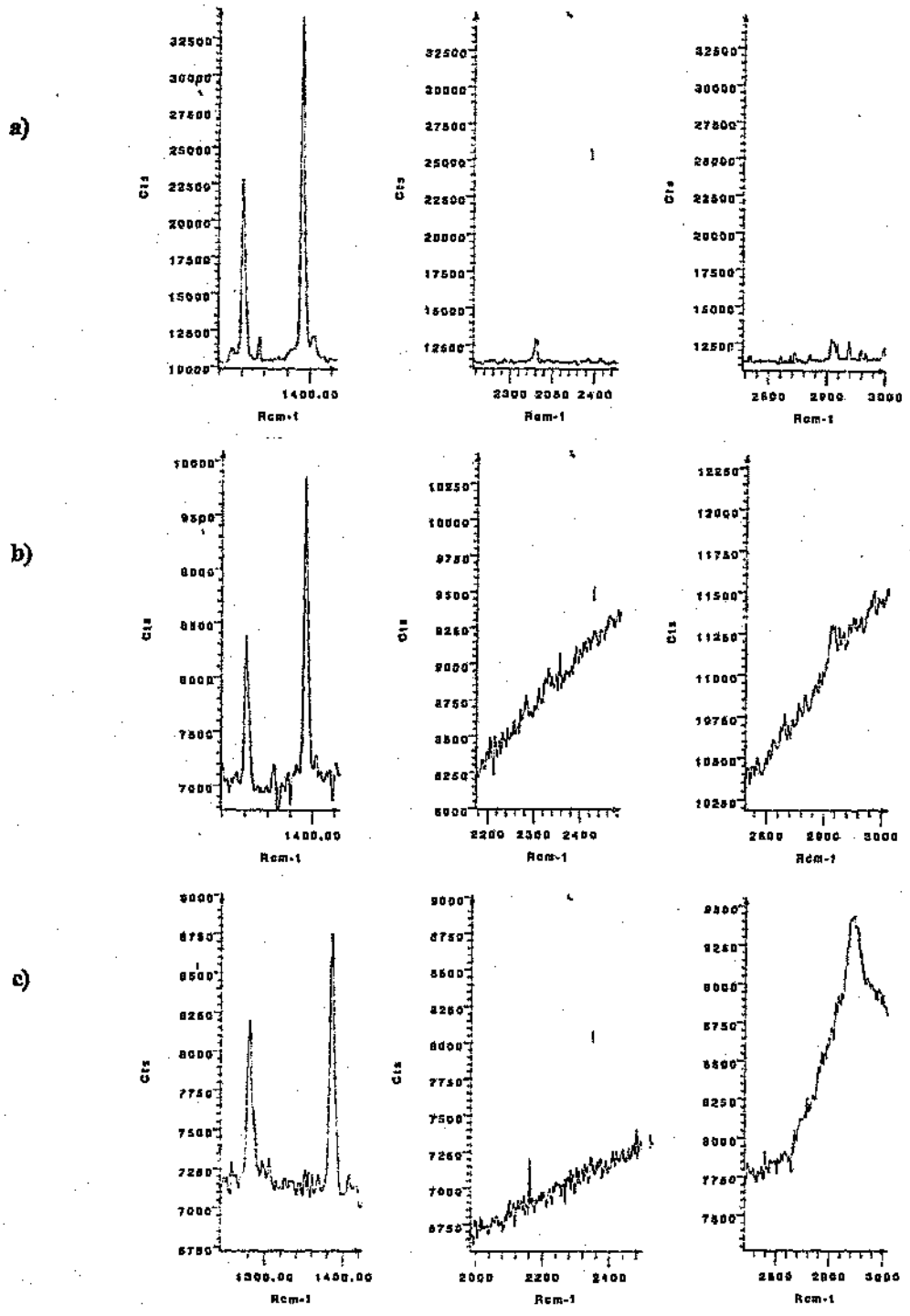


**Figure 6.26** a-c) Raman spectra of three different fluid inclusions showing $CO_2$ (left) $N_2$ (middle) and $CH_4$ (right) in quartz-hosted fluid inclusions from Grass Valley.

The methane peak position has been used to determine the pressure of methane inside the inclusions (Fabre and Couty, 1986). Table 6.6 shows the methane pressure for the observed methane peaks. These values are superimposed on Figure 6.27, which is taken from Goldstein and Reynolds (1994), and shows the relationship between relative wave number and methane pressure.

**Table 6.6** Methane peak positions and the corresponding methane pressure.

| SAMPLE | PEAK POSITION ($cm^{-1}$) | METHANE PRESSURE (bars) |
|---|---|---|
| GV02 (MM1-A) | 2913.8 | 110 ( density $8.7.10^{-2}$ ) |
| GV02 (MM2-C) | 2910.4 | 450 (density $26.6.10^{-2}$) |
| GV02 (MM3-A2) | 2942 | 0 (surface contamination) |
| SP3 | 2917.9 | 0 (surface contamination) |
| SP6 | 2910.4 | 450 (density $26.6.10^{-2}$) |

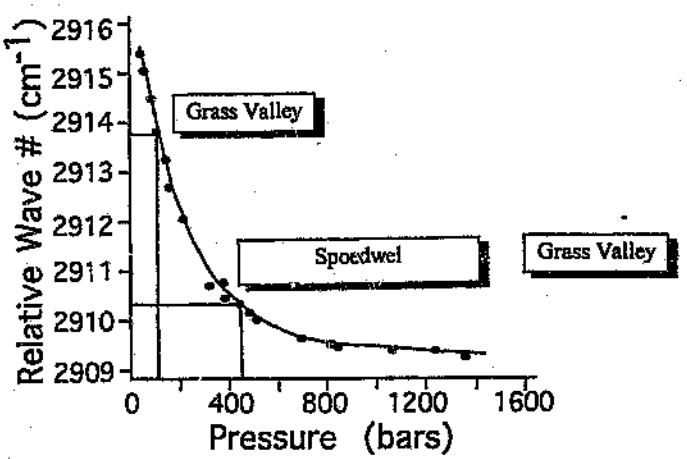


**Figure 6.27** Relationship between relative wave number and methane pressure determined from the laser Raman microprobe. Data from Fabre and Couty (1986) (in Goldstein and Reynolds, 1994).